Heterogeneous enantioselective catalysis:

The behaviour of reactants, products and modifiers

on single crystal surfaces

Thesis submitted in accordance with the requirements of the University of Liverpool for

the degree of

Doctor of Philosophy

By

Delphine Le Roux

Department of Chemistry

University of Liverpool

November 2002

Declaration

I declare that this thesis has not previously been submitted and is not currently being submitted for any other degree other than that of the degree of Doctor of Philosophy at the University of Liverpool.

All the work reported in this thesis is my own except where due reference is made.

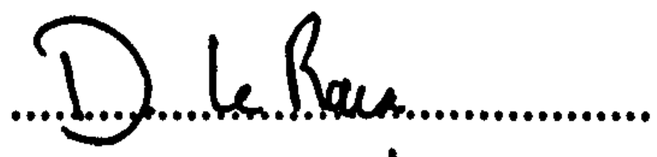

.....D. le Roux..... (Candidate)

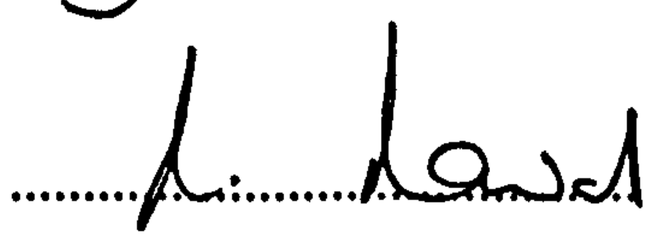

..... (Supervisor)

Acknowledgements

I would like to thank my supervisor Professor Rasmita Raval for offering me the opportunity to work in her research group, for her guidance, help and encouragement over these three years.

I am extremely grateful to Dr Vincent Humblot for his numerous explanations when I needed to learn the way UHV chambers work, the way an experiment is carried out and the way some pieces can be repaired; thanks for his support, advice and answers to my questions.

Many thanks as well to Dr Sam Haq and Dr Carsten Winkler for their valuable discussions, their experimental skills and useful advice. I would like to thank Dr Sue Barlow for reading and correcting this manuscript, for her encouragements and support.

It has been a great pleasure to work in Professor Raval's group: Alex Carew, Maria Ortega Lorenzo, Keith Middleman, Eva Mateo Marti, Lucy Bloxham, Alex McNutt, Christopher Bingham and Nick Brabner; and with people from Daresbury Laboratory: Professor Elaine Seddon, Dr Cephise Cacho, Dr Andrew Malins, Lee Jones, Dimitra Tsoutsou and James Grayson.

I do not forget other friends from the Leverhulme Centre for Innovative Catalysis and the Department of Chemistry who have made these three years enjoyable and who have given the feelings these years have been too short.

A special thought to Gwilherm Kerhervé for his love, help and support.

Abstract

Heterogeneous enantioselective catalysis: The behaviour of reactants, products and modifiers on single crystal surfaces

In the hydrogenation reaction of methylacetoacetate (MAA) to methyl-3-hydroxybutyrate (MHB) over a metal catalyst, the amino acid alanine is used as a chiral modifier to direct the reaction towards a particular MHB enantiomer. The work presented in this thesis considers the fundamental adsorption behaviour and interactions of the enantiomers of alanine and MHB at single crystal metal surfaces.

Both enantiomers of alanine adsorbed on Ni (110) in vacuo have the same behaviour. Reflection Absorption Infrared Spectroscopy (RAIRS) has shown that they adsorb in the anionic form at low coverage, through the two oxygens of the carboxylate group and through the nitrogen of the amino group. At high coverage, another phase grows in alongside the low coverage phase with both the anionic and the zwitterionic forms appearing to be present. This high coverage phase is attached to the surface through only one oxygen of the carboxylate group. The alanine molecules do not follow any long-range order on the surface with no Low Energy Electron Diffraction (LEED) pattern observed. With increasing temperature, the alanine molecules decompose into fragments before beginning to desorb around 350 K at low coverage and exploding off the surface at 400 K at high coverage.

RAIRS has shown that at room temperature both enantiomers of MHB are bonded to the Cu (110) surface through the C = O part of the ester group. This bond is strong and in a position quite normal to the surface. The alcoholic part of the MHB molecule does not maintain any bonding with the surface. The MHB molecule is subject to thermal changes. Both RAIRS and Temperature Programmed Desorption (TPD) experiments prove that the MHB molecule dehydrogenates into MAA even at room temperature with the rate increasing as the temperature increases. The activation energies for (R)-MHB and (S)-MHB to transform into MAA are 100 ± 20 kJ. mol^{-1} and 94 ± 17 kJ.mol^{-1} respectively. The MAA created then desorbs from the surface at a temperature of 450 K.

Experiments involving the co-adsorption of (S)-alanine with the enantiomers of MHB have shown that the MHB molecules can only co-adsorb with a low coverage phase of (S)-alanine. RAIR spectra have shown a small deformation of some of the alanine bands on co-adsorption of the (R)- or the (S)-MHB but the interaction between the enantiomers of MHB and (S)-alanine is weak and does not seem to be intimate. The TPD spectra have not revealed any change in the temperature of desorption of the molecules from the surface on co-adsorption. The activation energy for the transformation of (R)-MHB into MAA in the presence of (S)-alanine has been calculated as 96 ± 15 kJ. mol^{-1}. Thus, the activation energy of the dehydrogenation reaction is not influenced by the presence of (S)-alanine. At no point, has it been possible to observe any chiral discrimination by (S)-alanine between the enantiomers of MHB.

Glossary

acac	acetylacetone
AES	Auger Electron Spectroscopy
ee	enantiomeric excess
fcc	face centred cubic
EELS	Electron Energy Loss Spectroscopy
FTIR	Fourier Transform Infra-Red
IR	Infra-Red
LEED	Low Energy Electron Diffraction
MAA	Methyl-acetoacetone
MCT	Mercury Cadmium Telluride
MHB	Methyl-3-hydroxybutyrate
MRNi	Modified Raney Nickel
MSSR	Metal Surface Selection Rules
RAIRS	Reflection Absorption Infra-Red Spectroscopy
SERS	Surface Enhanced Raman Spectroscopy
STM	Scanning Tunnelling Microscopy
TDS	Temperature Desorption Spectroscopy
TPD	Temperature Programmed Desorption
TSP	Titanium Sublimation Pump
UHV	Ultra High Vacuum

Contents

Chapter One

Introduction

1.1 About stereochemistry

1.1.1 Pasteur's discovery

The first manifestation of optical activity was pointed out by Arago [1] in 1811, in his study of the action of a quartz plate on polarised light. Several years later, Biot [2] showed that this phenomenon was not limited to crystalline substances. Solutions of certain natural products also possessed the property of rotating the plane of polarisation of plane-polarized light. Biot studied the physical laws of the phenomenon in detail and showed, in particular, that the rotation angle (α) depends on the nature of the substance and its solvent, on the concentration of the substance in solution passed through by the polarised light, on the wavelength of the light used and on the temperature the test is conducted. The characteristic rotation for each optically active substance can be positive or negative according to the sign of the rotation angle. This is defined positive to show that the optically active substance is dextrorotatory and negative if the substance is laevorotatory, as shown in Figure 1.1.

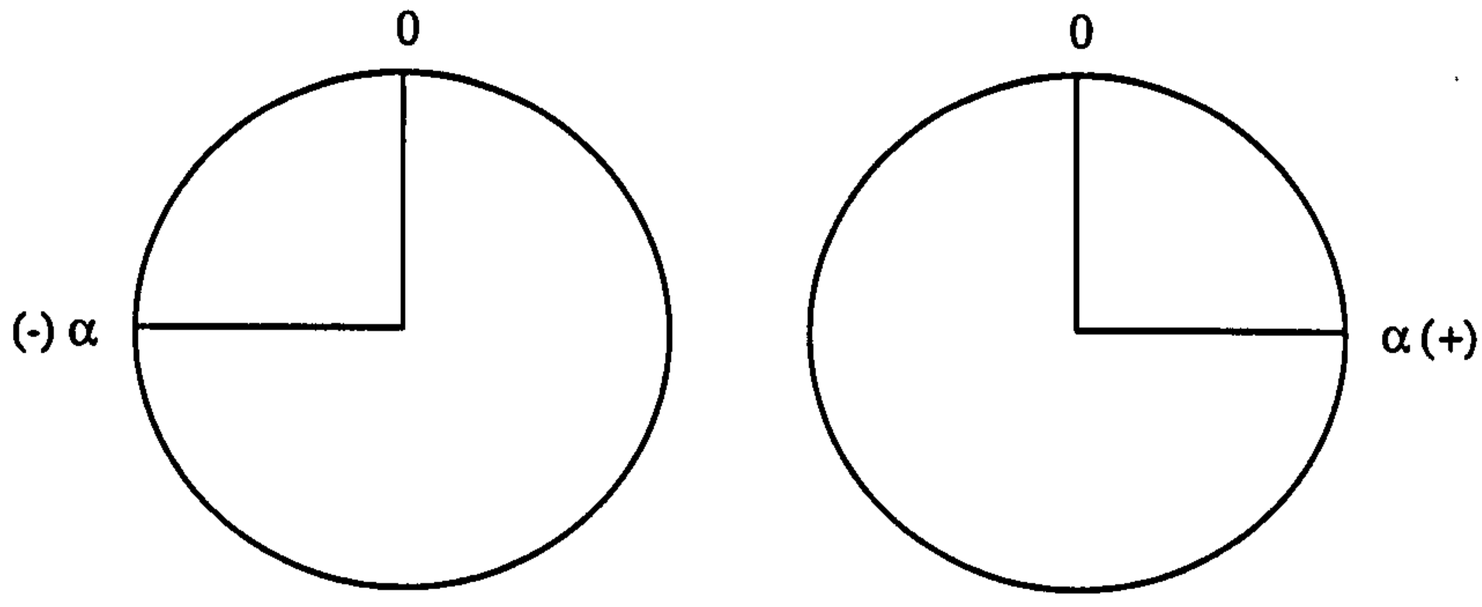

Figure 1.1: The rotation of plane-polarised light by two opposite optically active substances.

When Pasteur discovered the optical resolution of racemic tartrates [3], this was considered as a great advance. He was working for his doctorate in chemistry, on the crystallisation of different compounds; one of them was tartaric acid. Crystals of tartaric acid are present in large amounts in the sediments of fermenting wine, but they are also accompanied by a second acid called paratartaric acid or "racemic acid". A few years earlier, the chemical compositions of these two acids had been determined to be the same. But in solution, whereas tartaric acid rotated a beam of polarised light passing through it to the right, paratartaric acid did not rotate the light. Pasteur could not believe that two compounds having the same chemical composition could act so differently with respect to the rotation of light. He thought that the internal structure of the two compounds was different and this difference would show itself in the crystal form. Upon examination beneath his microscope, he saw that all crystals of pure tartaric acid looked identical to each other. When he examined the paratartrate crystals, he saw two types of crystals: one type was the mirror image of the other. With a dissecting needle and his microscope, he separated the left and right crystal shapes from each other to form two piles of crystals. He then showed that in solution, one form rotated polarised light to the left, the other to the right. This experiment proved that organic molecules with the same chemical composition can exist in space in unique stereospecific forms. Pasteur deduced that the rotatory power was connected with the existence of non-superimposable asymmetry in the molecule. With this work Pasteur gave birth to the new science of stereochemistry.

The work by Le Bel [4] and van't Hoff [5] introduced the concept of a carbon atom situated at the centre of a tetrahedron with its valence bonds directed toward the apices. If four different substituents are attached to the carbon atom, the mirror image of the structure is not superimposable with the original; the molecule now possesses rotatory power. The theory of the asymmetric carbon atom was developed up to a point where it was next thought that the presence of at least one such carbon atom in the molecule was necessary to give rise to optical activity. However, this has been revealed to be wrong. The true version is Pasteur's concept of molecular dissymmetry which ascribes optical activity to any molecule whose mirror image is not superimposable with the original.

1.1.2 Important definitions

Stereochemistry: The science which deals with structure in three dimensions is called stereochemistry. One aspect of stereochemistry is stereoisomerism; isomers that differ from each other only in the way that the atoms are oriented in three dimensional space are called ***stereoisomers*** [6]. The (D)-isomer of the optically active substance which turns the polarised light plane to the right is called dextrorotatory; the (L)-isomer of the optically active substance which turns the polarised light plane to the left is called laevorotatory.

Chiral: This word comes from the Greek word for hand. A chiral molecule is a molecule that is not superimposable on its mirror image. Thus a molecule is chiral if and only if it lacks an axis of improper rotation, that is an n-fold rotation (rotation by 360°/ n) followed by a reflection in the plane perpendicular to this axis which maps the molecule on to itself. A chiral molecule has no internal plane of symmetry. In addition, a chiral molecule exhibits optical activity. It has the property of rotating the plane of polarisation of plane-polarised monochromatic light that is passed through it.

Chirality is a property of the molecule as a whole. It is incorrect, therefore, to say that a molecule contains a chiral centre. It is preferable to refer to ***asymmetric centres*** or ***stereogenic centres***.

Enantiomers: A molecule presenting a stereogenic centre can exist as two different compounds that are stereoisomers and have identical chemical properties in an achiral (symmetrical) environment. The structures of these compounds are nonsuperimposable

mirror-images of each other. Figure 1.2 shows enantiomers of an amino acid, alanine. All amino acids are chiral except glycine.

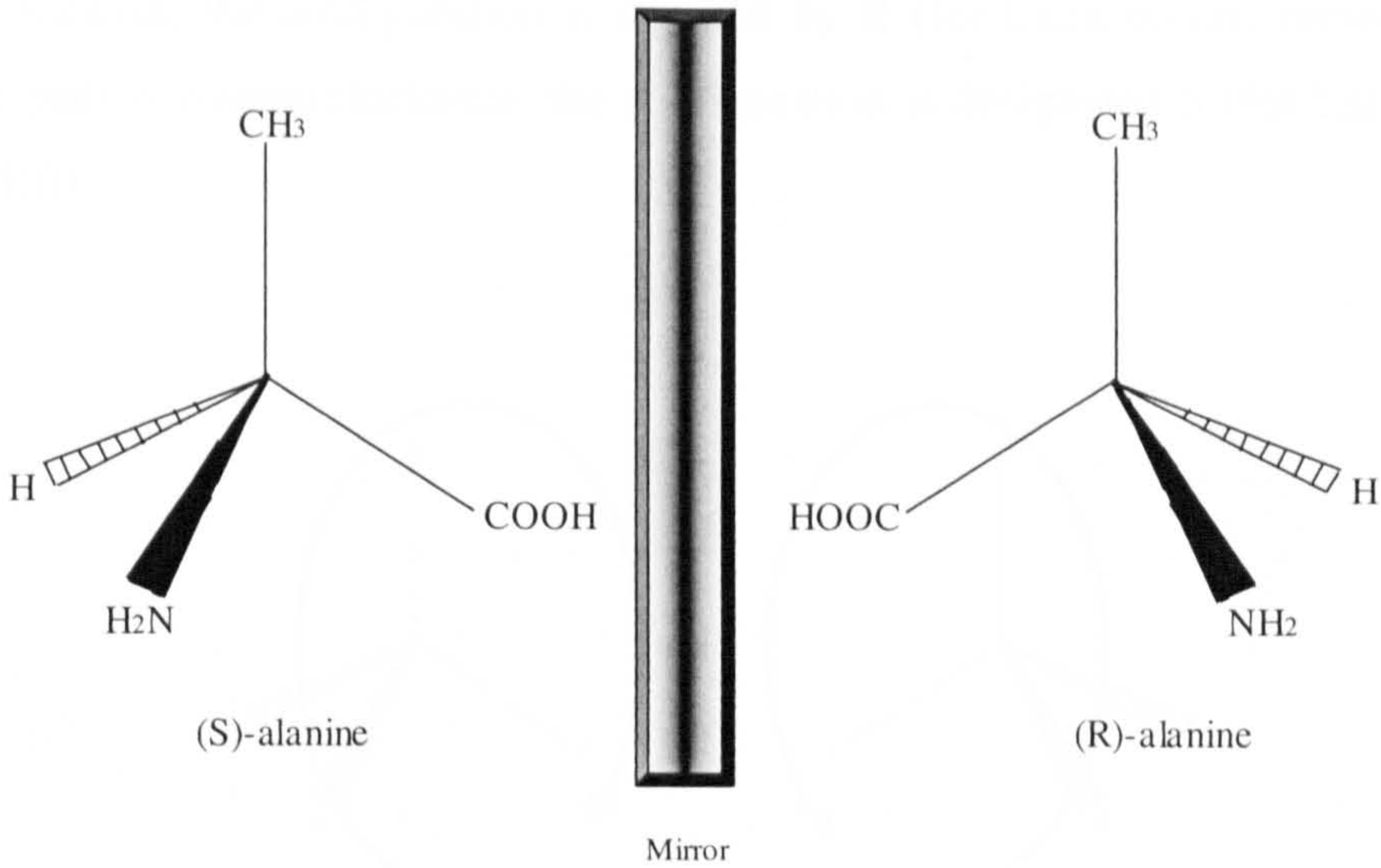

Figure 1.2: (S)- and (R)-alanine enantiomers.

Cahn-Ingold-Prelog convention: At Pasteur's time, it was only possible to distinguish between enantiomers with the sign of optical rotation, that is the dextrorotatory or the laevorotatory forms. However, this method did not allow the deduction of the spatial arrangement of the substituents around a stereogenic centre, which is the definition of ***configuration***. Thus two enantiomers have opposite configurations. An enantiomer can assume various ***conformations*** by rotation of groups around single bonds but a change in configuration requires the breaking of bonds at the stereogenic carbon. For assignment of configuration, the ***Cahn-Ingold-Prelog convention*** is used also known as the sequence rule or the R and S nomenclature [7, 8]. The Cahn-Ingold-Prelog convention is a set of arbitrary but consistent rules which allow a hierarchial assignment of the substituents at any stereogenic centre, Figure 1.3. The four substituents are first ordered according to the ***Sequence Rule***. This rule states that the groups are arranged in decreasing atomic number of the atoms by which they are bound to the stereogenic centre. It is next determined whether the sequence describes a right- or left-handed pattern on the molecular model as viewed according to the ***Conversion Rule*** [9]. When the four groups in the molecule are ordered in the priority a, b, c, d, the conversion rule states that their spatial pattern shall be described as right- or left-handed according to whether the sequence a $\rightarrow$ b $\rightarrow$ c is clockwise or anti-clockwise when viewed from an external point on the side remote from

d (the atom with the lowest priority), as shown in Figure 1.3. The stereogenic centre is viewed with the group of lowest priority (d) pointing away from the observer. When the path is clockwise, the configuration is denoted by R (for Latin rectus, meaning right). When the path is counterclockwise, the configuration is designated S (for Latin sinister, meaning left).

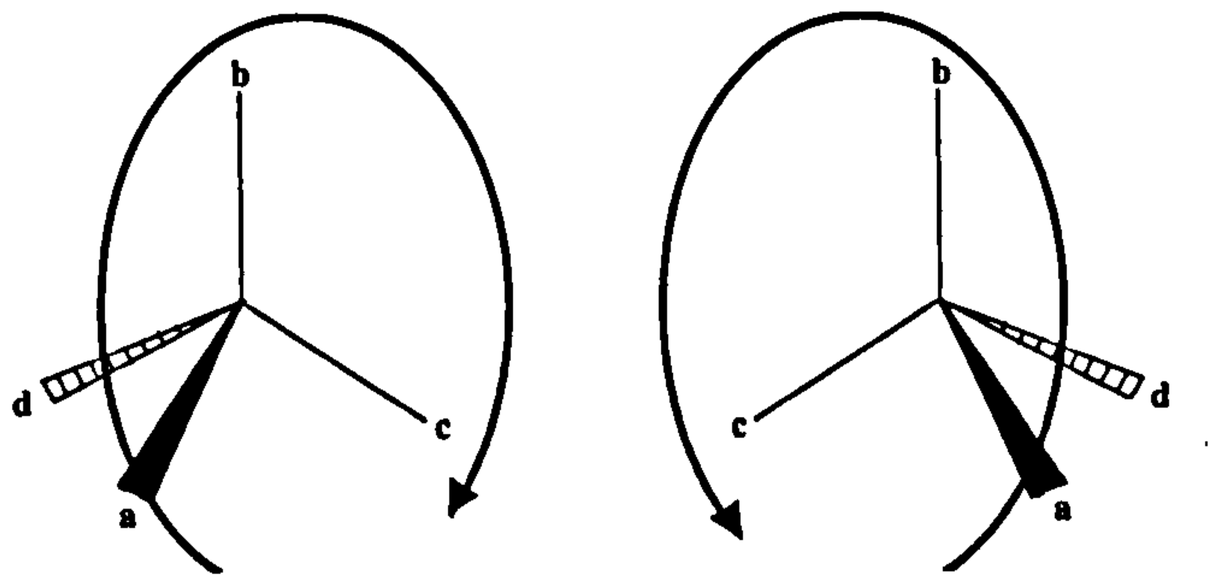

Figure 1.3: The Cahn-Prelog-Ingold convention.

1.2 The importance of chirality

It has been noticed that asymmetry pervaded at the origin of life and seems to be one essential factor of life on Earth. Recently, it has been discovered that an excess of (L)-amino acids is present in the Murchison and Murray meteorites indicating that a preference for (L)-amino acids existed in solar system material before there was life on Earth. This supports an idea, first proposed by Rubenstein [10], for an extraterrestrial origin for homochirality. This homochirality was sent to Earth via molecules which were materials available for the origin of life and which tipped the scales for life to develop with (L)-amino acids and (D)-sugars. On Earth, living bodies are made up of only those amino acids that exist in the left-hand form. The mirror image right-hand amino acids are not used by human or animal cells. Likewise, our cells burn only the right-handed form of sugar, not the left-handed form that can be made in the test tube. All amino acids in proteins are "left-handed", while all sugars in DNA and RNA, and in the metabolic pathways, are "right-handed". Racemic polypeptides could not form the specific shapes required for enzymes, because they would have the side chains sticking out randomly. Also, a wrong-handed amino acid disrupts the stabilizing α-helix in proteins. DNA could not be stabilised in a helix if even a single wrong-handed monomer were present, so it could not form long chains. This means it could not store much information, so it could not support life [11].

As a consequence, the human body reacts differently to opposite enantiomers. The most potent example that can be cited here is the "Thalidomide drama". 3-phthalimidoglutarimide was sold worldwide as the drug thalidomide in 1957 as a racemic mixture form. It was particularly sold to pregnant women to combat morning sickness. However, it was found to be responsible for the birth of 10,000-20,000 babies born with limb malformation and other severe birth defects. The explanation of this drama has been the bad reaction of the body to one of the enantiomers of the molecule, the 3-phthalimidoglutarimide. The (S)- form, presented in Figure 1.4, was found to be responsible for producing the birth defects, while the (R)- form would produce the sedative effect. Thalidomide was thus withdrawn from the market in 1960. Other examples, illustrating the different effect of enantiomers on the human body include (L)-DOPA, which controls Parkinson's Disease whereas the (D)-enantiomer is inactive; (S,S)-Ethambutol, presented in Figure 1.4, is a tuberculostatic drug but the (R,R)-isomer

causes blindness. Today, the differences in biological responses to opposite enantiomers of a molecule have to be catalogued. In 1992, the US Food and Drugs Administration (FDA) and the European Committee for Proprietary Medicinal Products asked the manufacturers of drugs to research the effect of each enantiomer on the human body. Thus, any new drug containing chiral centres must be prepared in a homochiral form if it is to be approved. Asymmetric synthesis is also desirable for environmental reasons. For example, (R,R,S)-Deltamethrin, shown in Figure 1.4, is a potent insecticide whereas the (S,S,R)-isomer is inactive. Thus, administration of the (R,R,S)-isomer rather than the racemic mixture halves the amount that needs to be applied and so minimises environmental pollution.

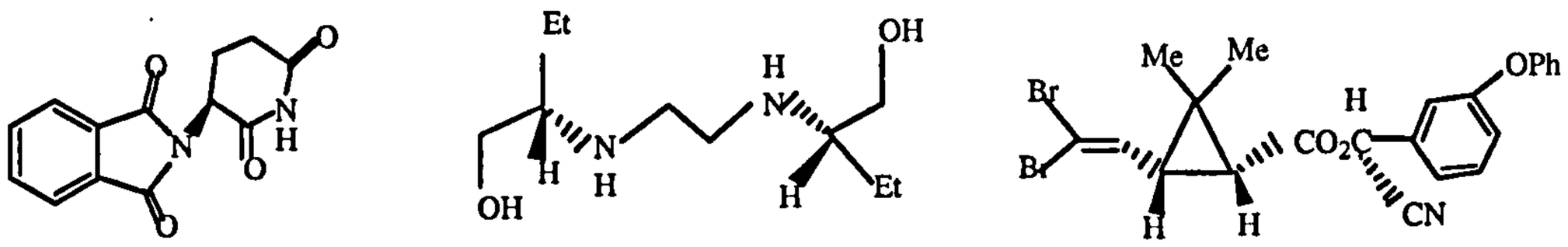

(S)-thalidomide (S,S)-Ethambutol (R,R,S)-Deltamethrin

Figure 1.4: Example of enantiomers whose knowledge of fabrication and effects are crucial.

Research of the manifestation of chirality and its effects involves the efforts of both academics and industrialists, to follow public legislation and public requirements.

1.3 Enantioselective Synthesis

Asymmetric synthesis (i.e. the enantioselective generation of asymmetric centres) is a chemical transformation of a prochiral substrate generating a preference for one enantiomer of the product. The term ***prochiral*** is used for a compound or group that has two enantiotopic atoms, faces, or groups. Atoms or groups in molecules are ***enantiotopic*** when they are related by symmetry elements such as mirror plane, inversion centre or rotation-reflection axis. For example, the two groups c in a grouping Cabcc are enantiotopic. Replacement of one of a pair of enantiotopic groups forms one of a pair of enantiomers. Analogously, if complexation or addition to one of the two faces defined by a double bond or other molecular plane gives rise to a chiral species, the two faces are called enantiotopic. The efficiency of an asymmetric synthesis is measured by optical yield or enantiomeric excess, ee, given by:

$$\% \text{ ee} = \{([R] - [S]) / ([R] + [S])\} \times 100.$$

However, asymmetric synthesis is only possible if the reaction is directed by a neighbouring stereogenic centre [12]. In general, the asymmetric centre can be present in a substrate, a reagent or a catalyst.

1.4 Heterogeneous Enantioselective Catalysis

In this thesis, the chiral centre of interest is the modified catalyst. An enantioselective catalyst must fulfil two functions: firstly, it has to activate the different reactants, and secondly, it has to control the stereochemical outcome of the reaction. Its advantage for asymmetric synthesis is that from grams of a chiral modifier, kilograms or tonnes of a chiral product can be made. Heterogeneous catalysis has some advantages over homogeneous catalysis; these advantages are the easier way of separation, handling, stability, recovery and re-use. Besides, some interesting reactions are efficiently catalysed by chiral heterogeneous catalysts. Finally, from theoretical and conceptual points of view, enantioselective catalysis with chiral solids is a challenging area of chemistry. Indeed, compared to soluble catalysts, there is an additional structural dimension involved. However, it must be kept in mind that heterogeneous catalytic chiral systems are rare because the stereo-differentiating mechanisms involved in these reactions are not fully understood. At this time, there are less than ten well-established reaction systems, because of the lack of fundamental information about the stereo-differentiating procedure. But, because of the advantages of heterogeneous catalysis, many research groups are looking for new types of chiral heterogeneous systems. Since the mode of action of the existing ones is not well understood, this search is done either on an intuitive trial and error basis or with simple hypotheses. Efficient metallic catalysts modified with an optically active additive have been discovered and developed. A survey of these studies was published in review articles [13-15]. Excellent enantiomeric excesses have been achieved for example in the hydrogenation of α-keto-esters in the presence of a platinum catalyst modified by cinchona alkaloids, and in the hydrogenation of prochiral ketones such as β-keto-esters and β-functionalised ketones with nickel catalysts modified with tartaric acid, as shown in Figure 1.5 [13, 22, 23].

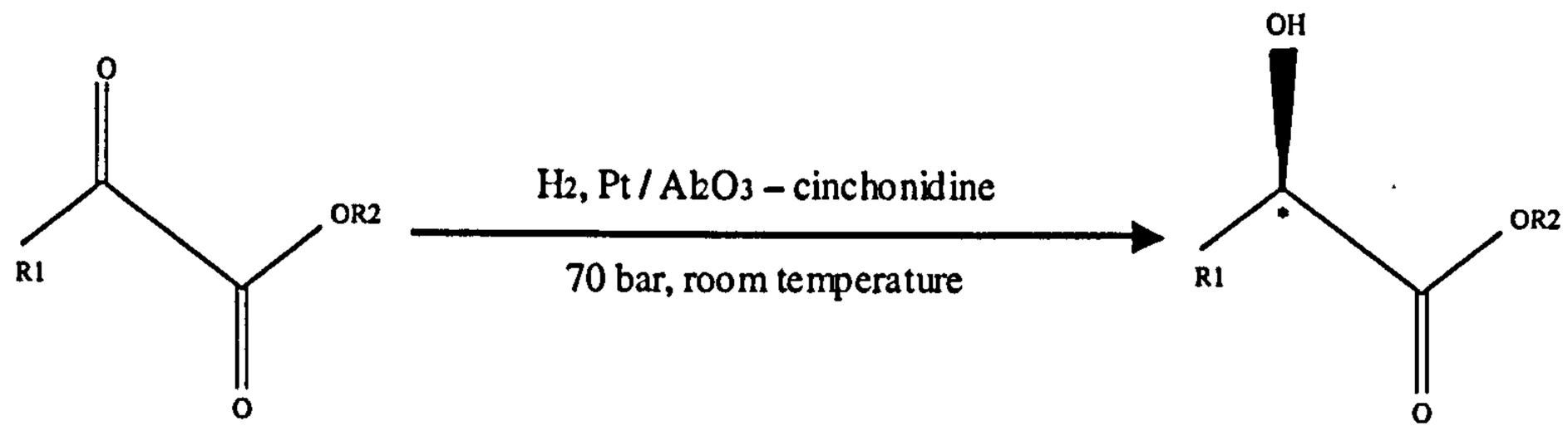

Figure 1.5: Examples of successful enantioselective reactions using metallic catalysts modified with an optically active additive.

In these optically modified catalytic systems, the metal catalyst / chiral modifier / reactant interaction is specific to the reaction in order to obtain high enantioselectivities. Although several detailed mechanisms have been proposed for these hydrogenations [16-21], this metal catalyst / chiral modifier / reactant interaction is still not fully understood.

1.5 Hydrogenation of Methyl-acetoacetate (MAA) into Methyl-3-hydroxybutyrate (MHB)

The heterogeneous enantioselective catalytic system which is the object of this thesis involves an asymmetric addition of hydrogen to methyl-acetoacetate to generate methyl-3-hydroxybutyrate (MHB). The (R)-(-)- form of MHB is of particular interest as it is an important intermediate in the synthesis of a carbonic anhydrase inhibitor used in the treatment of glaucoma [24]. Conventional nickel catalysts possess no inherent chirality and the bare nickel metal generates a racemic product [25-26], as presented in Figure 1.6.

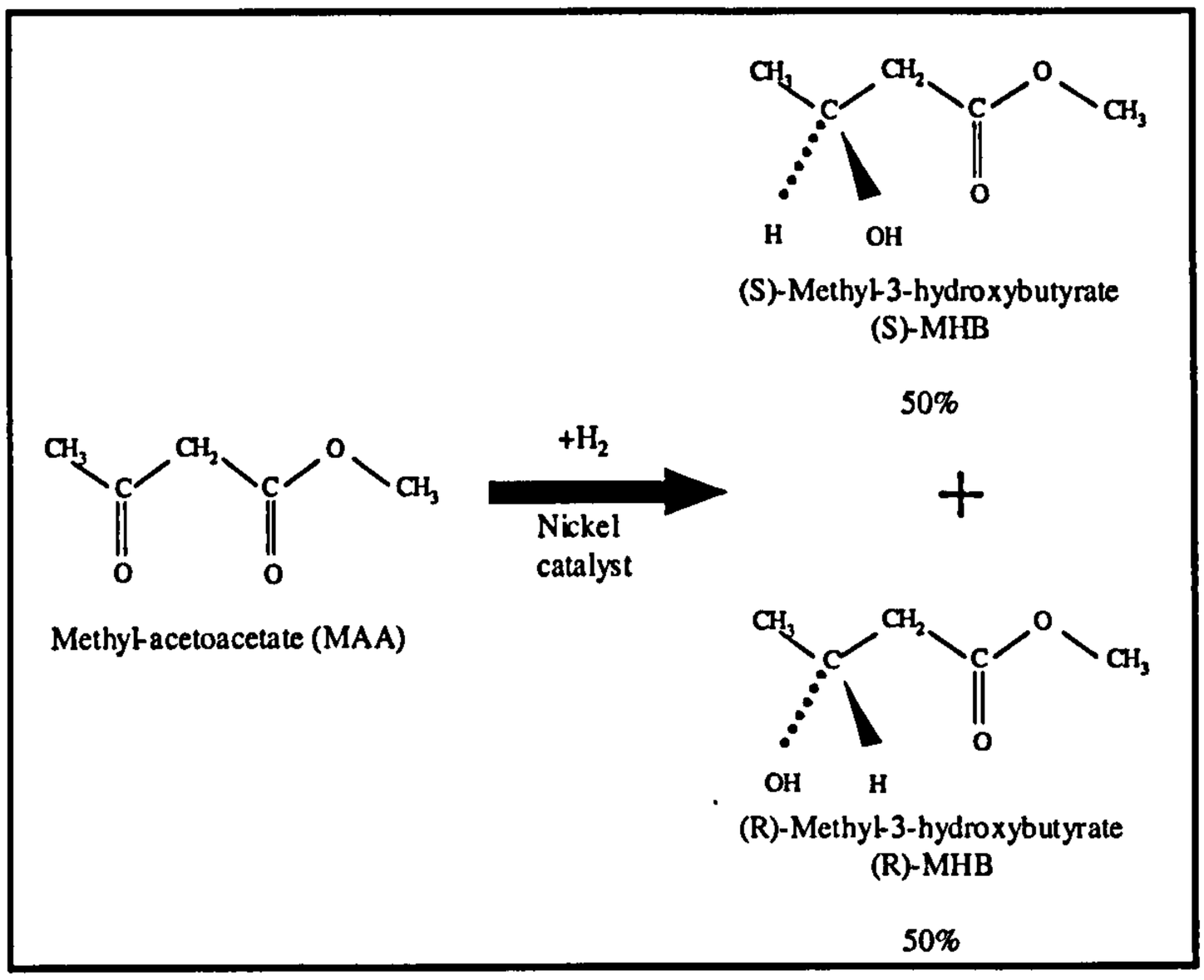

Figure 1.6: The hydrogenation of MAA into MHB, leading to the production of a racemic mixture.

A chiral environment is achieved by treating the activated catalysts with an optically pure reagent or catalyst modifier [25-30]. Such a modification has been shown not only to induce enantioselectivity but also to increase the overall reaction rate [28-29]. The enantioselective hydrogenation of β-keto esters over nickel catalysts modified with the optically pure isomer of an α-amino or α-hydroxy acid is well established and has been the subject of a comprehensive review by Izumi [22]. Such modifications are highly

specific in that the nickel catalyst is selective for the asymmetric hydrogenation of β-keto derivatives rather than α-keto compounds and the direction of the enantioselectivity is dependent upon the modifier. Thus, (R)-hydroxy or (S)-amino acids yield excess of (R)-product, whereas (S)-hydroxy and (R)-amino acid modifiers yield (S)-products [15, 22, 31, 32, 33]. As has been shown before, tartaric acid as a modifier gives great optical yield; this modified catalyst produces the synthesis of just one enantiomer with an e.e of ~95%. But the interest in this thesis concentrates on the amino acid alanine as a modifier. Figure 1.7 shows this taking alanine as the catalyst modifier.

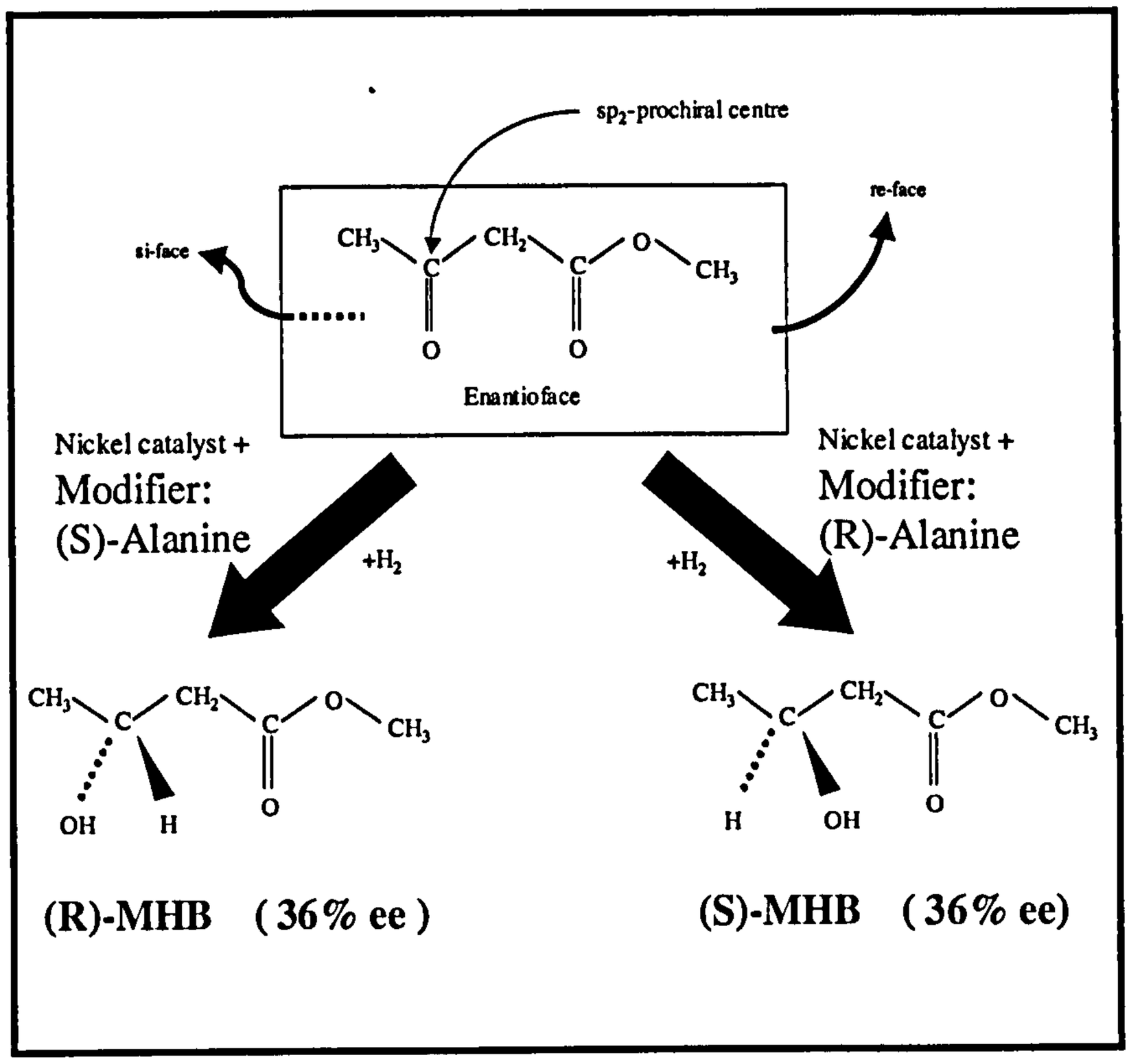

Figure 1.7: The hydrogenation of MAA into (R)-/ or (S)-MHB, depending on the chirality of the modifier added, (R)- or (S)-alanine.

The enantioselective hydrogenation of MAA into MHB using alanine, α-amino acid, as a chiral modifier has given an optical yield of 36 % [27, 33]. It has been demonstrated that it can even help to achieve better enantioselectivities, under certain conditions, for the hydrogenation of methyl acetoacetate than those modified using the same process, with tartaric acid [27]. Alanine has even been found to be responsible for the increase of the rate of hydrogenation of MAA into MHB [27].

In the study of these enantio-differentiating hydrogenations, one of the major difficulties encountered by number of workers [32, 34-38], has been to obtain some reproducible reaction rates and enantiomeric excesses. In spite of this, however, there is a general agreement that the enantioselectivity is strongly dependent on the method of catalyst preparation and on the nature of the modification procedure employed. In a number of investigations, the effects of varying a range of modification conditions on enantioselectivity have been considered, for example, the influence of the modification times [31, 39, 40], temperature [22, 32, 39-41], pH [22, 31, 37, 39, 41-45], modifier concentration [46, 47] and the introduction of a co-modifier [22, 34, 35, 46, 48, 49]. However, despite the vast body of information which has been accumulated, there still remains little or no consensus of opinion regarding the actual source of the enantio-differentiation and the nature of the enantioselective hydrogenation sites. A number of models have been proposed to date [22]. At an early stage, Groenewegen and Sachtler have proposed a model to illustrate the stereochemistry of the hydrogenation process using α-amino acid and α-hydroxy acid modified Raney nickel (MRNi) [50] as shown in Figure 1.8.

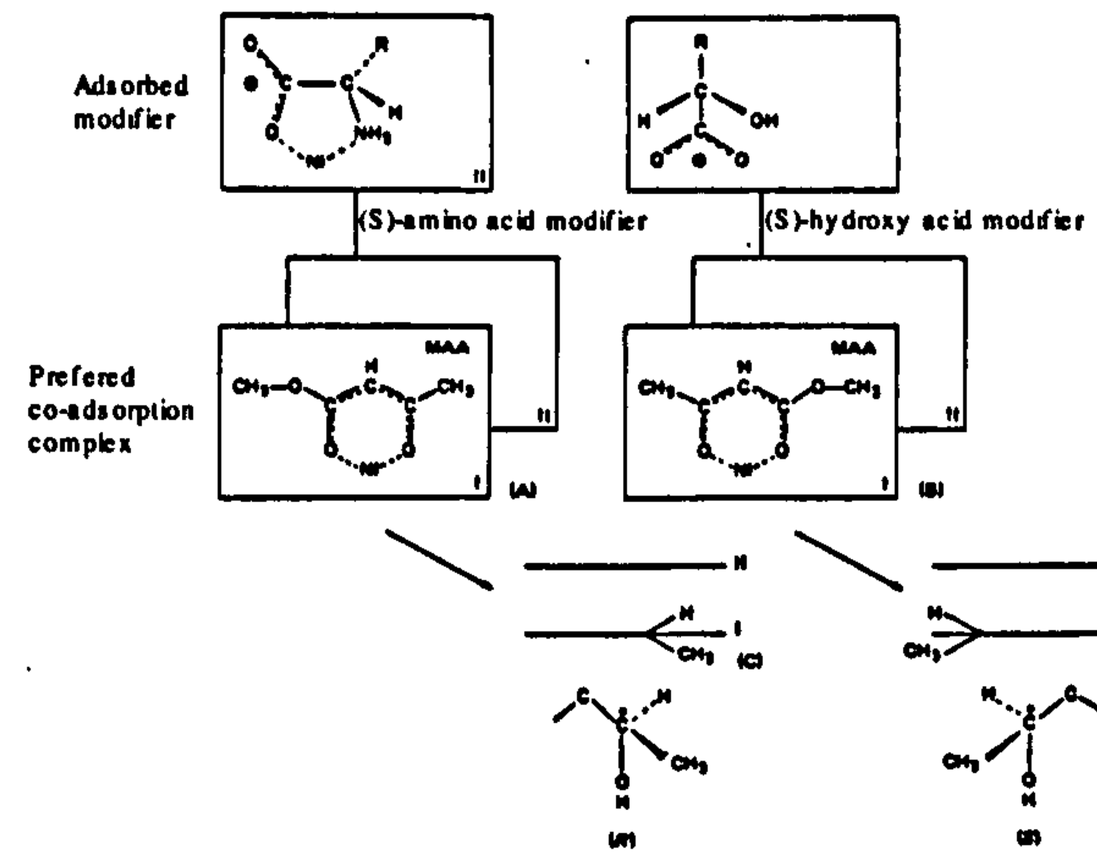

Figure 1.8 :Schematic representation of enantio-differentiating hydrogenation of MAA with α-amino acid-MRNi and α-hydroxy acid-MRNi, respectively [50].

In this model, the modifying reagent and MAA are adsorbed onto two adjacent nickel atoms arranged perpendicularly to the nickel surface. However, this model did not accord with the results of further investigations [15]. In 1983, Izumi and co-workers proposed the model shown in figure 1.9 [22]. For them, differentiation is the factor which rules the prior step of the reaction.

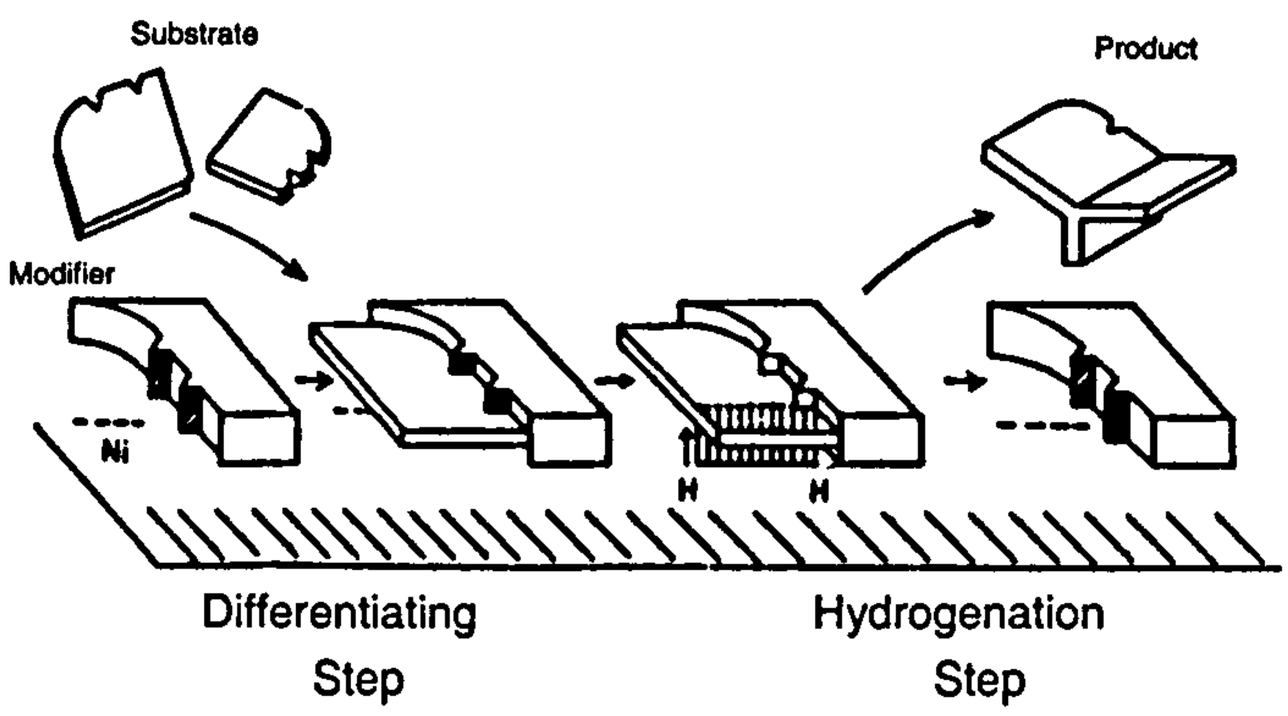

Figure 1.9: Schematic illustration representing the enantio-differentiating steps taking place during the enantioselective hydrogenation suggested by Izumi [22].

Some new studies whose aim is to mimic the chiral catalyst and to reveal its interaction with metal surfaces and MAA have been performed recently. These studies involve the adsorption of chiral modifiers, tartaric acid and alanine, on single metal crystals.

The study of the adsorption of two enantiomers of tartaric acid [54], the (R, R)- and the (S, S)- forms on Cu (110) resulted in the creation of several surface phases. These phases are created depending on the amount of tartaric acid deposited on the crystal, on the temperature of the crystal and the on holding time of the temperature of the sample [51].

The phases, which have been created by the adsorption of (R, R)-tartaric acid on Cu (110), are presented in Figure 1.10.

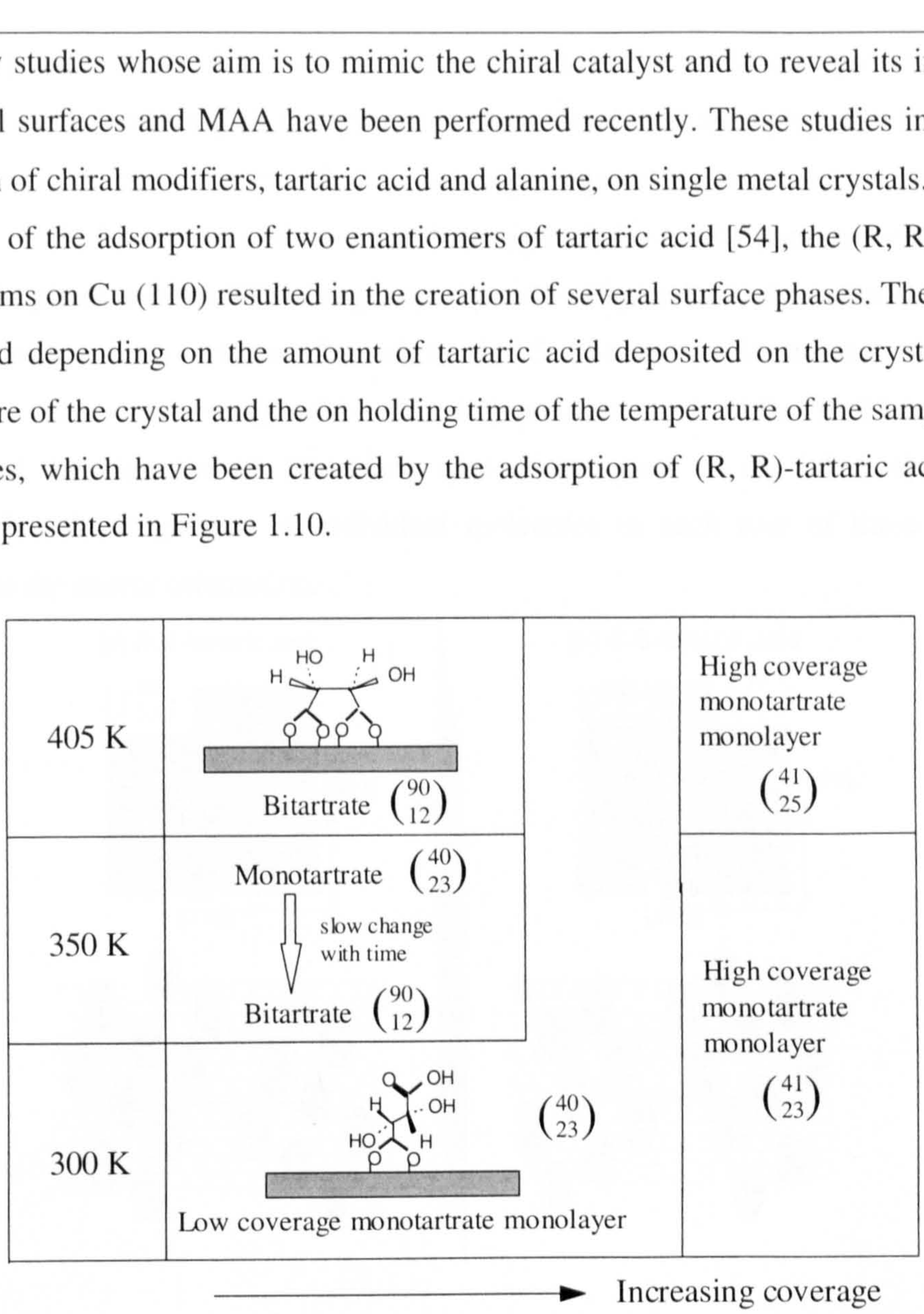

Figure 1.10: Adsorption phase diagram for (R, R)-tartaric acid on Cu (110), reproduced from [52].

An important element in this phase diagram is that each of these phases are highly ordered since they can present some very precise and very clear LEED patterns. The phases (4 0, 2 3) and (9 0 1 2) are thought to be important for the enantioselective reaction. Indeed, some STM images of the (9 0, 1 2) phase confirm the presence of long-range order, with a unit cell containing three molecules. They reveal that the bitartrate molecules are self-assembled in rows of three, each row stacking in parallel with others to form long chains, as can be seen in Figure 1.11. These long chains are aligned along the [1 –1 4] surface direction, which does not coincide with any of the symmetry

directions present on the Cu (110) surface. As a result, this molecular growth direction has the effect of destroying all the symmetry elements of the underlying metal, leading to the creation of a chiral surface that is non-superimposable on its mirror image. The behaviour of (S, S)-tartaric acid was also investigated; the LEED pattern for this (S, S)-tartaric acid phase and the STM images, presented in Figure 1.11, show that the chirality of the surface has been switched. Indeed, for the (S, S)-tartaric acid, the structure (9 0, -1 2), which is a true mirror image of the (9 0, 1 2) structure obtained for (R, R)-tartaric acid is observed. Besides, the (S, S)-tartaric acid chains grow in the [-1 1 4] direction, meaning that the alignment of individual molecules in each row of three has been switched to the mirror orientation.

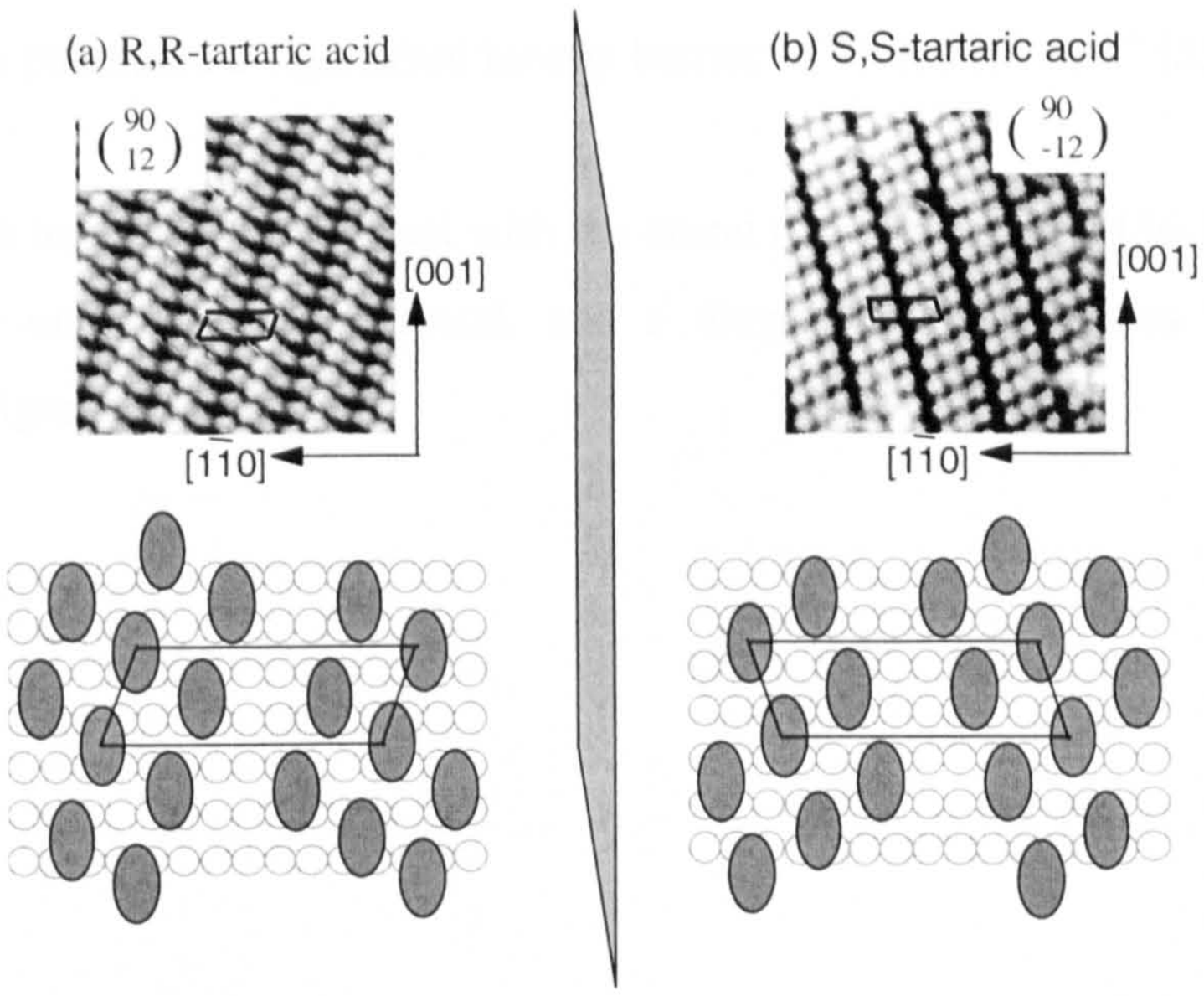

Figure 1.11: STM images showing mirror chiral surfaces created by (R, R)- and (S, S)-tartaric acid adsorbed on Cu (110). Shown are 108 Å × 108 Å STM images of the (9 0, 1 2) (R, R)-tartaric acid bitartrate phase and the (9 0, -1 2) (S, S)-tartaric acid bitartrate phase. Below each STM image is a schematic diagram displaying the position of the molecular features observed relative to the Cu (110) surface [53].

It is interesting to note that MAA has been shown to co-adsorb on the (4 0, 2 3) phase of (R, R)-tartaric acid. The (4 0, 2 3) phase then recombines into the (9 0, 1 2) incorporating the MAA molecules if the temperature of the Cu (110) crystal is increased up to 350 K [54]. It has even been shown that there is an interaction between the tartaric acid and the MAA molecules. The recombination of the (4 0, 2 3) phase into the (9 0, 1 2) phase can be explained by the fact that this last phase, which has been shown to be chiral, is the thermodynamically preferred phase. The conversion is associated with a local chemical transformation from the monotartrate to the bitartrate form, accompanied by a change in the two-dimensional organisation of the adsorbed modifier molecules which involves significant molecular mass transport and expansion in adsorption area. The transformation possesses a significant kinetic barrier of 73 ± 2 kJ. mol^{-1} [55].

Similar studies have been performed with the chiral modifier alanine [56-57]. (S)-alanine was adsorbed on a Cu (110) crystal, and a diagram of phases has been obtained, presented in Figure 1.12.

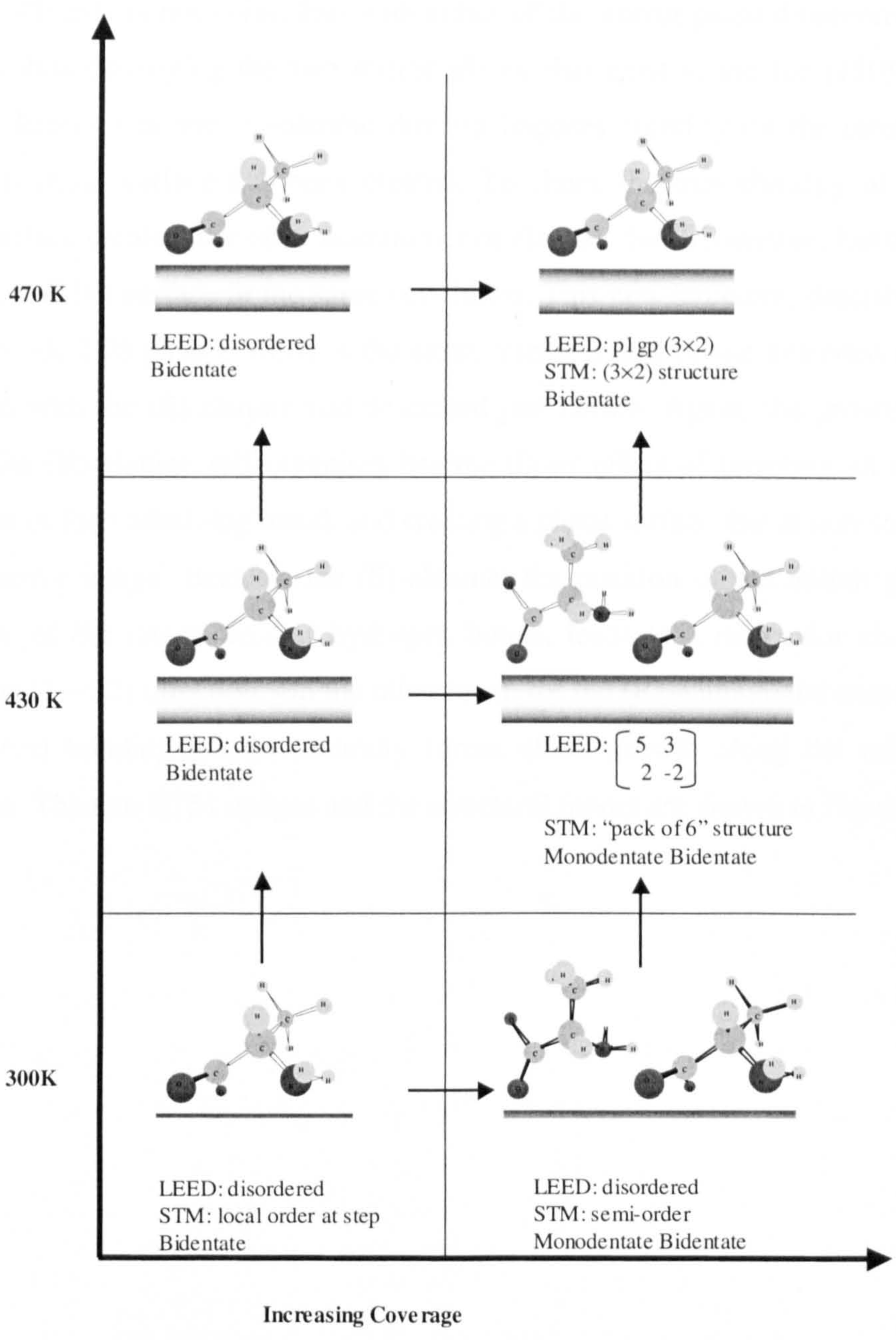

Figure 1.12: Adsorption diagram for (S)-alanine on Cu (110), reproduced from ref [56].

The most interesting phase is the (5 3, 2 -2) structure, since the STM images reveal that the two-dimensional order of the (S)-alanine extends over long distances (> 400 Å) across the surface. The (S)-alanine molecules seem to be arranged in regular groups of six or eight, which are aligned at a definite angle along the surface. Most interestingly, this growth axis is not coincident with either of the mirror plane directions of the metal surface, thus destroying the two mirror planes that exist at the fcc (110) surface. The growth direction of the (S)-alanine directly imposes chirality on the metal surface; an extended chiral surface has been created. To check the true chirality of the extended chiral surface created, the other enantiomer of alanine, the (R)-alanine, has been adsorbed on the Cu (110) surface in the same conditions. This new structure, described by LEED, is the (5 –3, 2 2) phase, which is the exact mirror image of the extended chiral surface obtained with the (S)-alanine and described just before. Again, the growth direction in which the (R)-alanine self-organises has the direct effect of breaking all the symmetry elements of the underlying metal, and creating a chiral surface that is non-superimposable to its mirror image. Besides, for (S)-alanine, the position of the amino group and the direction of the intermolecular hydrogen bonds, leads to a molecular chain alignment along the [1 –1 2] direction. On the other hand, for the (R)-alanine, the mirror positioning of the two bonding groups naturally forces chain growth along the mirror [-1 1 2] direction. The two STM images and the structural model are shown in Figure 1.13.

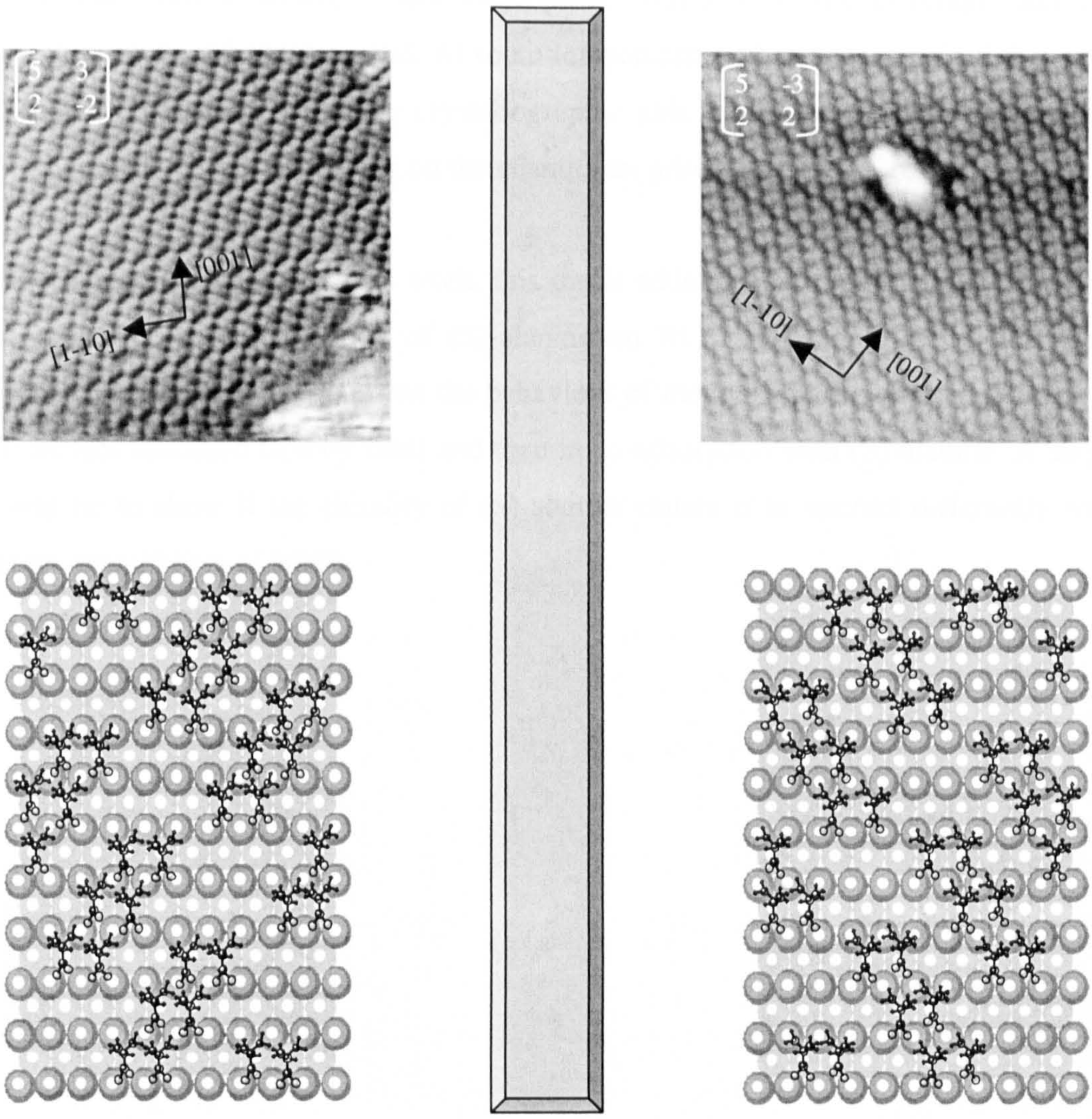

Figure 1.13: STM images showing mirror chiral surfaces created by (S)- and (R)-alanine adsorbed on Cu (110). Shown are 150 Å × 150 Å STM images of the (5 3, 2 -2) (S)-alanine and the (5 -3, 2 2) (R)-alanine, as well as their reciprocal model [56].

These (5 3, 2 –2) and (5 –3, 2 2) structures are also interesting because they present some channels which are opposite enantiomeric docking sites for incoming reactant molecules. It has even been noticed that the MAA molecules could adsorb onto these channels [58] under precise experimental conditions. A low coverage of (S)-alanine and some MAA molecules should be co-adsorbed on the Cu (110) surface. Once the mixture has been warmed up, the (S)-alanine molecules have been seen to re-organise themselves into pack of six molecules incorporating the MAA molecules into the channels [56].

Tartaric acid has also been studied on Ni (110) [58]. Again, a complex adsorption phases diagram has been obtained, where each phase varies with the coverage and the temperature of the Ni (110) crystal. At room temperature, it has been reported that each enantiomer aligns along the same crystallographic axis. However, at high temperature, the surface reconstructs depending on the enantiomer adsorbed.

As a continuation of the previous work, this thesis addresses two main points. The first point is to study the adsorption of (S)-alanine on Ni (110), and to reveal its phase diagram. The second point concerns the behaviour of methyl-3-hydroxybutyrate on a Cu (110) surface adsorbed first by itself and then in co-adsorption with (S)-alanine. A major aim will be to show if the chirality of (S)-alanine causes it to interact differently with different enantiomers of MHB.

1.6 Catalysis and Surface Science

As shown in the previous sections, little is known about the catalytic systems and their mechanisms. In recent years however, it has been shown that surface science techniques could answer some of the questions. These questions are about the structures of a catalytic surface, the adsorption of molecules on surfaces, their bonding and their orientation with respect to the surface or their organisation on the surface. Surface science techniques could answer these questions. In general, surface science uses single crystal surfaces. This limits the type of adsorption site available and makes the experiments easier to interpret. In order to keep these single crystal surfaces clean, the work is carried out under ultrahigh vacuum (UHV) conditions. Since no single technique can provide a complete description of a surface or adsorbate layer, a combination of several techniques is used. The combination Reflection Absorption Infra-Red Spectroscopy (RAIRS) - Low Energy Electron Diffraction (LEED) - Scanning Tunnelling Microscopy (STM) is used in this thesis. RAIRS provides information on the identity and conformation of the adsorbate as well as the nature of the surface-adsorbate bond and bonding site. A LEED pattern shows the basic two-dimensional periodicity of the ordered component of the surface structure. The STM provides the location of adsorbates on surfaces giving a contour map of single crystal surfaces at or close to atomic resolution and helps clarify the structure determinations made using LEED. Most surface science techniques require UHV conditions. Indeed, many characterisation techniques utilise electrons or particles which have a small mean free path, and therefore are sensitive to the outer layer of the sample.

Although surface studies have been able to contribute in a number of ways to the understanding of mechanism in heterogeneous catalysis [39], it must be born in mind that these studies are carried out under special conditions and they are only a model approach to what happens *in situ* .

References

[1] F. Arago, Mem. Classe Sci. Math. Phys. Inst. Imper. France **12 I,** 93 (1812).

[2] J.B. Biot, Ann. Chim. Physique **4,** 90 (1817); Mem. Acad. Roy. Sci. Inst. France **2,** 41 (1819).

[3] L. Pasteur, Ann. Chim. Physique **24,** 442 (1848); **28,** 56 (1850); C.R. hebd. Seances Acad. Sci. **28,** 477 (1849); **29,** 297 (1849).

[4] J. A. Le Bel, Bull. Soc. Chim. France **22,** 337 (1874).

[5] J. H. van't Hoff, Bull. Soc. Chim. France **23,** 295 (1875).

[6] R. A. Sheldon, Chirotechnology. Industial synthesis of optically active compounds, p. 6 (Marcel Dekker, New York, 1993).

[7] R. S. Cahn, C. K. Ingold, V. Prelog, Experimentia, **12,** 81 (1956).

[8] R. S. Cahn, C. K. Ingold and V. Prelog, Angew. Chem. Int. Ed. Engl. **5,** 385 (1966).

[9] R. A. Sheldon, Chirotechnology. Industrial synthesis of optically active compounds, p. 13 (Marcel Dekker, New York, 1993).

[10] Rubenstein, Nature, **306,** 118(1983).

[11] Thiemann, W., ed., 1973. International Symposium on Generation and Amplification of Asymmetry in Chemical Systems, Julich, Germany, p32-33, 1973; cited in: Wilder-Smith, A.E., 1981. The Natural Sciences Know Nothing of Evolution, Master Books, CA.

[12] R.A. Sheldon, Chirotechnology. Industrial synthesis of optically active compounds, p.73 (Marcel Dekker, New York, 1993).

[13] H.U. Blaser, Tetrahedron: Asymmetry **2,** 843 (1991).

[14] H.-U. Blaser, H.-P. Jalett, M. Muller, M. Studer, Catal. Today **37,** 441 (1997).

[15] A. Tai and T. Harada, Taylored Metal Catalysts, p.265 (Y. Iwasawa, Reidel, Dordrecht, 1986).

[16] B. Minder, T. Mallat, A. Baiker, G. Wang, T. Heinz, A. Pfaltz, J. Catal. **154,** 371 (1995).

[17] P. Johnston, P.B. Wells, J. Catal. **156,** 180 (1995).

[18] J.L. Margitfalvi, M. Hegedus, E. Tfirst, Tetrahedron: Asymmetry **7,** 571 (1996).

[19] R.L. Augustine, S.K. Tanielyan, J. Mol. Catal. **112,** 93 (1996).

[20] Y. Sun, J. Wang, C. LeBlond, R.N. Landau, D.G. Blackmond, J. Catal. **161**, 752 (1996).

[21] A. Baiker, J. Mol. Catal. **115**, 473 (1997).

[22] Y. Izumi, Adv. Catal. **32**, 215 (1983).

[23] H. U. Blaser, M. Muller, Stud. Surf. Sci. Catal. **59**, 73 (1991).

[24] R. A. Holt and S. R. Rigby, Proceedings of the Chiral Europe '95 Symposium, Spring Innovations Ltd., London, 1995, p. 13.

[25] A. Bennett, S. Christie, M.A. Keane, R.D. Peacock, G. Webb, Catal. Today **10**, 1619 (1991).

[26] M. A. Keane, G. Webb, J. Catal. **136,** 1 (1992).

[27] M. A. Keane, G. Webb, J. Mol. Catal. **73,** 91 (1992).

[28] M. A. Keane, Can. J. Chem. **72,** 372 (1994).

[29] M. A. Keane, G. Webb, Langmuir **10,** 4560 (1994).

[30] M. A. Keane, Catal. Lett. **19,** 197 (1993).

[31] M.J. Fish, D.F.Ollis, J. Catal. **50**, 353 (1977).

[32] A. Hoek, W.M.H. Sachtler, J. Catal. **58**, 276 (1979).

[33] M. A. Keane, Langmuir **10,** 4560 (1994).

[34] L. J. Bostelaar, W. M. H. Sachtler, J. Mol. Catal. **27,** 387 (1984).

[35] A. Hoek, H.M. Woerde, W.M.H. Sachtler, Proc. 7th. Cong. Catal., Tokyo, p.376 (1980).

[36] G.V. Smith, M. Musoiu, J. Catal. **60**, 184 (1979).

[37] G. Wittmann, G.B. Bartok, M. Bartok, G.V. Smith, J. Molec. Catal. **60**, 1 (1990).

[38] T. Harada, K. Haraki, Y. Izumi, J. muraka, H. Ozaki, A. Tai, Proc. 6th Int. Congr. Catal. London, p 1024, (1976).

[39] L. Fu, H.H. Kung, W.M.H. Sachtler, J. Molec. Catal. **42**, 29 (1987).

[40] S. Tatsumi, Bull. Chem. Soc. Jpn. **41**, 408 (1968).

[41] Y. Izumi, M. Imaida, H. Fukawa, S. Akabori, Bull. Chem. Soc. Jpn. **36**, 155 (1963).

[42] T. Harada, M. Yamamoto, S. Onaka, M. Imaida, H. Ozaki, A. Tai, Y. Izumi, Bull.Chem. Soc. Jpn. **54,** 2323 (1981).

[43] E. I. Klabunovskii, Russ. J. Phys. Chem. **47,** 765 (1973).

[44] A. A. Vedenyapin, E. I. Klabunovskii, Telanov, M. Yu, N. P. Sokolova, Kinet. Catal. **16,** 436 (1975).

[45] E. I. Klabunovskii, A.A. Vedenyapin, B.G. Chankvetadze, G.C. Areshidze, Proc. 8th Int. Congr. Catal., Berlin, p. 543 (1984).

[46] D.R. Richards, H.H. Kung, W.M.H. Sachtler, J. Molec. Catal. **36**, 329 (1986).

[47] S. Tatsumi, Bull. Chem. Soc. Jpn. **41**, 408 (1968).

[48] T. Harada, A. Tai, M. Yamamoto, H. Ozaki, Y. Izumi, Proc. 7th. Cong. Catal., Tokyo, p.364 (1980).

[49] T. Harada, Y. Izumi, Chem Lett. 1195 (1978).

[50] J.A. Groenewegen, W.M.H. Sachtler: J. Catal. **38**, 501 (1975).

[51] M. Ortega Lorenzo, S. Haq, T. Bertrams, P. Murray, R. Raval, C. J. Baddeley, J. Phys. Chem. B **103,** 10661 (1999).

[52] R. Raval, Cattech. **5,** 12 (2001).

[53] M. Ortega Lorenzo, C. J. Baddeley, C. Muryn, R. Raval, Nature **404,** 376 (2000).

[54] M. Ortega-Lorenzo, PhD Thesis, Complexities and dynamics of the enantioselective site in heterogeneous catalysis : tartaric acid and methylacetoacetate on Cu(110) (Liverpool University, 1999).

[55] M. Ortega Lorenzo, V. Humblot, P. Murray, C. J. Baddeley, S. Haq, R. Raval J. Catal. **205,** 123 (2002).

[56] S. Louafi, PhD Thesis, Creating model enantio-differentiating surfaces: alanine enantiomers and methylacetoacetate adsorptions studies on Cu(110) (Liverpool University, 2001).

[57] J .Williams, PhD Thesis, Adsorption and characterisation of chiral amino acids on Cu (110) single crystal surfaces, (Liverpool University, 1988).

[58] V. Humblot, PhD Thesis, Complexities and dynamics of the enantioselective site in heterogeneous catalysis: tartaric acid on Ni (110) (Liverpool University, 2002).

Chapter Two

Theory and Experimental Details

2.1 Reflection Absorption Infra Red Spectroscopy (RAIRS)

Vibrational spectroscopy is one of the oldest and most powerful analytical techniques to study the chemical structure of molecules in virtually any physical state. It has developed into one of the most powerful surface science techniques used to study the adsorption of molecules on metal surfaces.

Reflection Absorption Infrared Spectroscopy (RAIRS), Electron Energy Loss Spectroscopy (EELS) and Surface Enhanced Raman Spectroscopy (SERS) are the three useful techniques. SERS and EELS have the advantage of having a wide spectral range beginning at 5000 cm^{-1} and reaching 100 cm^{-1} in the case of EELS and 10 cm^{-1} for SERS. EELS has a high sensitivity but has the disadvantage of having a relatively poor resolution (20-40 cm^{-1}). There have been improvements in the resolution capabilities of EELS within recent years [1, 2] with the advancement in High Resolution Electron Energy Loss Spectroscopy (HREELS) but nevertheless the resolution has only increased to 8 cm^{-1}. RAIRS has the advantage of having high resolution (< 1cm^{-1}) but the disadvantage of a limited spectral range which is generally 4000-800 cm^{-1} although. However, the use of high intensity sources such as synchrotron radiation and sensitive detectors such as liquid helium cooled bolometers have extended the spectral range into the far-IR region of 200 cm^{-1} [3, 4].

The development of the RAIRS technique has been discussed by several authors [5-9]. The first studies of CO on supported Ni, Pd and Pt had been done using transmission infrared [10-11] but subsequent studies required the use of defined single crystal surfaces. This meant that the experiment had to be done using a reflection mode. The first experiments by RAIRS were done using multiple reflections mode in 1959 by Pickering and Eckstrom [12] and Francis and Ellison [13]. Greenler [14-16] considered the possibility of carrying out these experiments using single reflection. He showed that the

RAIRS experiment is most efficient when performed in single reflection mode rather than multi reflection mode. This is due to the balance of the loss of intensity during reflection at grazing incidence and the increased absorption by the extra molecules available with each additional reflection [14]. The work done by Pritchard and Sims [17] on the study of CO on copper confirmed this.

2.1.1 Presentation of the RAIRS set-up

One possible set-up of RAIRS is presented in Figure 2.1.

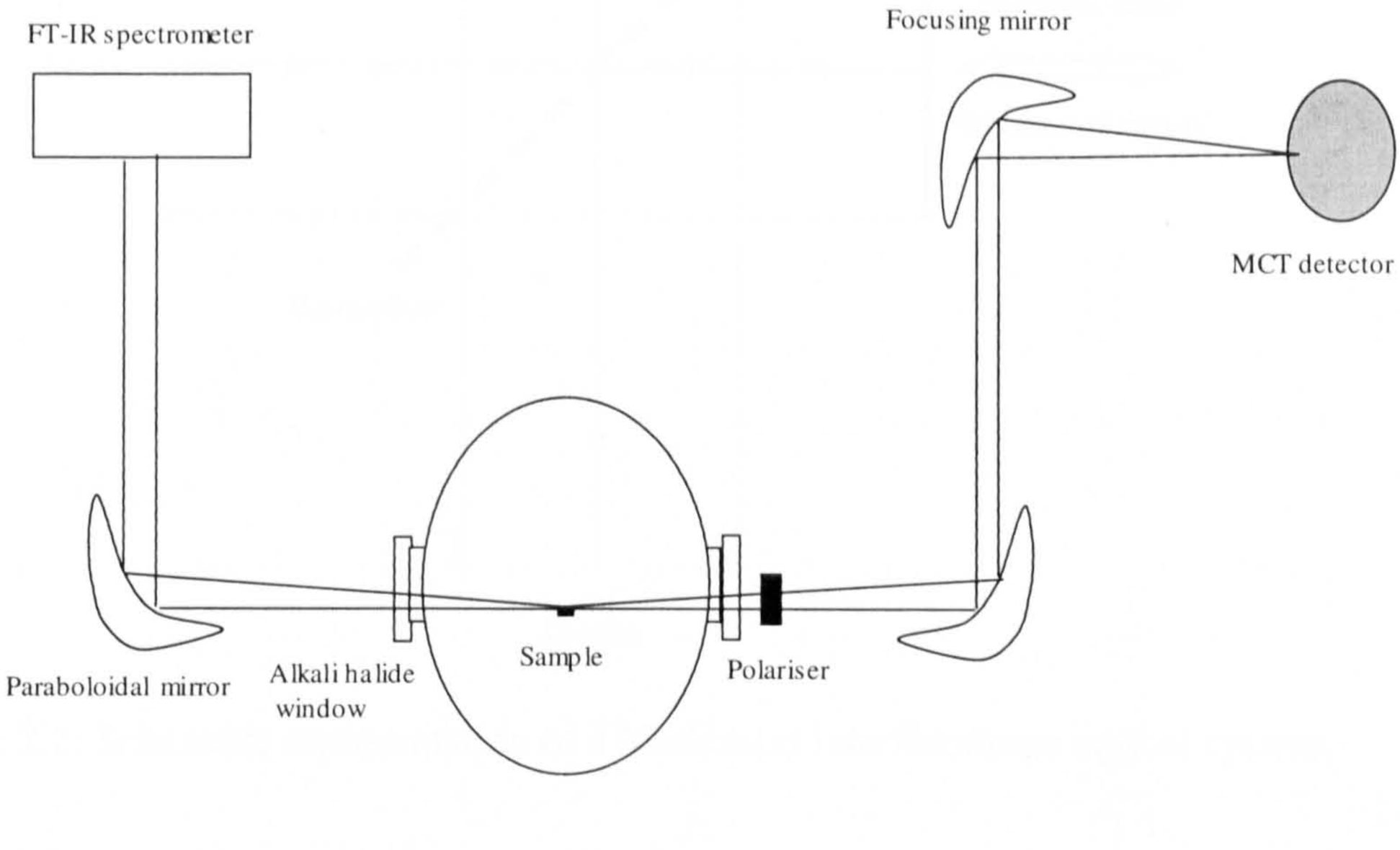

Figure 2.1: Possible set-up of the RAIRS (adapted from reference 18).

In a RAIRS set-up, the infrared radiation is focused through an IR-transparent window (a KBr window) on to the sample surface. As will be explained later in this section, the IR beam must come to the sample surface at grazing incidence. It is then reflected off the sample back outside the chamber and recollimated on to a photoconductive semiconductor detector such as mercury cadminum telluride (MCT).

The theory of FTIR spectrometry has been discussed by several authors [19-21] and is based on the mathematical treatment of the physical phenomenon of interferometry and the use of Fourier transformation to obtain spectral information. FTIR spectrometers utilises the Michelson interferometer [22] shown in Figure 2.2.

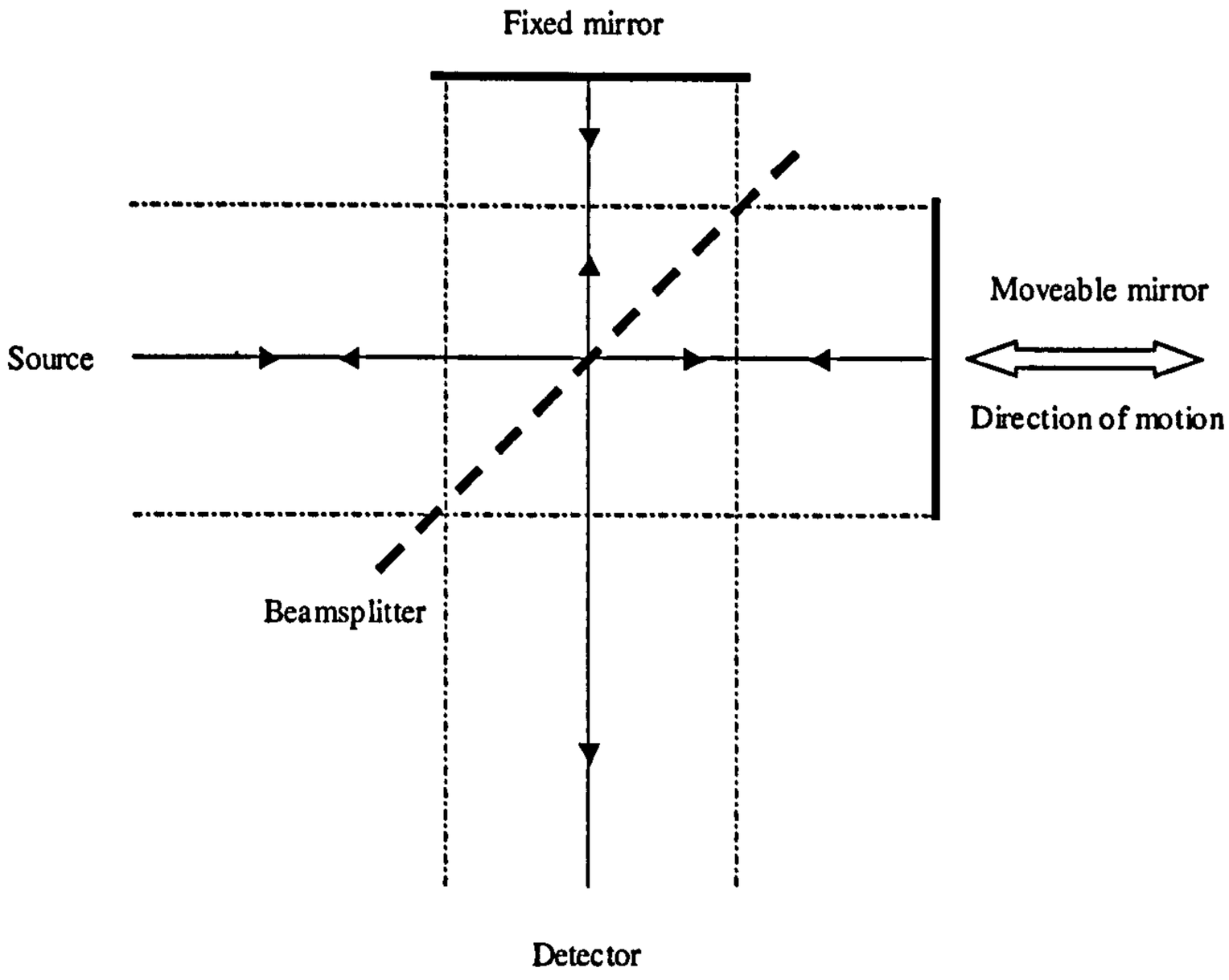

Figure 2.2: Schematic representation of a Michelson Interferometer optical system.

The infrared radiation is produced in a heated source and is generally composed of several frequencies of different intensities. However, if the source of the FTIR spectrometer is sufficiently stable, and if sufficient time is allowed to heat up the source thoroughly, a constant pattern of intensities over a defined frequency range is produced. This infrared radiation, produced by the source, is then sent to a mirror (not represented in Figure 2.2) which directs the beam into the interferometer. This beam is then split into two beams by a beamsplitter. One of the secondary beams is then sent to a fixed mirror. The other part is sent to a moving mirror. These two mirrors send the secondary beams back to the beamsplitter where they are recombined and interfere with each other. These important interferences are due to the moving mirror which travels back and forth along a precisely controlled track reflecting the beam from a position that is constantly changing. This movement causes the intensity of the recombined beam to change constantly. This change in intensity is different for each frequency of radiation. When the infrared beam exits the interferometer, it is deflected by a couple of mirrors before it reaches the detector. The detector produces an electrical signal in response to the radiation striking it. The detector measures the total intensity of infrared radiation reaching it across all frequencies. This measurement is read many times per second to generate the

interferogram. When a sample is placed in the path of the infrared beam, certain frequencies of the recombined beam may be absorbed or partially absorbed. As a result, the beam that comes out of the sample is different than the one that went in. It is as if the sample left a "fingerprint" in the infrared beam.

The instrument is calibrated internally using a laser whose beam follows the same path as the infrared light and whose frequency is known to great accuracy. As the laser beam passes through the interferometer and beamsplitter, it undergoes the same interference that occurs with the infrared beam. The cycles of the encoded laser beam are used as a sampling clock. The clock determines the number of times the detector is read during a scan and the precise location of the moving mirror at each reading. This ensures the accuracy of each frequency measurement and explains what is meant by "internal calibration". The laser also ensures that the readings taken during multiple scans are precisely synchronized, which maintains instrument precision. Because the laser beam is visible and travels through the focal point of the infrared beam, it is useful for aligning lenses and mirrors necessary to focus the beam on the crystal sample.

The performance of an FTIR spectrometer is an order of magnitude higher than that obtained with a dispersive instrument with respect to the signal to noise ratio for a given scan time and resolution. This improvement arises because of three well-known advantages of FTIR spectrometers: the Fellgett, the Jacquinot and the Connes advantages.

The Fellgett (or multiplex) advantage arises from the fact that each point on the interferometer contains information from the entire spectral range. Unlike dispersive instruments, which access each wavelength individually by means of gratings, the Fourier transform spectrometer samples the whole wide spectral range simultaneously leading to the scan time being greatly reduced in terms of sensitivity. Measurements taken over the same spectral range with the same resolution in the same time on an FTIR spectrometer will have a signal to noise (S/N) ration $n^{0.5}$ times greater than that taken using a dispersive spectrometer, where n is the number of resolution elements. Therefore, measurements taken using the same S/N can be n times faster on an FTIR spectrometer.

The Jacquinot advantage arises from the fact that resolution depends on the distance of mirror travel and not the slits and gratings. By removing the slits and gratings, there is more energy allowed to pass through the simple optical path so more of the source energy reaches the detector.

The Connes advantage is concerned with frequency precision and the fact that the interferometer contains its own internal frequency standard. The mirror movement and

the detector sampling of signal are clocked by interferometric fringes from monochromatic light, which is generally a He-Ne laser, whose operation was explained earlier. All frequencies in the output spectrum are calculated from the known frequencies for the laser light and as a result, an FTIR spectrometer achieves frequency precision of better than 0.01 wavenumbers.

2.1.2 Physical basis of RAIRS

Classically, the general infrared selection rule states that for a vibration to be infrared active, the electric dipole moment of the molecules must change during the vibration. Quantum mechanically the dipole is expressed in terms of the transition dipole moment, which, for a transition between states Ψ_i and Ψ_f, is defined as [23]:

$$\mu_{fi} = -e\int\psi_f^* \times r \times \psi_i \times d\tau \qquad (2.1)$$

The intensity of the transition I is proportional to the square of the transition dipole moment μ_{fi} and so only if the transition dipole moment is non-zero does the transition contribute to the spectrum [23].

For a molecule adsorbed on a metal surface, the interaction of the infrared radiation with the adsorbate dipole is influenced by the dielectric behaviour on the metal. This gives rise to the following selection rule for RAIRS:

'ONLY VIBRATIONAL MODES WITH A DIPOLE MOMENT CHANGE NORMAL TO THE SURFACE WILL BE OBSERVED'

Not only is the first monolayer under the substrates influence, but the surface selection rule extends to molecules adsorbed in the multilayer of thicker films, illustrated by Poling [24] with a 25 nm thick layer of Cu oxalate on copper.

The influence of a metallic substrate on absorption of infrared radiation by adsorbed molecules was originally treated by Francis and Ellison [13] and the classical electrodynamic macroscopic model was then pursued by Greenler [14], leading to the derivation of the optimum conditions for the RAIRS experiment. Greenler showed that for metal surfaces only the component of the electromagnetic vector normal to the surface is effective in exciting dipole-active vibrations. It was also shown that the experiment is only effective at high angles of incidence and that a single reflection from the surface is sufficient to achieve the desired experimental performance.

When infrared radiation reflects from a clean and highly reflective metal surface the interaction can be described using the Fresnel equation [13]. Such a process produces changes in the intensity (R) and phase (δ) of the reflected light which are dependent upon the orientation of the electric vectors of the radiation. Therefore analysis of this process requires the reduction of the electric field vectors into their components; s-polarised light with the electric field vector perpendicular to the plane of incidence and p-polarised light with the electric vector parallel to the plane of incidence, as presented in Figure 2.3.

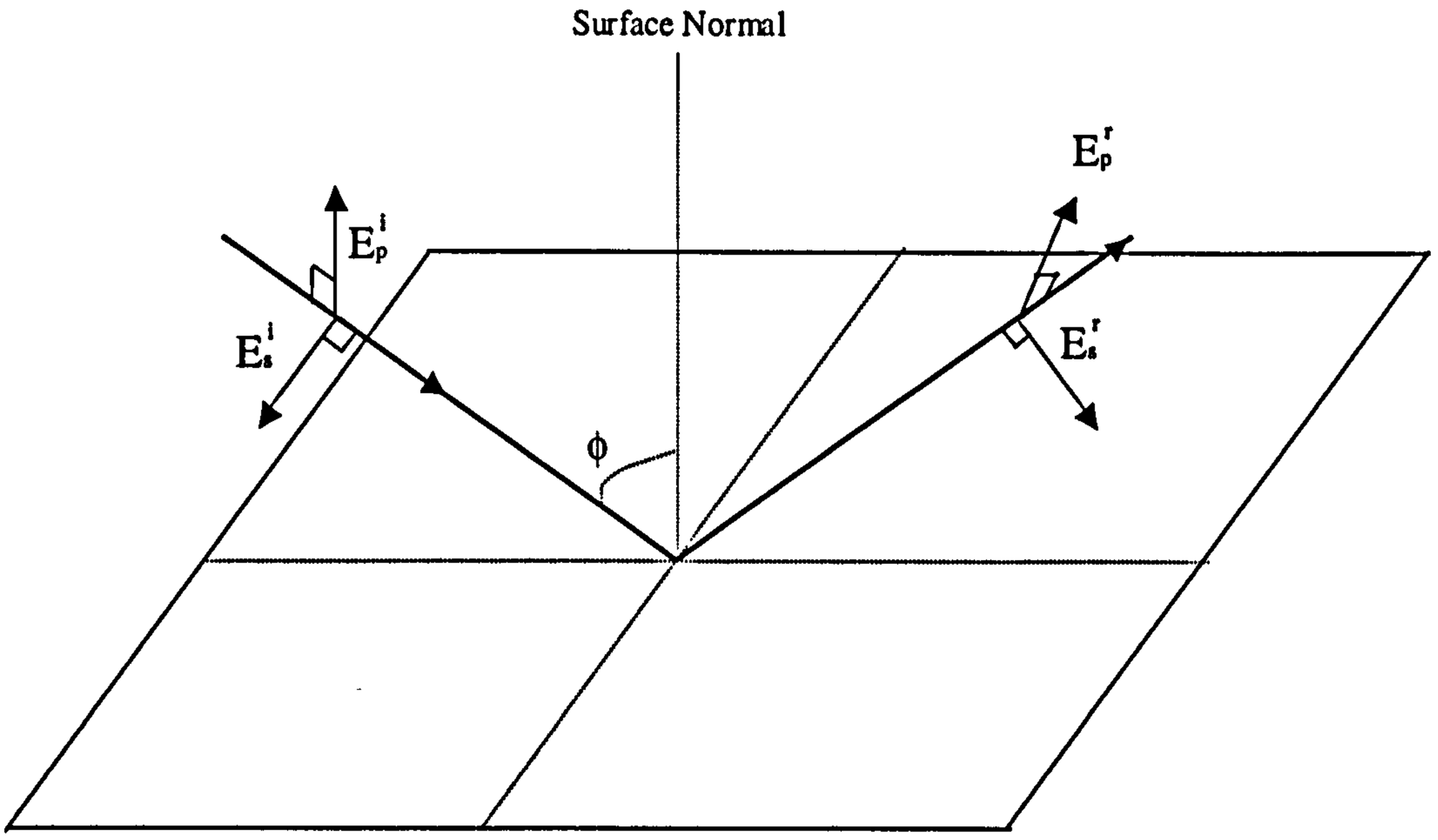

Figure 2.3: A schematic diagram of the reflection of infrared from a metal surface showing the s and p components of incident (E^i) and reflected (E^r) radiation, (adapted from reference 6).

The complex index of refraction for each of the phases constituting the interface can be written as:

$$\mathbf{n} = n + ik \qquad (2.2)$$

If: $n^2 + k^2 >> 1$, where n and k are the refractive index and absorption constants of the metal respectively, which is the case for light in the infrared wavelength region reflecting from a metal surface, the following formulae apply for reflected light incident on a clean metal surface:

$$Rp = \frac{(n-\sec\phi)^2 + k^2}{(n+\sec\phi)^2 + k^2} \qquad (2.3)$$

$$Rs = \frac{(n-\sec\phi)^2 + k^2}{(n+\sec\phi)^2 + k^2} \qquad (2.4)$$

$$\tan\Delta = \tan(\delta_p - \delta_s) = \frac{(2k \times \tan\phi \times \sin\phi)}{\tan^2\phi - (n^2 + k^2)} \qquad (2.5)$$

where Rp and Rs are the reflected intensities for p - and s - polarised light, δ_p and δ_s are the phase shifts experienced by the p and s polarised light upon reflection and ϕ is the angle of incidence. Using appropriate values for n and k typical of a highly reflecting metal surface (n = 3, k = 30) [6], Rp and Rs, and δ_p and δs, can be calculated as a function of incidence ϕ, shown in Figure 2.4.

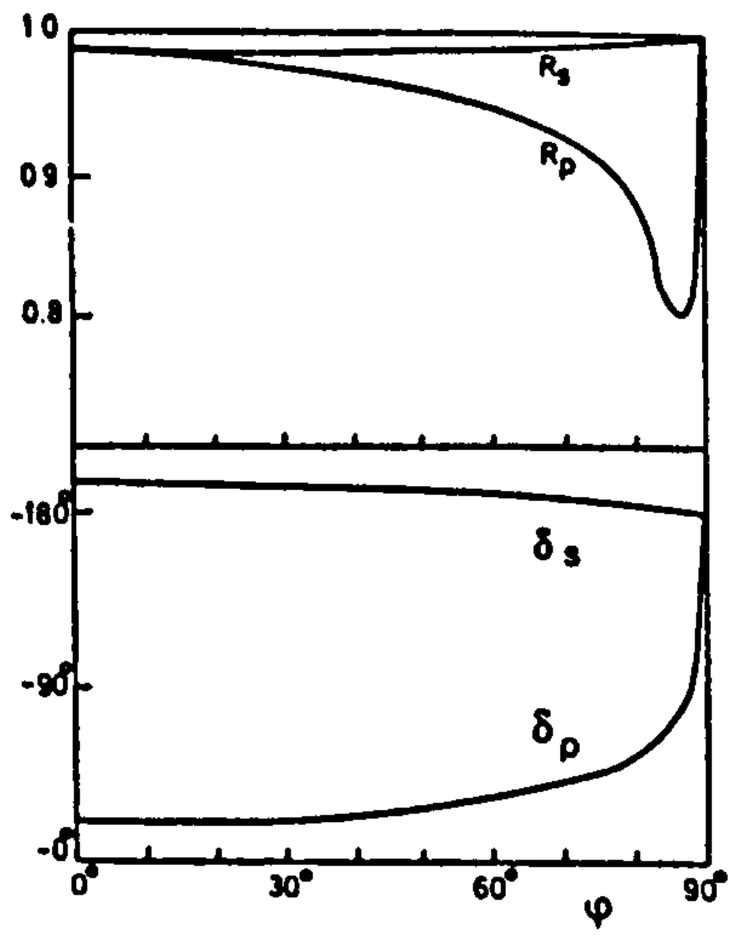

Figure 2.4: The reflection coefficient (R) and phase shifts (δ) of the s and p components of the infrared radiation on reflection from a metal surface as a function of angle of incidence (ϕ), (reproduced from ref 6).

The adsorbate dipole will interact with the total electric field vector at the surface. Thus the electric field components of the incident, reflected and refracted waves have to be considered, although the optical properties of the metal are such that most of the incident intensity is reflected, and the refracted wave contribution to the surface electric field is negligible [6]. If the amplitude of the incident electric field is $E^i \sin\theta$, (where θ is an arbitrary phase), the field due to the reflected wave is $E^i\, r \sin(\theta+\delta)$, where r is the reflection coefficient and δ is the phase shift. The resulting field at the surface is therefore given by:

$$E = E^i[\sin\theta + r\sin(\theta+\delta)] \qquad (2.6)$$

The phase shift (δ) of the s and p components of the infrared radiation on reflection from a metal surface are shown in Figure 2.4. If we first consider the case of s-polarised light, equation 2.6 yields:

$$E_s = E_s^i[\sin\theta + r_s \sin(\theta + \delta_s)] \qquad (2.7)$$

From Figure 2.4 it can be seen, for s-polarised light, a uniform 180° phase shift is observed for all angles of incidence and $r_s \approx 1$, therefore destructive interference occurs. The incident and reflected beams cancel and an electric field vector parallel to the surface will not exist. Thus vibrational modes with the vibrational dipole moment change parallel to the surface will not be excited. This is the main reason for the strict validity of the metal surface selection rule for dipole excitation of vibrational modes by infrared light on metal surfaces; there is no electric field parallel to the surface to interact with the dipole moment of a vibrational mode parallel to the surface.

If we now consider the case of the p polarised light, the incident and reflected electric wave fields have components both parallel, $E_p^{\parallel}$, and normal $E_p^{\perp}$ to the surface. Figure 2.5 shows how the magnitude of each changes with increasing angle of incidence. As ϕ increases so does the perpendicular component of p polarised light, with a simultaneous decrease in the parallel component. It can also be seen that reflected $E_p^{r\parallel}$ and incident $E_p^{i\parallel}$ are equal in magnitude but opposite in direction, and therefore cancel upon reflection of radiation from the surface.

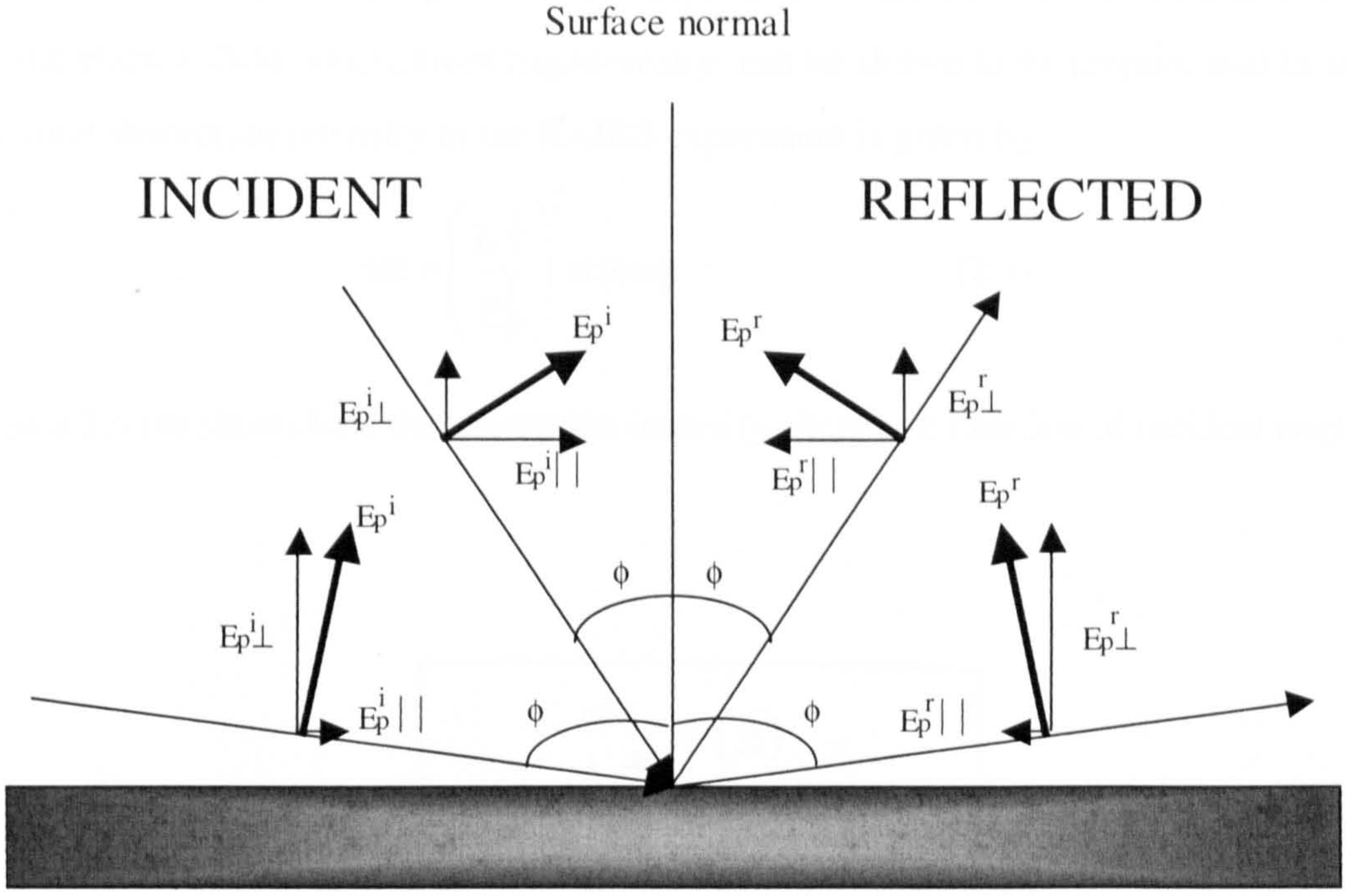

Figure 2.5: A schematic diagram of the magnitude of the p component of the electric vector parallel ($E_p^{\parallel}$) and perpendicular ($E_p^{\perp}$) to the surface as a function of angle of incidence.

In contrast, the reflected $E_p^{r\perp}$ and incident $E_p^{i\perp}$ are in the same direction and therefore reinforce. More specifically, for the perpendicular component of p-polarised light, equation 2.6 yields

$$E_p^{\perp} = E_p^{i} \sin\phi \times \left[\sin\theta + r_p \sin\left(\theta + \delta_p\right)\right] \qquad (2.8)$$

Figure 2.4 shows that the phase change for p polarised light remains small for a wide range of angles of incidence leading to constructive interference, but increases to 180° near grazing incidence resulting in cancellation. It is concluded, therefore, that incident p polarised radiation can give rise to significant electric fields at the metal surface, but only in a direction normal to the surface and at grazing angles of incidence. Greenler has shown that the optimum angle for the RAIRS experiment is 80-88 degrees from the surface normal depending on the metal [14]. Figure 2.6 (a) shows the relative amplitude of the electric field perpendicular to the surface as a function of incident angle ϕ for a typical metal. Assuming that the intensity of the absorption depends on the square of the

surface electric field E_p [25], and is also dependent on the number of molecules excited by the electric field which, from trigonometry, can be shown to be proportional to sec ϕ, the total absorption intensity in the RAIRS experiment is given by

$$\Delta R = \left(\frac{E_p^1}{E_p^i} \right)^2 \times \sec\phi \qquad (2.9)$$

Figure 2.6 (b) shows how the absorption intensity alters as a function of incident angle.

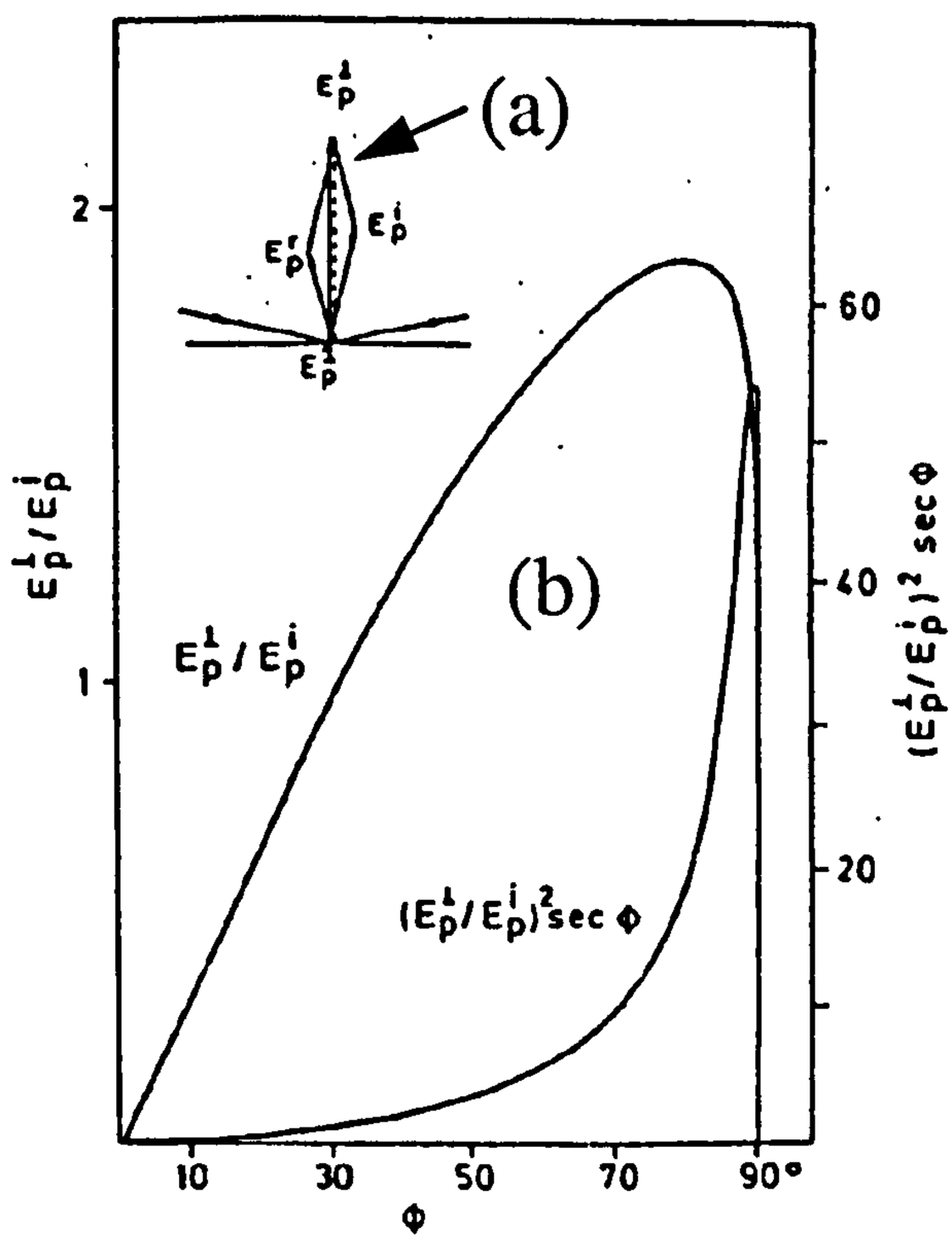

Figure 2.6: (a) The relative amplitude of the electric field perpendicular to the surface as a function of incident angle, (b) the absorption intensity as a function of incident angle [5].

Greenler extended the two phase (vacuum/solid) system to a three phase system which includes a homogeneous isotropic layer placed on the surface, characterised by an estimated complex dielectric constant for the adsorbate layer in the calculations [14] and the theoretical treatment has been greatly simplified by McIntyre and Aspnes [26]. Figure 2.7 presents a schematic diagram of the system under investigation. Greenler calculated

the change in reflectivity over the whole angle of incidence range using the Fresnel equations and it was found that a third layer does not make a significant difference when considering the general basis of the RAIRS experiment [14]; only light with a component of the electrodynamic vector normal to the surface will be absorbed and the change in reflectivity for a metal has a maximum at angles of incidence near to grazing.

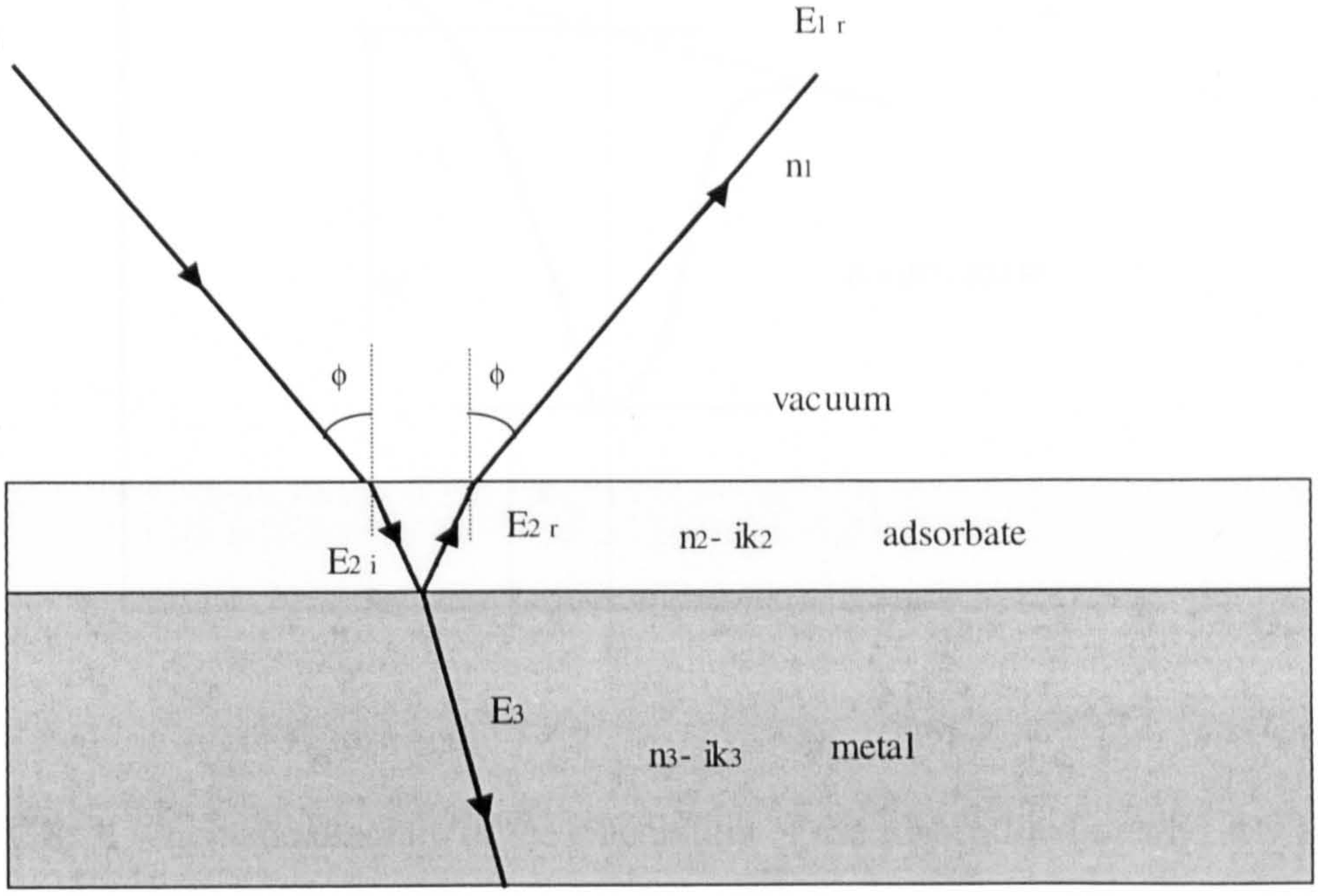

Figure 2.7: The classical three phase model of an adsorbate layer (n_2-ik_2) of thickness d on a metal (n_3-ik_3), (adapted from ref 5).

Incorporating the third layer also enabled the calculation of an absorption function, A.

$$A = \frac{\Delta R}{R^{\circ}} \qquad (2.10)$$

where

$$\Delta R = R^{0} - R \qquad (2.11)$$

is the reflectance in the three phases system with a non-absorbing adsorbate and R is the reflectance of the modelled adsorbate, see Figure 2.8.

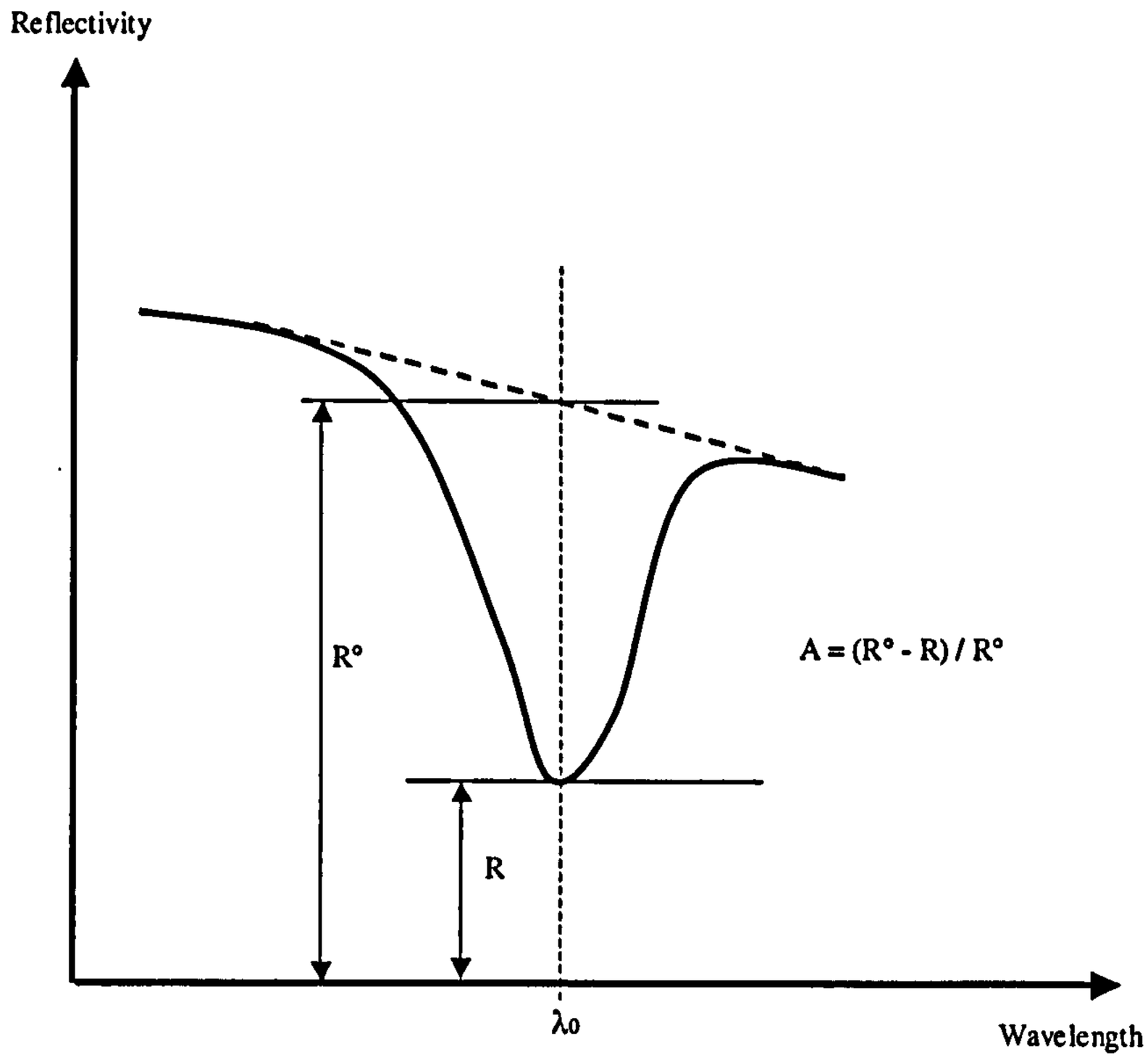

Figure 2.8: A schematic diagram of the calculation of the adsorption function $A = \Delta R / R^0$, where $\Delta R = (R^0 - R)$ is the reflectance in the three phase system with a non-adsorbing adsorbate and R is the reflectance of the modelled adsorbate, (reproduced from ref 5).

The results of the classical optical reflectivity treatment in restricting absorption to only those vibrations with a dipole moment perpendicular to the metal surface forms the basis of the so-called 'metal surface selection rule' (MSSR) and is entirely equivalent to the result obtained using image dipole theory [27-29]. The image dipole theory of the surface selection rule is expounded in Figure 2.9. The long range electromagnetic field of the infrared radiation will interact with the metal electrons as well as the dipole moment of a molecular vibration, i.e. the electromagnetic field of the infrared radiation cannot distinguish the dipole from its image, and interact with the sum of their dipole fields. In the case of a perpendicular dipole (left hand side of Figure 2.9) this leads to an increased response (and hence absorption). In the case of a dipole parallel to the surface, the net summation yields a quadrupole component, and no dipolar field remains for interaction (right hand side of Figure 2.9).

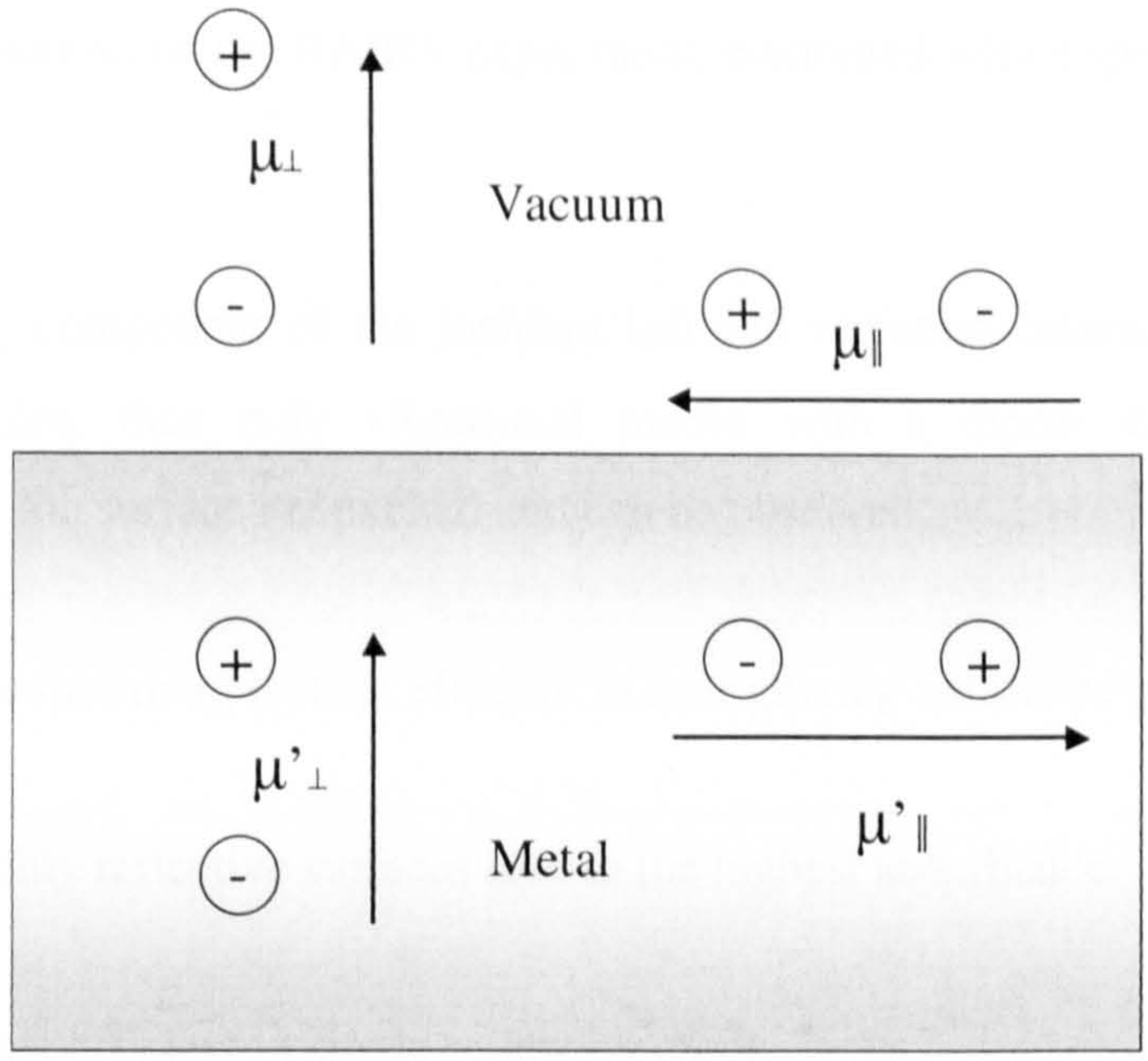

Figure 2.9: The image dipole picture of the screening of a dipole oriented parallel to a metal surface, and the enhancement of a perpendicular dipole, (adapted from ref 6).

Summary

Theoretical evaluation of the RAIRS experiment, combined with experimental evidence has shown that:

(1) Only the $p_{\perp}$ component of the incident infrared radiation interacts with adsorbate vibrational dipoles, thus only vibrational modes with a dipole component change perpendicular to the surface are excited and can be observed.

(2) The RAIRS experiment is most efficient in near grazing incidence geometry.

(3) The most highly reflective surfaces lead to the highest absorbance.

(4) RAIRS is most efficient in single reflection mode.

2.2 Scanning Tunnelling Microscopy (STM)

The scanning tunnelling microscope (STM) was invented by Binning and Rohrer at IBM, Switzerland, in 1982, for which they received the Nobel Prize for Physics in 1986.

Tunnelling can occur between a tip and a metallic surface simply by bringing them sufficiently close together. The electron clouds of the two start to overlap. A small positive bias on the tip is sufficient to cause a measurable tunnelling current over the gap between the tip and the metal. The voltage V shifts the position of all electrons in the metal up with respect to those of the tip and the Fermi levels are separated by an energy e V. If the tunnelling gap is sufficiently small, valence electrons from positions close to the Fermi level can tunnel to unoccupied states of the tip. Figure 2.10 illustrates this principle. The tunnelling current is in the range of pico to nano amperes and varies exponentially with the distance between tip and surface according to the formula:

$$j_T = \alpha_1 \frac{\sqrt{\varphi_{av}}}{d} V_T \exp\left(-\alpha_2 \sqrt{\varphi_{av}}\, d\right)$$

where j_T is the current density, d is the distance between the tip and the surface, V_T is the potential difference between the tip and the surface, φ_{av} is the average between the work functions of the tip and the surface, α_1 and α_2 are constants.

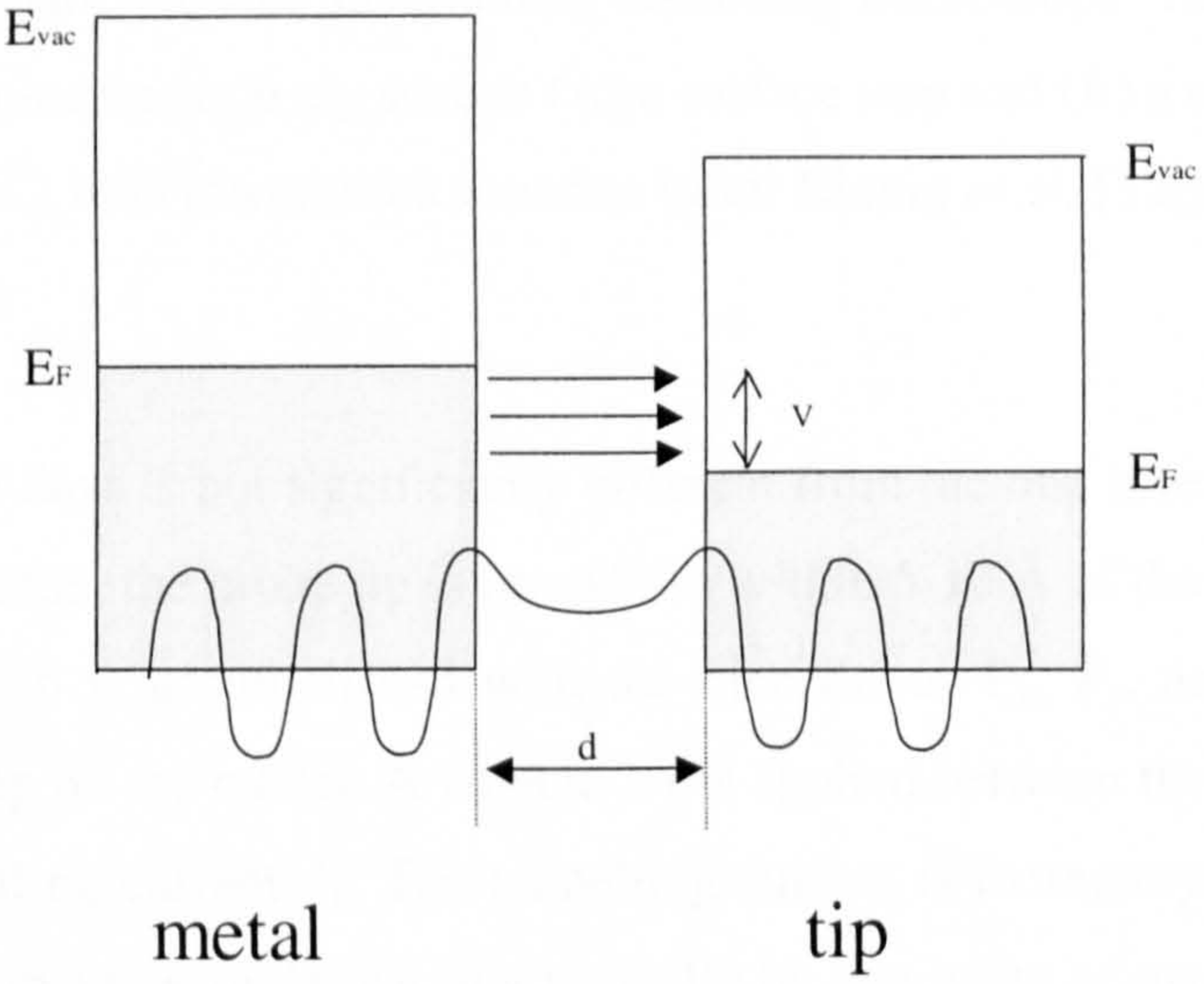

Figure 2.10: Principle of tunnelling between two metals with a potential difference V, separated by a gap d: electrons tunnel horizontally in energy from occupied states of the metal to unoccupied states of the tip (adapted from ref 30).

Figure 2.11 shows a schematic view of the STM, taken from the original work of Binnig, Rohrer, Gerber, and Weibel [31].

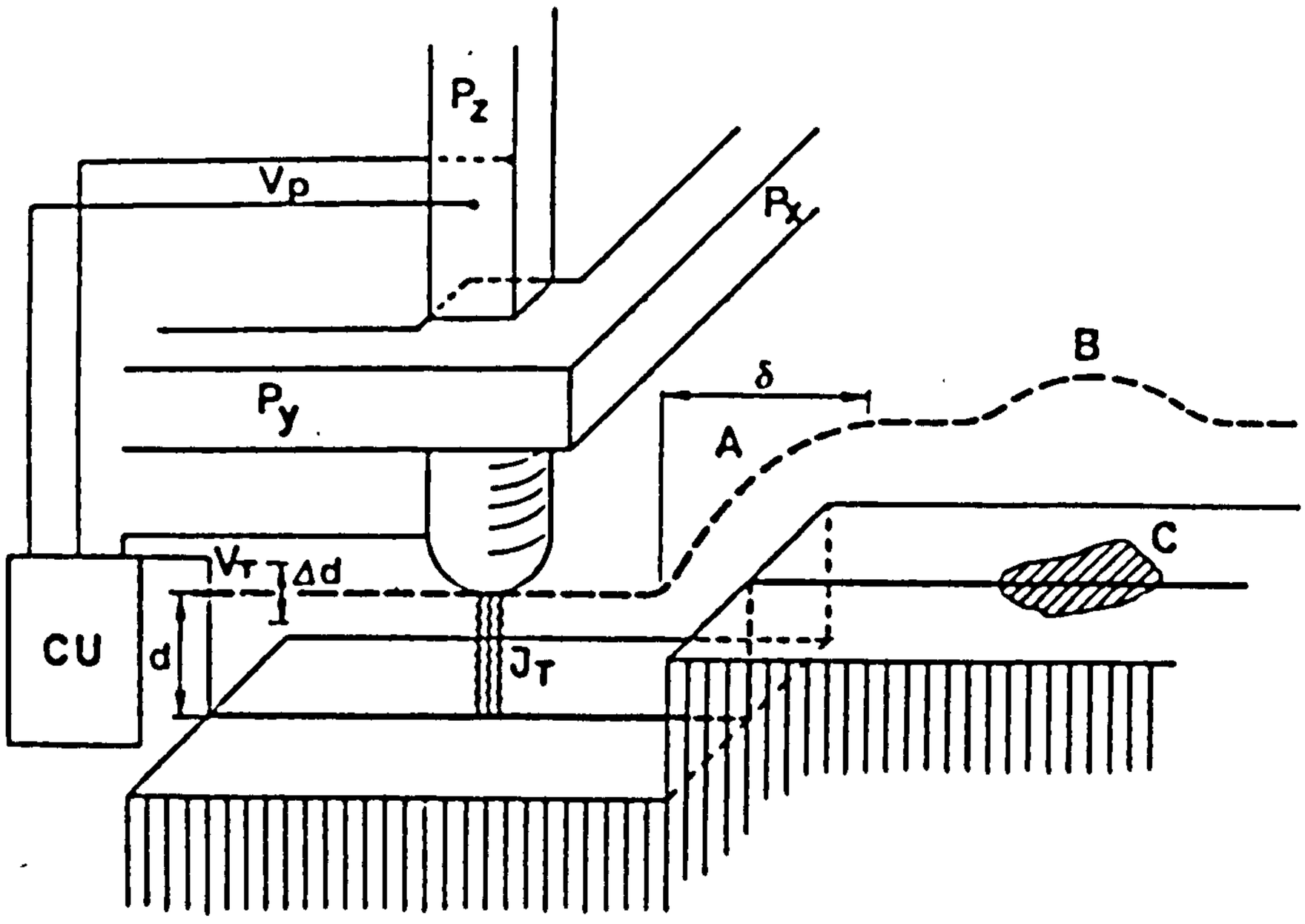

Figure 2.11: Schematic view of the scanning tunnelling microscope. The broken line indicates the z displacement in a y scan at (A) a surface step and (B) a contamination spot, C, with lower work function (after Binnig *et al.* [32]).

The STM used these days is not significantly different from the one invented by Binning and Rohrer. In operation, the probe tip is brought to within 5-10 Å of the sample surface. Fine motion of the tip is accomplished with the piezodrives P_x, P_y, and P_z or by one piezodrive, depending on the model. A voltage V_T is applied between the tip and sample, producing the tunnelling current J_T. The tunnelling current is extremely sensitive to the separation between tip and sample, varying typically by one order of magnitude for each Å change in tip-sample separation. Thus, by scanning the tip across the sample, one can obtain an image of the sample topography.

Two scanning modes can be used: the "constant current" mode or the "constant height" mode. In the constant current mode, the scan is accomplished by continuously adjusting

the tip height in order to maintain a constant tunnelling current. The tip height as a function of lateral position, z (x, y), thus constitutes a constant-current image of the surface. This mode offers a smoother image of the surface as constant adjustments are made. It is the best method to image a rough surface or large areas, but has the disadvantages of being slow and therefore more susceptible to thermal drift effects. In the constant height mode, the tip is scanned across the surface, at nearly constant height and voltage, while the current is being measured, or alternatively, the current is kept constant and voltage monitored. This method has the advantage of being fast, as it is not limited by the response time of the feedback loop, therefore minimising thermal effects and other distortions. It is often used on clean metal surfaces to obtain atomic resolution due to the small unit cell size. However, surfaces must be smooth to prevent the tip from crashing into the surface. For this reason, only small areas (< 100 Å) are normally scanned in this mode. In the simplest case, the collected images reflect the topography of the sample, as illustrated in figure 2.11 where the tip moves up over a surface step in constant current mode, which is the mode that is the most used.

Figure 2.12, also taken from the work of Binnig and Rohrer [32], illustrates a number of other aspects of the STM.

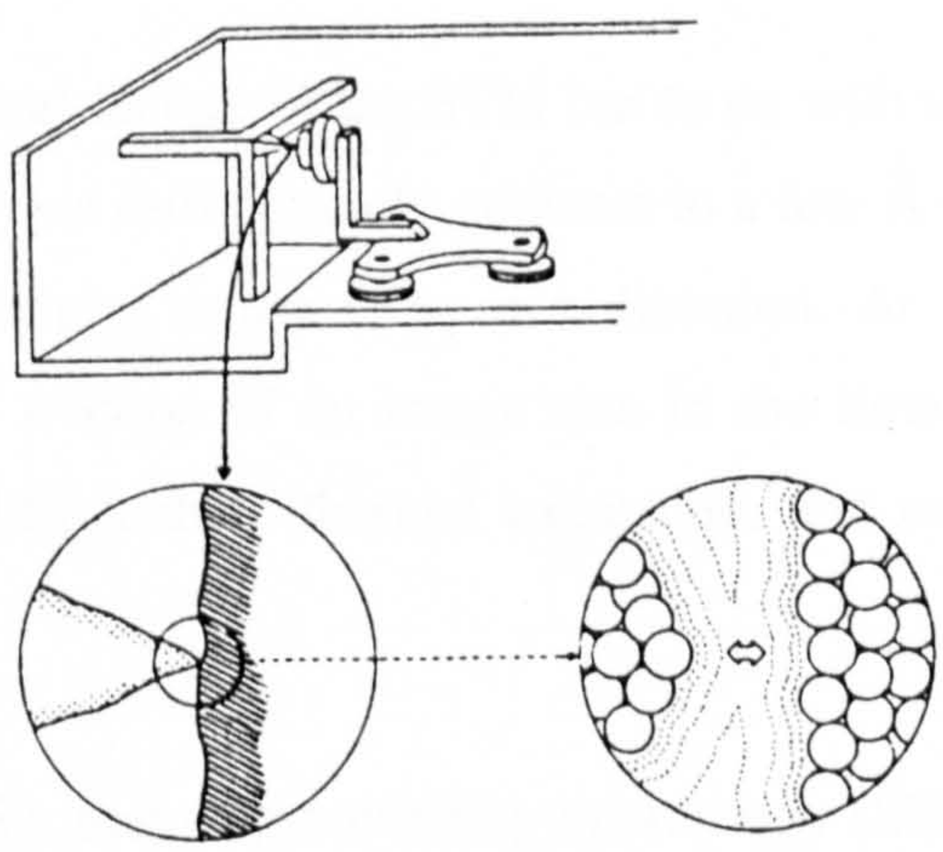

Figure 2.12: Schematic view of the physical principle and technical realisation of the STM. In the upper part of the figure, the three piezodrives, the tip, and the sample holder with the sample on the louse are shown. The bottom part of the figure shows amplifications of the tip-sample region down to the atomic level. The dotted curves denote electron charge-density contours on a logarithmic scale (after Binnig and Rohrer) [32].

It can be seen that the probe tip is mounted on a piezotripod, directed toward a sample attached on an electrostatic walker or "louse". This walker, described elsewhere [33], provides the coarse motion in the microscope, bringing the sample up to the tip within the scan range of the z-piezo (about 1 μm). The precise arrangement of atoms on the end of the tip affects the resolution of the microscope. This dependence of the images on the sharpness and shape of the tip must always be kept in mind when analysing STM images. Features which could result from asymmetric or multiple tips must be reproduced many times before they can be confidently identified as a property of the sample itself.

Clearly the mechanical stability between tip and sample must be very high to avoid vibrational noise in the tunnel current. Typical stability levels are in the range 0.01-0.1 Å. In the original STM designs, this stability was accomplished using the simple, but effective, method of building the microscope as compact as possible and then suspending it on soft springs. These springs damp out vibrations with frequency greater than their resonance frequency (about 1 Hz). The resonant motion of the springs themselves can be suppressed by eddy-current damping using permanent magnets. This original design of the STM remains today one of the very best methods for designing and building the microscopes. Nevertheless, a number of other designs have been developed which simplify and improve on various aspects of the instrument. A review of these designs is presented elsewhere [34].

Another important technical feature of the STM has to do with unintentional spatial drift between tip and sample. This drift typically amounts to a few Å per minute movement of the tip relative to the sample, in the x, y, or z direction. At this rate, the drift often amounts to a significant fraction of an image size in the time required to acquire the image. Sources of the drift include thermal expansion, and creep of the piezoelectric elements.

Since its inception in 1982, scanning tunnelling microscopy (STM) has proven its ability to be a powerful tool in the study of surfaces [31-36]. It has been possible to image ordered arrays of atoms on many metals and semiconductor surfaces, or clean surfaces as well as isolated adsorbates and thin overlayers. The STM can be used in UHV, air, various liquids, and at temperatures ranging from liquid helium to above room temperature.

The power of the tunnelling microscope lies in its ability to spatially and energetically resolve the electronic states on a surface. Spatially, the states can be observed with

atomic resolution; 5 Å lateral resolution is routinely achieved and features on the 3 Å scale can be resolved under favourable circumstances. Details of the geometric arrangement of atoms on the surface are reflected in the spatial distribution of electronic states, and the STM thus provides a probe of the atomic structure of surfaces. The connection between the electronic states and the atomic structure depends on the type of system. For metals, the states generally follow the atoms in a uniform fashion, and the STM thus provides a direct topographic view of the atoms.

2.3 Low Energy Electron Diffraction (LEED)

Low Energy Electron Diffraction (LEED) is a technique used to study the symmetry of a surface. A LEED pattern gives information on the size and shape of the two-dimensional unit cell of a surface, induced or not by atoms or molecules adsorption. It does not give information on the number of atoms in the unit cell or their location, i.e. the detailed atomic structure of the surface. This, however, can be obtained by varying the incident electron energy or its accelerating voltage V and measuring the intensity or current in the diffracted beams I but this IV LEED techniques [37] has not been used in the present work.

2.3.1 Operation of a LEED apparatus

A beam of electrons emitted by a hot filament and accelerated into a drift tube to a variable energy between 20 and 500 eV, is sent to the sample surface and is diffracted from it. The back-scattered beams move through field-free space between the crystal and the first grid, as shown in Figure 2.13. From a two-dimensionally periodic surface, electrons are backscattered in preferred directions according to whether Bragg diffraction conditions are met, as will be explained in the next section. The first grid is at sample (earth) potential while the second and third grid are negatively biased to ~ 97 % of the incident electron energy. By this process, those electrons that have been scattered inelastically in the sample or have lost ~ 3% of their energy in the scattering process can be rejected since they contribute only to a diffuse background in the diffraction pattern. Mainly elastically scattered electrons reach the screen. Between this first grid and the screen, the electrons are radially accelerated so that they are energetic enough to excite fluorescence in the screen and the spots of light so created can be viewed or photographed through the window. Bright spots observed, usually now from behind the screen, are a direct representation of the preferred back scattering directions. Disorder in surface layers, created for example by a dirty surface, generally leads to decreased

intensity in diffracted beams and an overall increase in background intensity associated with diffraction from random scattering centres.

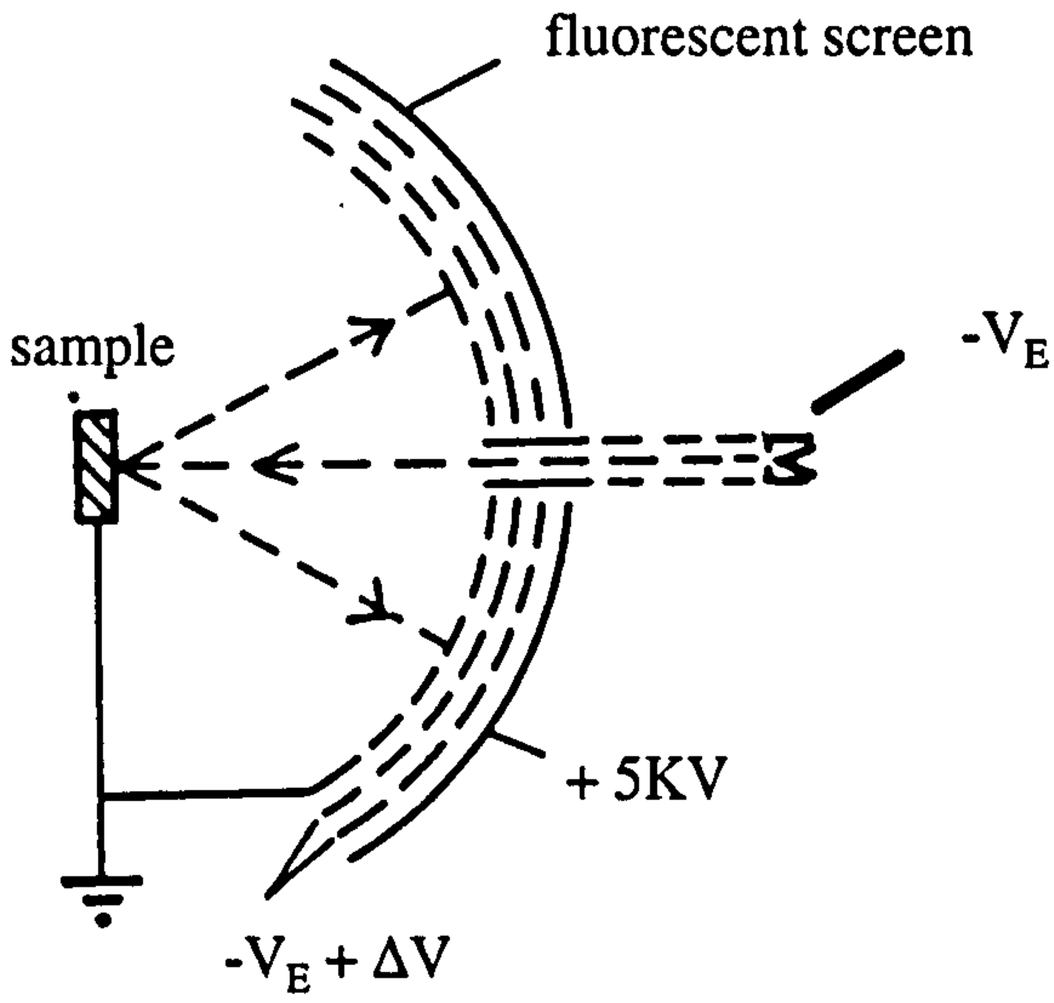

Figure 2.13: Schematic LEED instrument.

2.3.2 The LEED process

To get information from a LEED pattern, it is important to know how the incident electrons are scattered from a periodic surface to give the spots obtained in LEED patterns. The electrons which are elastically reflected undergo diffraction and are detected in the LEED experiment. They are considered as a wave with wavelength:

$$\lambda = \frac{h}{\sqrt{2 \times m_e \times E_{kin}}} \qquad (2.12)$$

where λ is the wavelength of the electrons, h is Planck's constant, m_e is the mass of an electron and E_{kin} is the kinetic energy of the electron. The electron wave, arising from a single electron, incident along the surface normal and scattered by a row of atoms, periodically spaced with a separation, a, undergoes constructive interference at an angle θ to the surface normal, as shown in Figure 2.14. This occurs if the Bragg scattering condition is met: the path difference ψ, must equal an integral number of wavelength, $n\times\lambda$, n being the order of the diffraction and λ the wavelength. This ensures that waves scattered from adjacent atoms are in-phase because the path length difference is an integral multiple of the wavelength:

$$n\lambda = a \sin\theta \qquad (2.13)$$

where θ is the angle between scattered electrons and the surface normal.

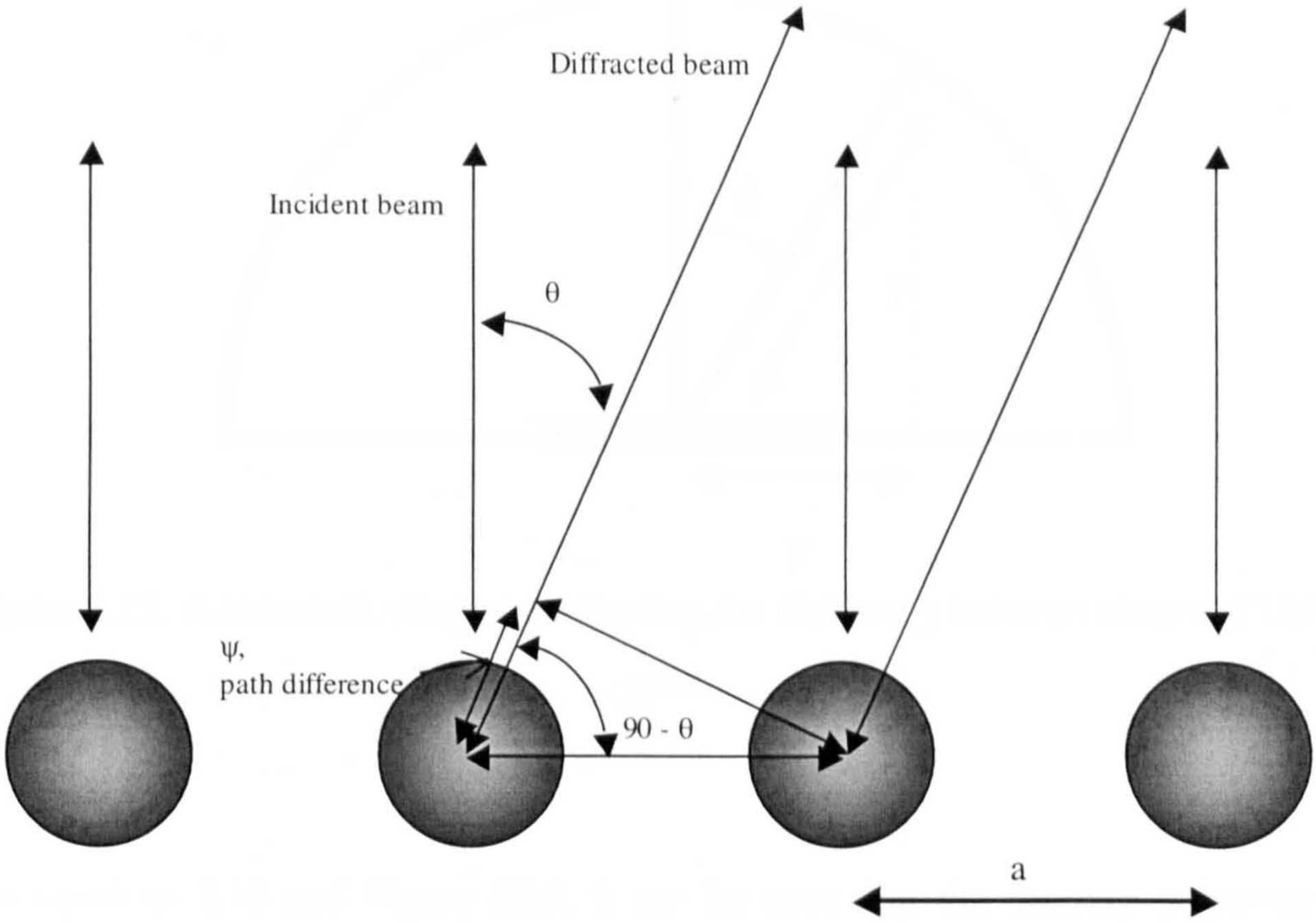

Figure 2.14: A schematic diagram of diffraction of a primary beam of electrons at normal incidence by a row of lattice points with separation a.

Hence, for a fixed wavelength, λ, and lattice spacing, a, only well-defined values of θ are allowed for which constructive interference will be observed corresponding to integer values of n. This means that discrete diffracted beams will be seen at particular angles.

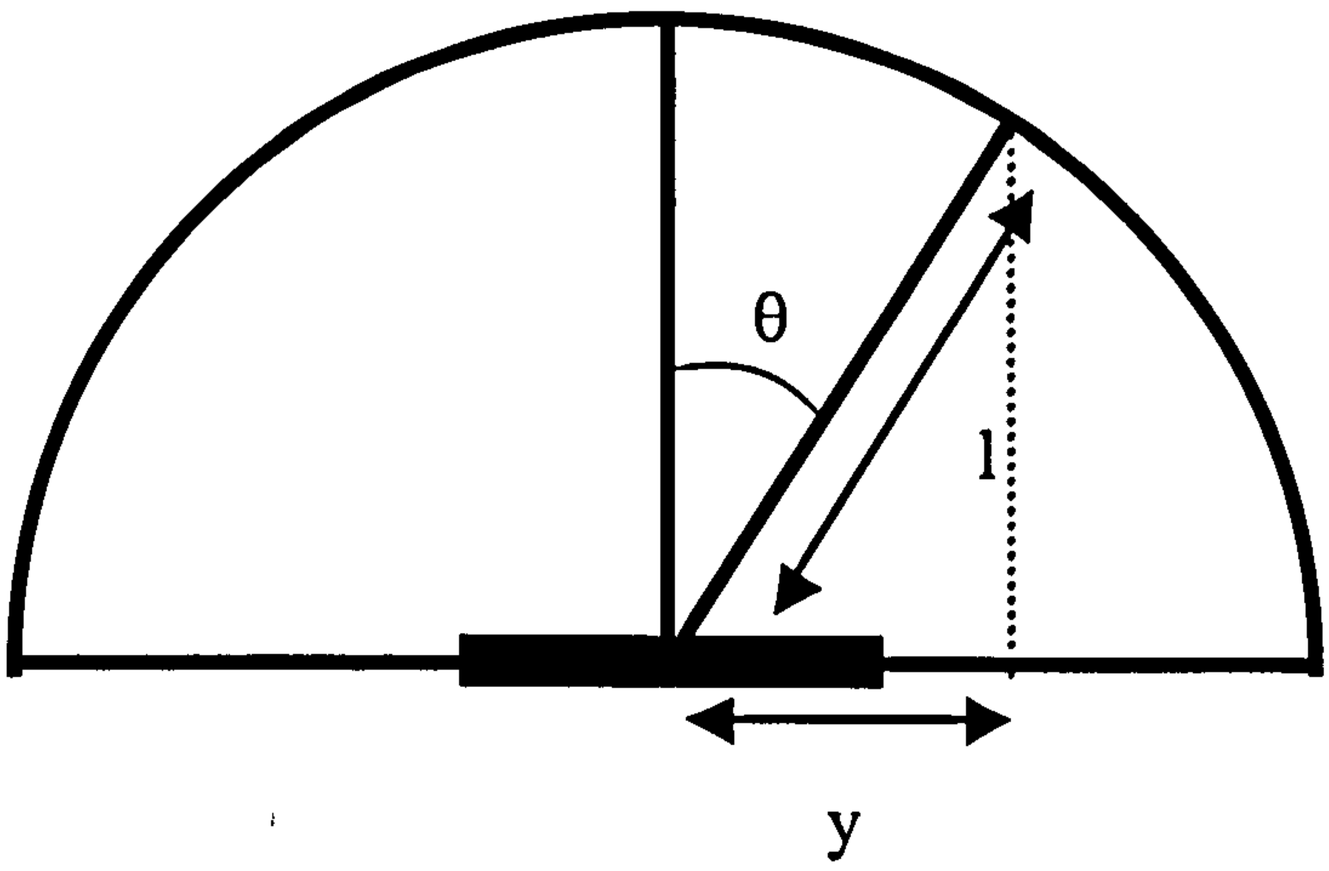

Figure 2.15: A schematic diagram indicating the distance y between observed LEED spots.

From equation 2.13 and Figure 2.15, it can be seen that the distance y between the observed LEED spots is proportional to 1 / a and the observed LEED pattern is a picture of the reciprocal space surface net. The real space surface net **r** in two dimensions is generated from a translational vector:

$$\mathbf{r} = m\,\mathbf{a} + n\,\mathbf{b} \qquad (2.14)$$

where m and n are integers and **a** and **b** are the unit mesh vectors.

An equivalent reciprocal space surface net **g** is generated by a reciprocal translation vector:

$$\mathbf{g}_{hk} = h\,\mathbf{a}^* + k\,\mathbf{b}^* \qquad (2.15)$$

where h and k are integers and **a*** and **b*** are the reciprocal unit mesh vectors.

Real and reciprocal space vectors are related through:

$$\mathbf{a} \cdot \mathbf{a}^* = 2\pi$$

$$\mathbf{a}^* \cdot \mathbf{b} = 0$$

$$\mathbf{b} \cdot \mathbf{b}^* = 2\pi$$

$$\mathbf{b}^* \cdot \mathbf{a} = 0$$

This means that **a*** and **b** and **b*** and **a** are perpendicular to each other respectively,

the length $|\mathbf{a}^*| = 2\pi / |\mathbf{a}|$ and the length of $|\mathbf{b}^*| = 2\pi / |\mathbf{b}|$.

The wavelength of an incident electron beam is also represented by its reciprocal space, the wavevector **k**:

$$\mathbf{k} = 2\pi / \lambda \qquad (2.16)$$

These diffraction conditions can be illustrated using the Ewald sphere construction, presented in Figure 2.16. The surface plane can be imagined as a raft of atoms which has been pulled away from the bulk, such that the distance between raft and bulk tends to infinity. Since distances in reciprocal space are inversely proportional to distances in real space the reciprocal lattice becomes a set of infinitely long rods normal to the plane of atoms. In the Ewald sphere construction, the incident radiation is represented by the wavevector **k**, which is drawn with the correct angle of incidence of θ and length $2\pi / \lambda$ and with its head at the origin O (already chosen for constructing the reciprocal lattice). To complete the Ewald sphere construction a circle of radius $2\pi / \lambda$ is drawn with its centre at the other end A of the vector. The circle corresponds to energy conservation, $|\mathbf{k}'| = |\mathbf{k}_0|$. Every point where the circle cuts a reciprocal lattice point represent a diffracted beam **k'** which satisfies the equation $\mathbf{k}'_{\|} = \mathbf{k}_{o\|} + \mathbf{g}_{hk}$ and amounts to the conservation of the component of momentum parallel to the surface.

This identifies the diffracted beams that are to be expected from a single set of lines, Figure 2.16, but when the full dimensional array is considered there are numerous sets of such lines to be drawn, with corresponding sets of reciprocal points and lattice rods. Each time the Ewald sphere construction is carried out for a new set of rods the circle is of the same diameter and touches the reciprocal lattice at the same origin O but its plane is rotated. The full construction thus consists of a sphere as if it were sitting on the plane of the reciprocal lattice, the point of contact being the origin O.

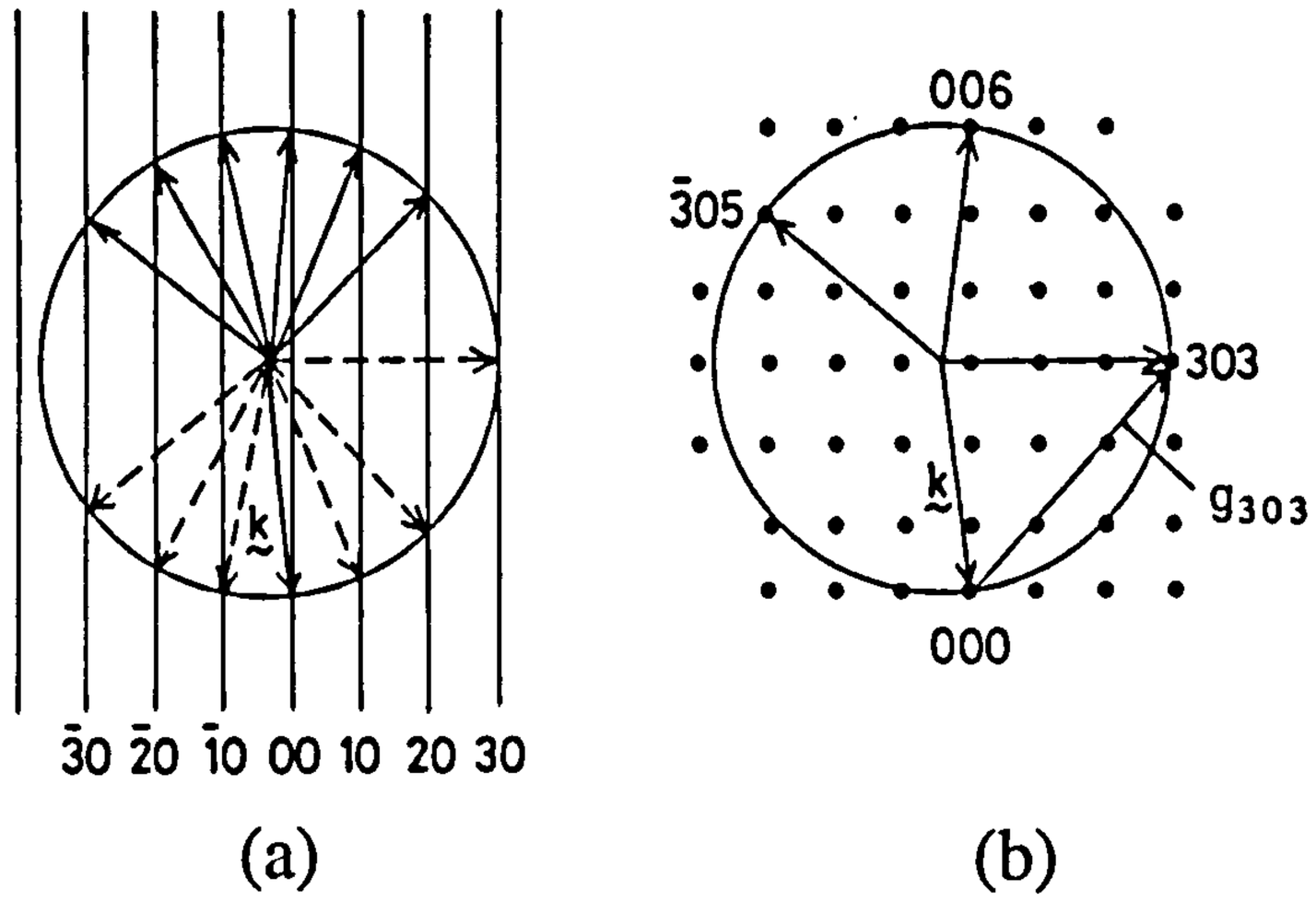

Figure 2.16: Ewald sphere construction in (a) two-and (b) three-dimensionally periodic systems. The incident electron is denoted by the vector **k** while all other radial vectors of the Ewald sphere correspond to outgoing diffracted beams **k'**. In the case of (a), the dashed vectors correspond to beams which do not emerge from the surface [38].

Thus the diffraction pattern has the same shape as the reciprocal lattice and the number and spacing of the spots depends on the radius of the Ewald spheres, i.e. the wavelength of the electrons. There is no requirement that the circle should go through any points other than O on the reciprocal lattice. If it does not, this means that for radiation of this particular wavelength incident at this particular angle there is no set of planes which fulfil the Bragg condition. Secondly, if **k** is less than 1/2 the spacing in the reciprocal lattice it is impossible to draw a circle through any two points on the reciprocal lattice. This implies to obtain diffraction $\lambda < 2a$ where a is the lattice spacing. Therefore for diffraction, the de Broglie wavelength of electrons should be appropriate:

$$\lambda = h / p \quad (2.17)$$

$$\lambda = \sqrt{\frac{150}{V}}\ \text{Å} \qquad (2.18)$$

where λ is the electron wavelength, p is the electron momentum, h is the Planck's constant and V is the potential in volts through which the electrons have been accelerated.

The positions of the spots from clean surfaces are important to determine if the bulk spacing persists on truncation, but most interest centres on the development of new diffraction patterns when adsorption occurs. The nomenclature commonly used to identify the overlayer is the Wood notation, which defines the ratio of lengths of the surface and substrate meshes, together with the angle through which the overlayer mesh vectors must be rotated to align the two pairs of translation vectors. In this notation if adsorbate A on the [hkl] surface of material X causes the formation of a structure having primitive translation vectors of length $|\mathbf{a}'| = p|\mathbf{a}|$ and $|\mathbf{b}'| = q|\mathbf{b}|$ with a unit mesh rotation of ϕ the structure is referred to as X{hkl}(p×q)-R $\phi°$ -A. This notation can only be used if the included angles of the surface and substrate unit meshes are the same, so while it is suitable for systems where the surface and substrate meshes have the same Bravais net, in general it is not satisfactory for mixed symmetry meshes. In this case an universally applicable matrix notation is used [39]. If a surface structure with basis vector $\mathbf{b}_1$ and $\mathbf{b}_2$ superimposed on a substrate lattice $\mathbf{a}_1$, $\mathbf{a}_2$ is present, then both lattices a and b may be related by b = ma or

$$\mathbf{b}_1 = m_{11}\,\mathbf{a}_1 + m_{12}\,\mathbf{a}_2$$

$$\mathbf{b}_2 = m_{21}\,\mathbf{a}_1 + m_{22}\,\mathbf{a}_2$$

The reciprocal lattice $\mathbf{b}^*$ may be correlated with the reciprocal $\mathbf{a}^*$ in a similar manner:

$$\mathbf{b}_1^* = m^*_{11}\,\mathbf{a}_1^* + m^*_{12}\,\mathbf{a}_2^*$$

$$\mathbf{b}_2^* = m^*_{21}\,\mathbf{a}_1^* + m^*_{22}\,\mathbf{a}_2^*$$

The reciprocal lattice parameters m_{ij}^* are obtained directly from the reading of the diffraction pattern.

It can be shown that m* is the inverse transpose matrix of m, so that $m^* = m^{-1}$ and $m = m^{*-1}$, which leads to the following relations:

$$m_{11} = 1 / \det m^* \,.\, m^*_{22}$$

$$m_{12} = 1 / \det m^* \,.\, m^*_{21}$$

$$m_{21} = 1 / \det m^* \,.\, m^*_{12}$$

$$m_{22} = 1 / \det m^* \,.\, m^*_{11}$$

where $\det m^* = m^*_{11}\, m^*_{22} - m^*_{21}\, m^*_{12}$. It is then possible from these equations to get the real surface lattice which is derived from the corresponding reciprocal lattice; the area of the unit mesh is given by the determinant of its matrix.

From these conditions, it is then possible to determine the size and shape of an adsorbate covered surface.

2.4 Thermal Desorption Spectroscopy (TDS)

Thermal desorption spectroscopy as it is used today was first described in the early 1960s by Redhead [40] and Carter [41], although it originated in flash desorption studies on metal ribbons by Apker [42]. The theory and practice of TDS have been discussed by a number of authors [43, 44].

TDS can also be known as temperature programmed desorption spectroscopy (TPD). The desorption of adsorbed atoms and molecules is one of the most fundamental elementary surface kinetic processes and can provide information concerning the strength of the interactions between the surface and the adsorbed species. If TPD spectra are collected as a family of curves of increasing initial surface coverage, the analysis can provide the adsorbate coverage (quantitatively), the adsorption energy which in general equals the activation energy of desorption, lateral interactions between the adsorbates through the coverage dependence of the adsorption energy, and the preexponential factor of desorption which on its turn reflects the desorption mechanism

In a TPD experiment, a temperature ramp is applied to the sample. The ramp follows the equation:

$$T = T_0 + \beta t$$

where T is the temperature, T_0 is the temperature at which the experiment starts and β is the heating rate.

The rate of desorption is followed by monitoring the amount of adsorbate desorbed into the gas phase (measured as the total pressure by an ion gauge, or a partial pressure by a mass spectrometer)as a function of temperature. If the pumping speed is infinitely high, readsorption may be ignored and the rate of desorption defined as the change in adsorbate coverage per unit of time is given by:

$$r = -\frac{d\theta}{dt} = k_{des}\theta^n = \nu\theta^n \exp\left(\frac{-E_{des}}{RT}\right) \text{[43]}$$

where r is the rate of desorption, θ is the coverage in monolayers, t is the time, k_{des} is the reaction rate constant for desorption, n is the order of desorption, ν is the preexponential factor of desorption, E_{des} is the activation energy of desorption, R is the gas constant.

2.5 Experimental details

2.5.1 RAIRS / LEED / TPD ultra high vacuum chamber

For the work on infrared and TPD, a multi-technique UHV chamber, has been used with RAIRS, LEED, RGA and TPD facilities, shown in Figure 2.17. This chamber also housed standard crystal cleaning techniques such as an Ar^+ ion gun. A base pressure around 10^{-10} mbar was generally achieved; the chamber was pumped using a 330 l / s turbomolecular pump and a titanium sublimation pump which flashed every 4 or 6 hours depending on the duration of the experiment. The chamber also had two KBr windows, which are transparent to infrared radiation between 4000-400 cm^{-1}. A gate valve isolated the powders sublimation doser and a leak valve isolated the liquids doser from the main chamber.

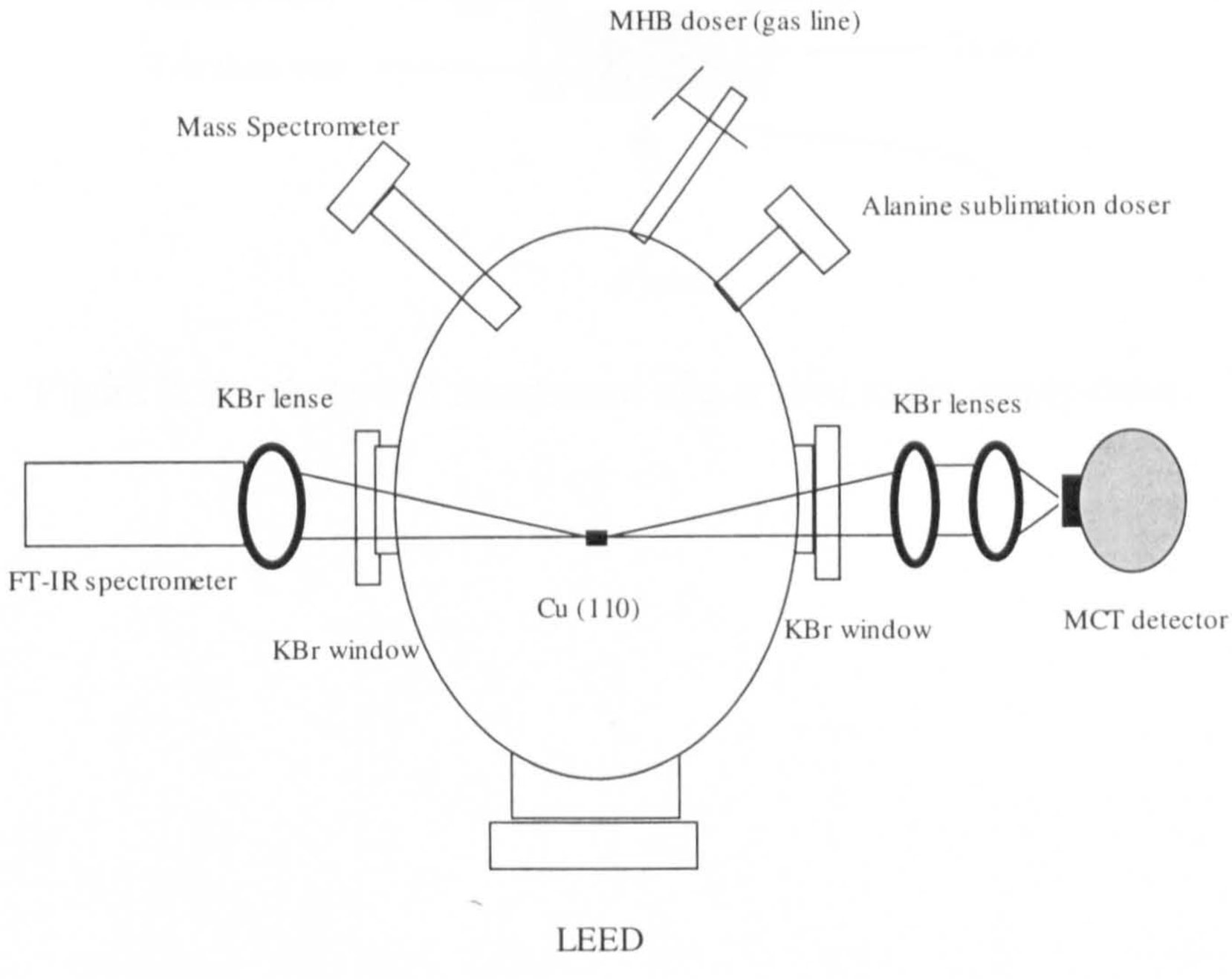

Figure 2.17: A schematic representation of the UHV chamber and optical set up used to perform the RAIRS, LEED and TPD experiment.

A Cu (110) crystal (9 mm × 17 mm × 1.4 mm) and a Ni (110) crystal (15 mm × 10 mm × 1.2 mm) were used as samples. The crystal used was mounted on the xyzθ manipulator using 0.25 mm Ta wires attached to the sample via two grooves spark-eroded into the two longest edges, Figure 2.18. It was resistively heated using a stabilised DC power supply. It was possible to heat the crystal to 1000 K. The crystal temperature was monitored with a chromel-alumel thermocouple wedged into a hole spark-eroded near one edge of the crystal. All temperatures were obtained by referencing the thermocouple to an ice / water junction and were corrected with respect to the calibration.

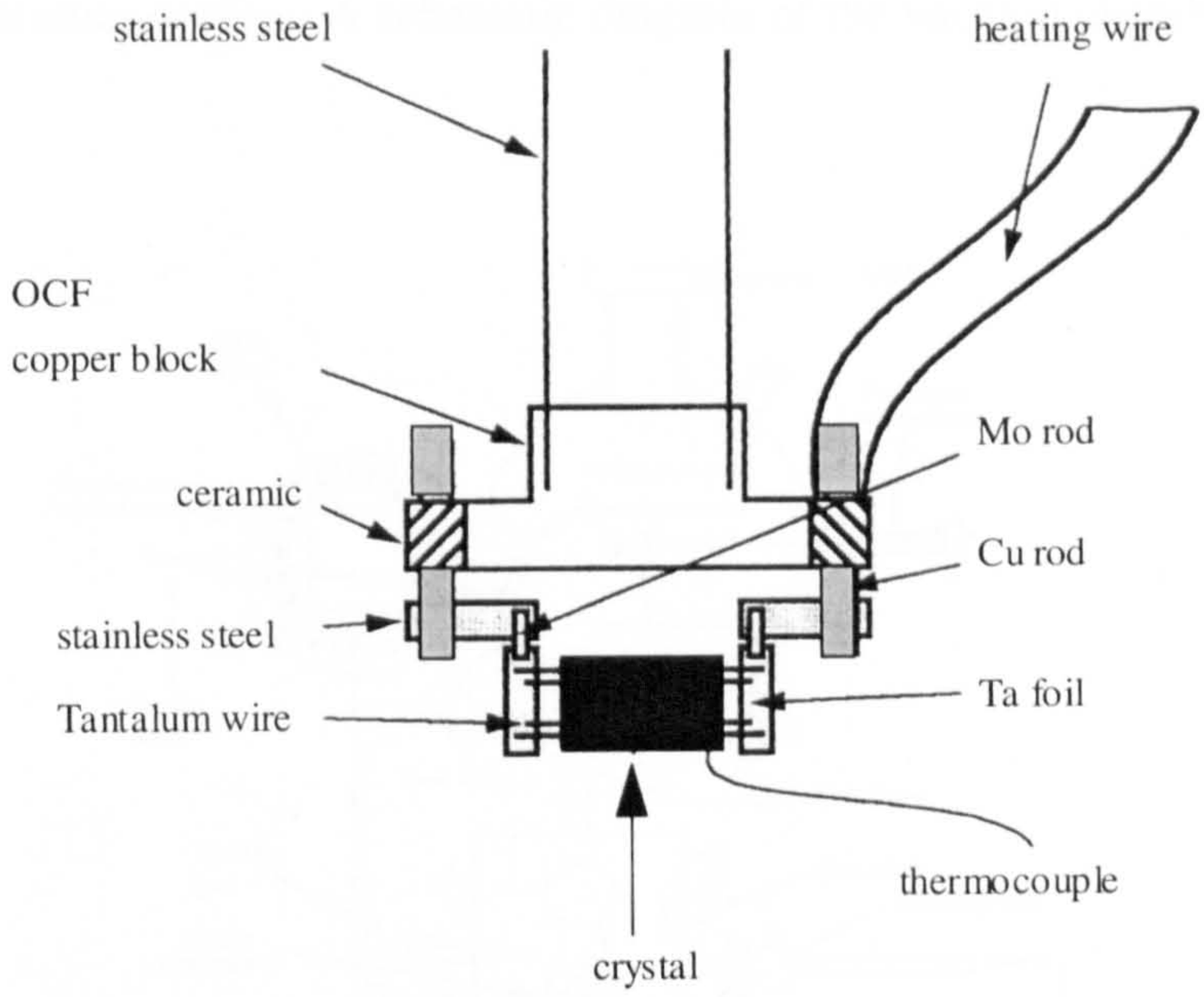

Figure 2.18: Method of attachment of a crystal to the manipulator.

2.5.2 STM / LEED ultra high vacuum chamber

This vacuum chamber was divided into a number of sections. Firstly, a fast entry lock for rapid transfer of samples into and out of vacuum, then a preparation chamber for sample treatment such as sample cleaning, gas or powder dosing, as well as an analytical chamber for surface analysis by LEED, AES and STM. This last chamber and the preparation chamber were separated by gate valves and thus could be at different pressures. Both the preparation and analytical chambers contained ports for the mounting of sample preparation devices. A schematic diagram of the vacuum chamber is shown in Figure 2.19.

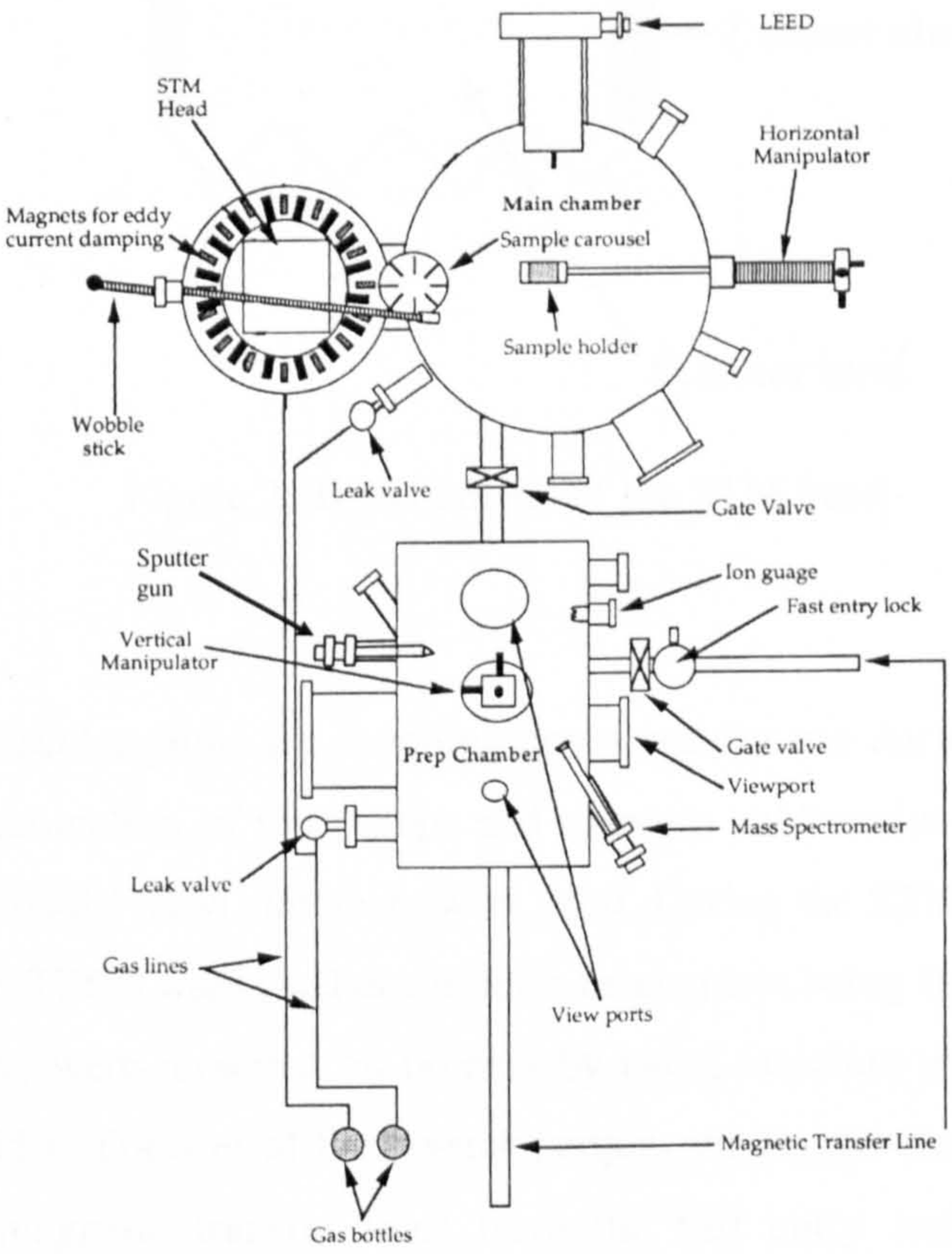

Figure 2.19: Diagram of the vacuum chamber as viewed from above.

Figure 2.20 presents the STM head.

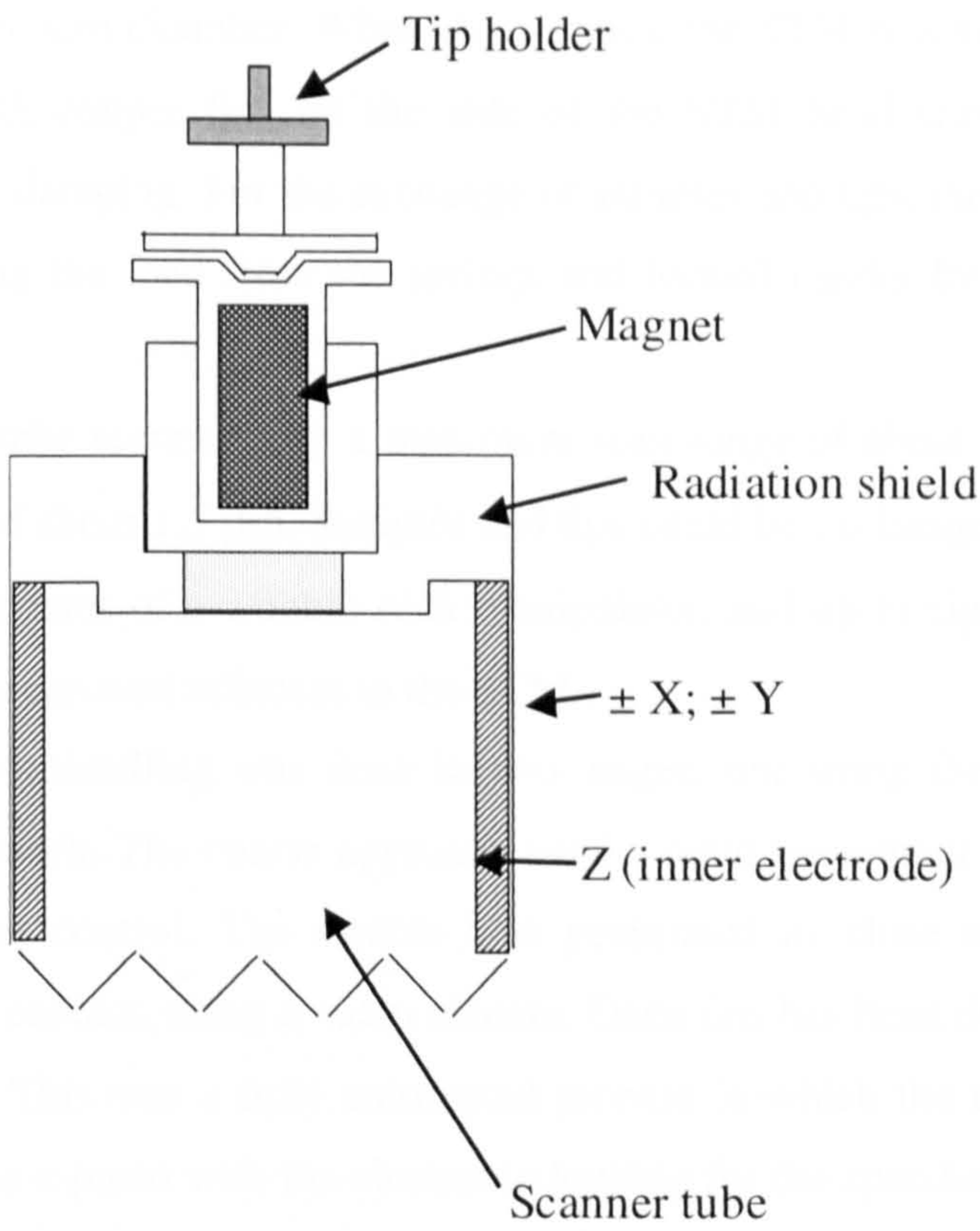

Figure 2.20: Schematic of the STM head.

A main turbo-molecular pump for roughing down and for use during sputtering and gas dosing, and a combination of ion pumps and titanium sublimation pumps (TSP) in the preparation, analytical / STM chambers were used. During the STM measurements, only the ion pumps and TPS's were used due to their mechanism being free from vibration.

The single crystals were mounted on holders by using tantalum wires which were spot welded to the holder. Transfer of the crystal samples within the chamber was done via a combination of magnetic transfer lines from the fast entry lock to the preparation chamber and then to the precision manipulators in either chamber. Both manipulators had X, Y, Z translation, 360 degrees rotation and heating facilities. The sample holder and manipulator were designed such that the manipulator could be rotated by 90 degrees to be either the sample transfer, sputter position, or LEED / AES position without falling. Samples were moved from the manipulator in the analytical chamber into the STM by means of a pincer-grip wobble stick.

The STM used in these studies was a commercial unit manufactured by Omicron Vakuumphysik GmbH. Vibration damping for the STM was achieved by an internal mechanism within the vacuum chamber. When in operation the STM was suspended by four vertical springs with copper fins on the side of the STM head sitting between magnets for eddy current damping. For the exchange of samples and tips, the STM could be raised vertically taking the load from the springs and locked rigidly by means of a linear motion drive.

The STM used a single tube scanner with a maximum scan range of about 12 μm × 12 μm with a Z translation of about 1.5 μm. Samples and tips could be exchanged in and out of the STM in UHV by means of a wobble stick manipulator, and up to eight samples / tips could be stored in the carousel adjacent to the STM.

Approach of the tip into tunnelling was done in two stages, one using the coarse, the other using the fine approach. The coarse approach used a rapid movement piezo louse, which was under manual control. The sample was positioned as close to the tip as possible without making contact, using a video camera. Once this has been done, the fine positioning could begin. This was a fully automated process in which the tip advanced towards the sample on the z-piezo with the electronic looking for the specified tunnelling current. If no current was found, the tip would pull back and the sample moved one step closer on the louse. This would continue until a tunnelling current was established.

The control of the STM was done via an Omicron STM control unit, interfaced to a Hewlett Packard 425 workstation.

The STM control software could also be used to analyse images. Distances and heights could be measured and a number of smoothing and filtering options were available.

During the course of scanning there were frequent tip changes which resulted in a line or lines of noise across an otherwise good image. These could be eliminated or reduced depending on how bad the noise is by filters in the image processing software. However, as well as removing noise they could also reduce the contrast of real features. Caution was required in all aspects of image manipulation.

2.5.3 Alanine sublimation doser

The alanine sublimation doser, presented in Figure 2.21, consisted of an electrical feedthrough flange containing two copper power (20 A) electrodes and two thermocouple electrodes, one in chromel and the other in alumel. Stainless steel barrel connectors were attached to the top of each copper electrode. One barrel connector held a small glass sample tube (ca. 2 mm bore) in which the alanine powder was placed; around the glass tube was evenly wrapped a 0.25 mm tantalum filament wire. Each side of this wire was attached to each barrel connector. Due to the low vapour pressure of the alanine sample the glass tube was resistively heated. The temperature was measured by a thermocouple attached to the end of the tube. A current of 0.85 A was sufficient to raise the temperature to above 90 °C. This doser formed part of a fourway cross, which was directly attached to the main chamber via a gate valve. The fourway cross was differentially pumped with a Varian turbo molecular pump (70 l / s) which allowed the sample to be baked independently from the rest of the chamber. The dosing line typically reached a base pressure of 5×10^{-9} mbar. A sharp pressure increase was noted when the sample was heated above ca. 90 °C, which was attributed to the sublimation of the sample. On opening the small gate valve the gaseous composition was analysed using a quadrupole mass spectrometer situated in the main chamber. It was believed the sample was successfully dosed when some characteristic sample cracking patterns was seen on the mass spectrometer. During dosing, the pressure in the chamber was typically 1-2 $\times$ 10^{-9} mbar.

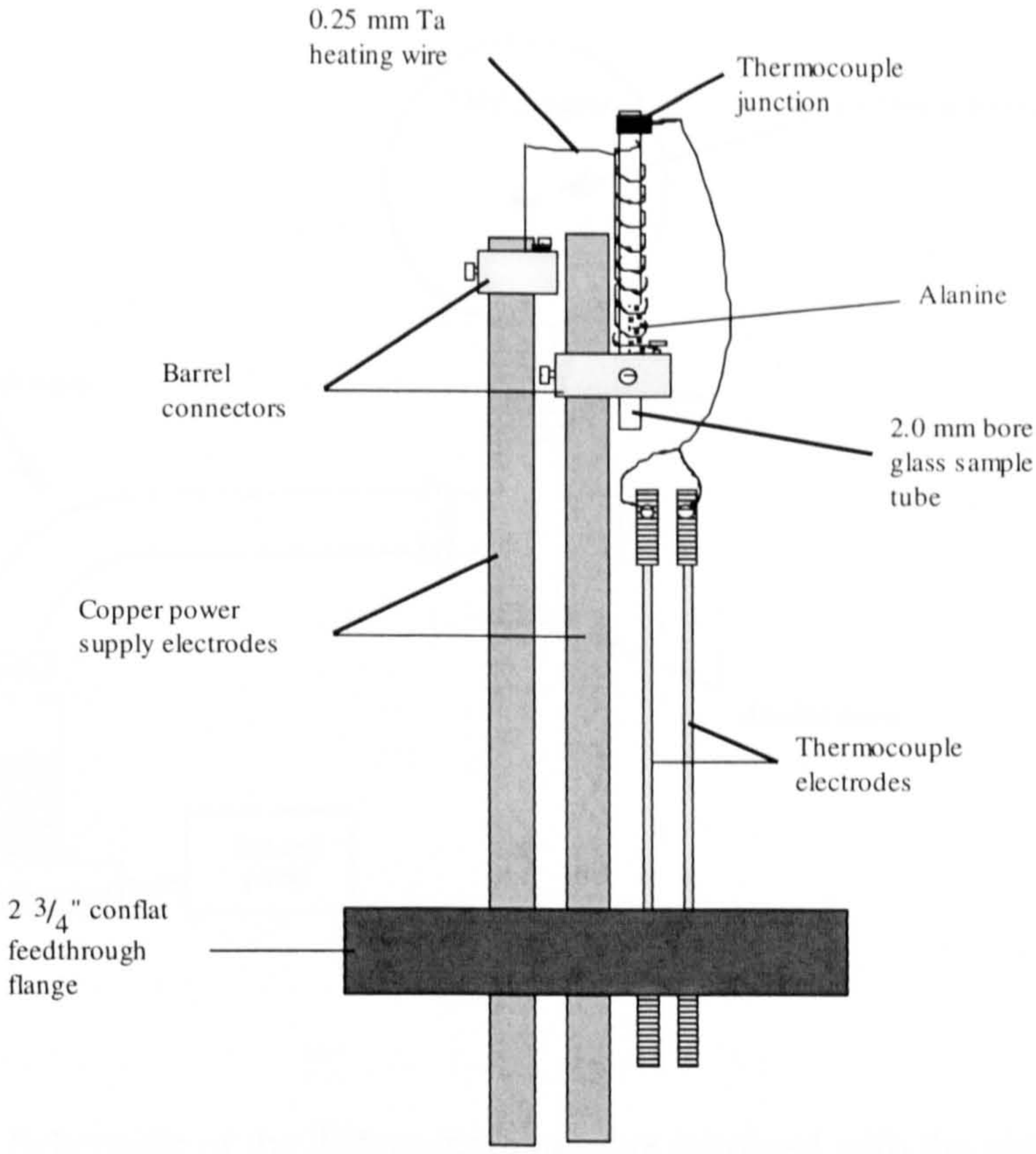

Figure 2.21: Schematic of the alanine sublimation doser.

This doser formed part of a fourway cross, which was directly bolted onto the main chamber at a port containing a gate valve. The fourway cross was differentially pumped with a Varian turbo molecular pump (70 l sec^{-1}) which allowed the sample to be baked independently from the rest of the chamber, as shown in Figure 2.22. The dosing line typically reached a base pressure of $5x10^{-9}$ mbar.

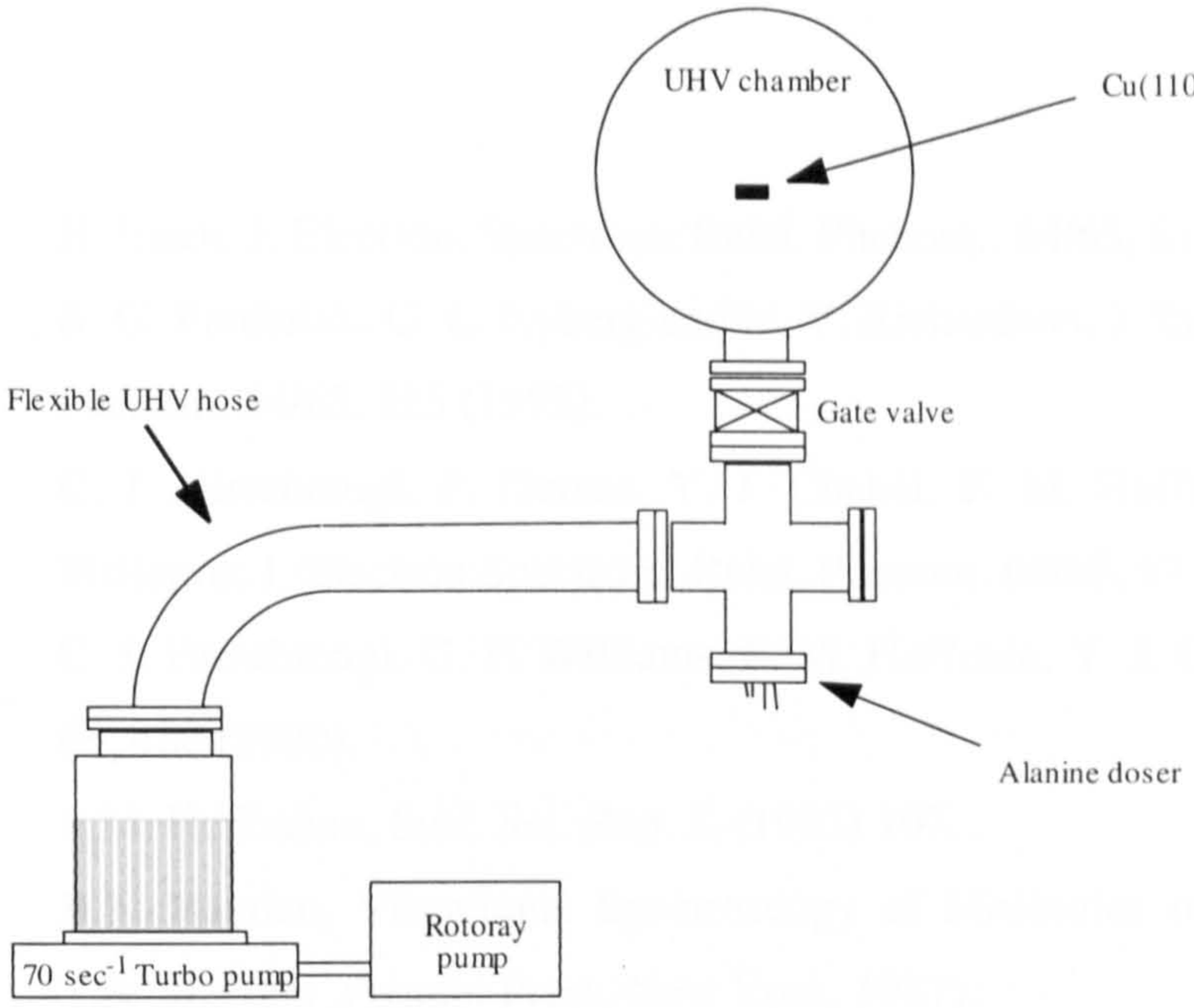

Figure 2.22: Schematic of the differential pumping involved with the alanine sublimation doser.

References

[1] H. Ibach, J. Electron. Spectrosc. Relat. Phenom.. **64/65,** 819 (1993).

[2] B. G. Frederick, G. L. Nyberg and N. V. Richardson, J. Electron Spectrosc. Relat. Phenom. **64/65,** 825 (1993).

[3] C. J. Hirschmugl, P. Dumas, Y. J. Chabal, F. M. Hoffman, M. Sohren, G. P. Williams, J. Electron Spectrosc. Relat. Phenom. **64/65,** 67 (1993).

[4] C. J. Hirschmugl, G. P. Williams, F. M. Hoffman, Y. J. Chabal, Phys. Rev. Lett. **65,** 480 (1990).

[5] F.M. Hoffmann, Surf. Sci. Rep. **3**, (1983) 107.

[6] B.E. Hayden, Vibrational Spectroscopy of Molecules on Surfaces, (Yates and T.E. Mayden ,Plenum Press, New York, 1987).

[7] Y. J. Chabal, Surf. Sci. Rep. **8**, 214 (1988).

[8] P. Hollis, J. Pritchard, Prog. Surf. Sci. **19,** 275 (1985).

[9] A. M. Bradshaw, E. Schweiser, in Spectroscopy of surfaces, (Eds R. J. H. Clark and R. E. Hester, Wiley 1988).

[10] R. P. Eischens, S. A. Francis, W. A. Pilskin, J. Phys.Chem. 60 (1956) 194; R. P. Eischens and W. A. Pilskin, Advan. Catal. **10,** 1 (1958).

[11] N. G. Yaroslavsky, A. N. Terenin, Dokl. Akad. Nauk SSSR, **66,** 885 (1949).

[12] H. L. Pickering, H. C. Eckstrom, J. Phys.Chem. **63,** 51 (1959).

[13] S. A. Francis, A. H. Ellison, J. Opt. Sci. Am. **49,** 131 (1959).

[14] R. G. Greenler, J. Chem. Phys. **44**, 310 (1966).

[15] R. G. Greenler, J. Vac. Sci. Tech. **12**, 1410 (1975).

[16] R. G. Greenler, J. Chem. Phys. **50**, 1963 (1969).

[17] J. Pritchard, M. L. Sims, Trans. Faraday Soc. **66,** 427 (1970).

[18] G. Attard, C. Barnes, Surfaces, (Oxford University Press, Oxford New York Toronto, 1998).

[19] P. R. Griffiths, Transform Techniques in Chemistry, (Plenum Press, New York, 1978).

[20] R. J. Bell, Introductory Fourier Transform Spectroscopy, (Academic Press, London, 1972).

[21] J. Chamberlin, The Principles of Interferometric Spectroscopy, (Wiley-Interscience, Chichester, 1979).

[22] A. A. Michelson, Phil. Mag. Fifth Series 31 (1891) 256; A. A. Michelson, Phil. Mag. Fifth Series **34,** 280 (1892).

[23] P.W. Atkins, in Physical Chemistry, (Oxford University Press, 1986).

[24] G.W. Poling, J. Colloid Interface Sci. **34**, 265 (1970).

[25] P. Hollis, J. Pritchard, in Vibrational Spectroscopy of Adsorbates, Eds R.; F. Willis, Springer Series in Chemical Physics, vol 15, (Springer, Berlin, 1980).

[26] J.D.E. McIntyre, D.E. Aspnes, Surf. Sci. **24**, 417 (1971).

[27] R.W. Ditchburn, Light, (Blackie, London, 1952).

[28] E.A. Stratton, Electromagnetic Theory, (McGraw - Hill, New York, 1941).

[29] O.S. Heaven, Optical Properties of Thin Films, (Butterworths, London, 1955).

[30] J. W. Niemantsverdriet, Spectroscopy in Catalysis, (VCH Publishers, Germany, 1995).

[31] G. Binnig, H. Rohrer, Ch. Gerber, E. Weibel, Phys. Rev. Lett. **49**, 57 (1982).

[32] G. Binnig, H. Rohrer, Surf. Sci. **152/153**, 17 (1985).

[33] G. Binnig, H. Rohrer, Helv. Phys. Acta **55**, 726 (1982).

[34] Y. Kuk, P.J. Silverman, Rev. Sci. Instrum. **60**, 165 (1989).

[35] G. Binnig, H. Rohrer, IBM J. Res. Dev. **30**, 355 (1986).

[36] P.K. Hansma, J. Tersoff, J. Appl. Phys. **61**, R1 (1987).

[37] D.A. King and D.P. Woodruff; The chemical physics of solid surfaces and heterogeneous catalysis, volume 1 , Clean surfaces, (Elsevier Scientific Publishing Company, 1981).

[38] D.P. Woodr, T. A. Delchar, Modern Techniques of Surface Science, p 25 (Cambridge Solid State Science Series, 1994).

[39] R.L. Park and J.R. Madden, Surf. Sci. **11** (1968).

[40] P. A. Redhead, Vacuum **12**, 203 (1962).

[41] G. Carter, Vacuum **12**, 245 (1962).

[42] L. Apker, Ind. Eng. Chem. **40**, 846 (1948).

[43] D. A. King, Surf. Sci. **47**, 384 (1975).

[44] M. W. Robert, C. S. McKee, Chemistry of the Metal Gas Interface, (Clarendon Press, Oxford, 1975).

Chapter Three

Adsorption of the Enantiomers of Alanine on Ni (110)

3.1 Introduction

Alanine is the simplest chiral α-amino acid, which presents two enantiomers, (S)- and (R)-alanine, or (L)- and (D)- respectively, which are non-superimposable mirror images, as shown in Figure 3.1. The (S)-alanine enantiomer is the natural compound. The molecule contains both an amino and a carboxylic acid functional group which are basic and acidic respectively, resulting in the compound having an amphoteric nature.

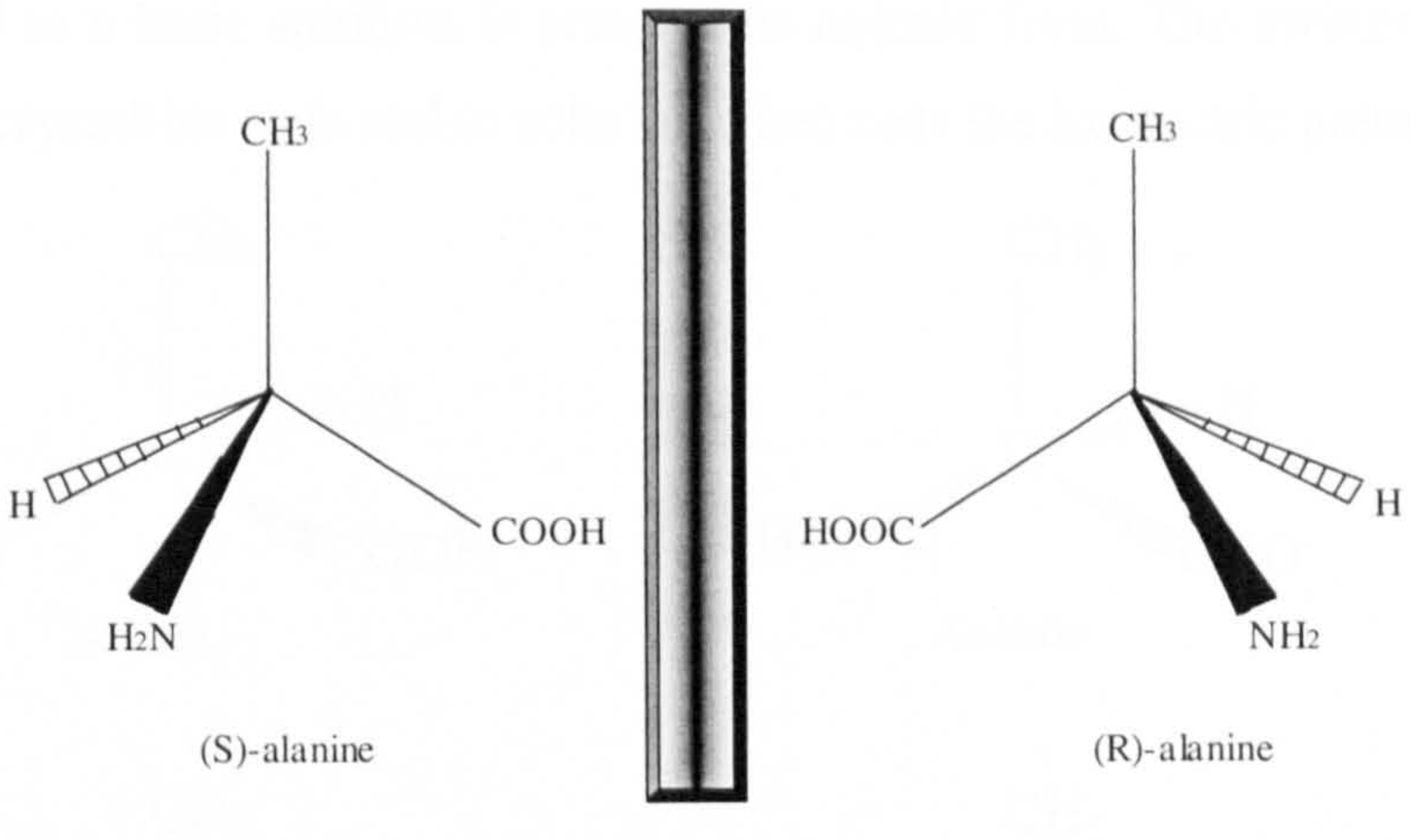

Figure 3.1: Two enantiomers of the alanine molecule: (S)-alanine and (R)-alanine.

The aim of this chapter is to study the adsorption of the enantiomers of alanine on Ni (110), more exactly the chemical form(s) of alanine on adsorption, its bonding and orientation, and the organisation of the molecules on the surface.

3.1.1. Chemical forms of alanine

This section describes the different chemical forms that can be taken by the alanine molecule. It will be important to recognise the chemical form present on adsorption on the surface; that is why this section includes the vibrational analysis of each of these different species.

Alanine is an amino acid, which as for all other amino acids, can exist in four different forms, presented in Figure 3.2 for the (S)-alanine enantiomer. The molecule can be in the neutral form (molecular form) [1-7], in the anionic form (with the COOH group deprotonated to give COO^-) [8-11], in the cationic form (with the NH_2 group protonated to give NH_3^+) [9-12] and in the zwitterionic form (with both NH_3^+ and COO^- groups) [9-24]. The molecule adapts its form to its immediate environment. The neutral form is present in the gas phase. The anionic and cationic forms are present in solutions, and their presence depend on the pH of the solution; in an acidic solution, the molecule presents its cationic form and in a basic solution, it presents its anionic form. The zwitterionic form dominates in the crystalline state and in solution when near the isoelectric point.

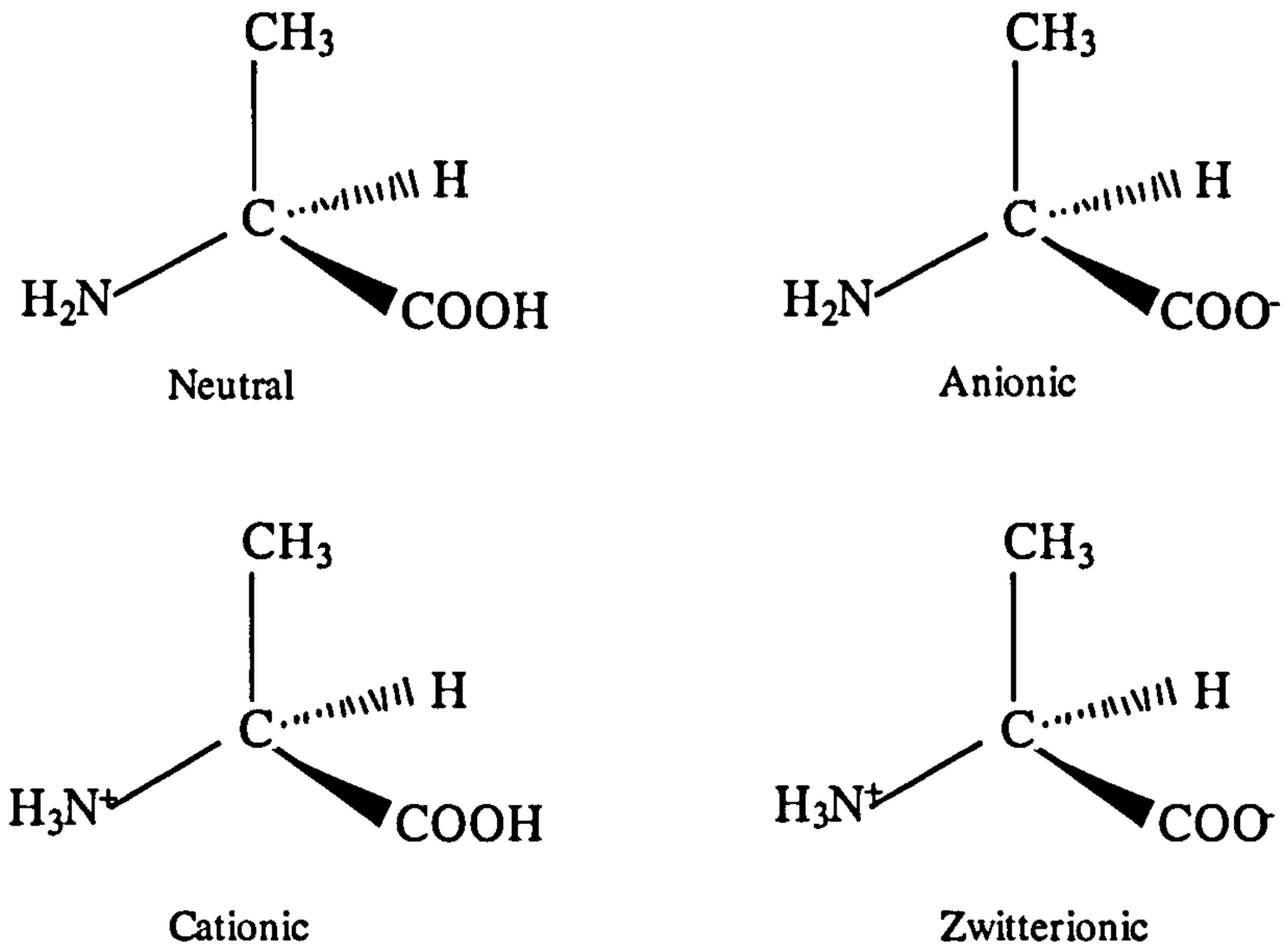

Figure 3.2: Three-dimensional representation of the possible structures taken by (S)-alanine.

3.1.1.1 (S)-alanine in the neutral form

In the gas phase [1-7], alanine is believed to exist in its neutral molecular form since intermolecular interactions have no effect. However, some authors [2, 5-7] suggest the coexistence of several gaseous conformers of (S)-alanine. Csaszar *et al* [2] suggest that the relative energies of the (S)-alanine conformers are determined by the interplay of several types of intramolecular hydrogen-bonds that can be formed, such as the (cis) versus (trans) arrangement of the carboxylic functional group, the steric strain and the repulsion of lone electron pairs on the N and O atoms. Csaszar *et al* predict two possible conformers of (S)-alanine [2], presented in Figure 3.3.

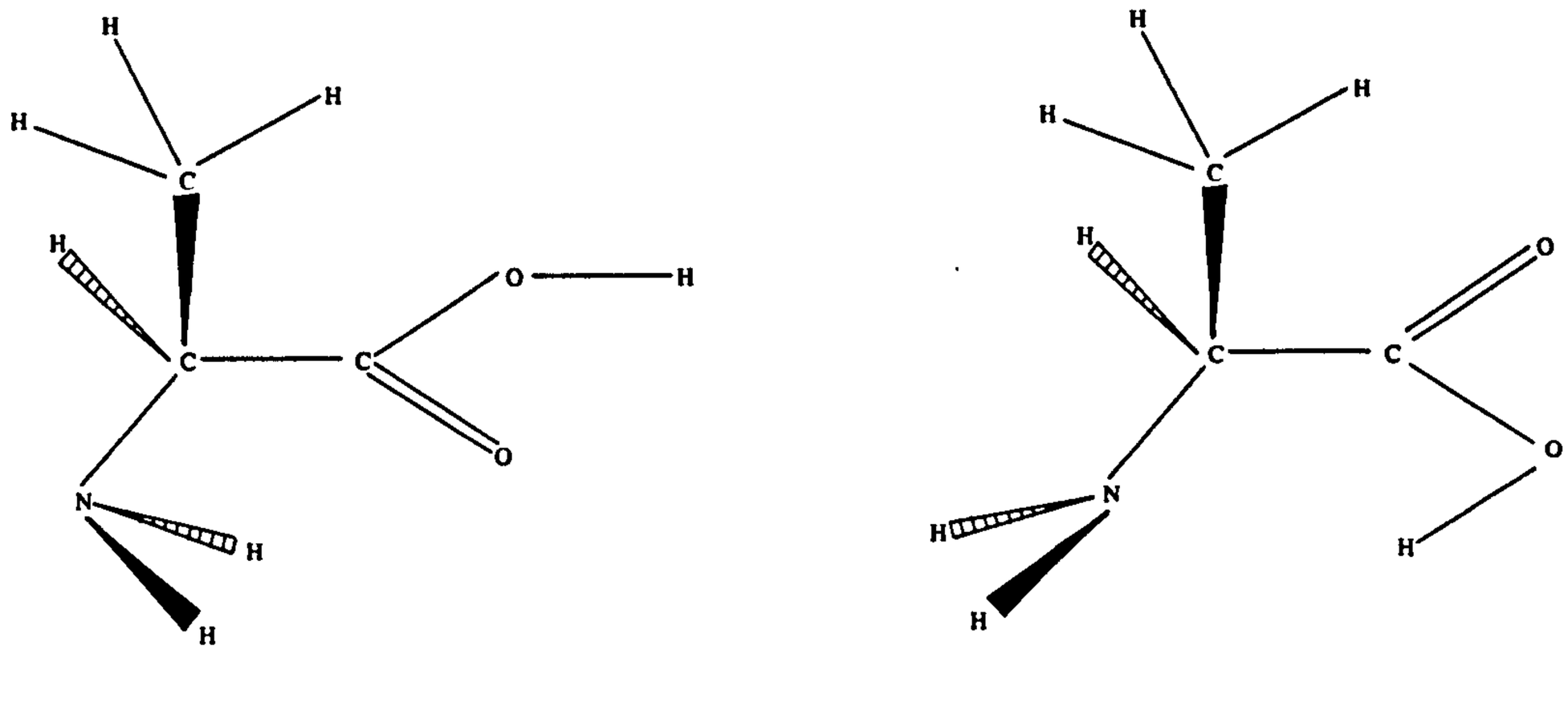

Conformer I Conformer II

Figure 3.3: Two conformers of gaseous (S)-alanine [2].

Conformer I has a configuration in which the hydrogens of the amino group are both "hydrogen bonded" to the carbonyl oxygen with the hydroxyl hydrogen in the normal (cis) configuration with respect to the carbonyl group. Conformer II involves a hydrogen bond between the lone pair of electrons of the amino group and the hydrogen atom of the hydroxyl group; this results in a (trans) configuration of the latter with respect to the carbonyl group. The conformer I is the most stable conformer since it is the lowest energy configuration.

Rosado *et al* [25], using matrix isolation infrared spectroscopy (MI-IR), and Cao *et al* [26] using and a technique involving sample dissolution, spray and deposition (DSD), have studied the vibrational frequencies of alanine in the neutral form. Their assignments are presented in Table 3.1.

MI-IR method [25] Wavenumbers (cm^{-1}) (S)-alanine	DSD method [26] Wavenumbers (cm^{-1}) Racemic mixture	Assignments
3560, **3555**, 3546	3587	ν (OH)
n. o.	3465	ν_{as} (NH_2)
2999, **2981**	3077	ν_{as} (CH_3)
2940	3027	ν_{as} (CH_3)
2886	2919	ν (CH)
n. o.	2830	ν_s (CH_3)
1791, 1787, **1774**, 1771	1747	ν (C=O)
1642, **1622**	1636	δ (NH_2)
1460	1470	δ_{as} (CH_3)
1454	1421	δ_{as} (CH_3)
1408	1377	δ (CH)
1386, **1376**	n.o.	δ_s (CH_3)
1368, **1335**	1340	δ (CH)
n. o.		tw (NH_2)
1215, **1206**	1295	δ (COH)
1153	1192	δ (C-O); [ν (C-O)][a]
1117, **1110**, 1105	1111	ν (CN)
1064	1051	ρ (CH_3)
1037, 1002	971	ρ (CH_3)
	916	ν (C-CH_3)
925, **920**	841	ω (NH_2)
852, 826		ν (C-CH_3)
805, **782**	810	ν (C-COOH)

Table 3.1: Vibrational frequencies of neutral forms of α-alanine [25-26].

For one band, assignment given in square brackets has been sought from [a]Ref. [25]; the most intense band of a group of bands assigned to the same vibration is shown in bold

3.1.1.2 (S)-alanine in the zwitterionic form

(S)-alanine exists in the zwitterionic form in the solid crystalline phase [13-22] or in liquid when near the isoelectric point [8-12, 23-24]. The presence in the molecule of two polar groups leads to very strong intermolecular electrostatic attractions within a crystal lattice. The results of some studies done by X-ray [13-14] and neutron [15] diffraction show that the molecules interact to form hydrogen-bonded columns in large well-ordered crystals [16], as shown in Figure 3.4.

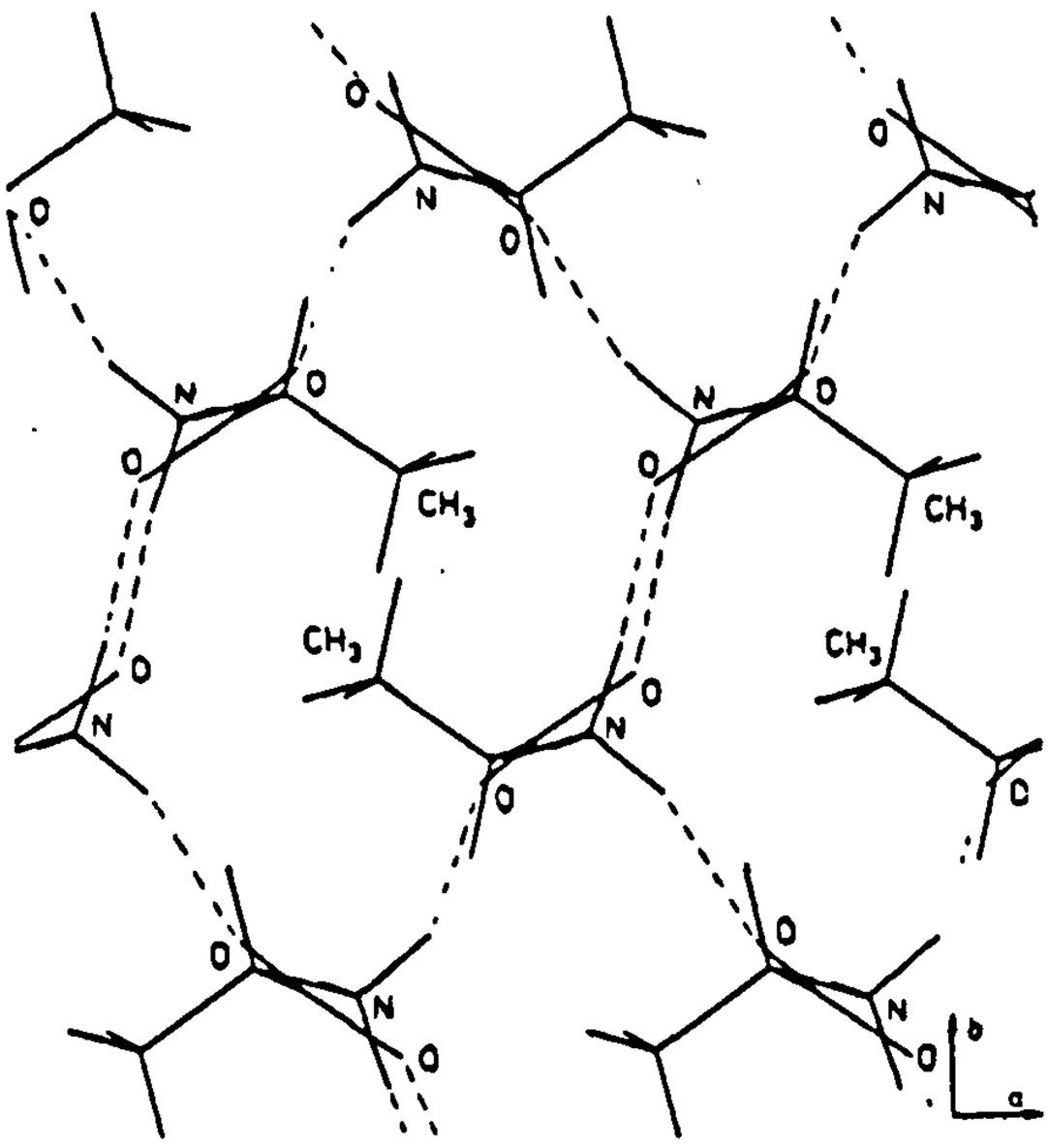

Figure 3.4: Diagram of the (S)-alanine crystal [15] (Dashed lines represent H-bonds).

Studies involving the infrared spectra of zwitterionic alanine in both the solid [12, 17-22] and liquid phases [12, 23, 24] have been reported in the literature. The fact that the (S)-alanine molecule is in the zwitterionic form involves some major changes in the infrared spectra compared to when it is in neutral form. The bands associated with the carboxylic acid group -COOH vanish being replaced by the three bands of the carboxylate group – COO^- [27]. In this carboxylate ion, the prevalent conjugation, Figure 3.5(a) and 3.5(b), makes the two C-O bond orders equal, Figure 3.5(c), as well as the interatomic distances (1.27 A). These distances are intermediate between the length of a simple C – O bond and a C = O double bond.

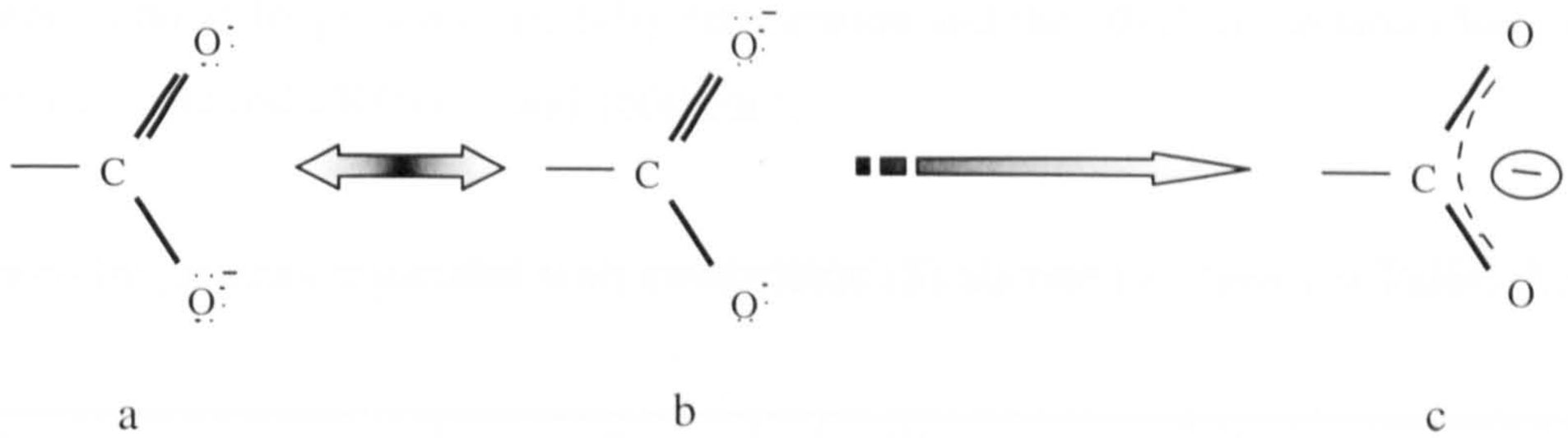

Figure 3.5: Schematic representation of a carboxylate ion.

The carboxylate group behaves as a unit and the frequency follows this behaviour. The $-COO^-$ group (carboxylate ion) has an asymmetric stretching vibration $\nu_{as}(COO^-)$ with a frequency at ~1600 cm^{-1}. This band is accompanied by a band representing the symmetric stretching vibration $\nu_s(COO^-)$ whose frequency is at ~ 1400 cm^{-1} and by a scissoring deformation δ_{sc} (OCO) around 700 cm^{-1} as presented in Figure 3.6 [28].

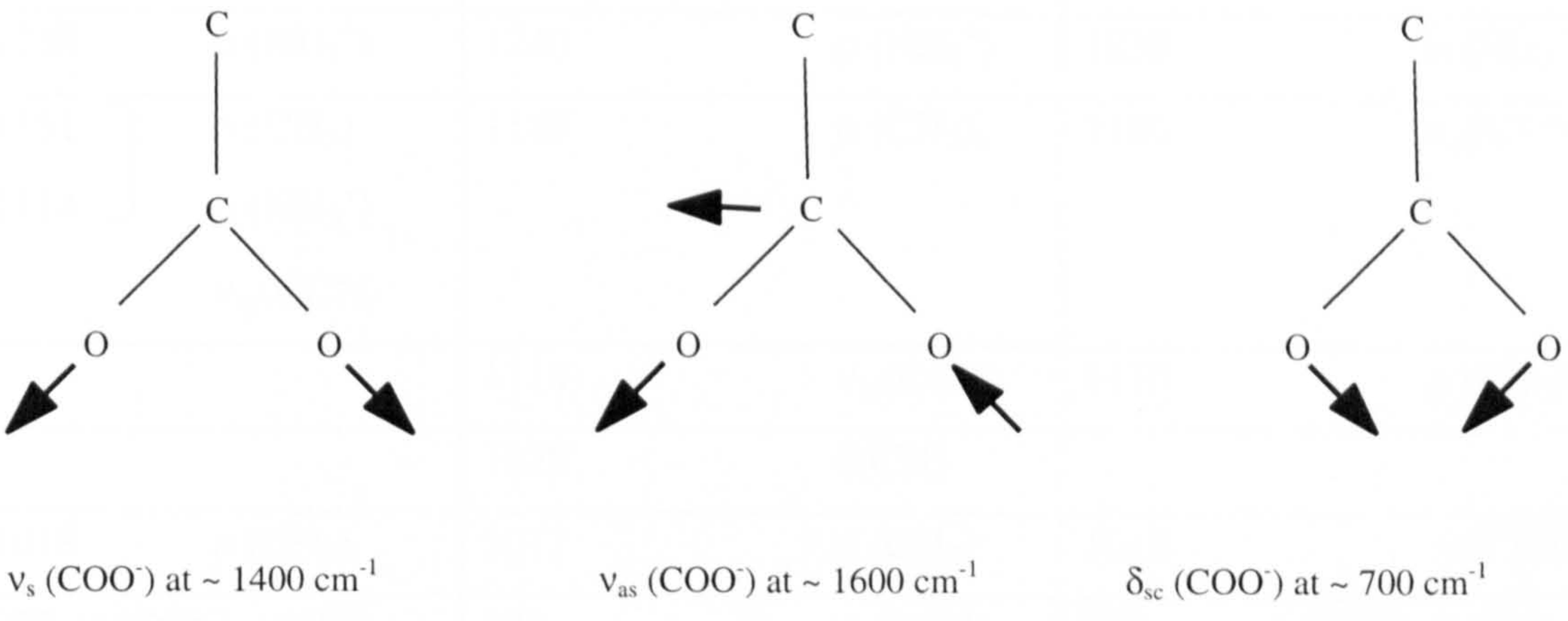

Figure 3.6: A schematic illustration of the symmetric and asymmetric vibrational modes associated with a carboxylate group.

The main difference observed between the spectra of the zwitterionic species and those obtained for the neutral form of alanine is the absence of the characteristic ν (C=O) stretch at about1700-1800 cm^{-1}.

The second major change is the appearance of the bands characteristic of the NH_3^+ group and the disappearance of the bands characteristic of the NH_2 group. However, these are

at rather similar frequencies: the NH_2 deformation and the NH_3^+ deformation have their frequencies around 1500 cm^{-1} and 1600 cm^{-1}.

Infrared frequencies associated with zwitterionic (S)-alanine are shown in Tables 3.2 and 3.3.

Frequency (cm^{-1}) [18]		Frequency (cm^{-1}) [19]		Frequency (cm^{-1}) [21]	
1623	δ_{as} (NH_3^+)	1621	δ_{as} (NH_3^+)	1615	δ_{as} (NH_3^+)
1597	ν_{as} (COO^-)	1591	ν_{as} (COO^-)	1590	ν_{as} (COO^-)
1534	δ_s (NH_3^+)	1524	δ_s (NH_3^+)	1505	δ_{as} (NH_3^+)
1451	δ_{as} (CH_3)	1451	δ_{as} (CH_3)	1450	δ_{as} (CH_3)
1411	ν_s (COO^-)	1411	ν_s (COO^-)	1404	ν_s (COO^-)
1356	δ_s (CH_3)	1354	δ_s (CH_3)	1360	δ_s (CH_3)
1308	δ(CH),	1309	δ(CH),	1310	δ_{sc} (NCH)
1238	ρ (NH_3^+)	1240	ρ (NH_3^+)	1235	ρ (NH_3^+)
1151 1114	ρ (CH_3) ρ (NH_3^+) ν_{as}(CCN)	1149	ρ (CH_3),	1150	ν_{as}(CCN)
		1114	ν_{as}(CCN)	1110	ρ (CH_3)
		1029	δ(CH)		
1018	ρ (CH_3)	1017	ρ (CH_3)	1018	ν_s(CCN)
923	ν_s(CCN)- ν(CC)	920	ν_s(CCN)	920	ν_s(CCN)+ ν(CC)
854	ν_s(CCN) + ν(CC)	851	ν_s(CCN)	.844	ν_s(CCN) + ν(CC)
773	δ(COO^-)	771	δ(COO^-)	769	w (COO^-)

Table 3.2: Infrared absorption bands and their assignments for crystalline (S)-alanine.

Frequency (cm^{-1}) Assignments [12]	Frequency (cm^{-1}) Assignments [23]	Frequency (cm^{-1}) Assignments [24]
	3080 ν_a (NH_3^+)	
	3020 ν_s (NH_3^+)	
	3003 ν_{as} (CH_3)	
	2993 ν_{as} (CH_3	
	2962 ν_s (CH)	
	2949 ν_s (CH_3)	
	2893 $2 \times \delta$ (CH_3)	
	1645 δ_{as} (NH_3^+)	
1623 δ_{as} (NH_3^+)	1625 δ_{as} (NH_3^+)	
1597 ν_{as} (COO^-)	1607 ν_{as} (COO^-)	1613 ν_{as} (COO^-) + ν_{as} (NH_3^+)
1534 δ_s (NH_3^+)	1498 δ_s (NH_3^+)	1503 δ_s (NH_3^+) + δ_{as} (CH_3) + ν_{as} (COO^-)
1451 δ_{as} (CH_3)	1459 δ_{as} (CH_3)	1457 δ_{as} (CH_3) + δ (CH)
1411 ν_s (COO^-)	1410 ν_s (COO^-)	1412 ν_s (COO^-) + δ_s (CH_3) + δ (CH) + δ_{as} (CC*C) + ρ (NH_3^+)
1356 δ_s (CH_3)	1375 δ_s (CH_3)	1374 δ_s (CH_3) + δ (CH) + ν_s (COO^-) + δ_s (NH_3^+) + δ_s (CC*C)
	1351 δ (CH)	1352 δ (CH) + ρ (NH_3^+)+ ρ (CH_3) + ν_s (COO^-)
1308 δ (CH)	1301 δ (CH)	1302 δ (CH) + ρ (NH_3^+) + ρ (CH_3) + ν_s (COO^-)
1238 ρ (NH_3^+)	1220 ρ (NH_3^+)	1217 ρ (NH_3^+) + ρ (CH_3) + δ (CH) + δ (CCN) + ν (C-COO^-)
1151 ρ (NH_3^+) 1114 ρ (CH_3) 1018 ν_{as} (CCN)	1145 ρ (NH_3^+)	1139 δ (CH) + ρ (NH_3^+) + ρ (CH_3) + w (COO^-) + δ (CC*C) + ν (CN)
	1110 ν_{as} (CCN) ρ (NH_3^+)	1113 δ (CH) + ρ (NH_3^+) + ρ (CH_3) + δ_{as} (CCN)
	1001 ν (C-COO^-)	1003 ρ (NH_3^+) + ρ (CH_3) + δ (CH)

	995 ρ (CH_3)	
923 [ν (CCN)- ν (CC)]	922 ρ (CH_3)	922 ν_{as} (^-O_2CCN) + δ (COO^-) + ρ (NH_3^+) + ρ (CH_3)
854 ν_s (CCN)	850 ν_s (CCN)	848 w (COO^-) + δ (COO^-) + ρ ($HCCO_2^-$) + ρ (NH_3^+) + ρ (CH_3)
773	775	781 w (COO^-) + δ (COO^-) + ν_{as} (CCN) + ρ ($HCCO_2^-$) + ρ (CH_3) + δ (CH)

Table 3.3: Summary of vibrational frequencies and assignments for zwitterionic (S)-alanine in liquid phase.

3.1.1.3 (S)-alanine in the cationic and anionic form

In solution, the form of the molecule of (S)-alanine depends on the pH. In an acidic solution, the molecule presents its cationic form [9-12]; in a basic solution [8-11], the (S)-alanine presents its anionic form. Table 3.4 gives the infrared and Raman vibrational frequencies of cationic alanine where the spectrum was recorded at pH 1 and anionic alanine where the spectrum was recorded at pH 12.

Cationic alanine		Anionic alanine		Assignments
[17][a]	[16][b]	[17][a]	[16][b]	[17]
1735 ss	1726			ν (C=O)
1600 sh				$\delta_{as}(NH_3^+)$
		1575 ss		$\nu_{as}(COO^-)$
1545 sb				$\delta_s(NH_3^+)$
1480 ms	1458	1475 ms	1455	$\delta_{as}(CH_3)$
		1420 ss	1413	$\nu_s(COO^-)$
1340 ms	1363	1375 ms	1359	$\delta_s(CH_3)$
	1321	1300 ws		δ(CH)
1265 ss				ν (C-O) + δ_s(O-H)
		1240 ws		
1225 sh				ρ (NH_3^+)

[a] Frequencies taken from Raman spectra of pure (S)-alanine [b] Frequencies taken from infrared spectra of a racemic mixture of (SR)-alanine

Table 3.4: Vibrational frequencies and band assignments of Raman and infrared data for anionic and cationic alanine.

3.1.2. Studies of alanine adsorption

There have been several studies concerning the adsorption of alanine from aqueous solution onto metal surfaces, for example, Pt (110) and Pt (100) polished electrodes [29], evaporated polycrystalline copper films with preferred (111) orientation [30], polycrystalline silver foil [31], colloid silver [32]. The studies of interest in this chapter consists of the adsorption of alanine on copper and nickel.

3.1.2.1 Copper

These studies concern the adsorption of alanine on different single well-defined copper single crystal surfaces, Cu (111), Cu (100) and Cu (110). Studies on the latter surface are very complete and supply some answers to the questions of bonding, orientation and organisation of the alanine molecules on the copper surfaces.

Atansasoska *et al* [33] conducted some experiments of the adsorption of (S)-alanine on Cu (111) and Cu (100) using Low Energy Electron Diffraction (LEED).

On Cu (111), the LEED suggested that (S)-alanine adsorbed into an ordered ($2\sqrt{13} \times 2\sqrt{13}$) R13°40' structure at a temperature of 435 K. The size of the unit cell, which was found to be (18.4 Å × 18.4 Å), suggested several molecules per unit cell. Figure 3.7 shows a schematic of one (S)-alanine molecule adsorbed on the surface along with its surface unit mesh. Atansasoska *et al* did not determine the position and orientation of the molecule on the surface. The drawn molecule, in Figure 3.7, is thus presented in an arbitrary position.

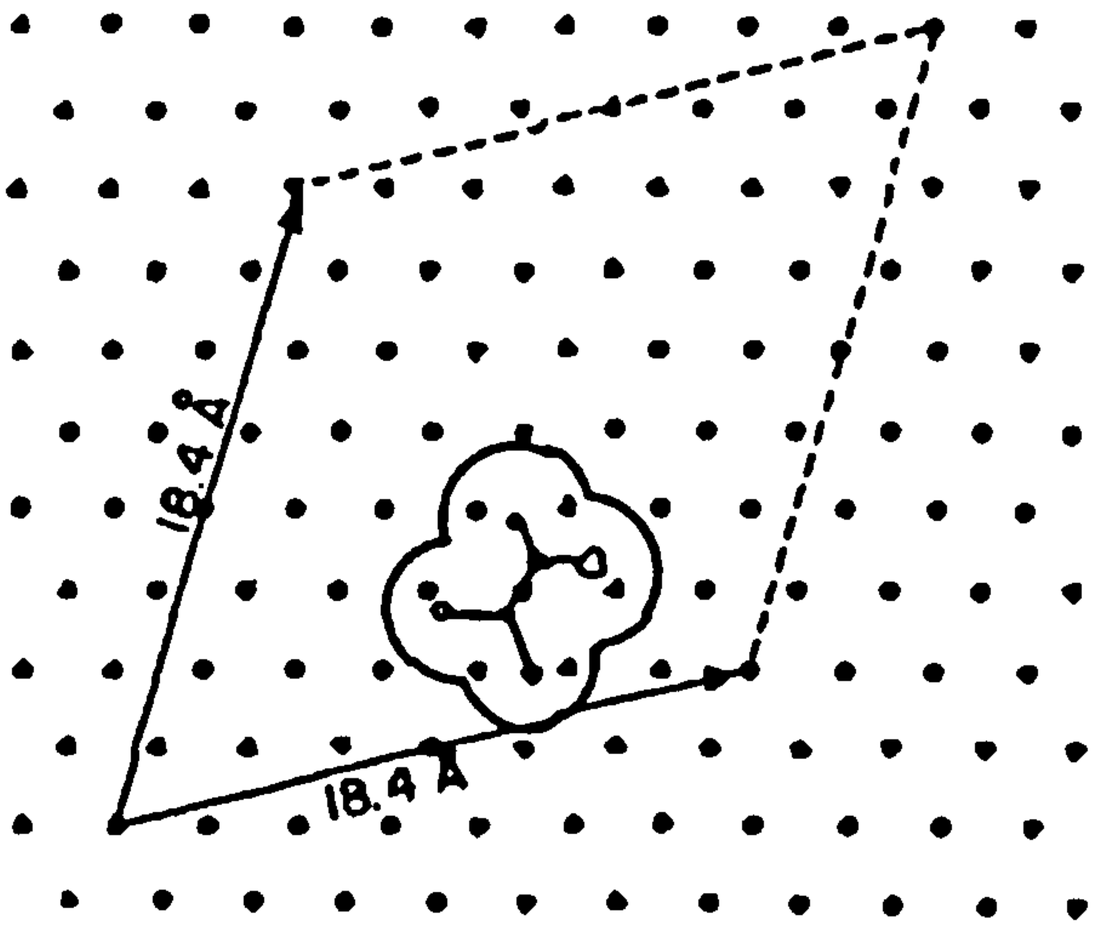

Figure 3.7: Real space unit mesh for the (S)-alanine monolayer structure superimposed on a Cu (111) surface model; the (S)-alanine size is also shown for comparison [33].

However, at room temperature, the LEED pattern was very poor suggesting the ordering in the adsorbed layer was poor whereas for temperature ≥ 435 K, the molecules started to form a well ordered structure.

On Cu(100), the LEED pattern obtained from the adsorption of (S)-alanine by Atansasoska et al [33] was very clear suggesting a well-ordered structure even at room temperature. A schematic of one (S)-alanine molecule adsorbed on the surface is presented in Figure 3.8. The unit mesh was found to be 5.81 Å × 5.81 Å.

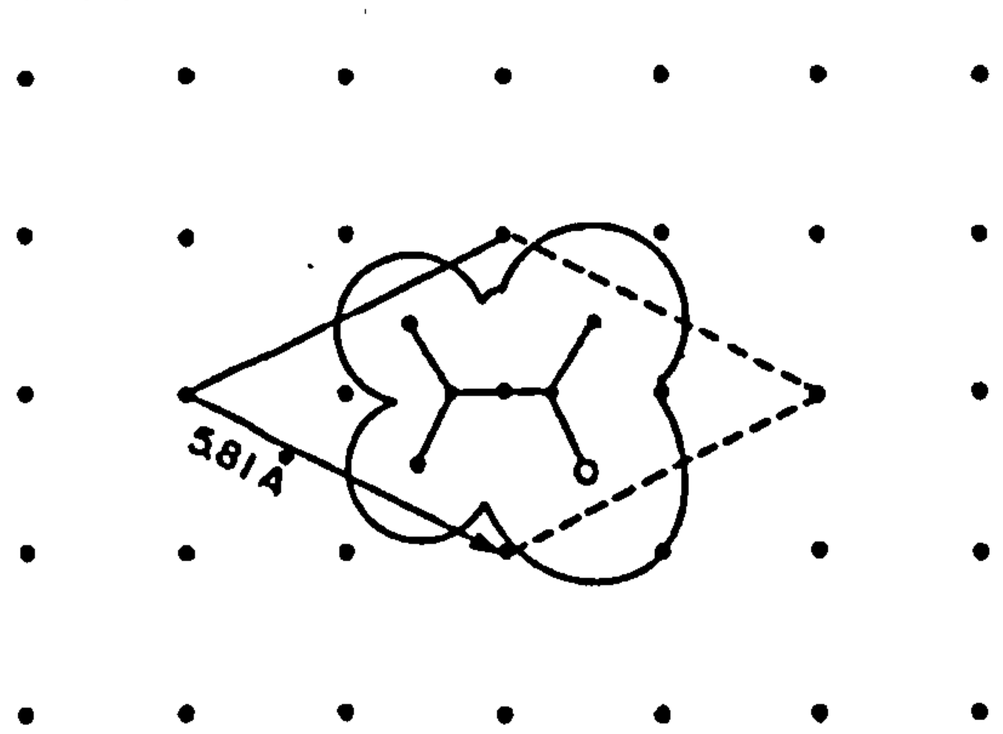

Figure 3.8: Real space unit mesh for the (S)-alanine monolayer structure superimposed on a Cu (100) surface model [33].

Zhao *et al* adsorbed (S)-alanine on Cu (001) and studied it using STM [34]. Figure 3.9 presents their proposed adsorption geometry showing the Cu (001)c(2 × 4)- structure on flat terraces and the Cu (3 1 1 7)1×1 structure on the steps.

In their model, they suggested that the two oxygen atoms and the nitrogen atom of the molecule were bonded to the copper substrate nearly at the atop site. The molecules were connected together by N – H- O hydrogen bonds, which formed chains in the [-1 3 0] direction. The authors favoured N – H $\cdots O^1$ hydrogen bonds rather than N – H $\cdots O^2$; this would induce the c(2 × 4) structure instead of a (2 × 2) structure. Zhao *et al* were able to image the adsorption of alanine at room temperature where the steps re-oriented to the [3 1 0] directions and some of the [3 1 0] steps bunched together to form {3 1 1 7} facets. Similarly as in the c(2 × 4) structure on the flat terraces, Zhao *et al* proposed that on the steps the molecules were connected by N – H $\cdots O^2$ hydrogen bonds to form chains in the [-1 3 0] direction (i.e. parallel to the steps).

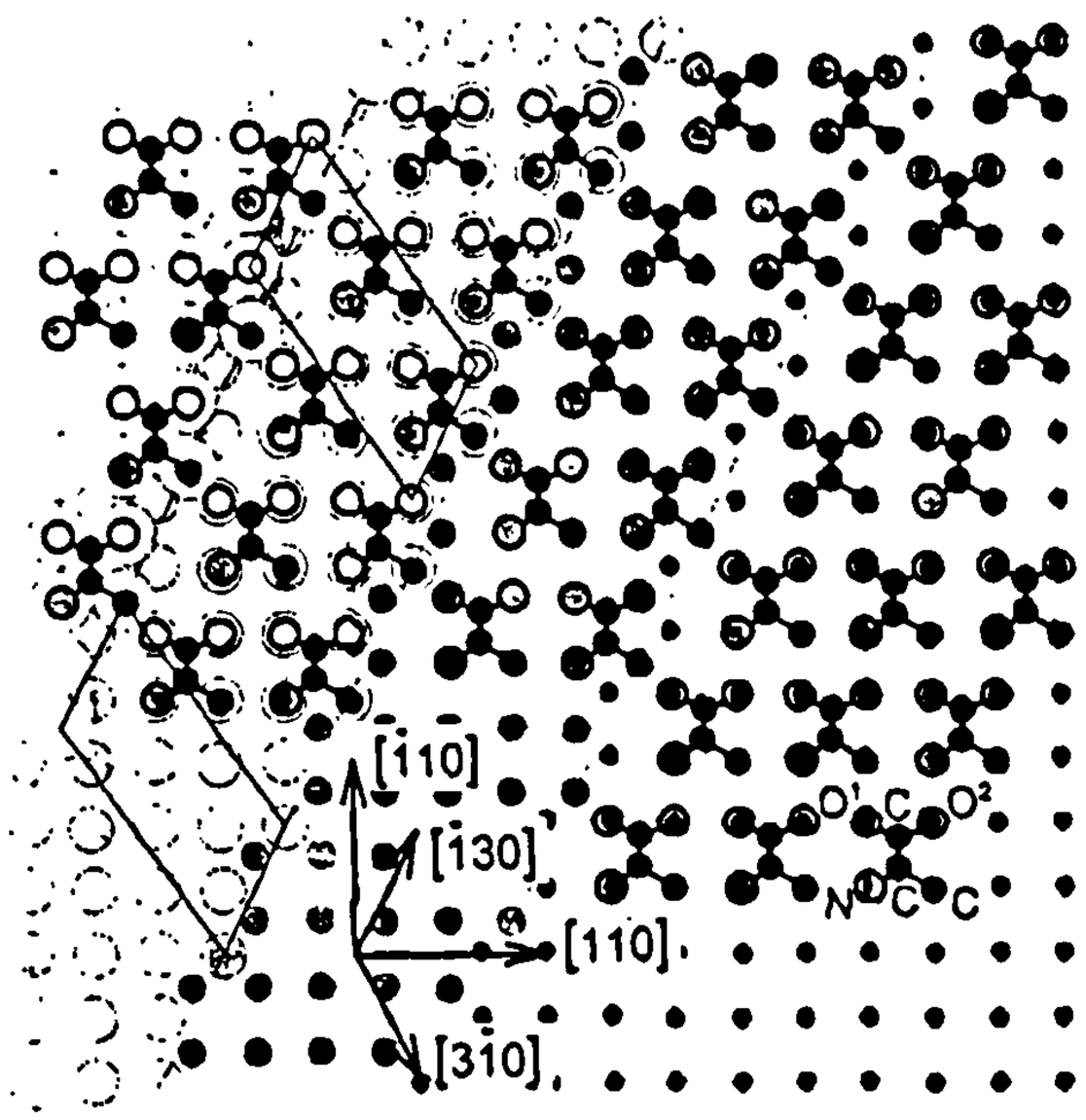

Figure 3.9: Schematic drawing showing the proposed adsorbed geometry of the alanine into Cu (001)c(2 × 4)- structure on flat terraces and Cu (3 1 1 7)1×1 structure on the steps. Two (3 1 1 7)1×1 unit cells are outlined [34]. (The N – H $\cdots O^1$ and N – H $\cdots O^2$ hydrogen bonded are marked in dashed line).

As discussed in Chapter One, the enantiomers of alanine on Cu (110) have also been investigated using the combination of RAIRS, LEED and STM [35, 36, 37]. Under certain conditions, the enantiomers of alanine on Cu (110) create extended chiral surfaces.

Figure 3.10 presents the successive RAIR spectra obtained during exposure of clean Cu (110) to (S)-alanine at 300 K with increasing time of exposure, as well as the bonding and orientation of the (S)-alanine molecule at low coverage (a) and high coverage (b). The assignments are given in Table 3.5.

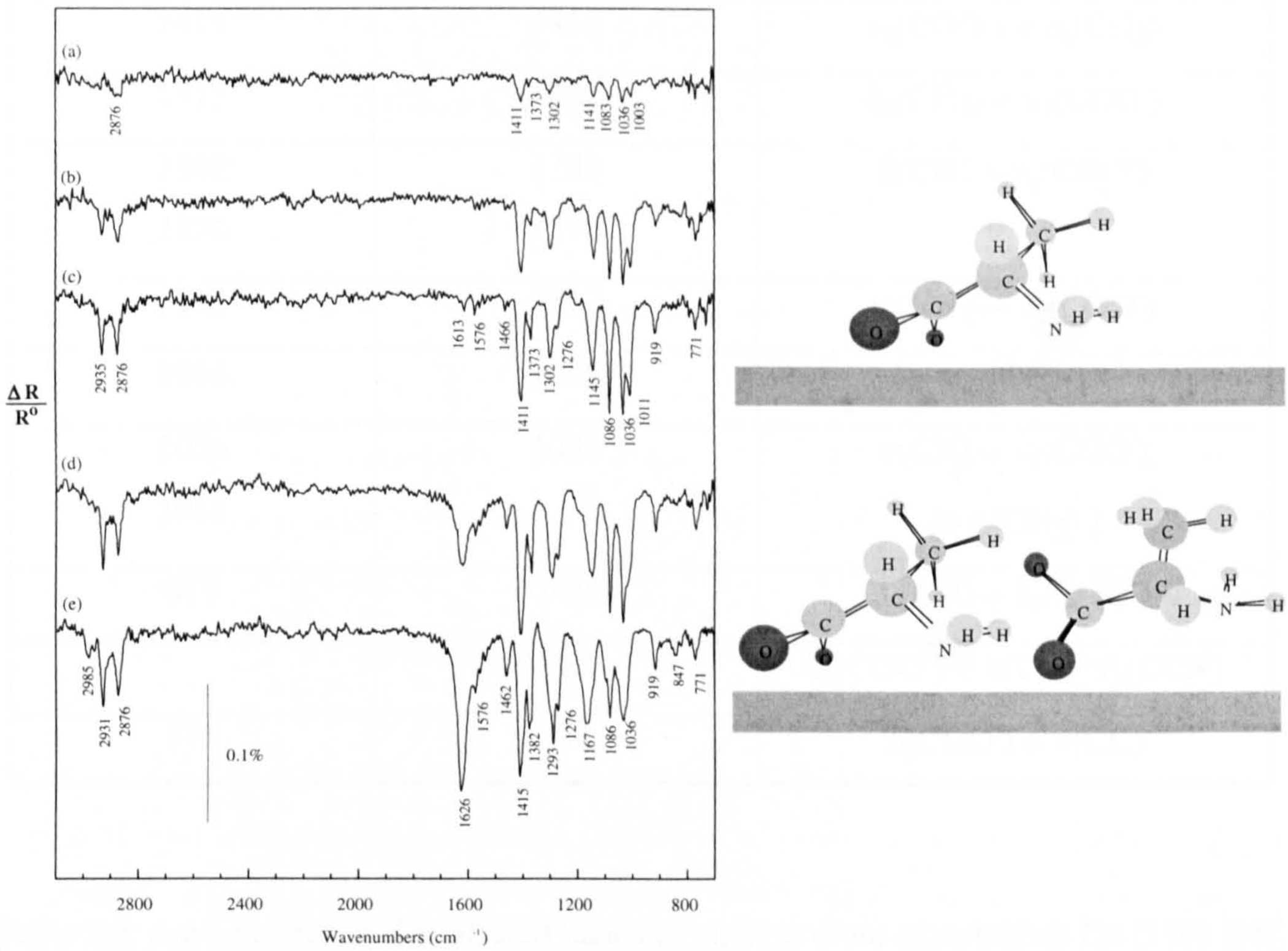

Figure 3.10: Successive RAIR spectra obtained during exposure of clean Cu (110) to (S)-alanine at 300 K when increasing time of exposure, as well as the bonding and orientation of the (S)-alanine molecule at low coverage (a) and high coverage (b) [35-36].

Low coverage	High coverage	Assignments
	2985	$\nu_a(CH_3)$
2935	2931	$\nu_s(CH_3)$
2876	2876	$2 \times \delta(CH_3)$
	1626	$\nu_{as}(COO^-)$
	1576	$\delta(NH_2)$
	1462	$\delta_{as}(CH_3)$
1411	1415	$\nu_s(COO^-) + \delta_s(CH_3)$
1373	1382	$\delta_s(CH_3) + \nu_s(COO^-)$
1302 1276	1293 1276	$\delta(CH) + \nu_s(COO^-)$
1145	1167	$\omega(NH_2) + \nu_s(COO^-)$
1086	1086	$\nu_{as}(CCN)$
1036 1011	1036	$\nu(CN) + \nu_s(COO^-)$ $[+ \rho(CH_3)]$
919	919	$\nu(CN) + \delta_s(COO^-)$
	847	$\delta_s(COO^-) + \nu(CN)/ \nu_s(CCN)$
771	771	$\delta(COO^-) + \nu(CC)$

Table 3.5: Assignments of the infrared bands of alanine when adsorbed on Cu (110) [35].

When adsorbed on Cu (110), at room temperature and above, the alanine molecules are in the anionic form. The low coverage phase is composed of alanine molecules bound to the surface via the amino group (NH_2) and both oxygens of the carboxylate group (COO^-) (bidentate form). The high coverage phase is composed of both molecules in the low coverage phase and others bound to the surface through only one oxygen of the COO^- group (monodentate form). A STM picture of the high coverage phase is presented in Figure 3.11.

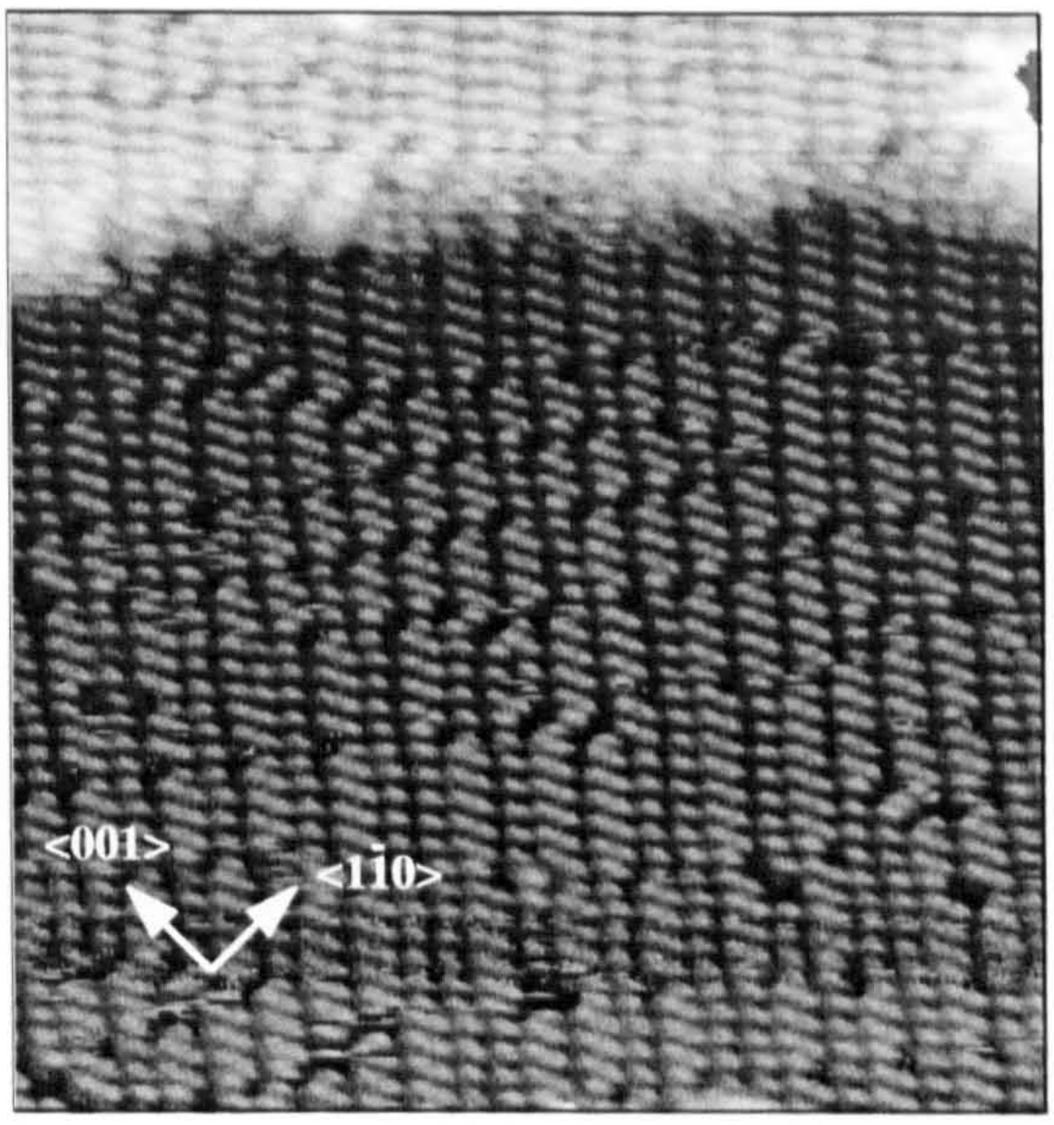

Figure 3.11: STM picture of a high coverage phase of (S)-alanine adsorbed on Cu (110), 140 Å × 140 Å [37].

As shown in Figure 3.11, the STM picture of the high coverage phase reveals that the (S)-alanine molecules organise themselves in a semi-ordered structure.

This high coverage phase is the most interesting phase in this study. When heated, it can lead to highly ordered phases. If the Cu (110) substrate is heated to 430 K, the LEED shows a (5 3 2 –2) structure given in Figure 3.12 (a). The STM picture of this structure shows the alanine molecule are arranged in packs of six molecules, presented in Figure 3.12 (b). The combination of RAIRS, LEED and STM results allowed the model, presented in Figure 3.12 (c) to be constructed. The pack of six molecules consists of molecules in both monodentate and bidentate orientations.

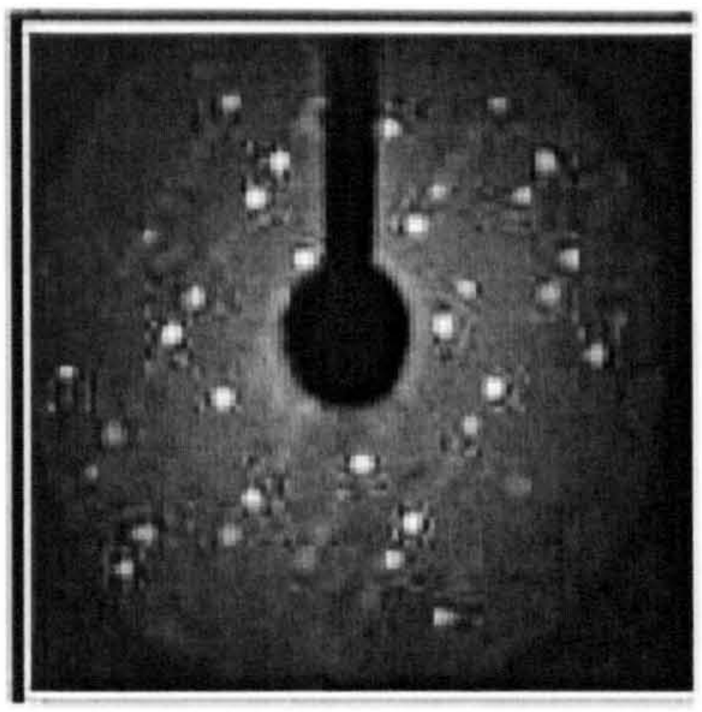

(a)

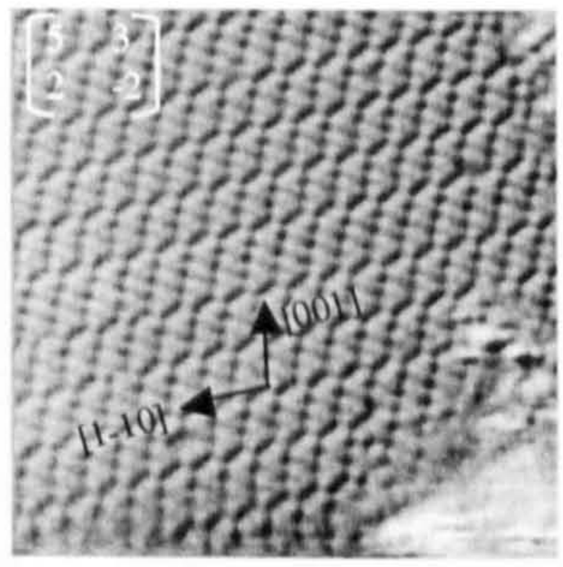

(b)

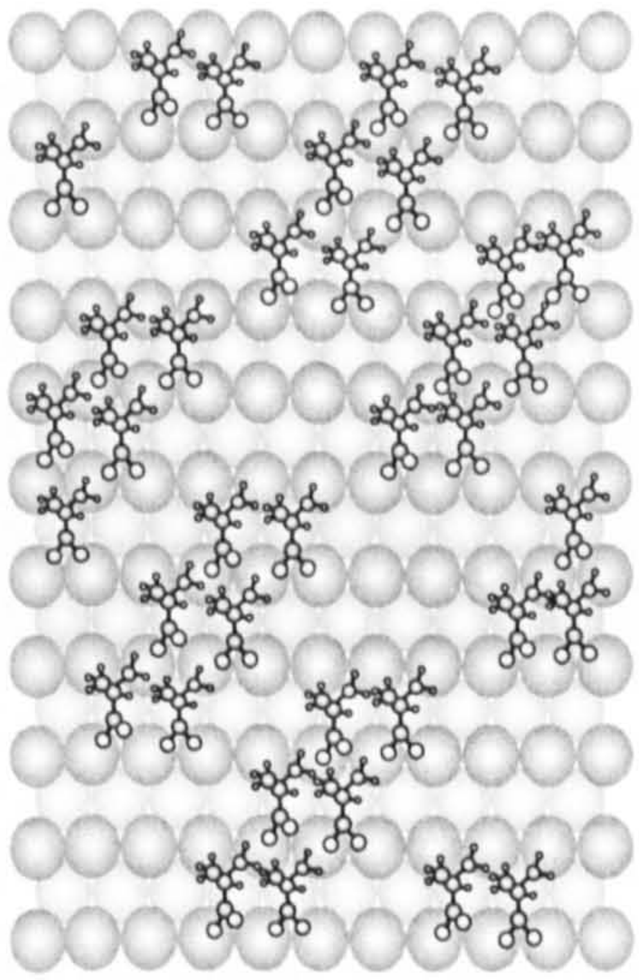

(c)

Figure 3.12: High coverage of (S)-alanine adsorbed on Cu (110) and annealed to 430 K; (a) LEED pattern of the (5 3 2 –2); (b) STM image, 100 Å × 100 Å; (c) model of the structure [37].

If annealed to 470 K, the alanine molecules re-organise into a (3 × 2) structure, shown by the LEED and proved by STM. Here only alanine molecules in the bidentate form are present.

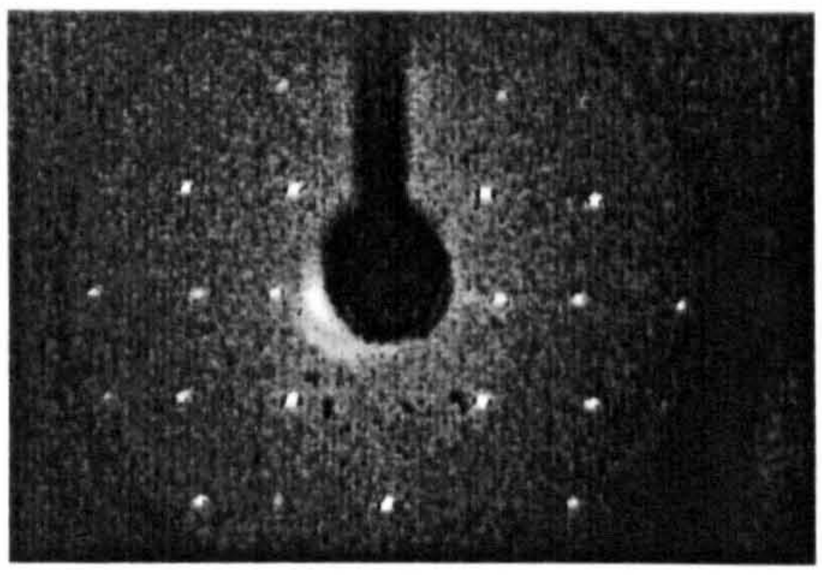

(a)

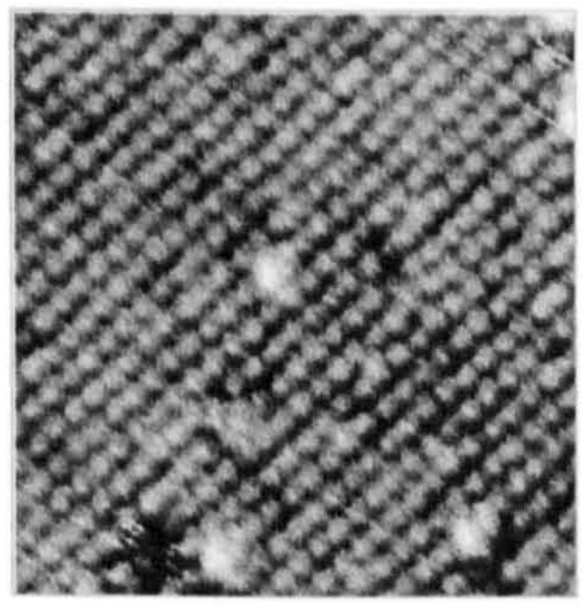

(b)

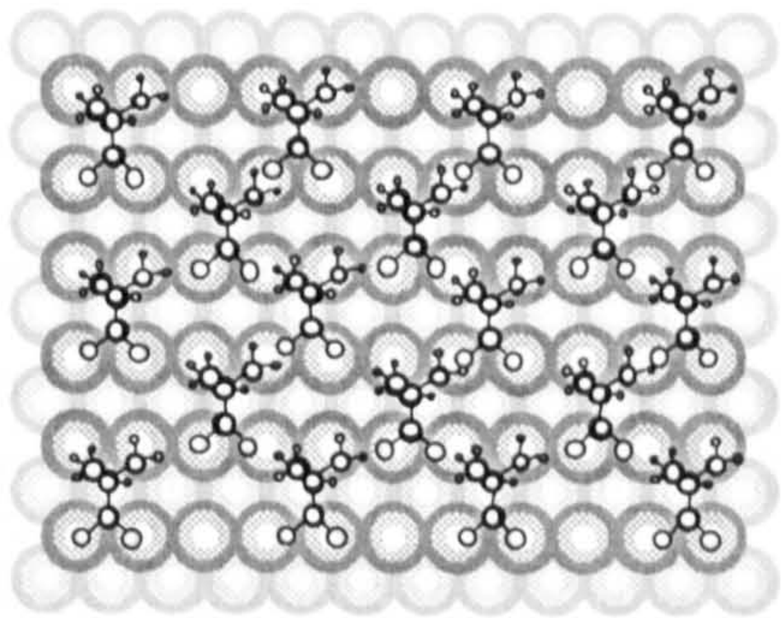

(c)

Figure 3.13: High coverage of (S)-alanine adsorbed on Cu (110) and annealed to 470 K; (a) LEED pattern of the (3×2) structure; (b) STM image, 100 Å $\times$ 100 Å; (c) model of the structure [37].

3.1.2.2 Nickel

A consideration of the studies which have involved the interaction between alanine molecules and the metal nickel should give an insight of what we should expect for our Ni (110) surface. Many studies have been done, involving nickel metal surfaces [38] and alanino-nickel complexes [39-45].

- ***Studies of nickel metal surfaces modified with optically active α-alanine from its aqueous solution [38]***

In this study, the infrared absorption spectra of thin films of α-alanine formed on pure nickel and Raney nickel surfaces have been measured. The orientations of the alanine molecules in the thin films were obtained. A change in the position of the molecule and a change in the chemical form of the molecule depending on the thin film have been indexed.

The first part considers bulk nickel plates modified at 5°C with 0.5 % aqueous solutions of (S)-alanine and (R)-alanine. Figure 3.14 shows the high-sensitivity reflection spectra obtained from bulk nickel plates modified with solutions of (a) (S)-alanine and (b) (R)-alanine.

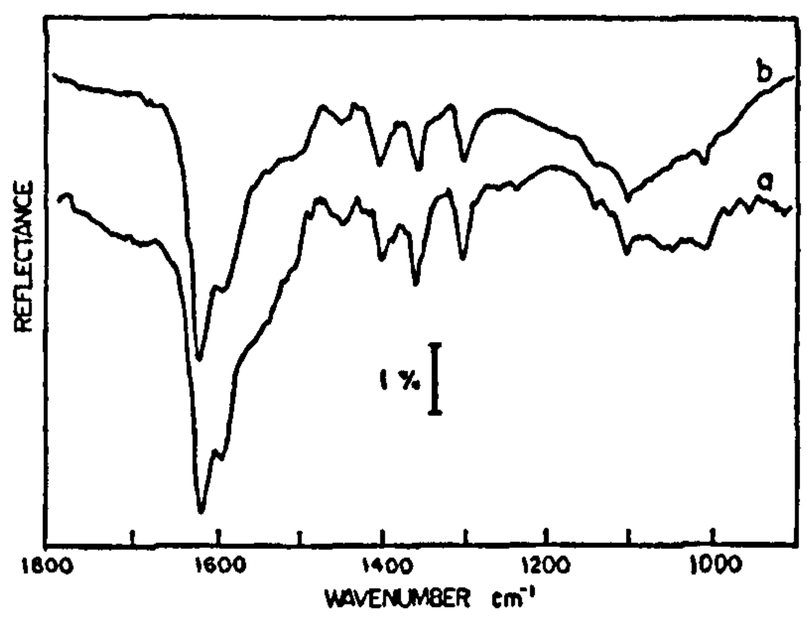

Figure 3.14: High-sensitivity reflection spectra of bulk nickel plates modified at 5°C with 0.5 % aqueous solutions of (a) (S)-alanine and (b) (R)-alanine.

The bands at 1620 and 1600 cm^{-1} were assigned to δ_{as} (NH_3^+) asymmetric deformation and ν_{as} (COO^-) antisymmetric stretching respectively. The broad band at 1515 cm^{-1} was attributed to the δ_s (NH_3^+) symmetric deformation. The orientation of the alanine molecule, in its zwitterionic form, on the thin film was deduced to be the one presented in Figure 3.15.

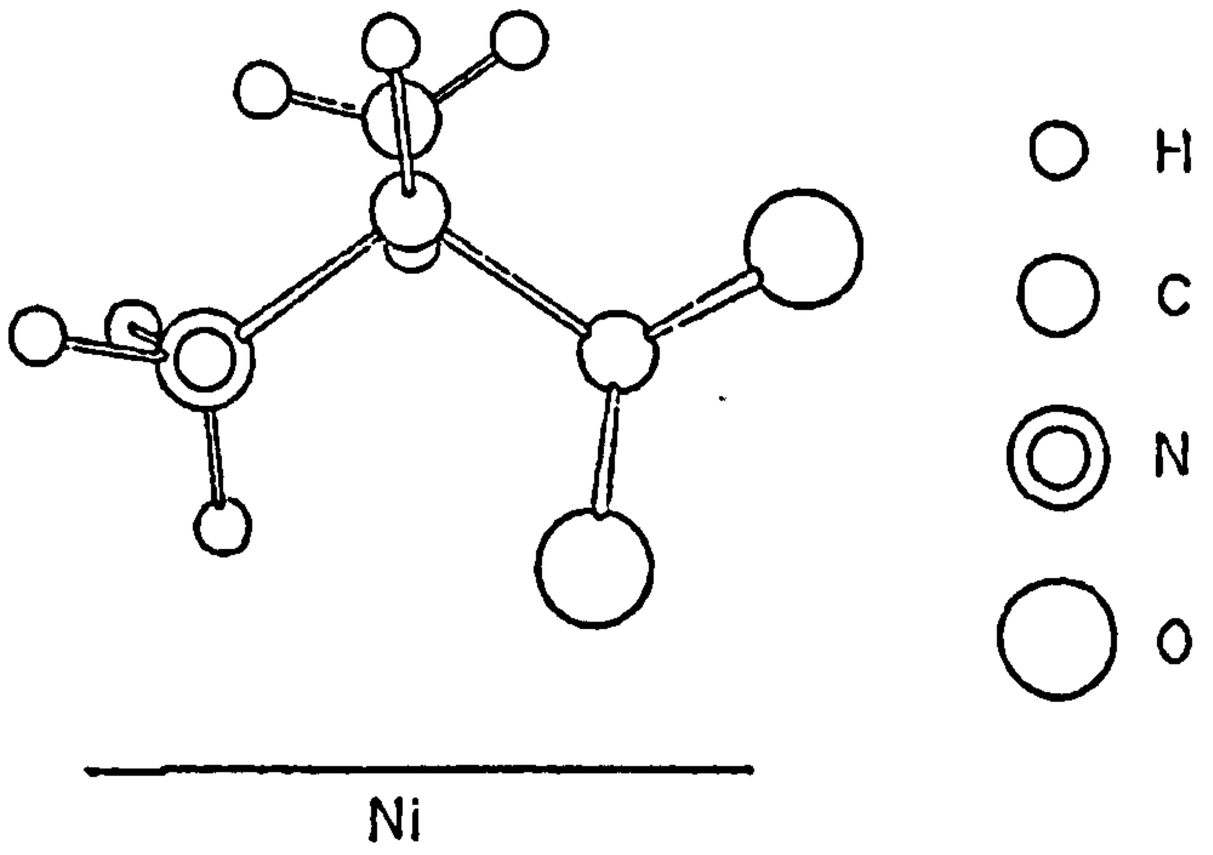

Figure 3.15: Orientational model in thin (R)-alanine crystal formed on nickel metal surface at 5°C.

The same experiment was done using Raney nickel (containing aluminium oxide) as thin film. The Raney nickel was modified with (R)-alanine at 100°C. The high-sensitivity reflection spectra of bulk nickel plates modified at 100°C with (R)-alanine is presented in Figure 3.16.

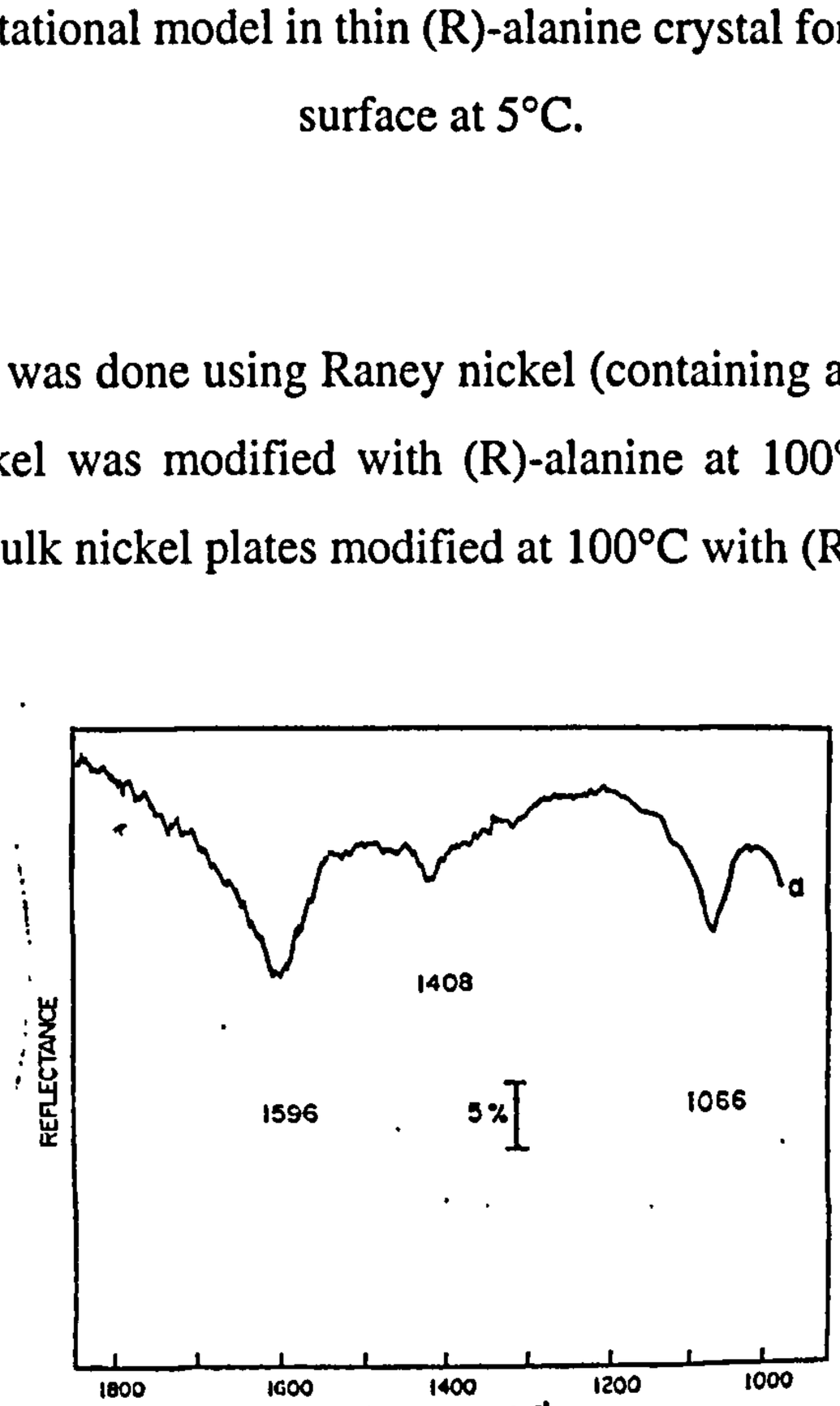

Figure 3.16: High-sensitivity reflection spectra of thin "Raney nickel" surfaces modified with (R)-alanine at 100°C.

The spectrum consists of a strong ν_{as} (COO^-) antisymmetric stretching absorption at 1596 cm^{-1} and a weak ν_s (COO^-) symmetric stretching absorption at 1408 cm^{-1}; this spectrum is also marked by the absence of the asymmetric and symmetric deformations of the NH_3^+ group. The proposed model of orientation of the (R)-alanine molecule on the Raney nickel is presented in Figure 3.17.

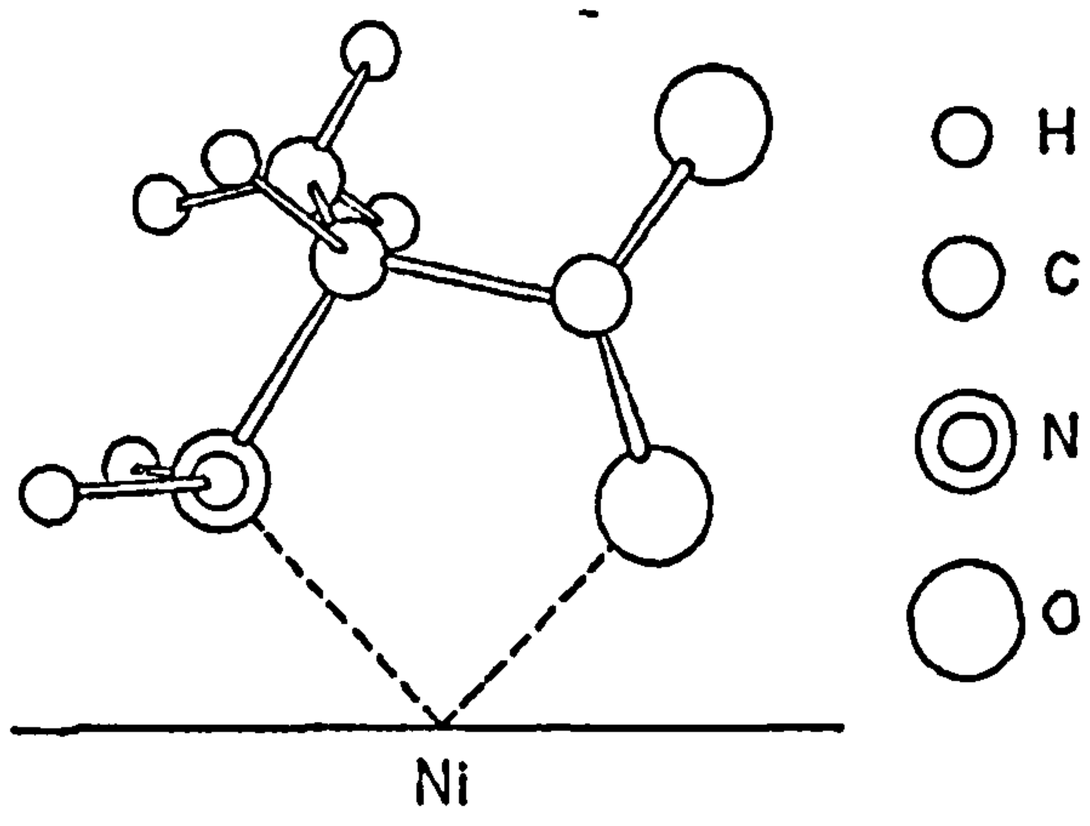

Figure 3.17: Orientational model in thin (R)-alanine crystal formed on "Raney nickel" surface at 100°C.

- ***Studies of alanino - nickel complexes***

There have been several studies of solid phase Ni (II) alaninato complexes [39-45]. A summary of the infrared frequencies and band assignments for solid phase nickel (II) complexes of alanine are presented in Table 3.6.

Frequency (cm^{-1}) [40]	Frequency (cm^{-1}) [41]	Frequency (cm^{-1}) [42]
3360 w		3379 w
3260 s ν (NH)		3366 w ν (NH)
		3275 m
2920 m ν (CH)		2982 sh
		2964 w ν (CH)
		2933 w ν (CH)
		2873 w
1590 vs ν_{as} (COO^-)	1588 ν_{as} (COO^-)	1584 s ν_{as} (COO^-)
1570 δ (NH_2)	1570 δ_{sc} (NH_2)	1566 δ (NH_2)
1483 vw		
1460 w δ_{as} (CH_3)	1477, 1462, 1409 δ_{as} (CH_3)	1457 w δ_{as} (CH_3)
1415, 1405 s ν_s (COO^-)	1402 ν_s (COO^-)	1394 s ν_s (COO^-)
1370 m ν_S (CH_3)	1368, 1365 ν_S (CH_3)	1354 m ν_S (CH_3)
1344 m		1344
	1341 δ (CH)	
1305 m		
	1327 tw (NH_2) tw	1334 m
		1298 sh
1295 m δ (CH)	1295, 1308 δ (CH)	1288 m δ (CH)
1231 vw	1232 ρ (CH_3)	1196 vw ρ (CH_3)
1205 vw	1206 ρ (CH_3)	1126 m

1136 m	skel. stretch	1134		1082 m ω (NH_2) + tw (NH_2) + δ (CH)
		1113	w (NH_2)	
1112 m	ω (NH_2)	1089	ν (CN)	1029 m
1085 s	ρ (CH_3)			
		1036	ν (CN)	
1030 w		1008	ν (CN)	1001 m
1000 w				
920 w	skel. vib.	925	ν (CN) + δ_{SC} (COO^-)	917 w ν (CCN) ± ν (CC)
852 m	skel. vib.	859	δ_{SC} (COO^-) +ν (CN)	850 m
775 m				
764 m	ρ (NH_2)	777	δ_{SC} (COO^-) +ν (CC)	776 w δ_{SC} (COO^-)

Table 3.6: Infrared frequencies and band assignments for solid phase nickel (II) complexes of alanine [40-42].

3.2 (S)-alanine on Ni (110)

3.2.1 RAIRS study of the adsorption of (S)-alanine on Ni (110) at 300 K

Figure 3.18 shows the development of the RAIR spectra with increasing exposure of (S)-alanine to Ni (110) at 300 K. These spectra present the bands in the region 3100 – 900 cm^{-1} wavenumbers. The assignments of these bands accompanied by the analysis of their intensities will provide the details of the orientation and bonding of this molecule on the Ni (110) surface. Indeed, the intensity of the bands may be rationalised in terms of the geometry of the adsorbed species leading to dipole activity of only selected modes, as dictated by the metal-surface selection rule [46-47]. To obtain the adsorption geometry of the (S)-alanine molecule on the Ni (110) surface, an analysis of the vibrational bands associated with each of the major functional groups in the molecule will be done.

It is important, first, to determine the form of alanine adsorbed on the Ni (110). The different forms of alanine, as well as their vibrational bands, have been described in the last section. As it has been shown, each form, on an infrared spectrum, should be distinguished by characteristic vibrational bands, associated with the main functional groups present. The zwitterionic form presents vibrations associated with the NH_3^+ and COO^- groups, identified by the deformations δ_{as} (NH_3^+), δ_s (NH_3^+), ν_{as} (COO^-) and the stretches ν_s (COO^-) and, sometimes a broad absorption feature from 3200 – 2000 cm^{-1} due to extensive intermolecular hydrogen bonding. The anionic form presents the vibrations associated with the COO^- group and also the NH_2 groups with the stretches ν_{as} (NH_2) and the ν_s (NH_2), the in-plane and out-of-plane deformation of the NH_2 and the NH_2 scissoring, rocking, wagging and twisting vibrations. The cationic form presents vibrations associated with the COOH and NH_3^+ groups. The COOH should present the following bands: three stretching vibrations of O-H, C=O and C-O bonds, two deformation vibrations of the O-H acid bond and a deformation vibration of the whole group COOH. The neutral form can be identified by the presence of the NH_2 and COOH vibrational modes.

When looking at the spectra presented in Figure 3.18, it is possible to distinguish two types of spectra. Spectra 3.18 (a) and (b) have essentially the same increasing bands, but from spectrum 3.18 (c) new bands start to increase and some bands tend to decrease in intensity. This suggests that the (S)-alanine is adsorbed on Ni (110) in two distinct phases whose characteristics depend on the coverage. These phases present different RAIRS bands and are formed as a result of different adsorption geometries of the (S)-alanine molecules on the Ni (110) surface. The first phase whose RAIR spectra are presented in Figure 3.18 (a) and (b) will be described as the "low coverage phase"; the second phase, whose RAIR spectra are presented in Figure 3.18 (c), (d) and (e) will be described as the "high coverage phase".

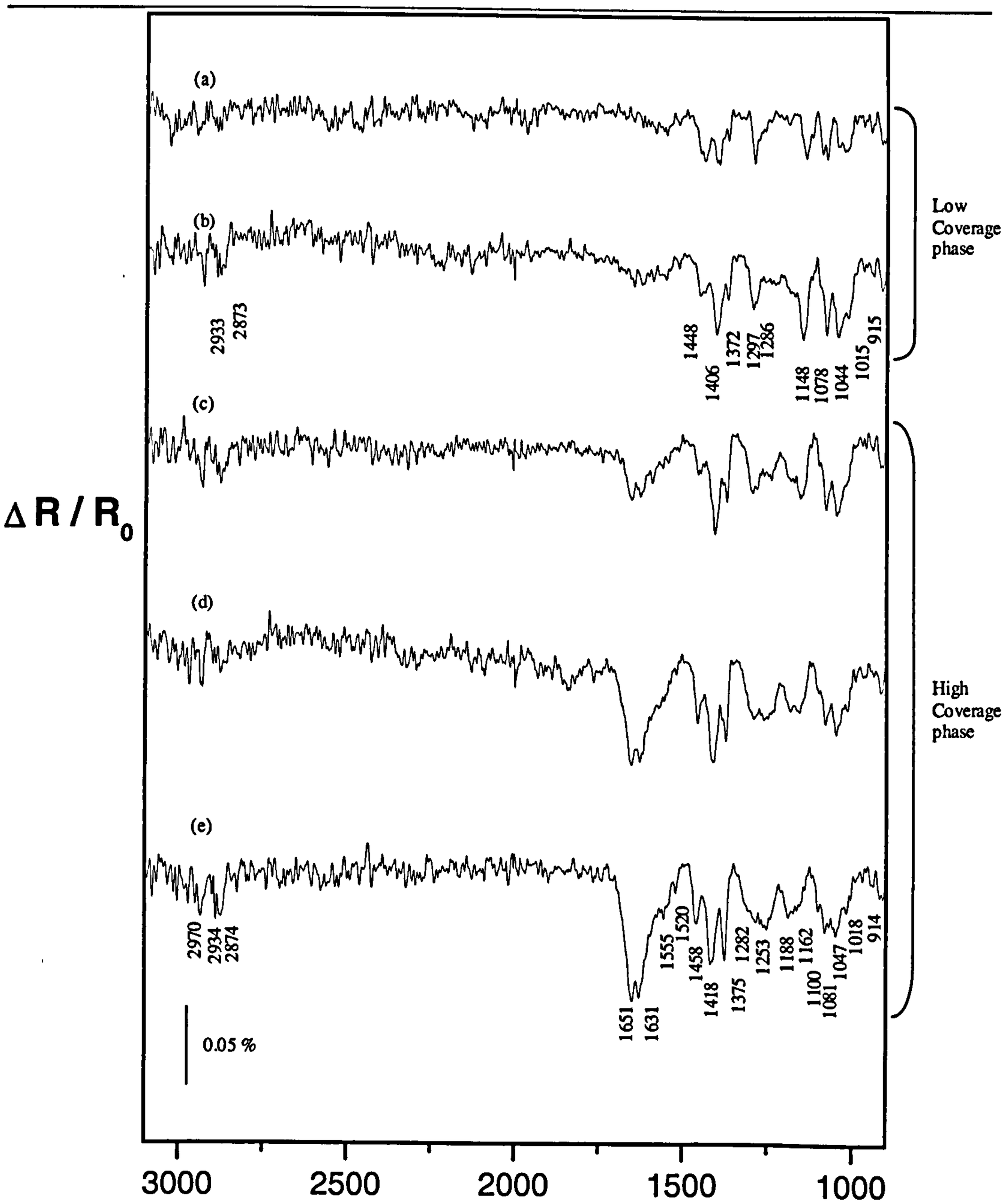

Figure 3.18: Successive RAIR spectra obtained during exposure of clean Ni (110) to (S)-alanine at 300 K after sublimation time of (a) 8 mins, (b) 11 mins, (c) 13 mins, (d) 15 mins, (e) 21 mins at 2×10^{-9} mbar.

3.2.1.1 The low coverage phase

The low coverage phase is illustrated by spectra (a) and (b) presented in Figure 3.18. To obtain the geometry of the (S)-alanine molecule adsorbed on the Ni (110) surface at low coverage, the functional groups of the molecule will be considered one by one.

As said before, the analysis of the relative intensity of the bands present on an RAIR spectrum can give the geometry of the adsorbed alanine molecule. The normal modes of the vibrations associated with each functional group of the molecule at low coverage are presented in Table 3.7.

The absence of the ν (C=O) stretching vibration in the 1700 cm^{-1} region in the spectrum (b) in Figure 3.18 indicates that upon adsorption the gas phase carboxylic group of the (S)-alanine molecule is deprotonated into a COO^- group. This is also confirmed by the presence of the vibrational mode associated with the COO^- whose vibration associated with the symmetric carboxylate stretch, ν_s (COO^-) is present at 1406 cm^{-1} wavenumbers in spectrum (b). The band assigned to the vibration associated with the asymmetric carboxylate stretch, ν_{as} (COO^-) is not present on this spectrum (b) meaning that this last vibration is inactive. Combining these two elements, it is conclusive to say that both the oxygen atoms of the carboxylate group are placed equidistant to the metal surface.

The wagging w (NH_2) vibration gives rise to an intense band at 1148 cm^{-1} which looks more intense in this spectrum than in the spectrum of the complex [41]. The δ (NH_2) scissoring deformation at ~ 1570 cm^{-1} does not manifest itself on the spectra. This means that the plane of the NH_2 group lies parallel to he surface. Besides, as there is a considerable enhancement of this band compared to the complex, it is suggested that the N lone pair interacts with the surface causing this vibration to induce a greater charge transfer.

The bands at 1078 cm^{-1} assigned to the ν_{as} (CCN), and at 1044 cm^{-1} and 1015 cm^{-1}, assigned to ν_{as} (CCN) + ν_s (COO^-) + ρ (CH_3) vibrations, have an intensity comparable to the bands at 1406 cm^{-1} and 1148 cm^{-1}. This means that the C – N bond is oriented largely normal to the surface.

The CH group gives a strong band, compared to that seen for this vibration in the Ni / alanine complex [41], at 1297 cm^{-1} representing the bending deformation δ (CH), meaning that this vibration projects a large component normal to the surface.

The CH_3 group presents two bands: a symmetrical deformation, δ_s (CH_3) at 1372 cm^{-1} and a asymmetric deformation δ_{as} (CH_3) at 1448 cm^{-1}. However, these bands are small compared to the bands obtained for the metal alanine complexes of Ni (II). The first two vibrations present dipole moments almost normal to each other. This means that the C – CH_3 bond is neither normal nor parallel to the surface.

Table 3.8 shows the assignment of the IR bands of (S)-alanine on Ni (110) compared to (S)-alanine adsorbed on Cu (110) and nickel complexes of alanine.

Wavenumbers (cm^{-1})	Assignment	Description of vibrational modes
1372	Symmetric methyl deformation δ_s (CH_3)	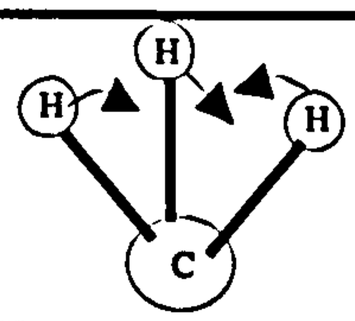
1448	Asymmetric methyl deformation δ_{as} (CH_3)	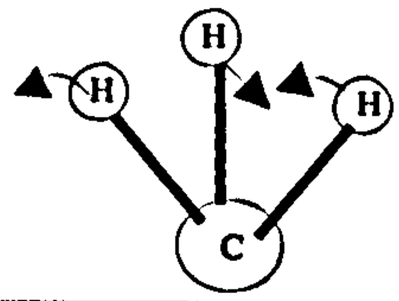
1297	(CH) deformation δ (CH)	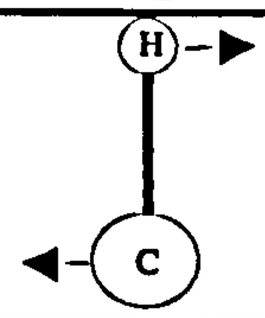
1148	Amine wag w (NH_2)	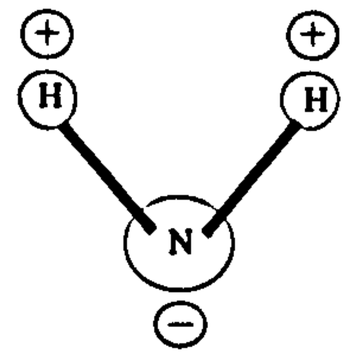
1406	Symmetric carboxylate stretch ν_s (COO^-)	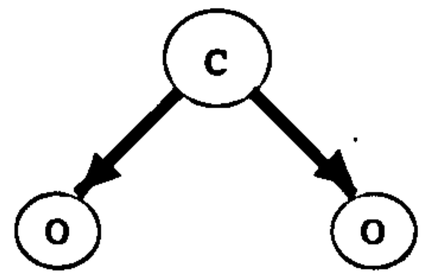

Table 3.7: Description of the normal modes of vibrations for the functional groups of (S)-alanine in the low coverage phase.

(S)-alanine on Cu (110) [35]		Ni-(L-ala)$_2$ [41]	(S)-alanine on Ni (110) This work	Assignments
Low coverage	High coverage		Low coverage	
-	2985			ν_a (CH_3)
2935	2931		2933	ν_s (CH_3)
2876	2876		2873	δ (CH_3)
1613	1626	1588		ν_{as} (COO^-)
1576	1576	1570		δ (NH_2)
1466	1462	1407	1448	δ_{as} (CH_3)
1411	1415	1402	1406	ν_s (COO^-) + δ_s (CH_3)
1373	1382	1365	1372	δ_s (CH_3) + ν_s (COO^-)
1302 1276	1293 1276	1308 1295	1297 1286	δ (CH) + ν_s (COO^-)
1145	1167		1148	w (NH_2) + ν_s (COO^-)
1086	1086	1089	1078	ν_{as} (CCN)
1036 1011	1036	1036 1008	1044 1015	ν (CN) + ν_s (COO^-) + ρ (CH_3)
919	919	925	915	ν (CN) + δ_s (COO^-)

Table 3.8: Vibrational assignments of (S)-alanine on Ni (110) in comparison with those of Ni-(ala)$_2$ complexes and (S)-alanine adsorbed on Cu (110) at 300 K.

The analysis of the spectra (a) and (b) in Figure 3.18 allows affirming that the (S)-alanine molecule at low coverage adsorbs in the anionic form, with both oxygen atoms of the COO^- group equidistant from the surface and bonds through the COO^- and NH_2 groups, as shown in Figure 3.19.

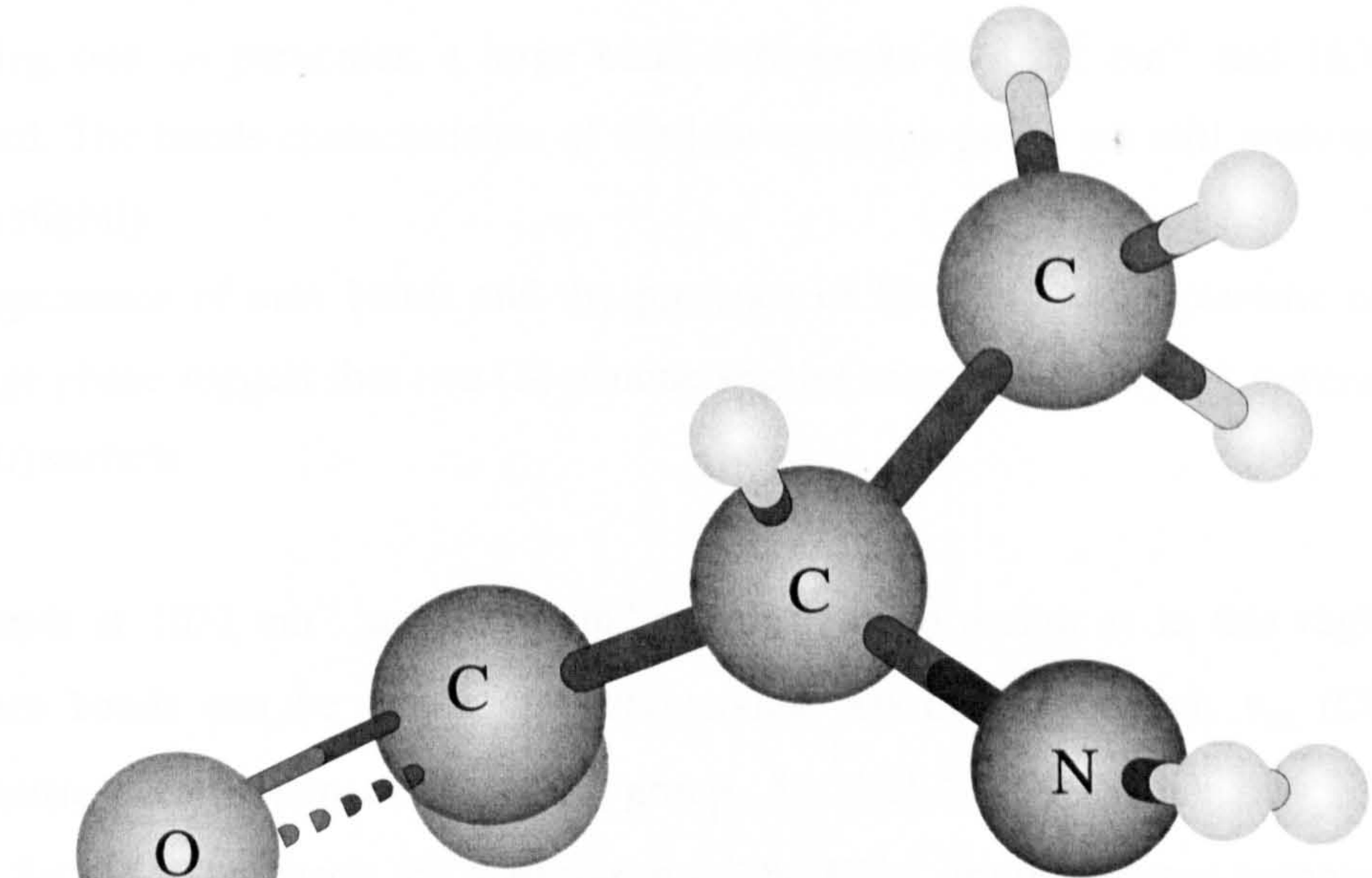

Figure 3.19: Schematic representation of one molecule of (S)-alanine adsorbed on the Ni (110) surface at 300 K in the low coverage phase.

3.2.1.2 The high coverage phase

The high coverage phase is illustrated on spectra (c), (d) and (e) in Figure 3.18. A number of new bands appears and their relative intensity increases from one spectrum to the following one, in particular, a large band with peaks at 1651 cm^{-1} and 1631 cm^{-1} is observed. The bands characteristics of the low coverage phase are still present but have shifted slightly.

The appearance of new bands and the presence of the bands characteristic of the low coverage phase suggest that two (S)-alanine species may coexist at high coverage on the Ni (110) surface.

The bands at 1631 cm^{-1} and 1651 cm^{-1} are difficult to assign as in this region of the spectrum bands can be due to the carboxylate asymmetric stretch ν_{as} (COO^-), the asymmetric deformation of the NH_3^+ group, δ_{as} (NH_3^+) and the bending of the NH_2 group, δ (NH_2). To check the appearance of the NH_3^+ group, another technique would have been welcome, such as X-ray Photoelectron Spectroscopy (XPS) which would have enabled the chemical form of the nitrogen to be determined, but this was not available.

The band at 1631 cm^{-1} can be assigned to the carboxylate asymmetric stretch ν_{as} (COO^-) vibration. For comparison, when alanine is adsorbed on nickel, as a nickel complex, the frequency of the carboxylate asymmetric stretch ν_{as} (COO^-) vibration is 1590 cm^{-1} [40-42]. This frequency is 1630 cm^{-1} when glycine is adsorbed on Cu (110) [48] and 1626 cm^{-1} when alanine is adsorbed on this same metal [35]. The appearance of the asymmetric carboxylate stretch represents a new phase involving the COO^- group with a sideways-tilted orientation in which the carboxylate oxygen atoms have an inequivalent interaction with the surface. This posture would lead to the asymmetric carboxylate stretch vibration exhibiting the greatest dipole activity.

The band at 1651 cm^{-1} can be assigned to the asymmetric deformation of the NH_3^+ group, δ_{as} (NH_3^+); indeed, when alanine is adsorbed on a nickel surface at 5°C, the frequency of this group has a higher value than the frequency of the carboxylate asymmetric stretch ν_{as} (COO^-) vibration, as shown in introduction [38]. The band at 1520 cm^{-1} can be assigned to the symmetric deformation δ_s (NH_3^+), as has been done when alanine is adsorbed on a nickel surface at 5°C [38]. This would allow assigning the bands at 1253 cm^{-1} to the rocking deformation ρ (NH_3^+). These three bands would be the witness of the appearance

of the NH_3^+ group on the surface. Besides, the combination of these two elements allows the suggestion that the C – NH_3^+ bond has a position almost parallel to the surface, with a small component normal to the surface, due to the small symmetric deformation δ_s (NH_3^+) at 1520 cm^{-1}.

The band attributed to the symmetric carboxylate stretch at 1418 cm^{-1} does not change upon further adsorption of molecules on the surface, confirming the low coverage phase is still present on the surface.

The wagging w (NH_2) vibration having given rise to the band at 1148 cm^{-1} in the low coverage phase is still present at 1162 cm^{-1} in the high coverage phase. It seems to have lost some intensity and is now on the side of a new w (NH_2) band at 1188 cm^{-1} which is suggested to be associated to the high coverage phase. These two bands are accompanied by the δ_s (NH_2) scissors at 1555 cm^{-1}. It can be concluded that in the new phase, both the δ_s (NH_2) scissors and the w (NH_2) wag of the NH_2 group presents some dipole activity normal to the surface. This confirms the appearance of a new species having the plane of its NH_2 group in a position between the normal and the parallel planes to the surface.

The vibration below 1100 cm^{-1} associated with the CCN stretches show no increase in intensity, indicating that the C-N bond of the new high coverage species may no longer be directed towards the surface.

The IR bands which characterise the CH_3 group in the low coverage phase, at 1375 cm^{-1}, and 1458 cm^{-1} are still present on the spectra representing the high coverage phase. The band representing the δ_s (CH_3) vibrations, at 1375 cm^{-1} has dramatically increased its intensity, meaning that the C-CH_3 bond of the new species is oriented to a position more normal to the surface.

In addition, the possibility of hydrogen bonding between the oxygen atoms of the carboxylate group and hydrogen atoms of other surrounding alanine molecules cannot be excluded. It has been also shown that the shifted absorption bands due to the hydrogen bonded A – H stretching vibrations are much broader than the corresponding bands of the non-hydrogen bonded A – H group [49]. Besides, the A – H deformation modes are shifted to higher frequencies but these modes do not show any substantial band broadening or intensity change. This might explain why some of the bands on the spectra are so broad in the high coverage phase; some are in fact composites of a large number of thin bands: some of these thin bands represent groups which are hydrogen bonded and some other thin bands represent groups which are not hydrogen bonded. The hydrogen

bonding implies the involvement of the NH_2 group, the CH and the NH_3^+ groups as these groups present broader bands.

Table 3.9 presents the vibrational assignments of (S)-alanine in the high coverage phase on Ni (110) at 300 K and Table 3.10 presents the description of the normal modes of vibrations for the functional groups of (S)-alanine in the high coverage phase.

Frequency (cm^{-1})	Assignments
1651	δ_{as} (NH_3^+)
1631	ν_{as} (COO^-)
1555	δ (NH_2)
1520	δ_s (NH_3^+)
1458	δ_{as} (CH_3)
1418	ν_s (COO^-) + δ_s (CH_3)
1375	δ_s (CH_3) + ν_s (COO^-)
1282	δ (CH) + ν_s (COO^-)
1253	ρ (NH_3^+)
1188 1162	w (NH_2) + ν_s (COO^-)
1100 1081	ν_{as} (CCN)
1047 1018	ν (CN) + ν_s (COO^-) [+ ρ (CH_3)]
914	ν (CN) + δ_s (COO^-)

Table 3.9: Vibrational assignments of (S)-alanine in the high coverage phase on Ni (110) at 300 K.

Wavenumbers (cm^{-1})	Assignment	Description of vibrational mode
1375	Symmetric methyl deformation δ_s (CH_3)	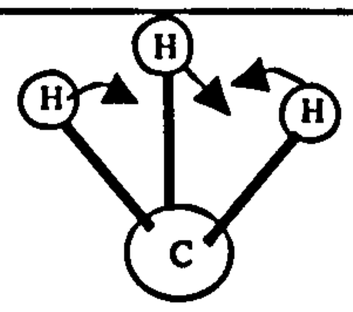
1458	Asymmetric methyl deformation δ_{as} (CH_3)	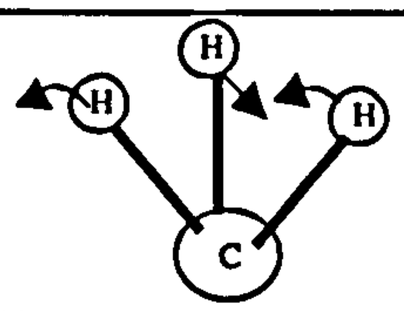
1282	(CH) deformation δ (CH)	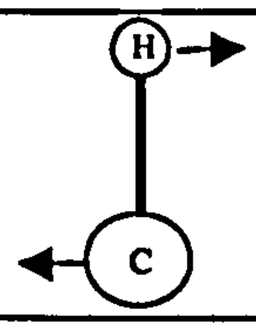
1162	Amine wag w (NH_2)	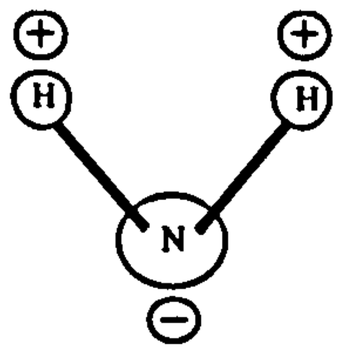
1555	Amine scissors	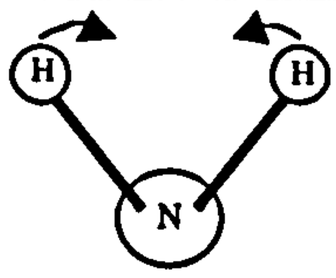
1418	Symmetric carboxylate stretch ν_s (COO^-)	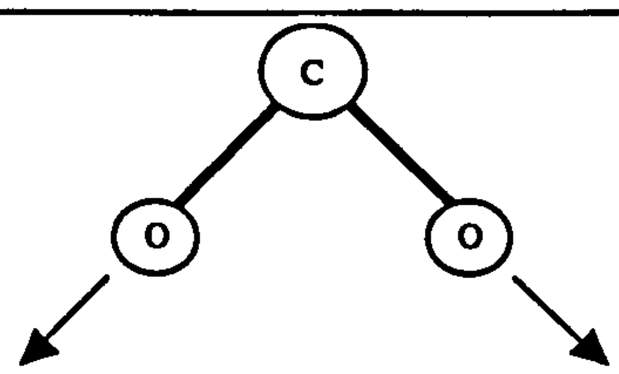
1631	Asymmetric carboxylate stretch ν_{as} (COO^-)	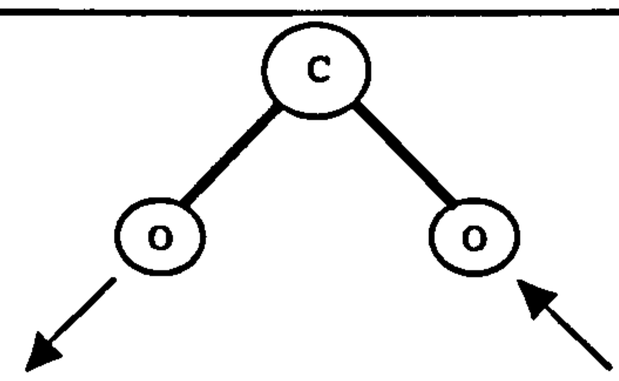

Wavenumbers (cm^{-1})	Assignment	Description of vibrational mode
1651	Asymmetric ionised amino deformation δ_{as} (NH_3^+)	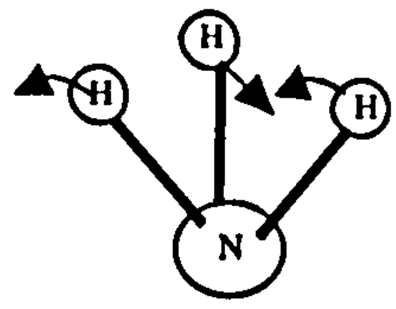
1520	Symmetric ionised amino deformation δ_s (NH_3^+)	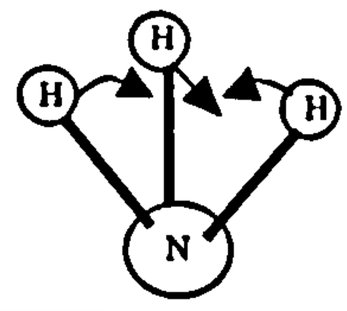
1253	Ionised amino deformation ρ (NH_3^+)	Association of the two deformation modes with the vibration of the C-CH_3 linkage

Table 3.10: Description of the normal modes of vibrations for the functional groups of (S)-alanine in the high coverage phase.

In addition to the differently oriented species created at high coverage, at least some of the molecules appear to be in a different chemical form. Strong vibrations associated with the NH_3^+ group indicate that the NH_3^+ group, may be formed by the addition of one hydrogen to the amino group of one of the high or low coverage species. As mentioned before, because the band representing the asymmetric deformation δ_{as} (NH_3^+) is a big broad one and because the band representing the symmetric deformation δ_s (NH_3^+) is a smaller one, the C – NH_3^+ bond is in a position quite parallel to the surface. Besides, since in the low coverage phase, the C – NH_2 bond is oriented largely normal to the surface and since in the new species present in the high coverage phase, this bond seems to be parallel to the surface, it can be suggested that the hydrogen is attached to the amino group of the new species appearing in the high coverage phase. Thus, the high coverage phase gives birth to two new species, drawn in Figure 3.20.

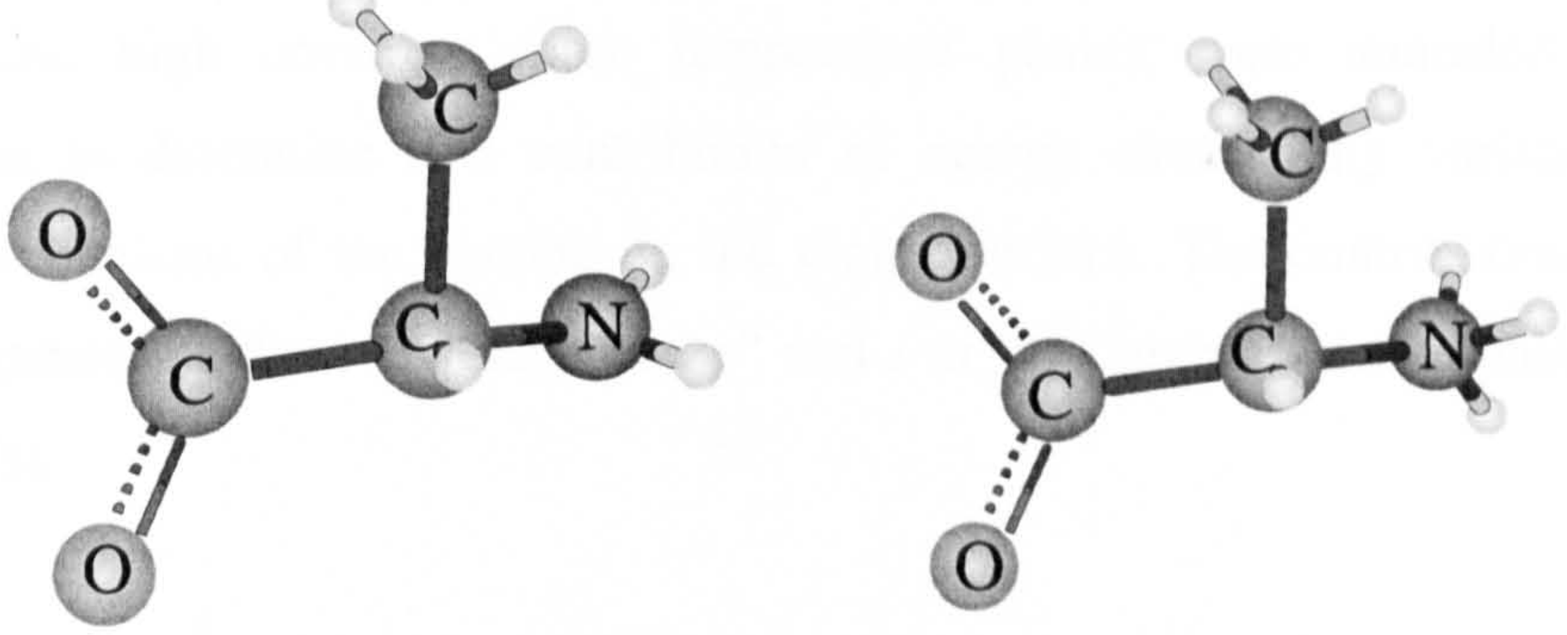

Figure 3.20: Schematic representation of two molecules of each of the new species created when (S)-alanine is adsorbed on the Ni (110) surface at 300 K in the high coverage phase.

3.2.2 RAIRS study of the adsorption of (S)-alanine on Ni (110) above 300 K

The low and high coverage room temperature phases were annealed to higher temperatures to determine if a contribution of energy caused any variations in the bonding mechanisms of the alanine on the nickel surface. The contribution of energy could reorganise the "low coverage phase" and / or the "high coverage phase" into (a) new phase(s).

3.2.2.1 The low coverage phase

The low coverage phase was heated slowly to a given temperature and the infrared spectra were taken as the system cooled down. As is shown in Figure 3.21, no new bands appear from spectra (a) to (c), no band shifts in frequency, and no bands disappear. The low coverage phase is stable until 333 K, and does not reorganise to form a new phase with increasing temperature. At the temperature of 333 K, some new bands around 1600 cm^{-1} are seen, which may suggest similarities to the high coverage phase described in the previous section. However, these bands are not accompanied by other bands characteristic of the high coverage phase. The TPD experiments discussed in the following section show that at a temperature around 333 K, the alanine molecules start desorbing, so these bands around 1600 cm^{-1} are probably some fragments of the molecule. It can also be added that from spectra (d) to (f), the band around 910 cm^{-1} is increasing and broadening which can also be a sign of the molecule decomposing.

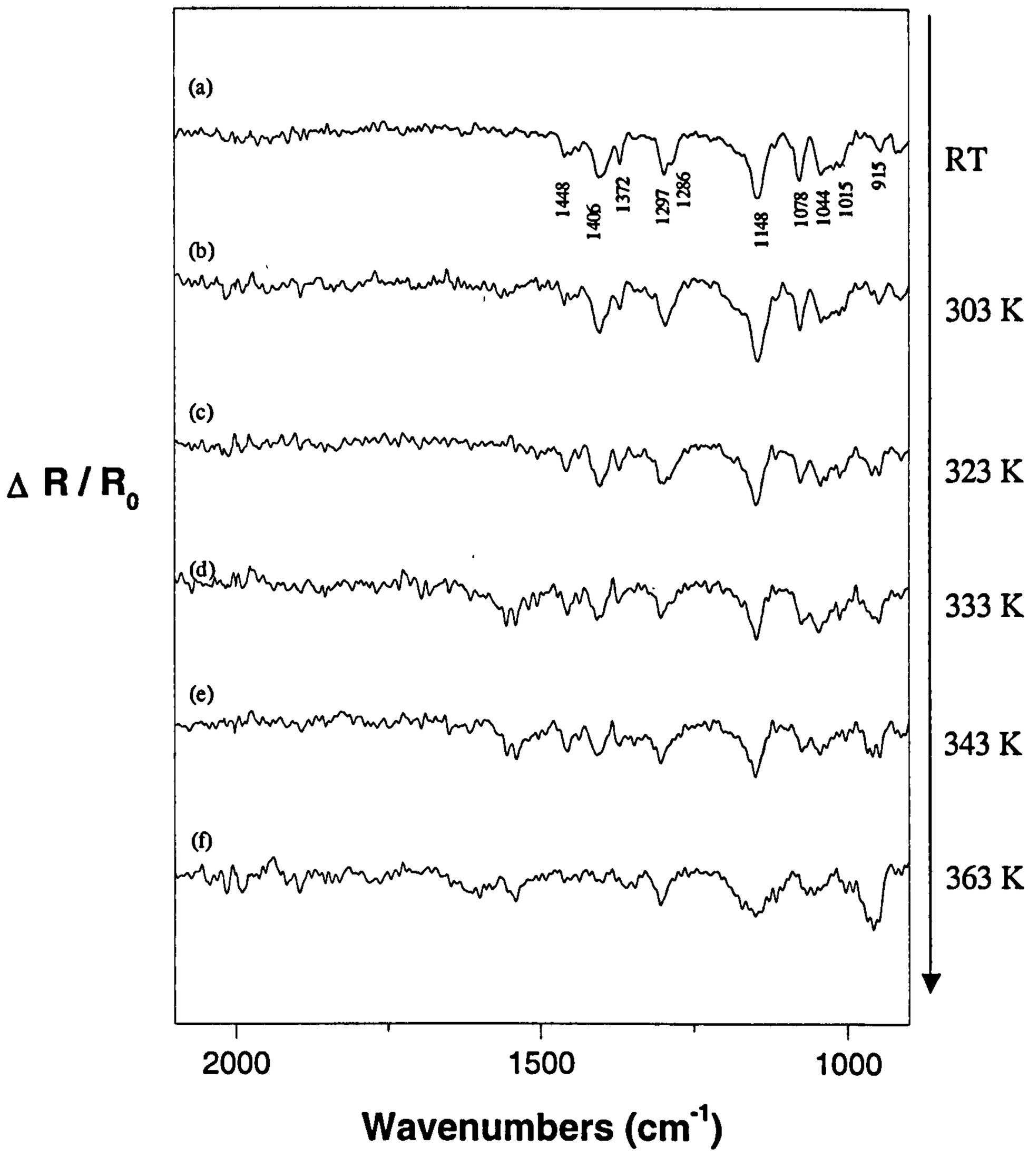

Figure 3.21: RAIR spectra of the low coverage phase of (S)-alanine obtained when heating the sample to different temperatures.

3.2.2.2 The high coverage phase

The spectra obtained when the room temperature high coverage phase was heated and cooled down are presented in Figure 3.22.

It might be expected that the energy sent to the surface could have modified the high coverage phase into another phase, such as the low coverage phase as is seen for Cu (110). However, from room temperature to 333 K, no change can be reported. The bonding of the alanine molecules in this high coverage phase is not sensitive to the heat until the temperature of 368 K. Indeed, in spectrum (d), all the bands start losing slightly some intensity. This cannot be attributed to a new way of bonding of the molecules on the surface but might be the witness of the beginning of decomposition of the molecules on the surface. In the subsequent spectra, the degeneration of the bands is increased. At 378 K, the band at 914 cm^{-1} appears to be splitting into two new bands. This could be a sign that the alanine molecules are decomposing on the surface before desorbing. Further information regarding degeneration of the bands with temperature can be obtained from the TPD results discussed in the next section.

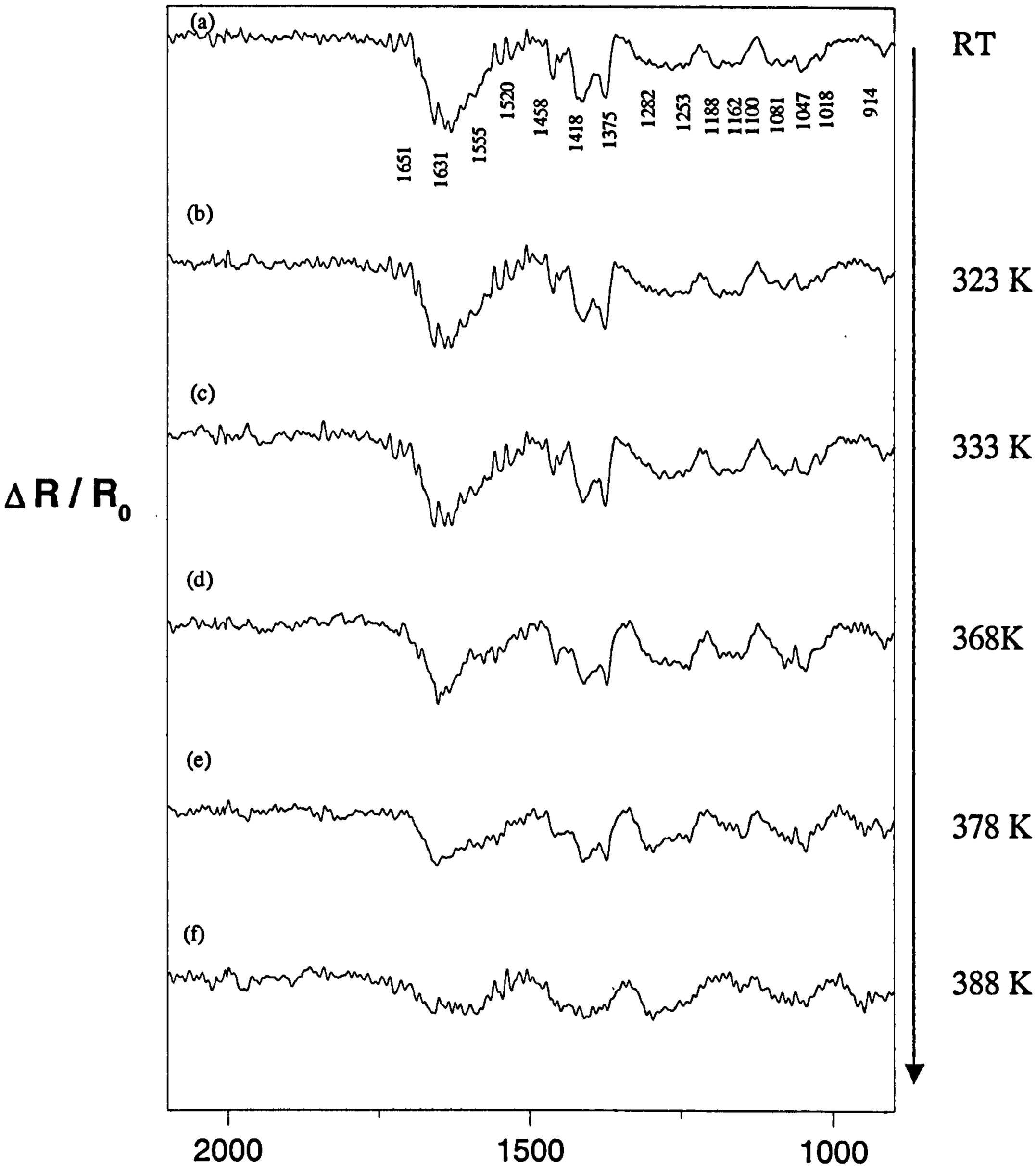

Figure 3.22: RAIRS spectra of the high coverage phase of (S)-alanine obtained when heating the sample to different temperatures.

3.2.3 TPD study of the adsorption of (S)-alanine on Ni (110) at 300 K

3.2.3.1 General remarks on the adsorption of hydrogen on Ni (110)

When adsorbed on Ni (110) surface, the alanine molecule initially deprotonates into its anionic form. However, hydrogen is easily adsorbed on Ni (110) and desorbs at quite a high temperature. Figure 3.23 shows a series of thermal desorption spectra obtained after adsorption of hydrogen at 120 K. Three distinct desorption states are observed at full coverage.

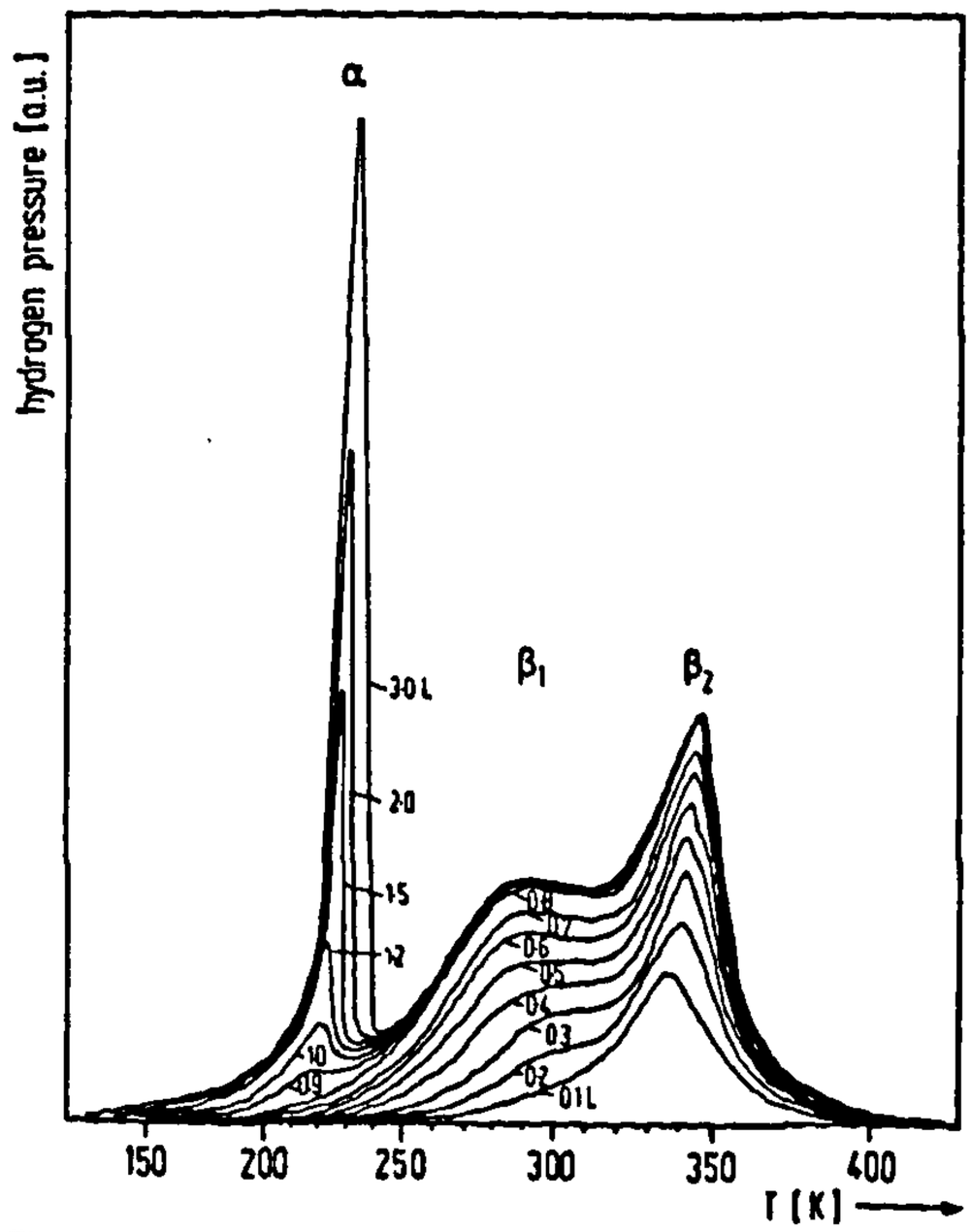

Figure 3.23: Series of thermal desorption spectra obtained after adsorption of hydrogen at 120 K; from ref [50].

In Figure 3.23, the first desorption state is the sharp α-state which desorbs at ~ 220 K. The two other states, β_1 and β_2 states desorb at 290 K and 340 K respectively. In our experiments, at 300 K, we can expect to have some hydrogen atoms adsorbed on the Ni

(110) surface coming from the deprotonation of the alanine molecules. This suggested process is presented in Figure 3.24.

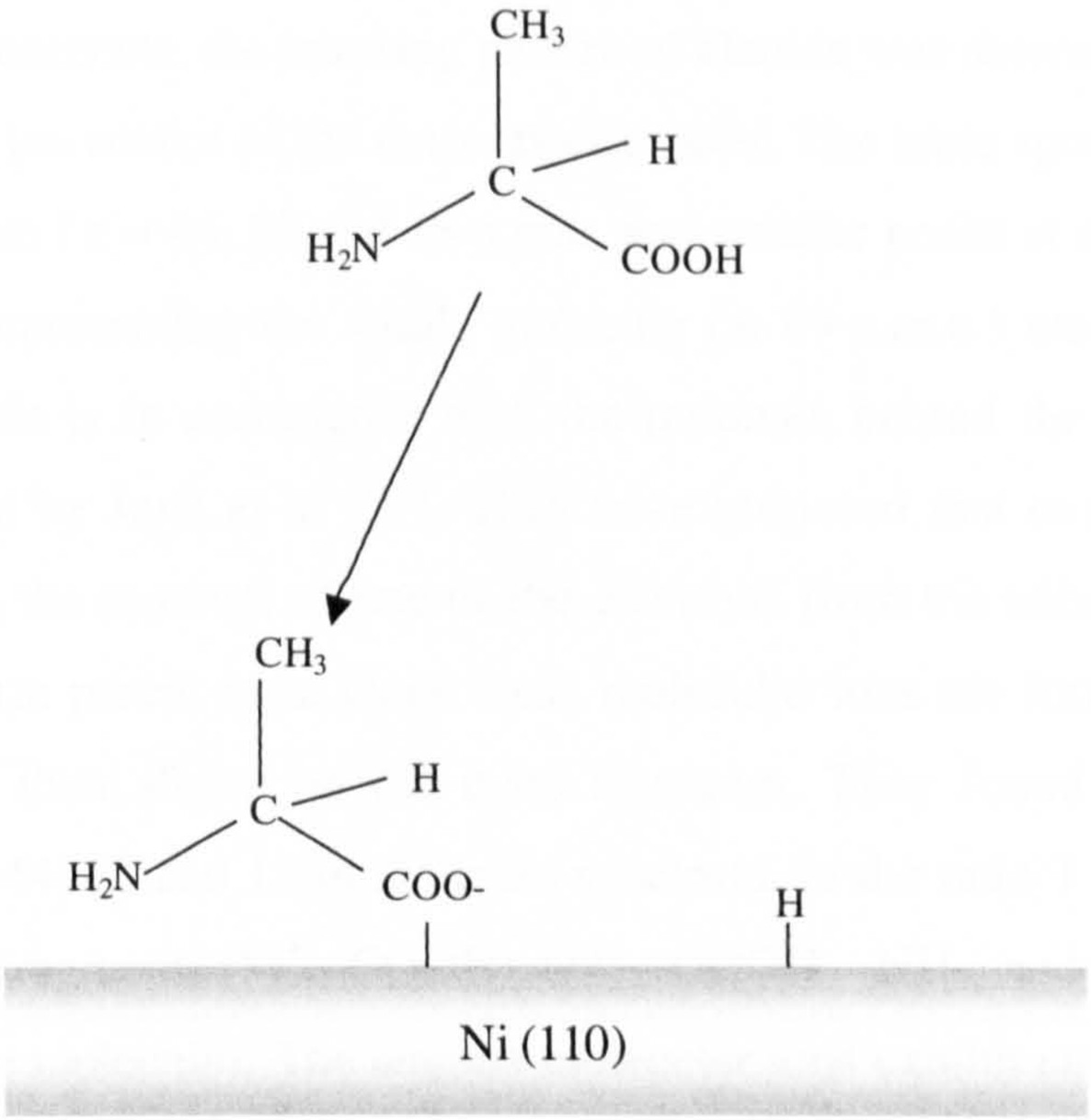

Figure 3.24: Proposed process of adsorption of the alanine molecule on the Ni (110) surface: deprotonation of the molecule and adsorption of the hydrogen on the surface.

At high coverage, this hydrogen can as well break off from the Ni (110) surface, attaches to the amino group of the alanine molecules, being responsible for the formation of the NH_3^+ group.

From the TD spectra presented in Figure 3.23, the hydrogen adsorbed during the adsorption of the alanine on the surface is expected to desorb around the temperatures of 340 K and 350 K approximately.

3.2.3.2 The low coverage phase

Before the TPD experiments, the cracking pattern of alanine was determined by its direct evaporation into the ion source of the mass spectrometer. The mass spectrum was seen to give major peaks at m / z = 44, 28 and 18 a.m.u. and smaller peaks at m / z = 15, 27 and 42 a.m.u.. A peak representing the whole molecule (at 89 a.m.u.) was absent from the cracking pattern. This is in accordance with the rationale behind the fragmentation of (S)-alanine proposed by Junk *et al* [51]. They have proposed that molecular ionisation occurs initially with the removal of one of the electrons from the unbonded pair on the nitrogen atom to form parent ions. Once these molecular ions are formed, they rapidly fragment becoming then absent on the mass spectrum. They found the major peaks appeared at m / z = 44, 28 and 18 in the mass spectrum, in the ratio 1 : 0.2 : 0.24. They are the peaks of the fragments (M^+ - COOH), (M^+ - COOH – NH_2) and H_2O, respectively (with M^+ the alanine molecule). The alanine molecular ions exhibit strong tendencies to rearrange one hydrogen atom upon fragmentation, leading to the production of H_2O, thus making the m / z = 18 mass fragment peak the second most predominent peak in the mass spectrum. They also reported that the intensity of the molecular ion at 89 a.m.u. is about 0.2 % of the most intense peak at m / z = 44 a.m.u.

The results of the TPD experiments conducted after the deposition of a low coverage of (S)-alanine at room temperature are shown in Figure 3.25. No peak at m / z = 18 corresponding to H_2O is observed but two peaks attributed to H_2, m / z = 2 are present. As explained before, the peak at 356 K is the peak of the H atoms desorbing from the Ni (110) surface. The second peak, at 387 K, is the hydrogen coming from the alanine molecules adsorbed on the surface. The peak at m / z = 28 and 44 a.m.u. are probably decomposition fragments and are identified as CO and / or H_2CN and CO_2 respectively. Figure 3.25 shows that this low coverage of alanine is stable until the temperature of 356 K where a small broad peak of m / z = 28 is present. The desorption of this species beginning at 342 K approximately, which is in accordance with the results obtained by RAIRS when heating this low coverage phase.

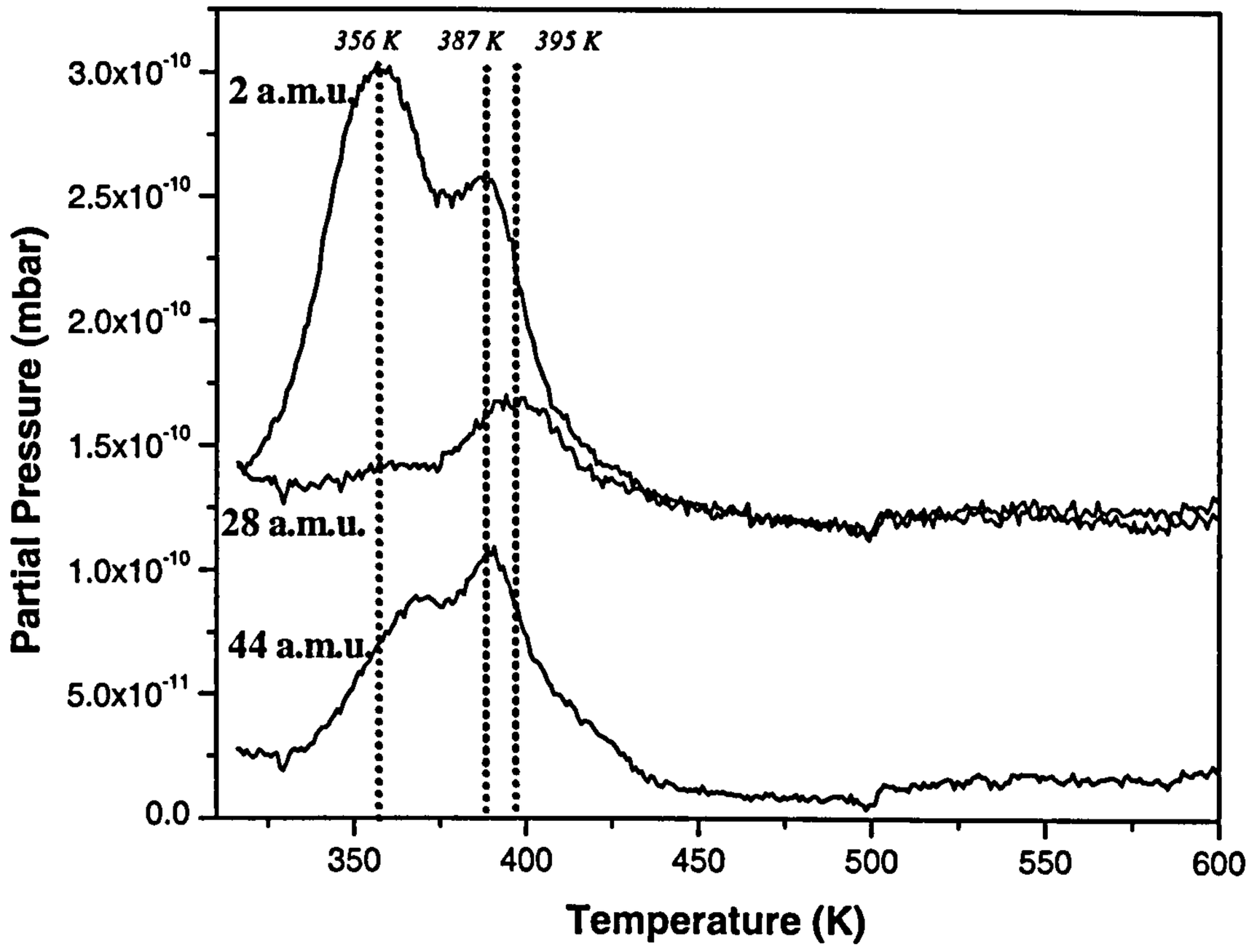

Figure 3.25: TPD spectra for the low-coverage phase of (S)-alanine on Ni (110) at 300K, monitoring fragments with m / z = 2, 28 and 44 a.m.u..

3.2.3.3 The high coverage phase

The same experiments were carried out on the high coverage phase. Figure 3.26 presents the TPD spectra obtained.

Here again, two peaks representing the hydrogen are present on the spectrum. The first peak is attributed to the hydrogen atoms adsorbed on the Ni (110) surface. The second peak is attributed to the fragments of the alanine molecules, which "explode" off from the surface at a temperature of ~ 400 K.

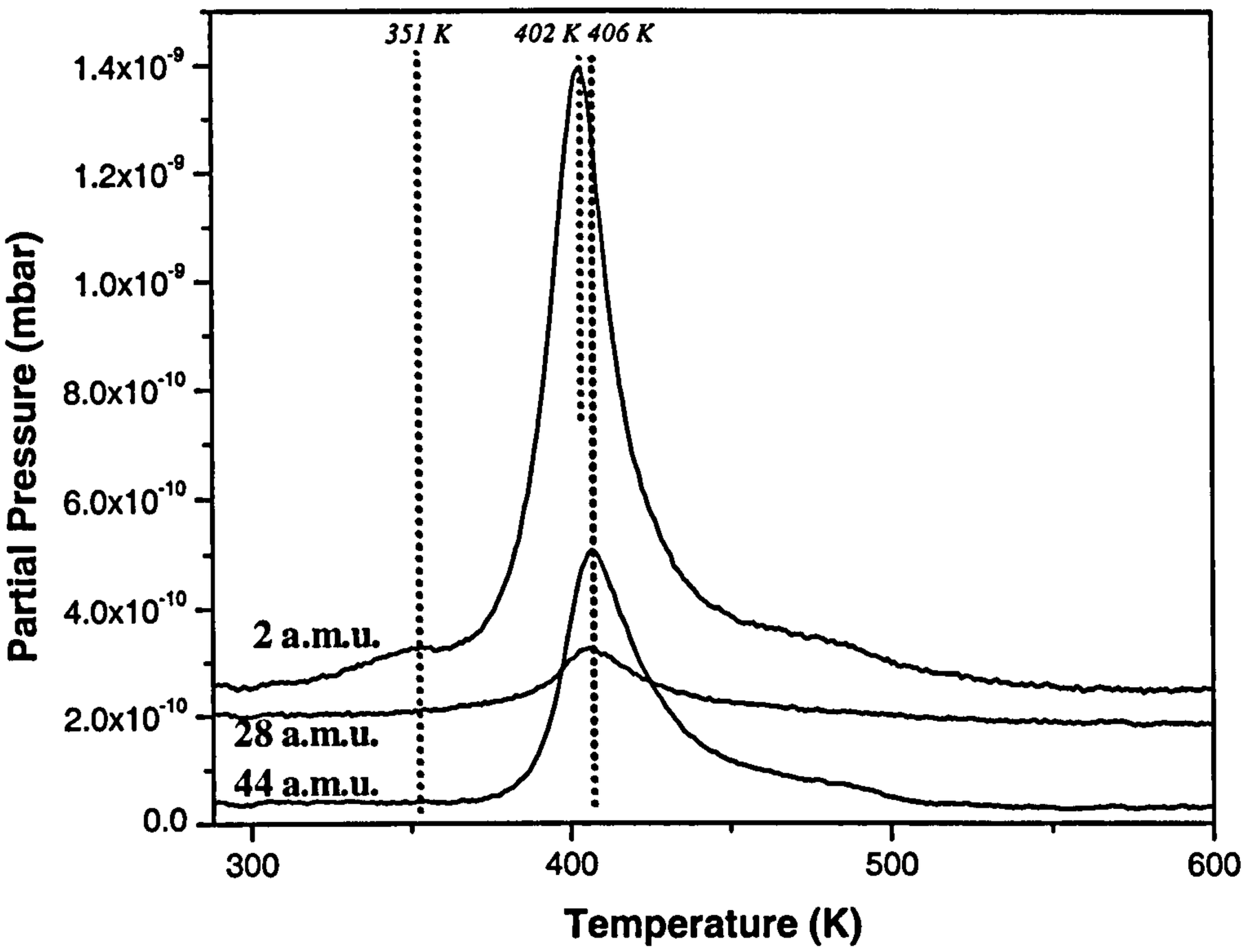

Figure 3.26: TPD spectra for the high-coverage phase of (S)-alanine on Ni (110) at 300K, monitoring fragments with m / z = 2, 28 and 44.

These TPD spectra reveal as well that the alanine fragments start desorbing from the surface at ~380 K, which is in accordance with the results given by the RAIRS analysis of the high coverage phase annealed to different temperatures.

3.2.4 LEED and STM study of the adsorption of (S)-alanine on Ni (110) at 300 K

A number of different LEED experiments have been tried for different coverages and temperatures. These were: (a) depositing a low coverage of (S)-alanine initially and increasing this coverage checking the LEED each time; (b) depositing a low coverage and annealing the crystal checking the LEED at each temperature and (c) depositing a high coverage and annealing the crystal checking the LEED at each temperature. However, unfortunately, a (1×1) LEED pattern with high background, similar to the one shown in Figure 3.27, had been obtained each time.

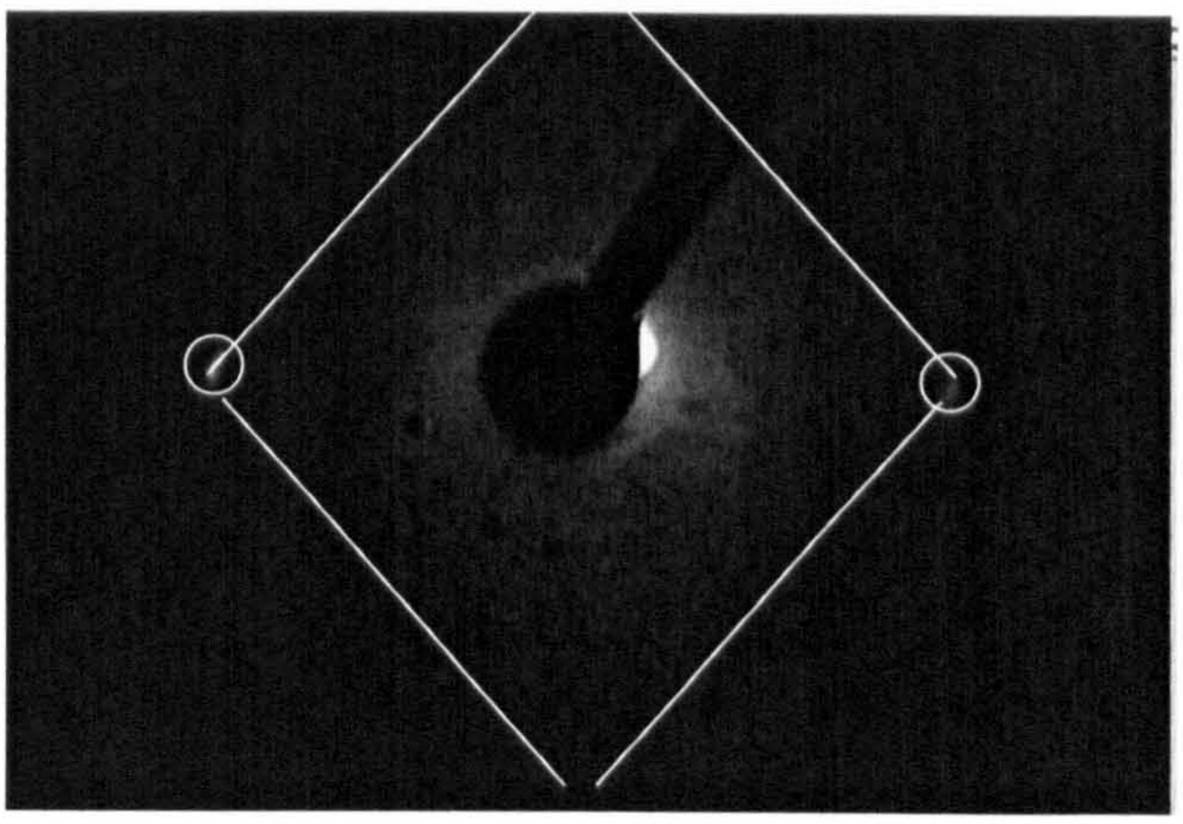

Figure 3.27: Example of LEED pattern obtained during the experiments with (S)-alanine on Ni (110) at 30 eV, with the unit cell drawn in white lines.

The systematic absence of a LEED pattern for each condition of low or high coverage and of sample at room temperature or heated to higher temperature reveals that there is absolutely no order on the surface. Thus the molecules do not self-organise into a periodic structure at the surface, in contrast to (S)-alanine on Cu (110).

The STM images taken at room temperature also reveal that there is no organisation of the (S)-alanine molecules in a proper structure, Figure 3.28. However, the (S)-alanine molecules seems to align in the [1 -1 0] direction. In contrast with Cu (110), where the (S)-alanine molecules can organise themselves even at room temperature, on Ni (110) this does not happen. This is presumably due to the greater strength of the interaction

between the Ni (110) surface and the (S)-alanine molecules. On the Ni (110) surface the (S)-alanine molecules appear to "hit and stick" whereas on Cu (110) they have sufficient mobility to move around and maximise the intermolecular interactions between the (S)-alanine molecules.

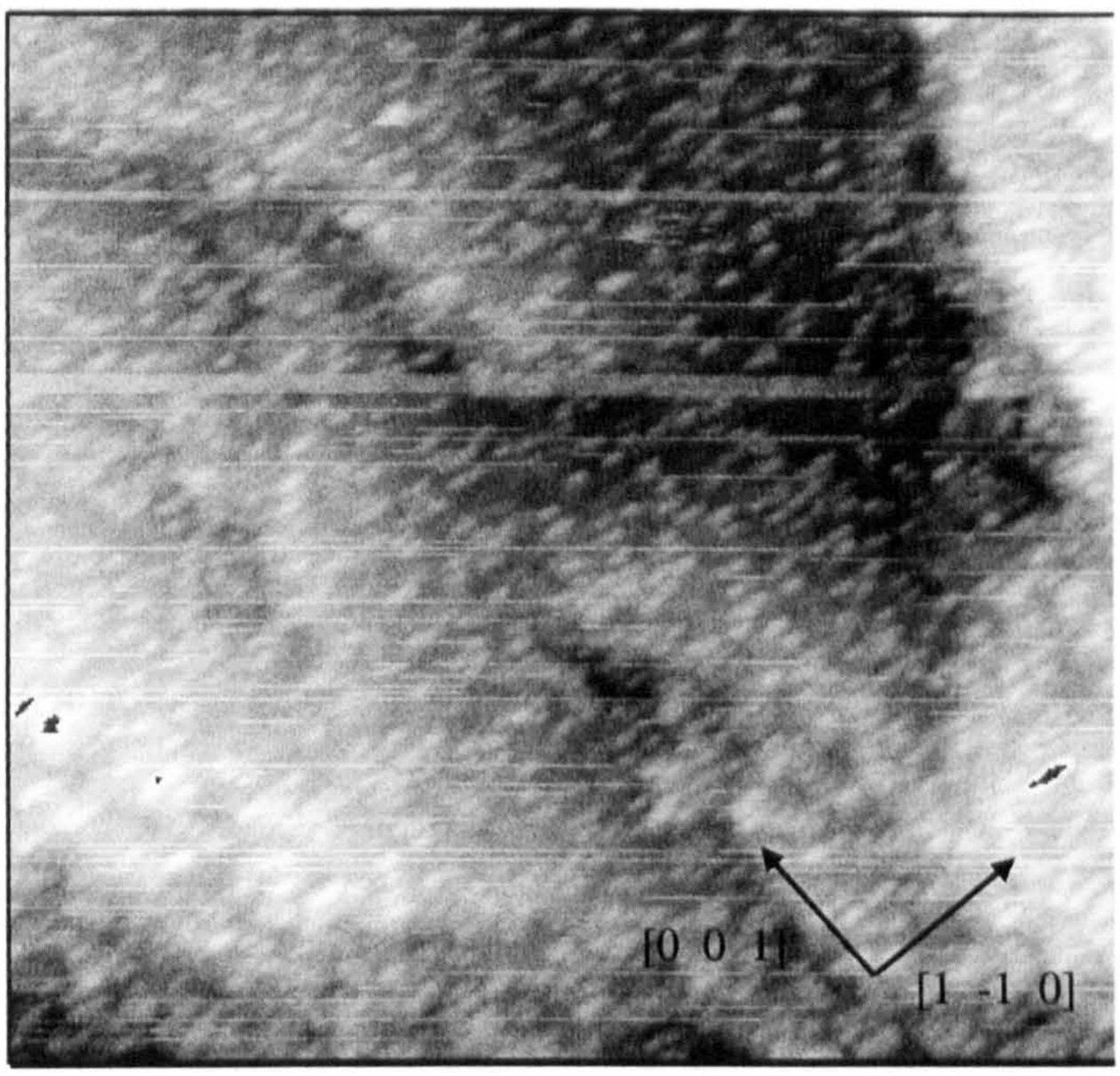

Figure 3.28: STM image of a high coverage of (S)-alanine on Ni (110) at room temperature; 500 Å × 500 Å (V_{tip} = -0.7 V; I_t = -0.33 nA) (Compare with Figure 3.11 on page 82).

The same processes have been observed when tartaric acid is deposited on Cu (110) and on Ni (110) [52-53]. On Cu (110), the tartaric acid molecules re-organise themselves depending on the coverage and on the temperature. On Ni (110), they form complexes with the nickel atoms. These complexes, depending on the temperature, reconstruct the surface [53].

3.3 (R)-alanine on Ni (110)

It is known that the chirality of the product MHB, in the dehydrogenation of MAA, is affected by the chirality of the alanine modifier [54-58]; so any variations in adsorption between (R) and (S)-alanine would be of particular interest. Thus, this section presents the RAIRS and TPD results which have been obtained with the (R)-alanine under the same experimental conditions as with (S)-alanine.

It is important to note, however, that attempts to distinguish enantiomeric forms of α-substituted dicarboxylic acids in the infrared have previously failed [59-60]. The reason for this is that enantiomers are chemically identical and the vibration frequencies of each enantiomer are expected to give identical infrared spectra. We can thus expect the same results for the amino acids, for (S) and (R)-alanine.

It has however been shown by STM and DFT calculations that if adsorbed on Ni (110), (R, R) and (S, S)-tartaric acid present different two-dimensional arrangements [53]. Unfortunately, during the period of this thesis, no STM images of the adsorption of (R)-alanine on Ni (110) have been taken. For completeness, however, the RAIRS and TPD results for (R)-alanine on Ni (110) are presented in the next section.

RAIR spectra were obtained as a function of increasing coverage during the adsorption of (R)-alanine on Ni (110). These spectra are presented in Figure 3.29.

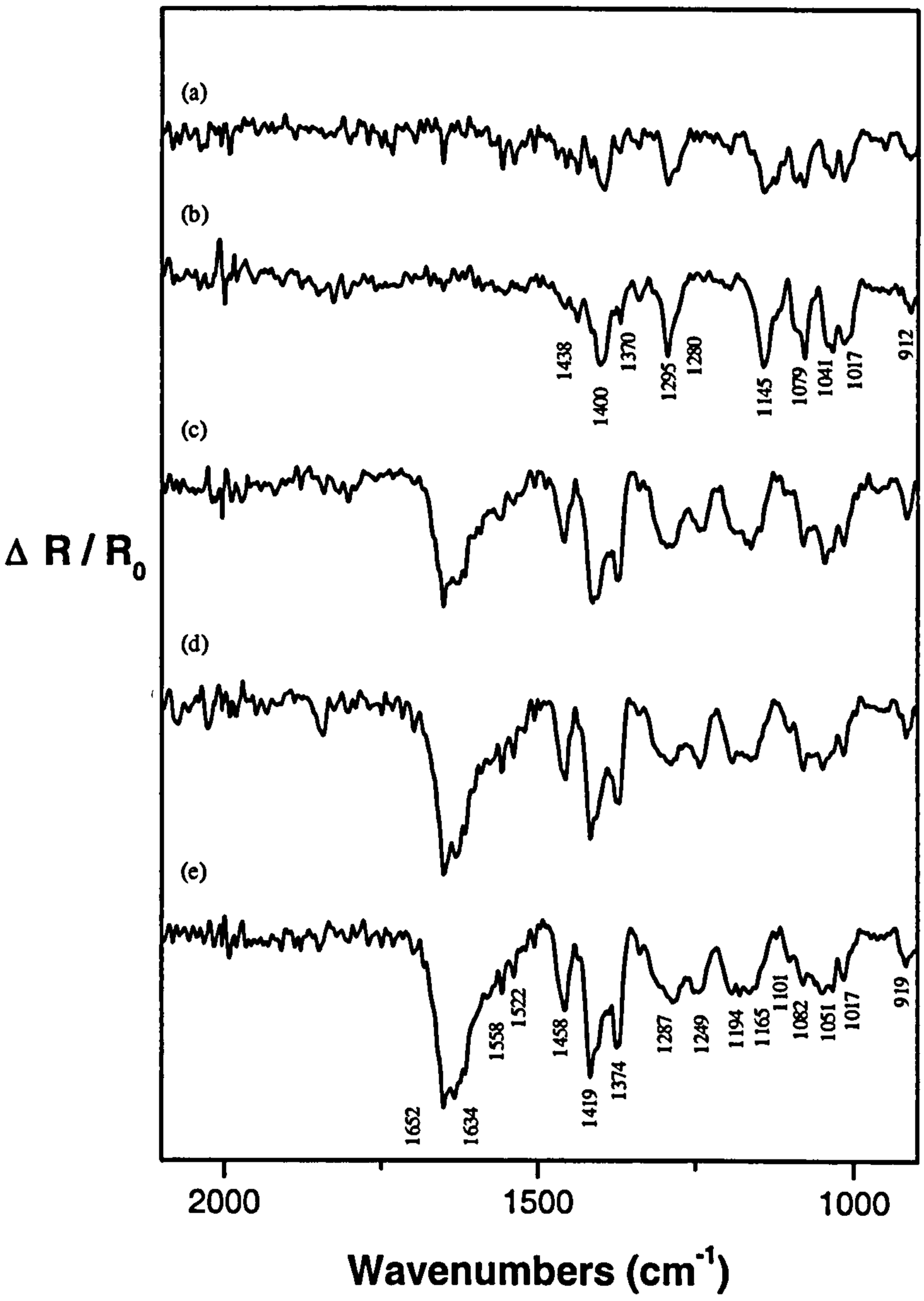

Figure 3.29: Successive RAIR spectra obtained during exposure of clean Ni (110) to (R)-alanine at 300 K after sublimation time of (a) 4 mins, (b) 6 mins, (c) 10 mins, (d) 12 mins, (e) 16 mins at 2×10^{-9} mbar.

As can be seen in Table 3.11, the infrared frequencies of the absorption bands of the (S)- and (R)-alanine are similar, since the resolution of the spectrometer is 4 cm^{-1}.

(S)alanine on Ni (110) adsorbed at 300 K		(R)-alanine on Ni (110) adsorbed at 300 K	
Low coverage	High coverage	Low coverage	High coverage
	2970		2965
2933	2934	2937	2932
2873	2874	2876	*2880*
	1651		1652
	1631		1634
	1555		1558
	1520		1522
1448	1458	1438	1458
1406	1418	1400	1419
1372	1375	1370	1374
1297	1282	1295	1287
1286	1253	1280	1249
	1188		1194
1148	1162	1145	1165
	1100		1101
1078	1081	1079	1082
1044	1047	1041	1051
1015	1018	1017	1017
915	914	912	919

Table 3.11: Comparison between the infrared frequencies for both the (S)- and (R)-enantiomers of alanine adsorbed on Ni (110) at low and high coverage at room temperature.

These data clearly suggest that both enantiomers are adsorbed with the same chemical form, anionic at low coverage and anionic plus zwitterionic at higher coverage. Thus both enantiomers are bonded to the Ni (110) surface in the same way.

When warmed above room temperature, both enantiomers also gave identical RAIR spectra, indicating that there are no variations between the adsorption geometry of the two enantiomers at any temperature.

Figure 3.30 shows the TPD spectra obtained for the (R)- and the (S)-alanine at low and high coverages.

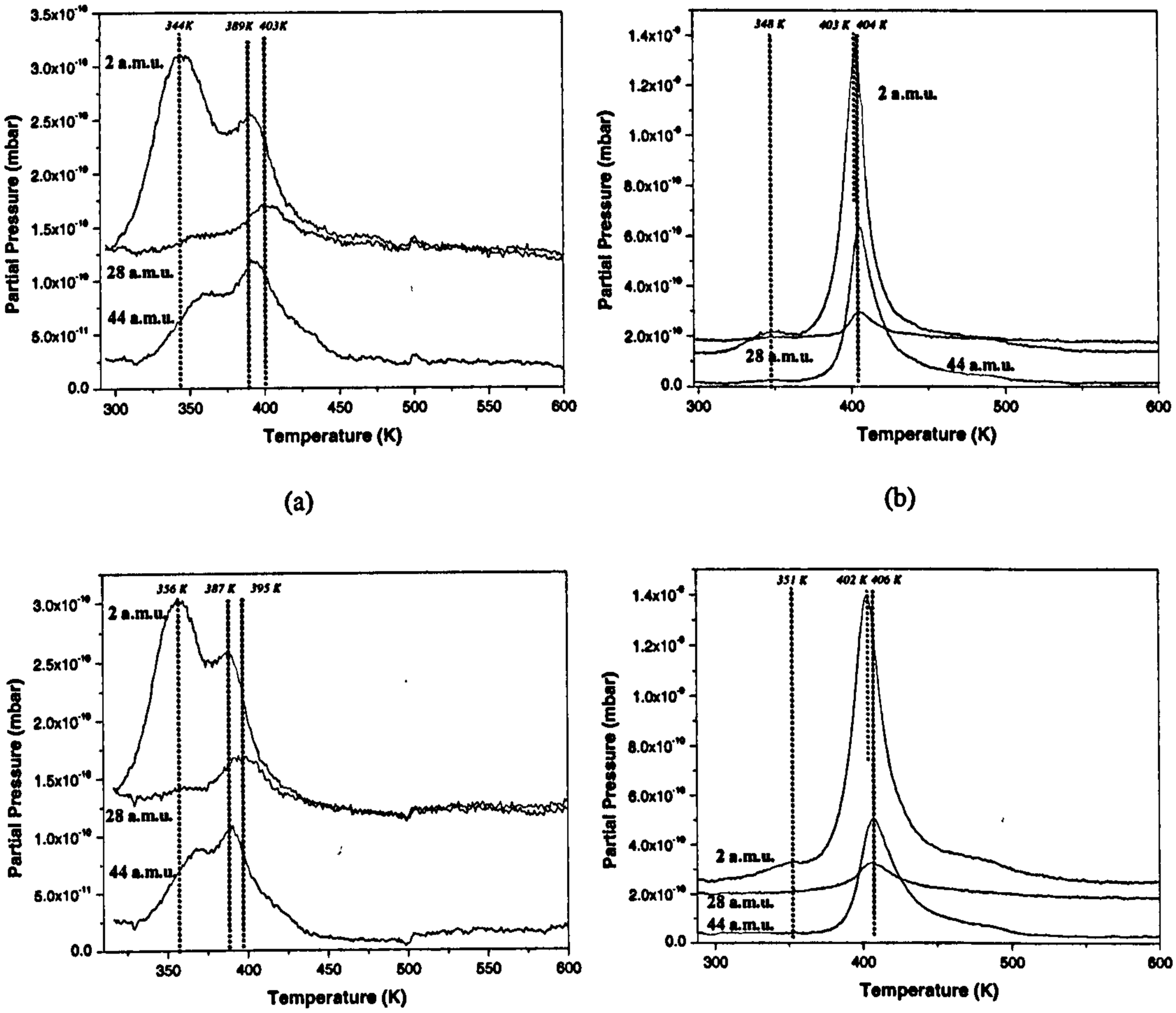

Figure 3.30: TPD spectra of (a) low coverage of (R)-alanine; (b): high coverage of (R)-alanine; (c): low coverage of (S)-alanine; (d): high coverage of (S)-alanine.

From Figure 3.30, both enantiomers desorb from the Ni (110) surface in the same way. This is expected as the Ni (110) is not a chiral surface. A difference of temperature of up to 12 K can be noticed, probably due to the experimental error.

3.4 Summary

The results can be summarised in the phase diagram presented in Figure 3.31. Only the (S)-alanine is represented, but this diagram is also valid for the (R)-alanine.

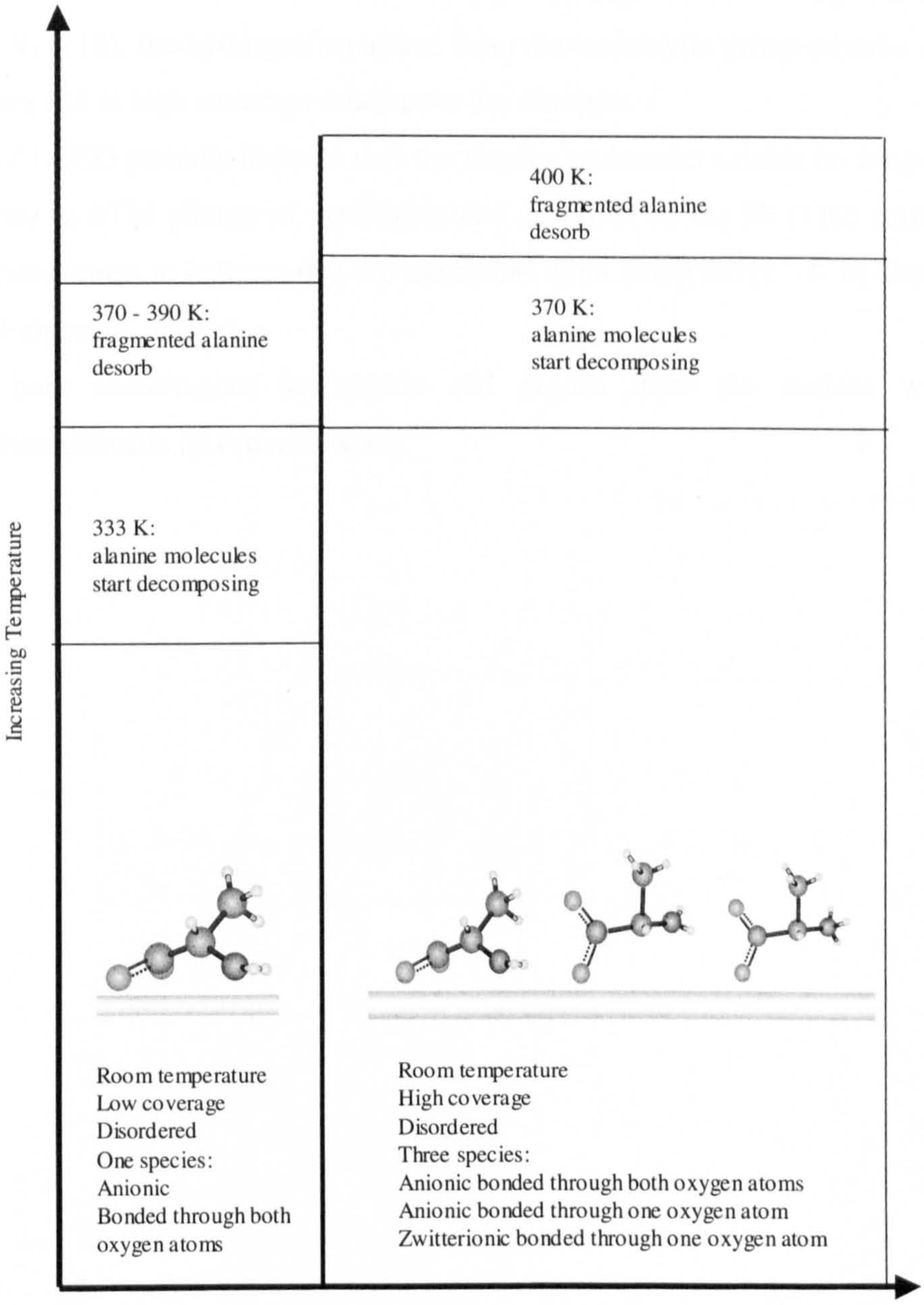

Figure 3.31: Adsorption phase diagram showing the nature adopted by (S)-alanine molecules on the Ni (110) surface as a function of temperature and coverage.

The alanine exists on the Ni (110) as two chemical forms: anionic and zwitterionic, depending on the coverage. At low coverage, the alanine molecules are present in the anionic form and are bonded through both oxygens of the carboxylate group as well as the electron lone pair of the nitrogen. At high coverage, another phase grows in alongside the low coverage phase with the molecule bound to the surface through one oxygen of the carboxylate group. At high coverage both the zwitterionic and ionic forms of alanine appear on the surface. It is believed that when the alanine molecules deprotonate to adsorb on the Ni (110), the hydrogen separated from the carboxylic group adsorbs on the Ni (110) surface and at high coverage attaches to the nitrogen.

The absence of LEED patterns indicate that the alanine molecules exhibit no long-range order. However, an STM picture of the (S)-alanine adsorbed on the Ni (110) surface at room temperature seems to indicate that the molecules align along the [1 -1 0] direction, but do not self-organise.

On heating, both enantiomers decompose and desorb from the surface without reorganising themselves in an ordered phase.

References

[1] G. Junk and H. Svec, J. Am. Chem. Soc., **85**, 839 (1963).

[2] A. G. Császár, J. Phys. Chem., **100**, 3541 (1996).

[3] C. J. Cassady, S. R. Carr, K. Zhang, A. C. Phillips, J. Org. Chem., **60**, 1704 (1995).

[4] Y. Ding and K. Krogh-Jespersen, Chem. Phys. Lett., **199**, 261 (1992).

[5] P. D. Godfrey, S. Firth, L. D. Hartherley, R. D. Brown, A. P. Pierlot, J. Am. Chem. Soc., **115**, 9687 (1993).

[6] A. G. Császár, J. Mol. Struct., **346**, 141 (1995).

[7] H. J. Simpson, Jr., R. E. Marsh, Acta Crystallogr., **20**, 550 (1966).

[8] J. T. Edsall, J. Chem. Phys. **4**, 1 (1936).

[9] L. D. Barron, A. R. Gargaro, L. Hecht, P. L. Polavarapu, Spectrochim. Acta A, **47**, 1001 (1991).

[10] M. Takeda, R. E. S. Iavazzo, D. Garfinkel, I. H. Scheinberg, J. T. Edstall, J. Chem. Phys., **80**, 3813 (1958).

[11] J. F. Pearson, M. A. Slifkin, Spectrochim. Acta A, **28**, 2403 (1972).

[12] K. Fukushima, T. Onishi, T. Shimanouchi, S. Mizushima, Spectrochim. Acta, 236 (1959).

[13] H. J. Simpson, Jr., R. E. Marsh, Acta Crystallogr., **20**, 550 (1966).

[14] R. Destro, R. E. Marsh and R. Bianchi, J. Phys. Chem., **92**, 966 (1988).

[15] M. S. Lehmann, T. F. Koetzle, W. C. Hamilton, J. Am. Chem., Soc. **94**, 2657 (1972).

[16] A. M. Mieu, D. Durand, M, Quilichini, M. J. Field, J. C. Smith, J. Phys.Chem., **99**, 5645 (1995).

[17] S. Suzuki, T. Ohshima, N. Tamiya, K. Fukushima, T. Shimanouchi and S. Mizushima, Spectrochim. Acta, **11**, 969 (1959).

[18] T. Oshima, N. Tamiya, Spectrochim. Acta, **17**, 384 (1961).

[19] S. F. A. Kettle, E. Lugwisha, P. Vorderwisch, J. Eckert, Spectrochim. Acta A, **46**, 921 (1990).

[20] M. Tsuboi, T. Takenishi, A. Nakamura, Spectrochim. Acta, **17**, 634 (1961).

[21] R. F. Adomowicz, M. L. Sage, Spectrochim. Acta A, **30**, 1007 (1974).

[22] R. F. Adomowicz, E. Fishman, Spectrochim. Acta A, **28**, 889 (1972).

[23] M. Diem, P. L. Polavarapu, M. Oboodi and L. A. Nafie, J. Am. Chem. Soc., **104,** 3329 (1982).

[24] G. Yu, T. B. Freedman, L. A. Nafie, Z. Deng and P. L. Polavarapu, J. Phys. Chem., **99,** 835 (1995).

[25] M. T. S. Rosado, M. L. R. S. Duarte, R. Fausto J. Mol. struct., **410-411,** 343 (1997).

[26] X. Cao, G. Fischer, Spectrochim. Acta A **55,** 2329 (1999).

[27]. M. Avram, Gh. Mateescu, Infrared spectroscopy, p 125 (Wiley-Interscience, Romania, 1972).

[28] B. A. Sexton, Surf. Sci. **88,** 319 (1979).

[29] D. A. Stern, G. N. Salaita, F. Lu, J. W. McCargar, N. Batina, D. G. Frank, L. Laguren-Davidson, C. Lin, N. Walton, J. Y. Gui, A. T. Hubbard, Langmuir **4,** 711 (1988).

[30] A. Ihs, B. Liedberg, K. Uvdal, C. Tornkvist, P. Bodo, I. Lundstrom, J. Colloid Interface Sci. **140,** 192 (1990).

[31] R. J. Colton, J. S. Murday, J. R. Wyatt, J. J. DeCorpo, Surf, Sci. **84,** 235 (1979).

[32] J. S. Suh, M. Moskovits, J. Am. Chem. Soc. **108,** 4711 (1986).

[33] L. L. Atanasoska, J. C. Buchholtz, G. A. Somorjai, Surf. Sci. **72,** 189 (1978).

[34] X. Zhao, R. G. Zhao, W. S. Yang, Surf. Sci. **442,** L 995-L 1000 (1999).

[35] J .Williams, PhD Thesis, Adsorption and characterisation of chiral amino acids on Cu (110) single crystal surfaces, (Liverpool University, 1988).

[36] J. Williams, S. Haq, R. Raval, Surface Science, 368 (1996) 303.

[37] S. Louafi, PhD Thesis, Creating model enantio-differentiating surfaces: alanine enantiomers and methylacetoacetate adsorptions studies on Cu(110), (Liverpool University, 2001).

[38] A. Hatta, Y. Moriya, W. Suetaka, Bull. Chem. Soc. Japan **48,** 3441 (1975).

[39] K. Nakamoto, Y. Morimoto, A. E. Martell, J. Am. Chem. Soc. **83,** 4528 (1961).

[40] D. Segnini, C. Curran, J. V. Quagliano, Spectrochim. Acta **16,** 540 (1960).

[41] G. C. Percy and H. Strenton, J. Chem. Soc., Dalton Trans. 2429 (1976).

[42] J. F. Jackovitz, J. A. Durkin, J. L. Walter, Spectrochim. Acta **23 A,** 67 (1967).

[43] K. Nakamoto, Infrared Spectra of Inorganic and Coordinated Compounds, 202 (1963).

[44] A. Rosenberg, Acta Chem. Scand. **10,** 840 (1956).

[45] C. A. McAuliffe, W. D. Perry, J. Chem. Soc. 634 (1969).

[46] R. G. Greenler, D. R. Snider, D.Witt, R. S. Sorbello,Surf. Sci. **118,** 415 (1982).

[47] H. A. Pearce, N. Sheppard, Surf. Sci. **59,** 205 (1976).

[48] S. M. Barlow, K. J. Kitching, S. Haq, N. V. Richardson, Surf. Sci. **401,** 322 (1998).

[49] Vinogradov, Linneell, Hydrogen Bonding, p 52 (Van Nostrand Reinhold Company, New York, 1971).

[50] K. Christmann, F. Chehab, V. Penka, G. Ertl, Surf. Sci. **152,** 256 (1985).

[51] G. Junk and H. Svec, J. Am. Chem. Soc., 85 (1963) 839.

[52] M. Ortega-Lorenzo, PhD Thesis, Complexities and dynamics of the enantioselective site in heterogeneous catalysis : tartaric acid and methylacetoacetate on Cu(110) (Liverpool University, 1999).

[53] V. Humblot, PhD Thesis, Complexities and dynamics of the enantioselective site in heterogeneous catalysis : tartaric acid on Ni (110) (Liverpool University, 2002).

[54] A. Tai and T. Harada, Taylored Metal Catalysts, p.265 (Y. Iwasawa, Reidel, Dordrecht, 1986).

[55] Y. Izumi, Adv. Catal. **32,** 215 (1983).

[56] M.J. Fish, D.F.Ollis, J. Catal. **50,** 353 (1977).

[57] A. Hoek, W.M.H. Sachtler, J. Catal. **58,** 276 (1979).

[58] M. A. Keane, Langmuir **10,** 4560 (1994).

[59] Bellamy, L.J., The Infrared Spectra of Complex Molecules, p.162 (Methuen, London, 1959).

[60] M. Avram, Infrared Spectroscopy - Applications in Organic Chemistry, p. 394 (Wiley, Interscience, 1972).

Chapter Four

Adsorption of the Enantiomers of Methyl-3-hydroxybutyrate on Cu (110)

4.1 Introduction

4.1.1 Presentation of the molecule of methyl-3-hydroxybutyrate (MHB)

Methyl-3-hydroxybutyrate (MHB) is a molecule with an alcohol and an ester group in β-positions as shown in Figure 4.1. The methyl-3-hydroxybutyrate molecule [1-2] is a molecule with a C = O and an alcohol group and as the similar molecules, in solution present two associations: intermolecular and intramolecular [1-6] hydrogen bondings. Indeed, the strongly electronegative oxygen atom attached through its two valencies to a hydrogen atom and a carbon from the organic group has two pairs of unshared electrons which enable the formation of hydrogen bonds with acceptors of electrons, such as C=O. The factor responsible for the posture of this molecule in solution is the hydrogen bonding between the alcohol group and the ketone group, as shown in Figure 4.2. The hydrogen bonding in MHB can be between OH and OCH_3 and / or between OH and O = C [2].

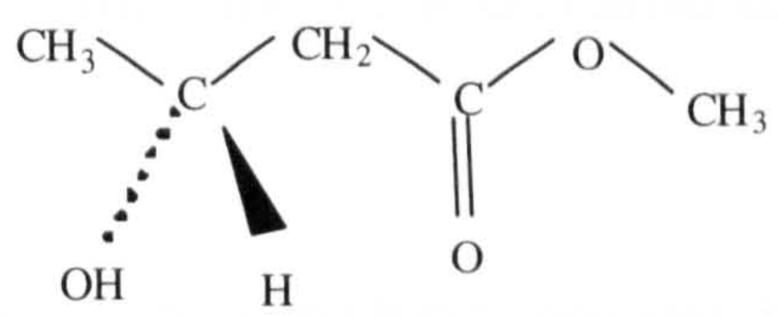

(R)-Methyl-3-hydroxybutyrate
(R-MHB)

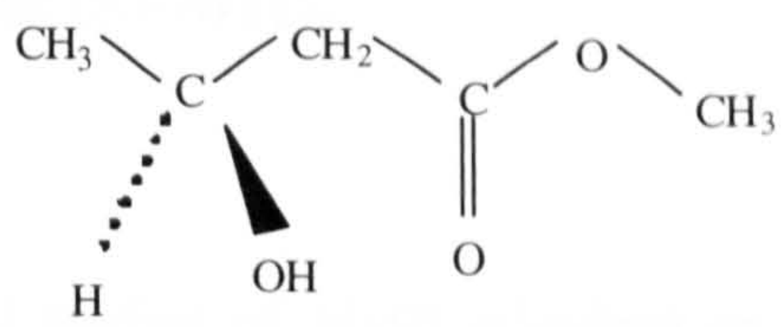

(S)-Methyl-3-hydroxybutyrate
(S-MHB)

Figure 4.1: Enantiomers of MHB; the asymmetric centre is the carbon bonded to the alcohol group.

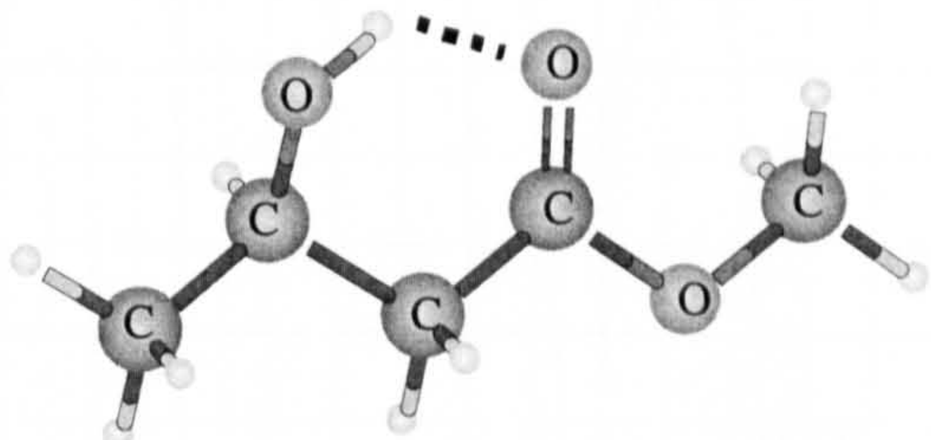

Figure 4.2: Hydrogen bonding between the ketone and the alcohol group in MHB; here shown for the (R) enantiomer.

4.1.2 Assignments of the infrared bands of (S)-MHB

To the best of my knowledge, previous infrared studies of MHB adsorbed on metal surfaces do not exist in the litterature. To assign the infrared bands obtained from the adsorption of MHB on Cu (110), it was necessary to consider the infrared spectrum of MHB in its liquid form. The infrared spectrum of (S)-MHB in the liquid form is presented in Figure 4.3.

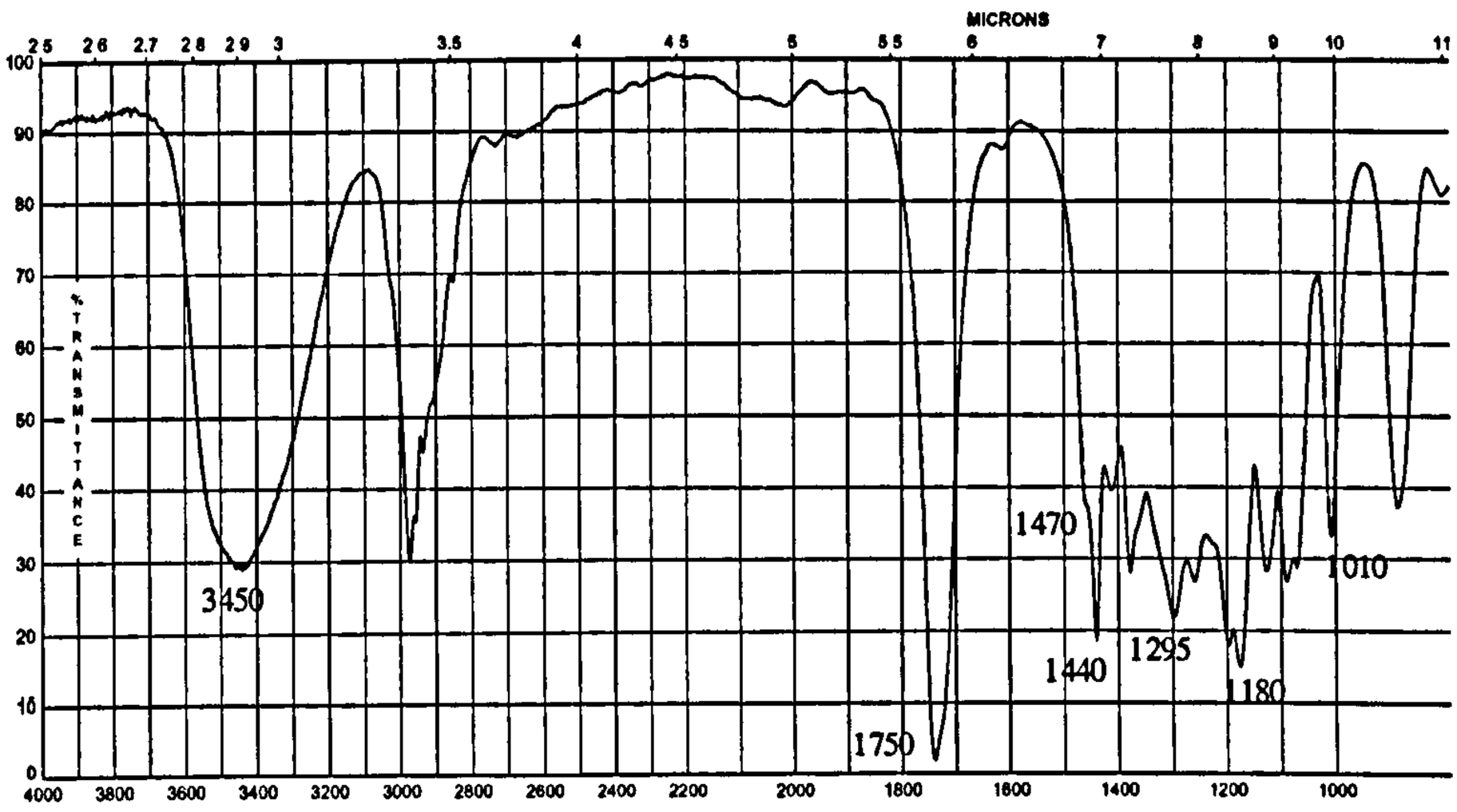

Figure 4.3: Infrared spectrum of (S)-methyl-3-hydroxybutyrate [7].

In order to assign these bands, the infrared spectra and / or assignments of polycrystalline sodium-β-hydroxybutyrate [8], (-) zinc lactate and ethyl lactate [9] are considered. A consideration of the infrared spectrum of polycrystalline sodium β-hydroxybutyrate helps to assign the bands of the alcoholic part of the MHB molecule whereas the bands associated with ethyl lactate are important in identifying the ester part of the molecule.

Figure 4.4 presents the infrared spectrum of polycrystalline sodium-β-hydroxybutyrate [8] and Figure 4.5 presents the IR spectrum of poly-(β-hydroxybutyrate) [10]. The major difference between the two spectra is the region correlated to the absorption of the ν (C = O) bond. Indeed, in the sodium β-hydroxybutyrate spectrum, one large band with a shoulder at 1560-1600 cm^{-1} is present but in the spectrum of the poly-(β-hydroxybutyrate), these two bands are replaced by a band at 1730 cm^{-1}. The structure of the polymer of poly-(β-hydroxybutyrate) does not allow its ionisation so consequently, the compound keeps its C = O bond. This is in contrast to sodium-β-hydroxybutyrate which ionises into $[CH_3CHOHCH_2COO]^-$. Indeed, the spectrum of this last compound presents two bands at 1595 cm^{-1} and 1410 cm^{-1}. These bands can be assigned to ν_{as} (COO^-) and ν_s (COO^-) vibrational modes respectively, as has been explained in Chapter Three.

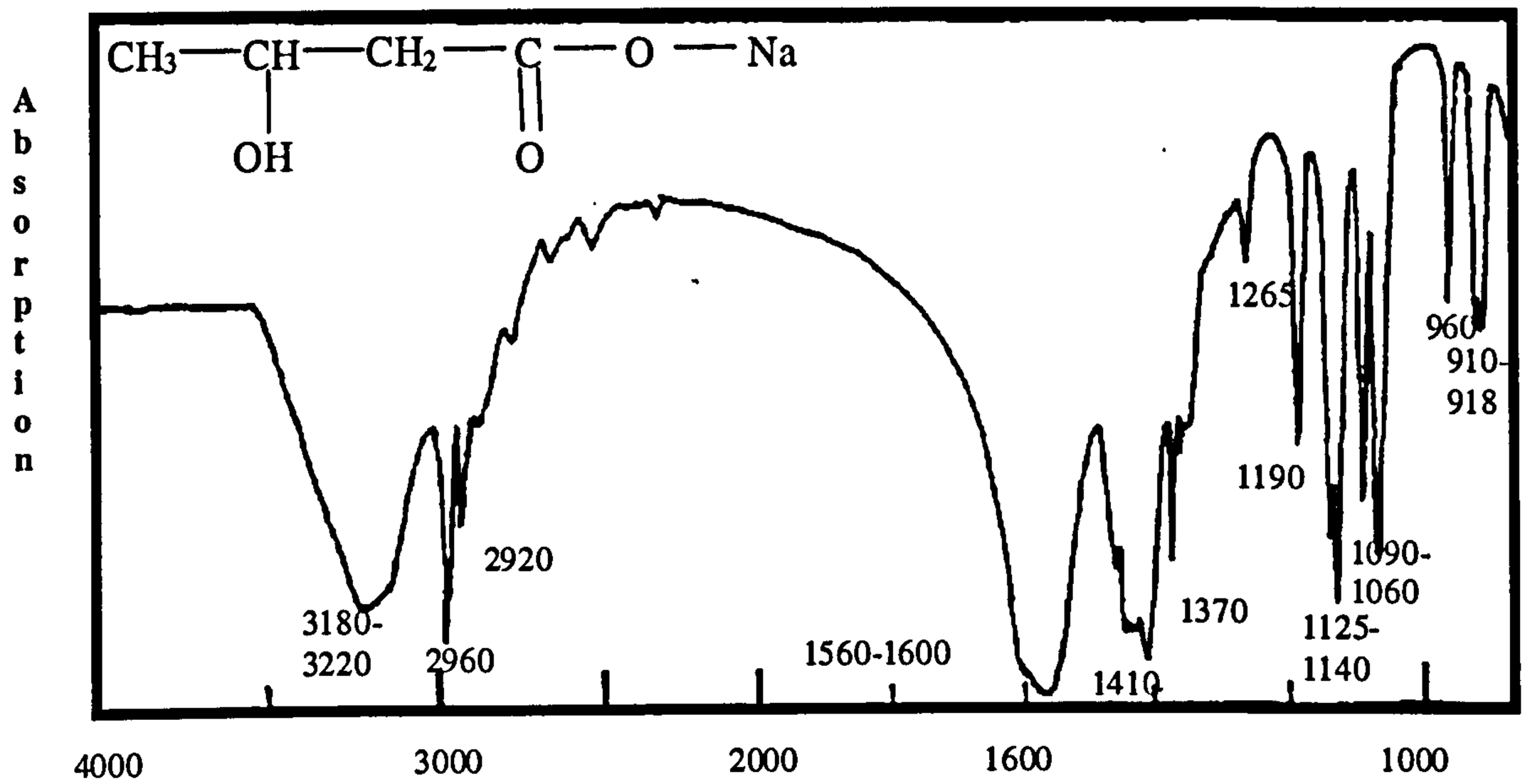

Figure 4.4: FTIR spectrum of polycrystalline sodium β-hydroxybutyrate [8].

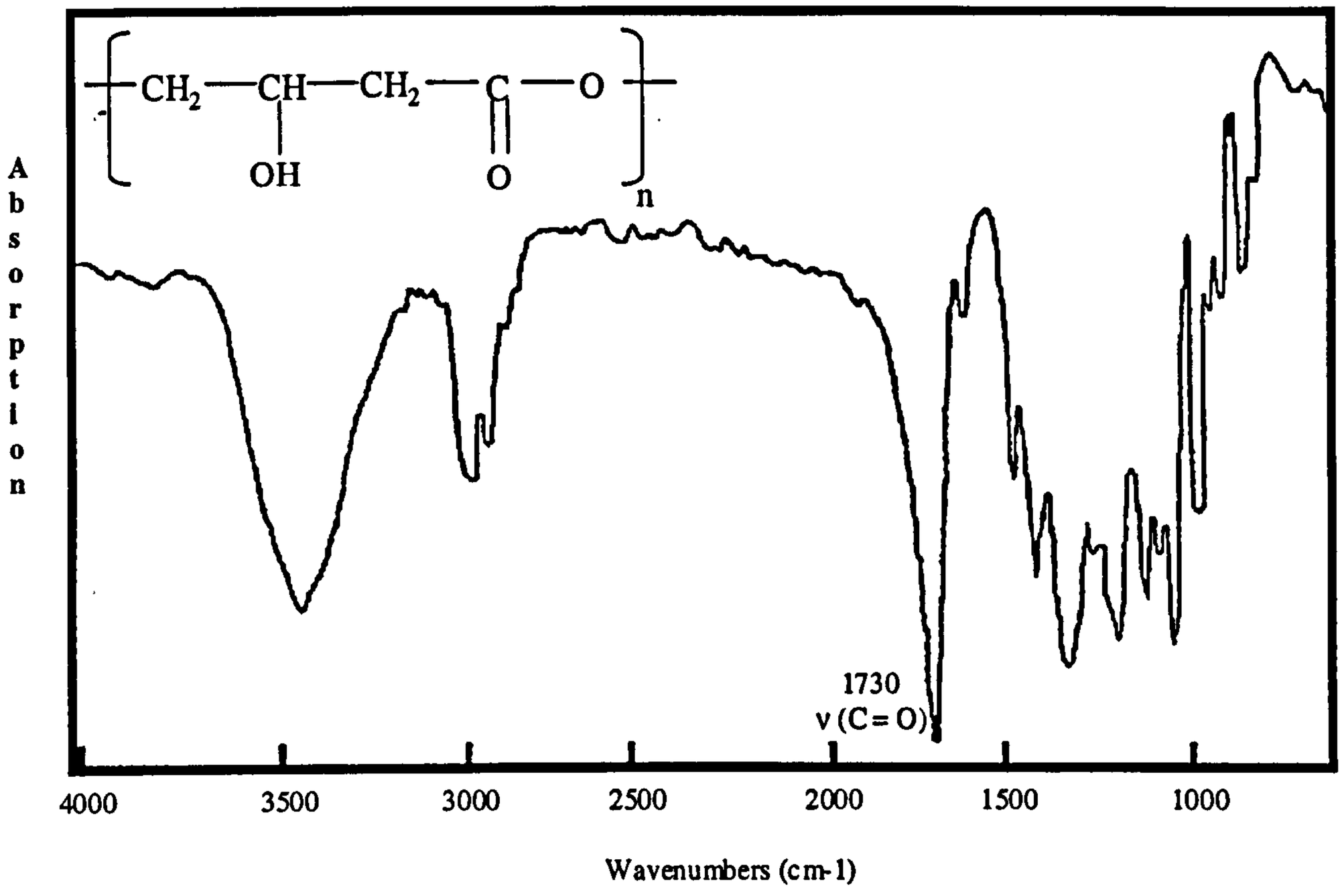

Figure 4.5: IR spectrum of poly-(β-hydroxybutyrate) [10].

Figure 4.6 presents a drawing of sodium-β-hydroxybutyrate in its ionised form.

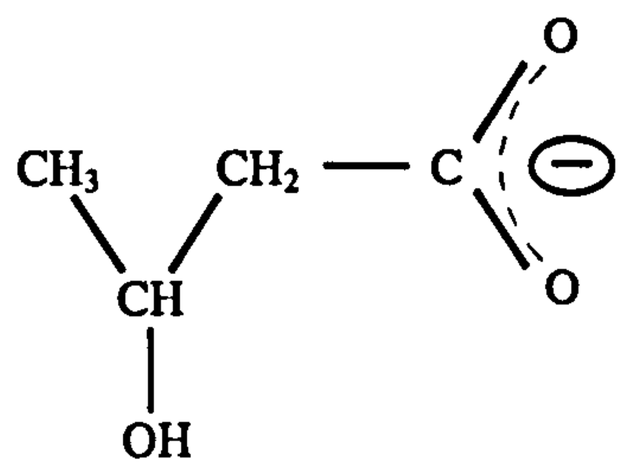

Figure 4.6: Ionic form of sodium β-hydroxybutyrate.

The assignments given for the polycrystalline sodium β-hydroxybutyrate [8] are shown in Table 4.1.

The strongly electronegative alcoholic oxygen atom has two pairs of unshared electrons which enable the formation of hydrogen bonds between the OH group and the C = O group. Consequently, in the infrared spectrum, the band arising from the stretching vibration of the hydroxyl group in free alcohol, which is at ~3600-3650 cm^{-1} disappears

and a new band, much broader and much stronger, at lower frequencies, at 3180-3215 cm^{-1} appears instead, arising from the –O-H...O bond, inter- or intra-molecule(s). This suggests that the ν (OH) band is a composite of a large number of thin bands corresponding to different modes of association of the molecules.

The ionic form of sodium β-hydroxybutyrate is a secondary alcohol, and its ν (CO) vibration is expected to arise around 1100 cm^{-1} [11]. This vibration is represented by a doublet on the spectrum of sodium β-hydroxybutyrate at 1125 cm^{-1} and 1140 cm^{-1}. The presence of intra- or intermolecularly OH-bonded conformations has been put, by Morssli et al [8], responsible for the presence of this doublet. The same phenomenon has been observed for the assignment of zinc lactate, which deprotonates into $[CH_3CHOHCOO]^-$ ion in aqueous solution [10]. The ν (CO) vibration gives a doublet at 1121 cm^{-1} and 1090 cm^{-1}, due to intra- or intermolecular hydrogen bonding according to Goulden [9].

The δ (OH) deformation mode, in the presence of hydrogen bondings, is shifted to higher frequencies but it does not show any substantial band broadening or intensity change when hydrogen bonding occurs [12]. This band has been assigned to the frequency of 1350 cm^{-1} by Morssli et al [8] and this high frequency is said to be representative of free alcohol groups. In zinc lactate, the δ (OH) deformation mode gives rise to two bands which have been assigned by Goulden et al at 1390 cm^{-1}, for the hydrogen bonded alcoholic group (CO_2^- --- H), and at 1279 cm^{-1} for the "more free" alcoholic group (C = O --- H_2O) [9].

Wavenumbers (cm^{-1})	Assignments
3215	ν (OH)
3180	ν (OH)
2960	ν (CH_3)
2920	ν (CH_2)
2895	ν (CH)
2880	
2800	
1560-1595	ν_{as} (COO^-)
1440-1460	δ_{as} (CH_3)
1425	δ (CH_2)
1410	ν_s (COO^-)
1370	δ_s (CH_3)
1355	w (CH_2)
1350	δ (OH)
1320	δ (CH)
1265	δ (CH)
1190	tw (CH_2)
1125-1140	ν (C - OH)
1065-1090	ν (C - C)

Table 4.1: Infrared bands and assignments in sodium β-hydroxybutyrate [8].

In this section, the ester part of the MHB molecule is taken into account. Esters are easily recognisable on an infrared spectrum because of their characteristic absorptions arising from the C=O and C-O groups. The carbonyl frequency is higher than that for normal ketones because of the influence of the oxygen atom. The single bond C-O is very strong in esters which allows it to be differentiated from the weaker C-C band of ketones which appear in the same spectral region. Figure 4.7 shows the vibrational motions associated with the ester functionality.

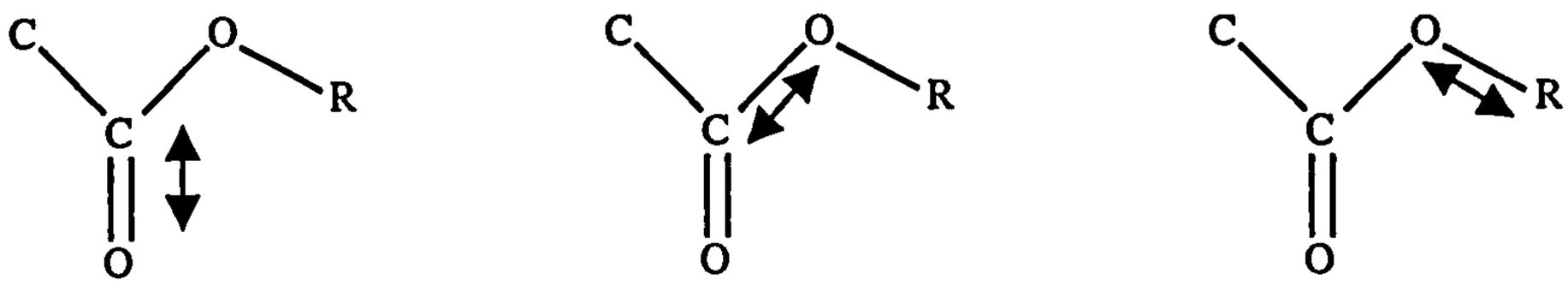

ν (C = O): ~ 1700 cm^{-1} ν (C – O_e): ~1200 cm^{-1} ν (O_e - R):~ 1050 cm^{-1}

Figure 4.7: Vibrational motions associated with the ester functionality.

As an example, Table 4.2 gives the infrared bands and assignments of ethyl lactate in aqueous solution [9].

Ethyl lactate 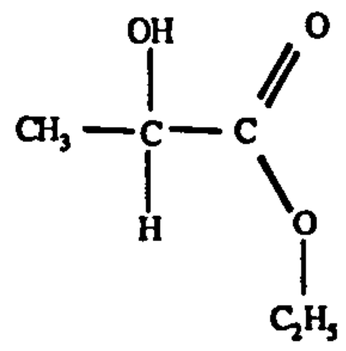	Assignments
1464	δ_{as} (CH_3)
1383	δ_s (CH_3)
1294	δ (OH)
1230	ν (CO – O_e C_2H_5)
1129	ν (C - OH)
1047	ν (C - CH_3)
1012	ν (O_e – C_2H_5)

Table 4.2: Infrared bands and assignments of ethyl lactate in aqueous solution [9].

From the assignments of sodium β-hydroxybutyrate and ethyl lactate, it is possible to assign the infrared spectrum of liquid methyl-3-hydroxybutyrate. The assignments are presented in Table 4.3.

Sodium-β-hydroxybutyrate [8]		Ethyl lactate [9]		Methyl-3-hydroxybutyrate [Spectrum from [7] Assignment, this work]	
3215	ν (OH)			3450	ν (OH)
3180	ν (OH)				
2960				2960 vs	
2920	ν (CH_3)			2920 m	ν (CH_3)
2895	ν (CH_2)			2895 m	ν (CH_2)
2880	ν (CH)			2880 m	ν (CH)
2800				2800 m	
				1750	ν (C = O)
1595-1560	ν_{as} (COO^-)				
1440-1460	δ_{as} (CH_3)	1464	δ_{as} (CH_3)	1440-1470	δ_{as} (CH_3)
1425	δ (CH_2)			1420	δ (CH_2)
1410	ν_s (COO^-)				
1370	δ_s (CH_3)	1383	δ_s (CH_3)	1380	δ_s (CH_3)
1355	w (CH_2)				
1350	δ (OH)			1360	δ (OH) or w (CH_2)
1320	δ (CH)				
		1294	δ (OH)	1295	δ (OH)
1265	δ (CH)			1260	δ (CH)
		1230	ν ($CO-O_eC_2H_5$)	1230	ν ($CO-O_e$ CH_3)
1190	tw (CH_2)			1195	tw (CH_2)
				1180	ρ (CH_3)
1125-1140	ν (C - OH)	1129	ν (C - OH)	1120	ν (C – OH)
1065-1090	ν (C - C)	1047	ν (C - CH_3)	1060-1090	ν (C – CH_3)
		1012	ν (O_e - C_2H_5)	1010	ν (O_e - CH_3)

Table 4.3: Assignments of methyl-3-hydroxybutyrate in the liquid form.

4.1.3 Adsorption of esters on surfaces

Some studies on the adsorption of some esters on single metal have been published by a number of authors [13-20]. It has been found that the wavenumbers of the ν (C=O) and ν (C-O_e) bonds of methyl formate, ethyl formate and methyl acetate shift when these molecules adsorb on a surface, as shown in Table 4.4.

	Methyl formate $HCOOCH_3$			**Methyl acetate CH_3COOCH_3**		**Ethyl formate $HCOOC_2H_5$**	
	Gas	Adsorbed on Ni(111)	Adsorbed on Cu(110)	Gas	Adsorbed on Ni(111)	Solution	Adsorbed on Ni(111)
ν(C=O)	1746	1659	1670	1747	1666	1732	1653
ν(C-O_e)	1205	1262	1260	1249	1302	1187	1255

Table 4.4: Shifts in the ν (C=O) and ν (C-O_e) modes of some esters caused by adsorption on single metal surfaces [13-14].

The interesting fact emerging from this table is that the wavenumbers of the ν(C=O) mode reduce from ~ 1750 cm^{-1} in the gas or liquid phase to ~ 1660 cm^{-1} when adsorbed onto a surface. In contrast, the wavenumbers of the ν (C - O_e) mode increase from the gas or liquid phase.

These esters have been found to bond to the metal surface through the carbonyl lone pair. Their molecular plane is perpendicular to the surface. Table 4.5 presents the assignments of the bands of methyl acetate adsorbed on Ni (111) [14].

Methyl Acetate on Ni(111) [14]

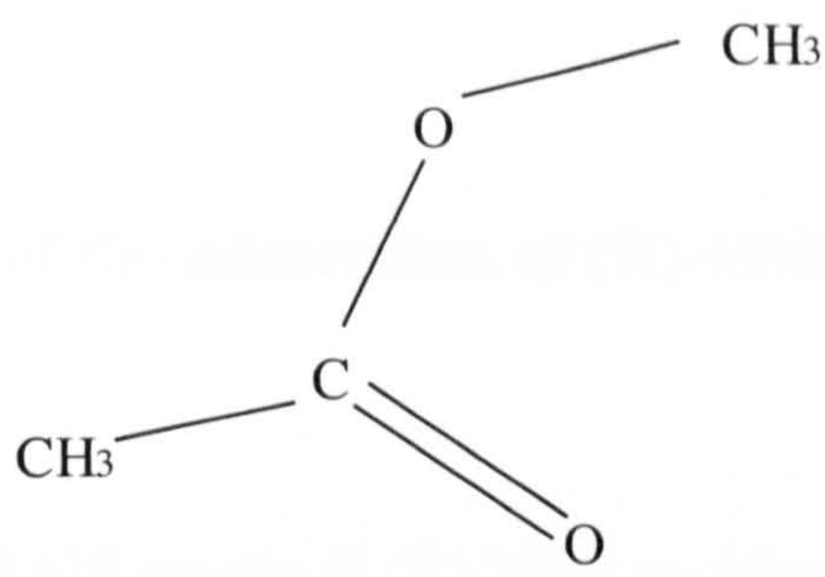

Ni(111)

Wavenumbers (cm^{-1})	Assignments
1666	ν (C = O)
1456	δ_a (CH_3)
1364	δ_s (CH_3)
1302	ν (C - O_e)
1041	ν (O_e - CH_3)

Table 4.5: Assignments of the bands of methyl acetate adsorbed on Ni (111), as well as its position on the surface [14].

Although the assignments of the main bands of MHB have been obtained, care will be needed when it is adsorbed on metal surface as bands are likely to change position.

4.2 (R)-MHB on Cu (110)

4.2.1 RAIRS study of the adsorption of (R)-MHB on Cu (110) at 300 K

Figure 4.8 presents the RAIR spectra of (R)-MHB adsorbed on a clean Cu (110) surface with increasing exposure from 3 L to 15 L.

The tentative assignments of the bands presented on these spectra have shown that these infrared bands are related to two different molecular species. Indeed, it will be shown in a later section that the appearance of new bands from one spectrum to the other (surrounded in grey in the spectra in Figure 4.8) is not linked to the increase in coverage, but is linked to the transformation of the MHB into methyl-acetoacetate (MAA), which has begun while dosing the MHB. Figure 4.9 presents the RAIR spectrum of the (R)-MHB before its transformation into MAA begins. In the following section, only this RAIR spectrum of the (R)-MHB molecule, obtained as soon as it is absorbed on the surface, and before it is transformed into MAA, will be considered.

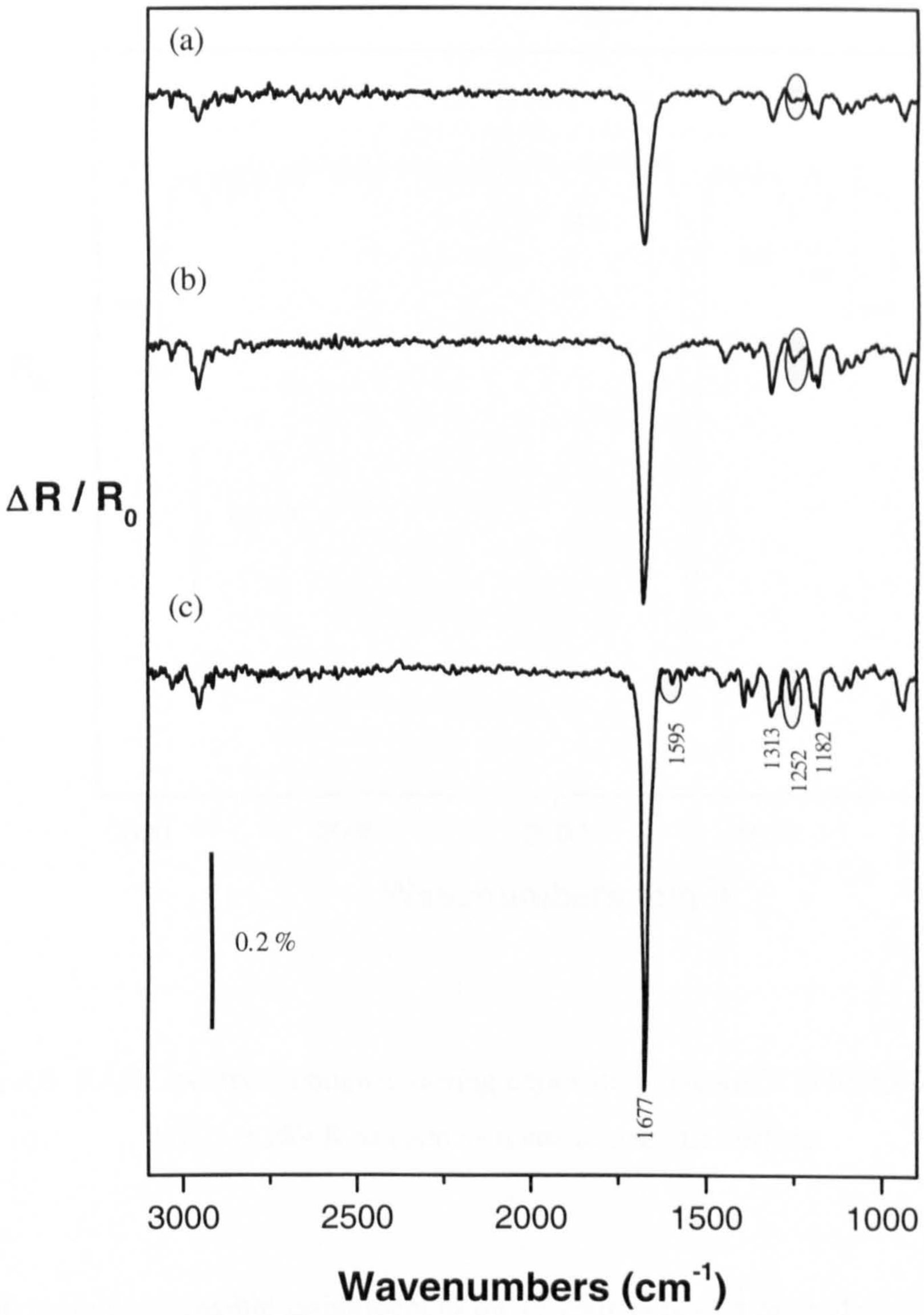

Figure 4.8: Successive RAIR spectra obtained during exposure of clean Cu (110) to (R)-MHB at room temperature; (a) 3L; (b) 5 L; (c) 15 L.

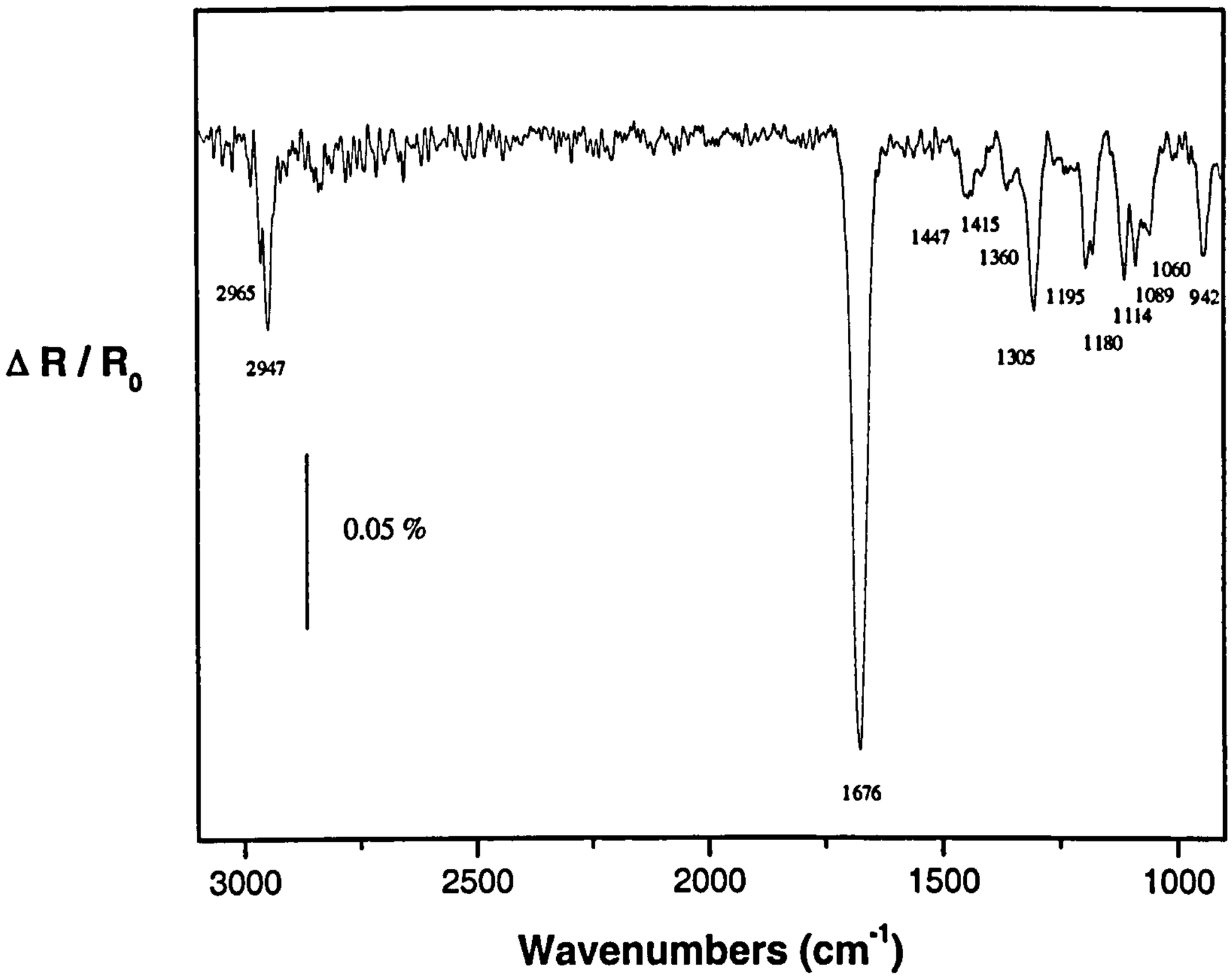

Figure 4.9: RAIR spectrum obtained during exposure of clean Cu (110) to 3 L of (R)-MHB at 289 K as soon as it adsorbs on the surface.

Table 4.6 presents a possible assignment of the (R)-MHB peak adsorbed on Cu (110).

Methyl-3-hydroxybutyrate in the liquid form (this work)		(R)-Methyl-3-hydroxybutyrate on Cu (110) (this work)	
3450	ν (OH)		
2960 vs 2920 m 2895 m 2880 m 2800 m	ν (CH_3) ν (CH_2) ν (CH)	2965 2947	ν (CH_3) ν (CH_2) ν (CH)
1750	ν (C=O)	1676	ν (C=O)
1440 - 1470	δ_{as} (CH_3)	1447	δ_{as} (CH_3)
1420	δ (CH_2)		
1380	δ_s (CH_3)	1415	δ_s (CH_3)
1360	δ (OH) or w (CH_2)	1360	δ (OH) or w (CH_2)
1260 - 1295	δ (CH)		
1230	ν (CO-O_eCH_3)	1306	ν (CO - O_eCH_3)
1195	tw (CH_2)	1195	tw (CH_2)
1180	ρ (CH_3)	1180	ρ (CH_3)
1120	ν (C – OH)	1114	ν (C – OH)
1060 - 1090	ν (C – CH_3)	1089	ν (C – CH_3)
1010	ν (O_e – CH_3)	1060	ν (O_e – CH_3)
942	tw CH_3	942	tw CH_3

Table 4.6: Assignments of (R)-MHB adsorbed on Cu (110) with comparison to assignments of MHB in the liquid form.

On the spectrum presented in Figure 4.9, the major band is present at 1676 cm^{-1}. This frequency is very close to the frequencies presented by the ν (C = O) vibration when esters are adsorbed on surfaces, as discussed earlier. This band is thus easily assigned to

the ν (C = O) vibration of the ketone part of the MHB molecule. Due to the high intensity of this band and its sharpness, it must be deduced that the carbonyl groups are oriented perpendicular to the surface. This first conclusion is not surprising if we consider the way the esters adsorb generally on clean surfaces [13-20].

However, the intensity of the other bands is very small relative to this first band. An assignment of the peaks can be proposed in Table 4.6, with the help of the work presented in the introduction section.

The other "easily" recognisable bands are the characteristic bands of esters. The assignment of MHB in liquid phase as well as the adsorption of other esters adsorbed on single metal surfaces, allows the band at 1060 cm^{-1} to be assigned to the ν (O_e - CH_3) stretching vibration.

The ν (CO - O_e CH_3) stretching vibration is expected to give a band around 1250 cm^{-1} in the liquid phase. In Figure 4.9, the band at 1305 cm^{-1} can be assigned to this vibration. It is the second most intense band of the spectrum and as has been observed for other esters in the gas phase [13-14], this frequency shifts to a higher value when adsorbed on a surface.

The description of these three ester bands gives already a first idea of the position of the MHB molecule on the surface. It can be deduced that the C = O bond is in a position very close to the normal of the surface; its position is "almost" normal to the surface plane but not "completely" normal as a consequence of the position of the CO - O_e CH_3 bond and O_e – CH_3 bond. As both ν (O_e – CH_3) stretching vibration and ν (CO - O_e CH_3) stretching vibration are seen, these bonds must be in a position situated between the normal and the parallel planes to the surface.

Bands due to the CH_3 group are low in intensity in Figure 4.9. Application of the infra-red metal surface selection rule indicates that the C - CH_3 bond is neither parallel nor perpendicular to the Cu surface. The ν (C – CH_3) stretch vibration has a medium component normal to the surface since it gives a medium band at 1089 cm^{-1}. If the C - CH_3 bond is parallel to the Cu surface, the δ_s (CH_3) symmetric vibration frequency should not be seen, while the δ_{as} (CH_3) asymmetric vibration should give rise to an infrared band at ~1450 cm^{-1}. On the other hand, when the C - CH_3 bond is normal to the Cu surface, the δ_s (CH_3) symmetric vibration frequency should give rise to an infrared band at ~1380 cm^{-1}, while the δ_{as} (CH_3) asymmetric vibration should not be seen. In the spectra of Figure 4.9, both 1447 and 1415 cm^{-1} bands, assigned to the δ_{as} (CH_3)

asymmetric vibration and δ_s (CH_3) symmetric vibration respectively, are weak in intensity.

The alcoholic group is believed to present one ν (C – OH) vibration represented by the band at 1114 cm^{-1}. This band is a medium one, indicating the C – OH bond is in a position almost normal to the plane of the surface.

The OH group deformation band is hard to define - it should be somewhere around 1300-1450 cm^{-1} [21]. In addition, the way the OH group is pointing with regards to the surface is hard to define as it has not been possible to identify the ν (O – H) vibration as formation of ice on the detector prevents the spectrometer seeing the bands in the region above 3000 cm^{-1}.

Around 1300 – 1400 cm^{-1}, the CH group deformation and the wagging of the CH_2 group are expected to give some bands [22].

Combining all these observations it can be deduced that the orientation of the (R)-MHB molecule when adsorbed on the Cu (110) surface, shown in Figure 4.10, would explain the intensity of the bands found in the spectrum given in Figure 4.9.

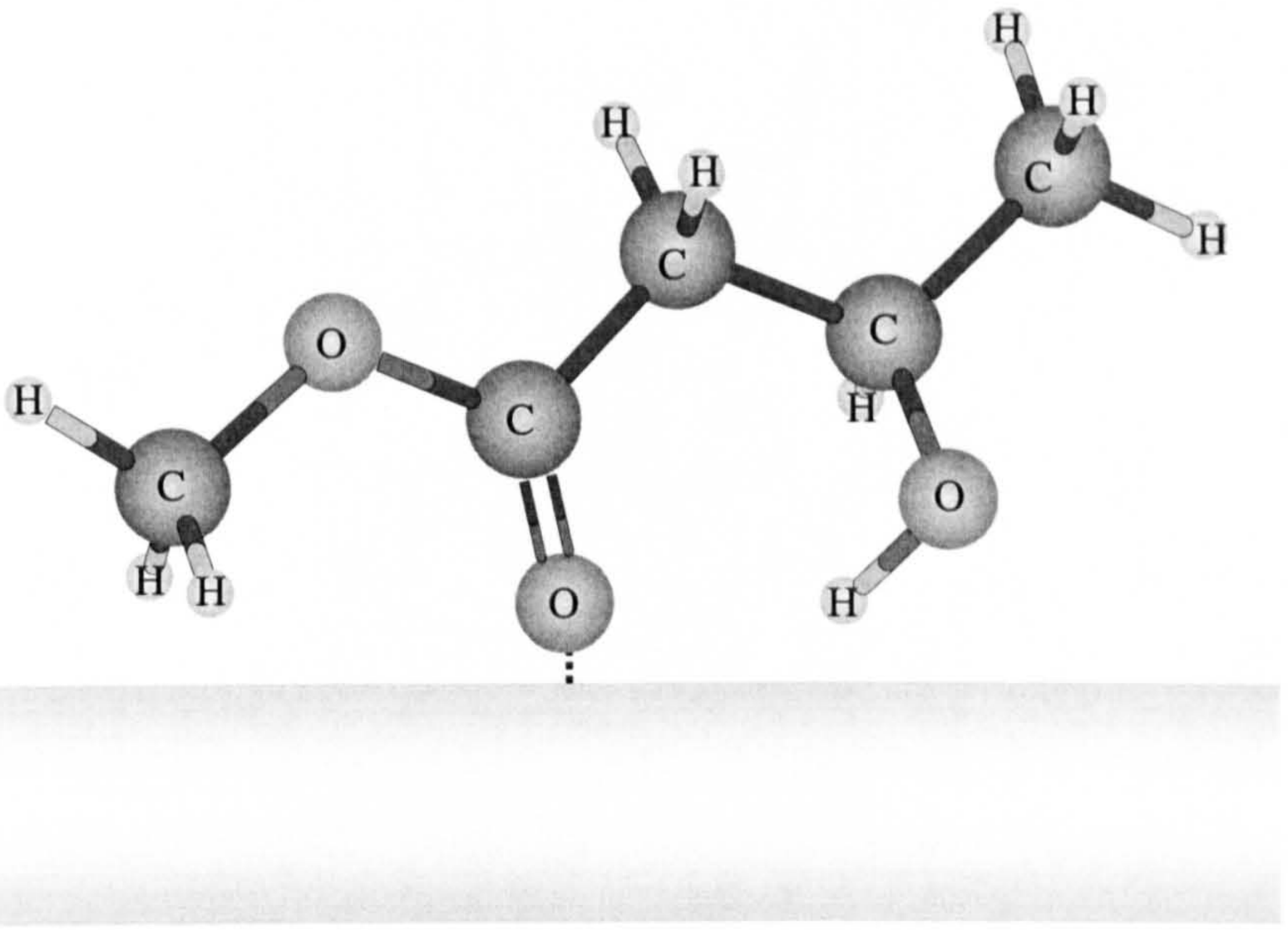

Figure 4.10: Schematic representation of one molecule of (R)-MHB adsorbed on the Cu (110) surface at 300 K.

4.2.2 RAIRS study of the adsorption of (R)-MHB on Cu (110) above 300 K

The (R)-MHB covered Cu (110) surface was annealed to different temperatures and RAIR spectra recorded. These spectra are presented in Figure 4.11 for a coverage of 15 L. By increasing the temperature, dramatic changes in the RAIR spectra can be seen. The clear disappearance of some stretching vibration bands representing ν (C – OH) and ν (C - CH_3) can lead to the possibility of a new orientation of the MHB molecule on the surface. The disappearance of the major peak attributed to the ν (C = O) stretching vibration and its replacement by two peaks at 1598 cm^{-1} and 1574 cm^{-1} leads to the possibility of a transformation of the MHB into another molecule. Other changes include the shift of the bands representing the deformation of the CH_3 group and the appearance of new bands at 1261 cm^{-1} and 1004 cm^{-1}.

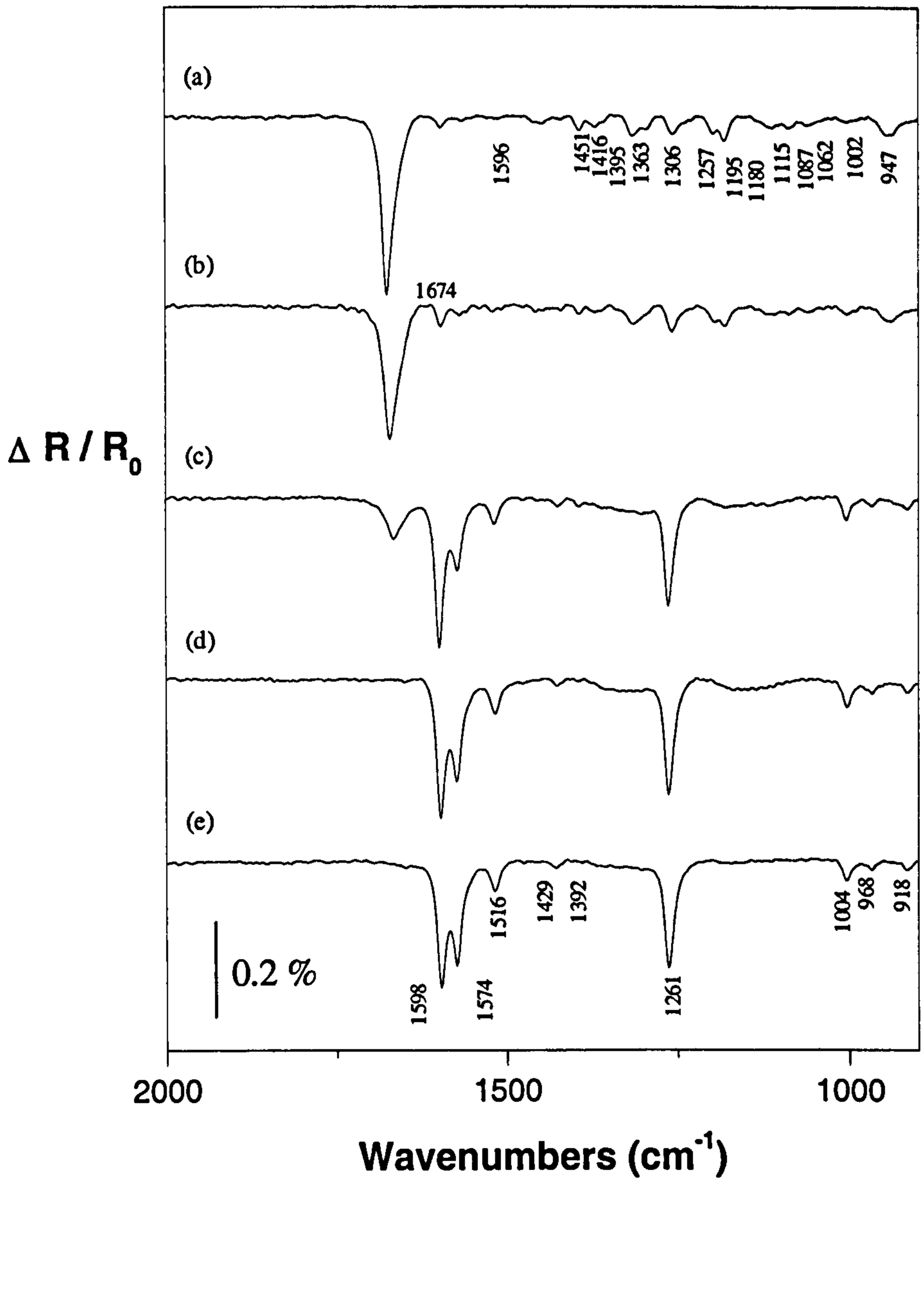

Figure 4.11: RAIRS spectra of 15 L of (R)-MHB obtained when heating the sample to different temperatures: (a) 300 K; (b) 323 K; (c) 348 K; (d) 373 K and (e) 398 K.

By considering the RAIR spectra of the annealed surface, the new species that appears has strong similarities to that of dehydrogenated MHB, the molecule of methyl-acetoacetate (MAA). This latter molecule has been the object of a previous study on Cu (110), so a direct comparison of the infrared spectra can be made [23]. The RAIR spectrum of MAA adsorbed on a Cu (110) surface is presented in Figure 4.12 [23].

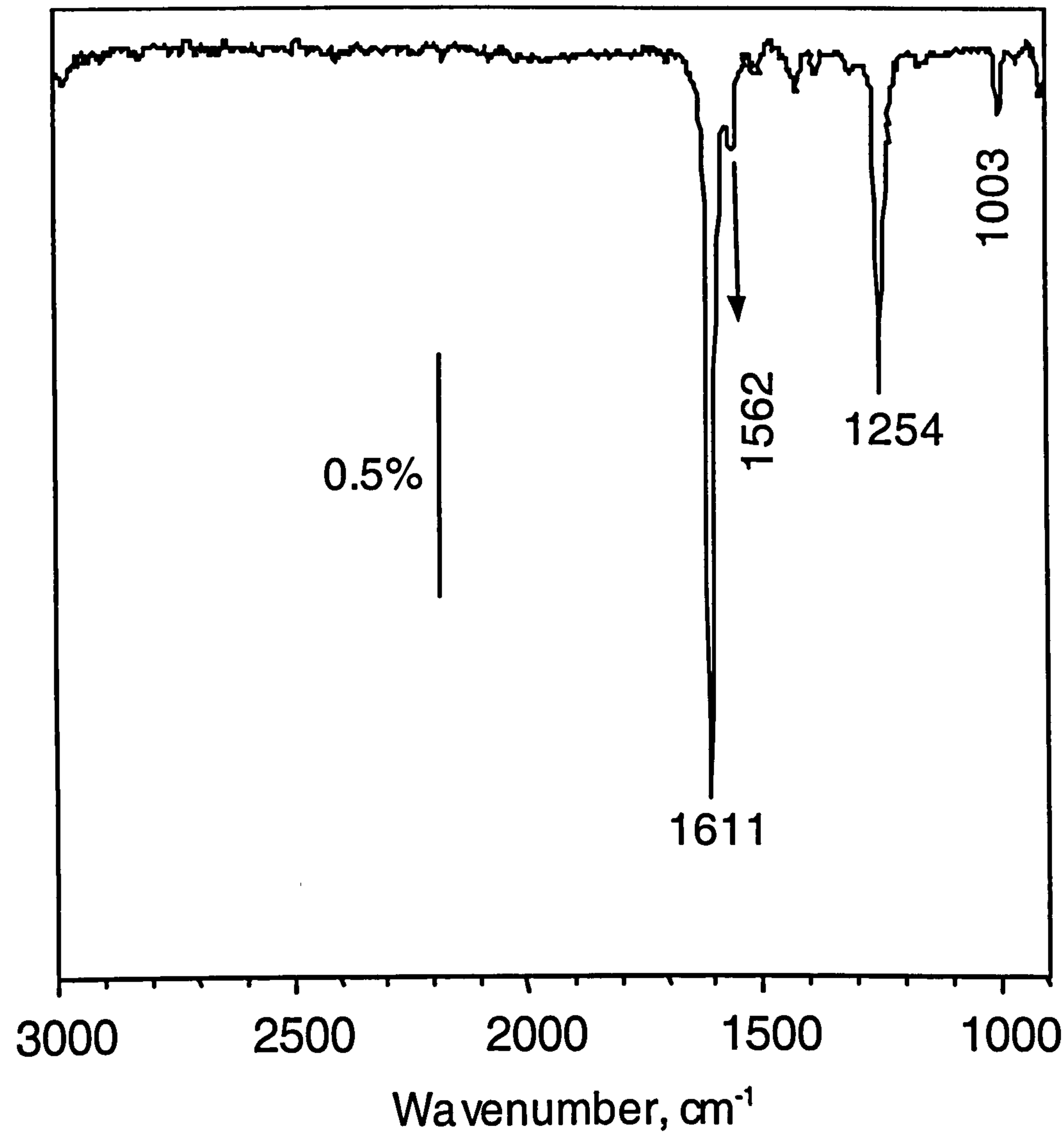

Figure 4.12: RAIR spectrum of 16 L of MAA adsorbed on Cu (110) [23].

To prove the appearance of the MAA on the surface and to find its orientation on the Cu (110) surface, the following points of study will be considered briefly. The assignment of the infrared bands of the spectrum of the MAA in the liquid form will be given and explained first.

It is important to know, before assigning the infrared bands of the MAA, that this molecule does not exist as an individual compound but as a mixture of keto - enol forms due to tautomerism [24]. These forms are drawn in Figure 4.13.

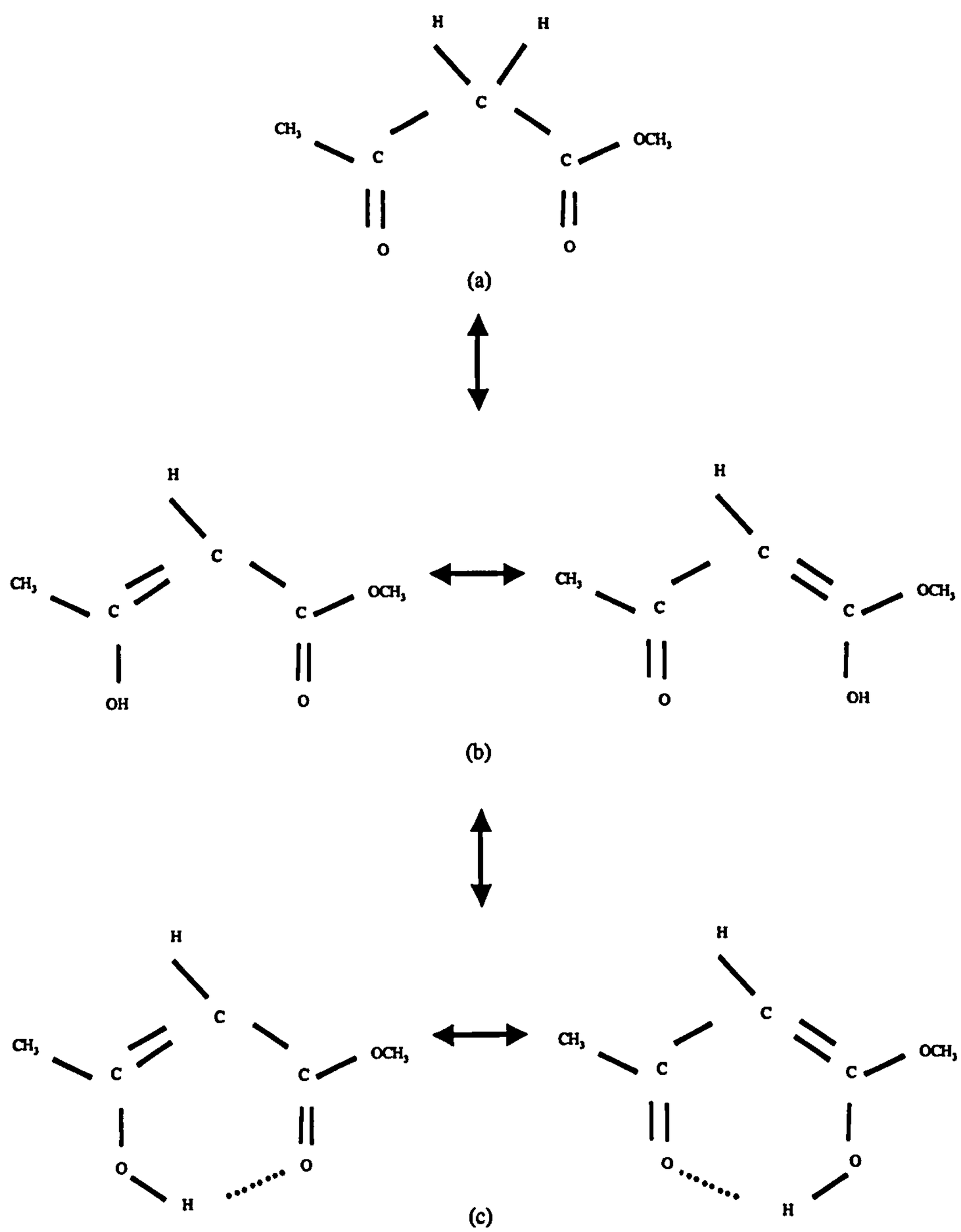

Figure 4.13: Five possible compounds present in a liquid solution of methylacetoacetate: (a): pure form; (b): α, β unsaturated carbonyl; (c) bonded carbonyl.

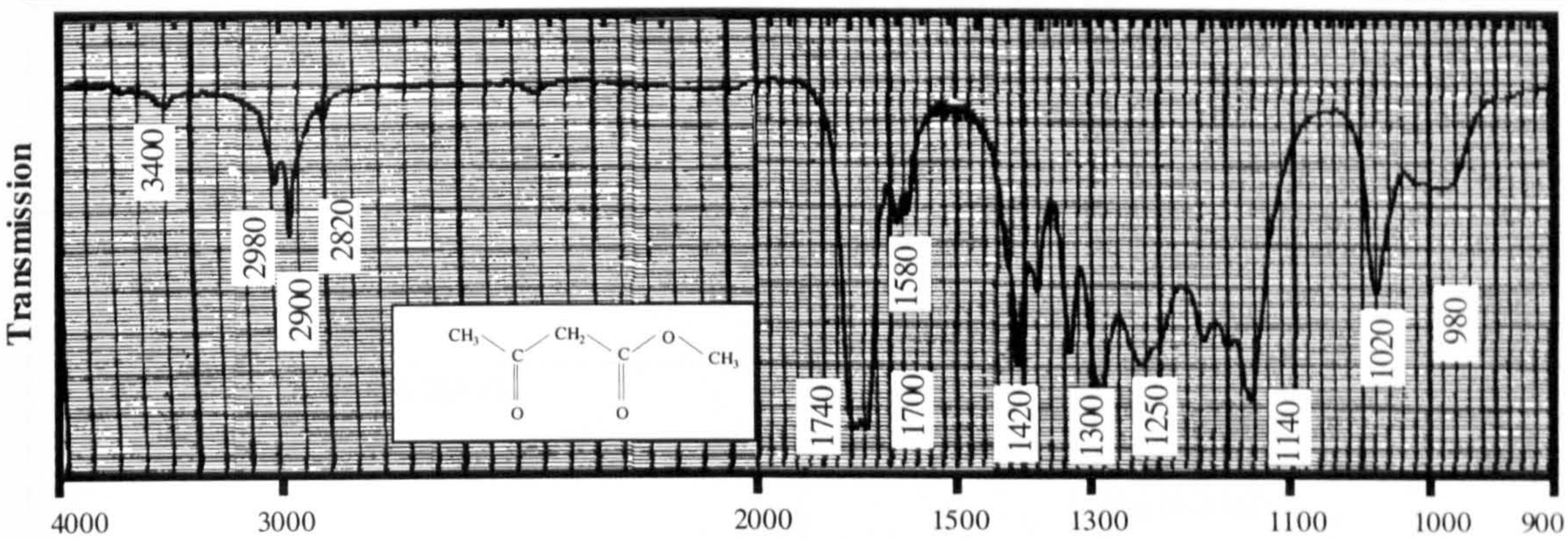

Figure 4.14: Infrared spectrum of methylacetoacetate in the liquid phase [25].

The spectrum of MAA in the liquid phase has been assigned elsewhere [23]. This spectrum, in Figure 4.14, shows a broad band (between 1740 and 1700 cm^{-1}) in the ν (C = O) region, corresponding to absorptions of the C=O group in the $COOCH_3$ and of the keto group in β-position [26]. In addition, bands between 1640 and 1580 cm^{-1} are due to ν (C = O) and ν (C = C) of the small amount of the enol form which is in equilibrium. The enol form in MAA corresponds to a chelate structure resulting from an intramolecular hydrogen bonding between the carbonyl group (acceptor) and the enolic hydroxyl group (donor). Proof of this is that on acetylation of the OH group (in the enolic form) the possibility of chelation disappears and carbonyl bands appear at ~1700 cm^{-1} [24].

The assignment of each of the bands present in the spectrum of MAA in the liquid phase is given in Table 4.7.

Methylacetoacetate in the liquid phase. Wavenumbers (cm^{-1})	Assignments
3400	ν (OH)
2980-2900	ν_{as} (CH_3) ν_{as} (CH_2)
2820	ν_s (CH_3) ν_s (CH_2)
1740-1700	ν (C = O) (pure form)
1640-1580	ν (C = C) + ν (C = O) (enol form)
1420	δ_{as} (CH_3)
1390-1340	δ_s (CH_3)
1300	w (CH_2)
1250	ν (CO - O_eCH_3)
1140	ρ (CH_3)
1020	ν (O_e- CH_3)
980	tw CH_3

Table 4.7: Characteristic vibrational bands (cm^{-1}) and assignments of methylacetoacetate in the liquid phase [23].

The behaviour of a molecule when forming a metal complex is sometimes similar to that observed when the molecule is adsorbed on a metal surface [27]. The behaviour of the (R)-MHB transformed into MAA on Cu (110) at high temperature can be compared to acetylacetone (acac) adsorbed on metals [24]. In the literature, an extensive amount of infrared data has been collected on the keto-enol tautomerism of acac [24, 28, 29]. The difference between the MAA molecule and acetylacetone is that a ketone group replaces the ester group as shown in Figure 4.15. The tautomerism of 1,3-dicarbonyl compounds has been reported to be the same as that of β-ketoesters [24].

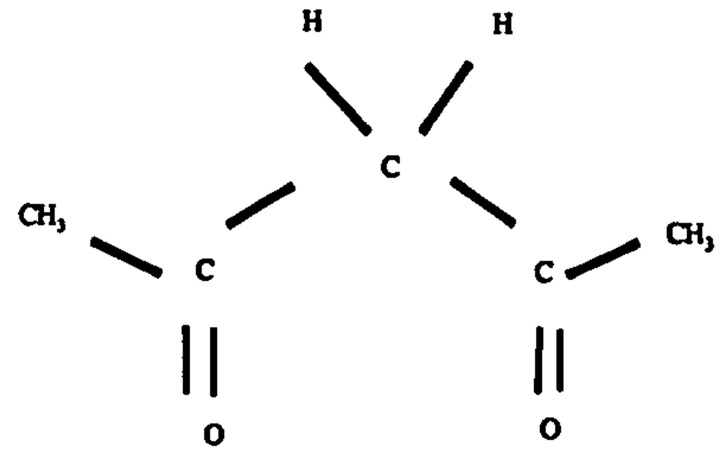

Figure 4.15: Schematic representation of the acetylacetone molecule.

The acac molecule can be found in two forms: the keto form and the enol form, presented in Figure 4.16.

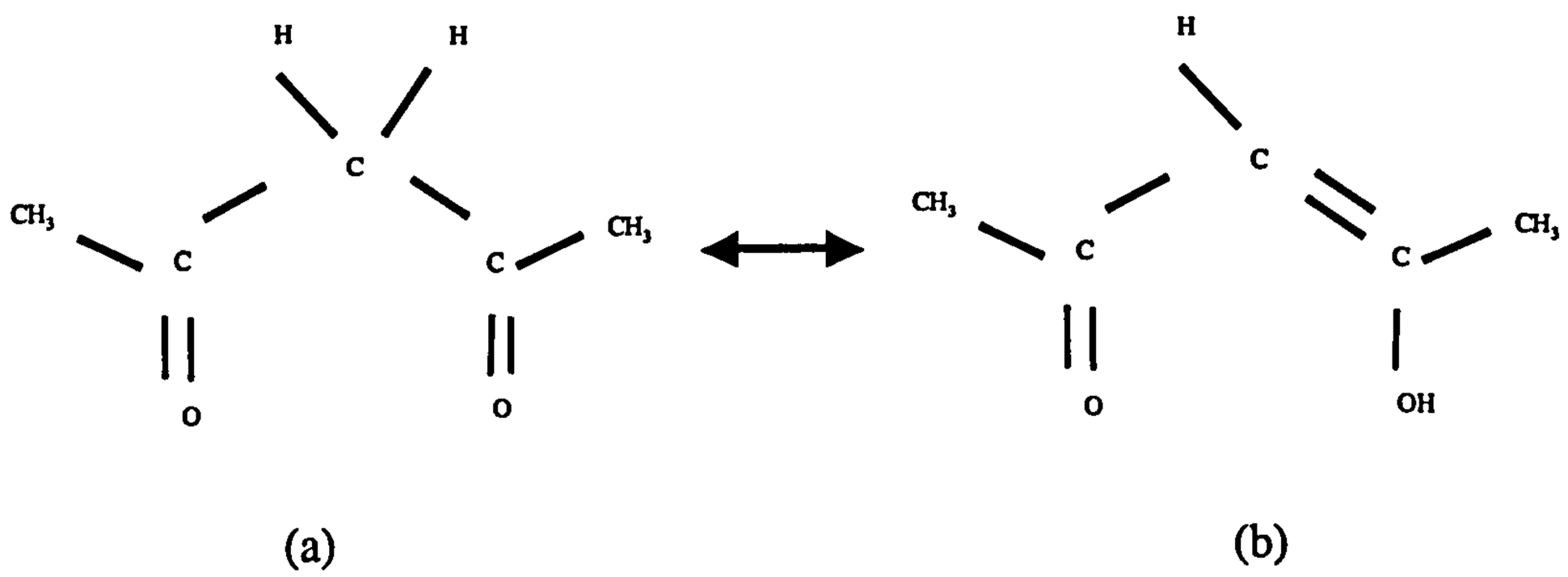

(a) (b)

Figure 4.16: The two forms of acetylacetone molecule: (a) the keto form; (b) the enol form.

Table 4.8 presents the keto and enol forms of acetylacetone, as well as their characteristic vibrational bands and their assignments [29].

Keto form		Enol form	
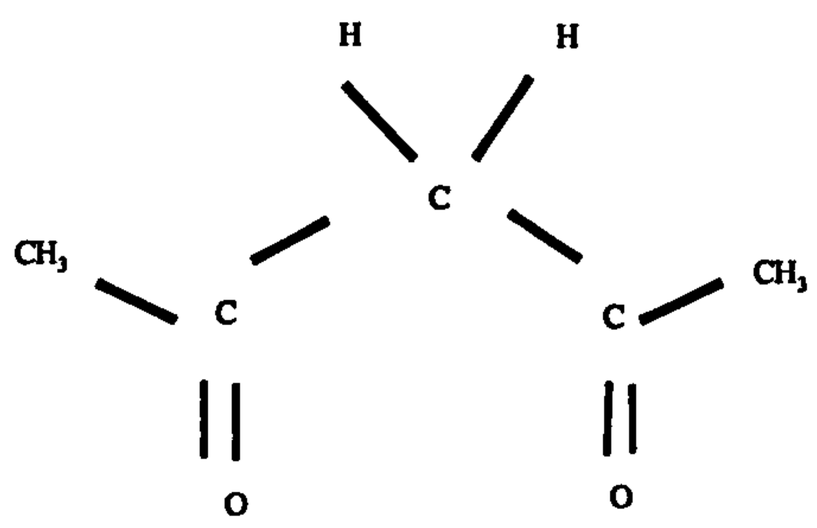		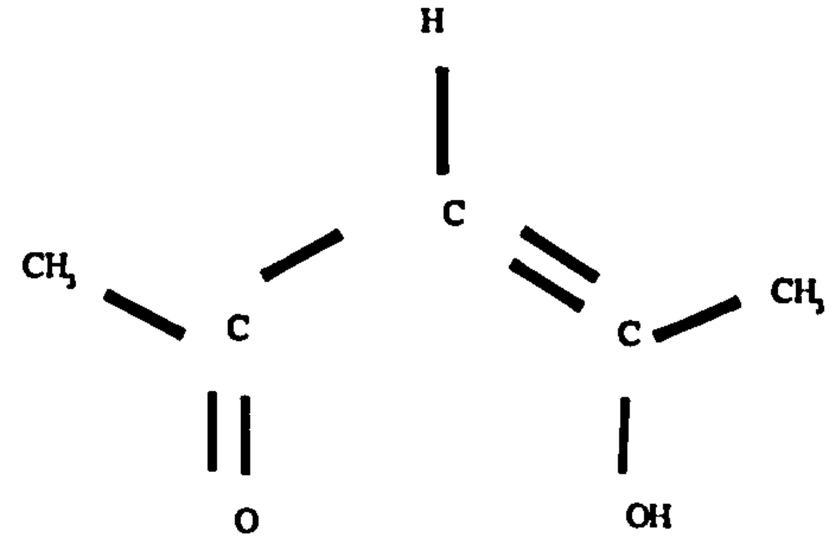	
1709-1729	ν (C = O)	1538-1640	ν (C = C) + ν (C = O)
1420	δ_{as} (CH_3)	1419	δ_{as} (CH_3)
1360	δ_s (CH_3)	1360	δ_s (CH_3)
1300	w CH_2		
1246	ν (C – C)	1247	ν (C – C)
1157	ρ (CH_3)	1170	ρ (CH_3)
998	tw CH_3	998	tw CH_3

Table 4.8: Keto and enol forms of acetylacetone, as well as their characteristic vibrational bands and their assignments [29-30].

It is then interesting to understand the behaviour of acac on metals and to relate it to the assignments of the bands in the ν (C = O) region in the IR spectra of the (R)-MHB transformed into MAA. The complexes of acetylacetonato ions, which have been studied extensively [28] can be classified into 6 types. The formation and the posture of the acac molecule, or ion, depend on the medium in which it has been formed. Table 4.9 describes these different types as well as the behaviour of the C=O bond and its position in the infrared spectra.

Type	Schematic representation	Description Infrared bands in the νC=O region
A	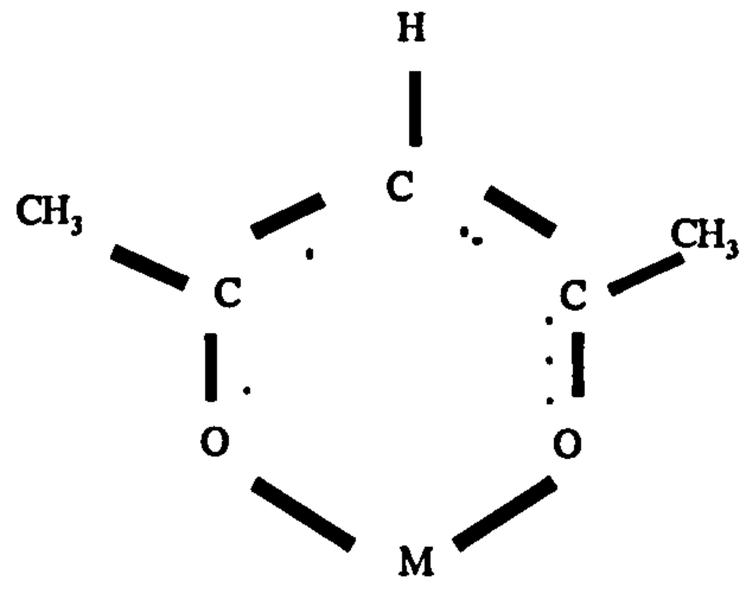	$Cu(acac)_2$ complex: 1577 cm^{-1}: ν(C⎓O) + ν(C⎓C) 1529 cm^{-1}; ν(C⎓C) + ν(C⎓O)
B	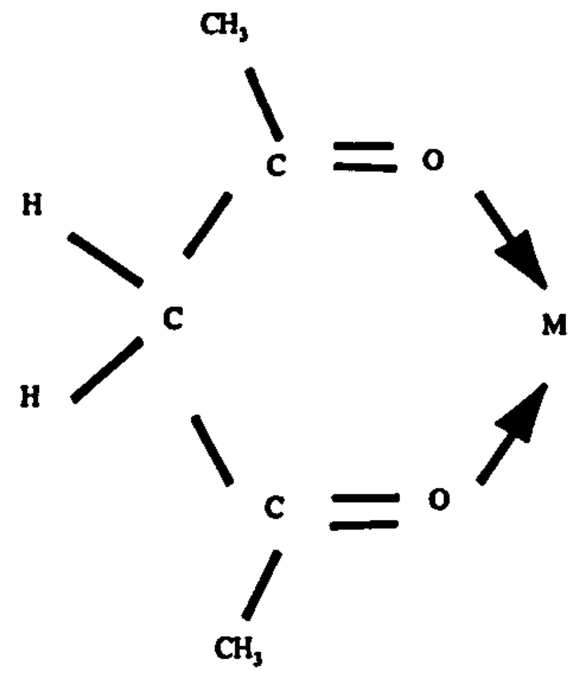	Coordination found in $[Ni(acacH)_3](ClO_4)_2$, $Co(acacH)Br_2$ and related compounds Described as ketonic coordination Strong band at 1700 cm^{-1}: ν (C = O) Compounds prepared in acidic or neutral media
C	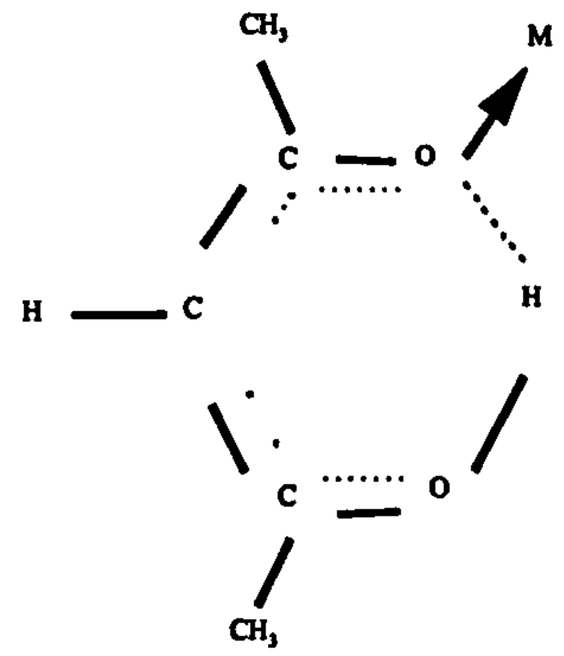	Coordination found in $Mn(acacH)_2Br_2$ Acetylacetone described in the enol form Band at 1627 cm^{-1}: ν (C⎓O) and at 1564 cm^{-1}: ν (C⎓C)

Type	Schematic representation	Description Infrared bands in the νC=O region
D	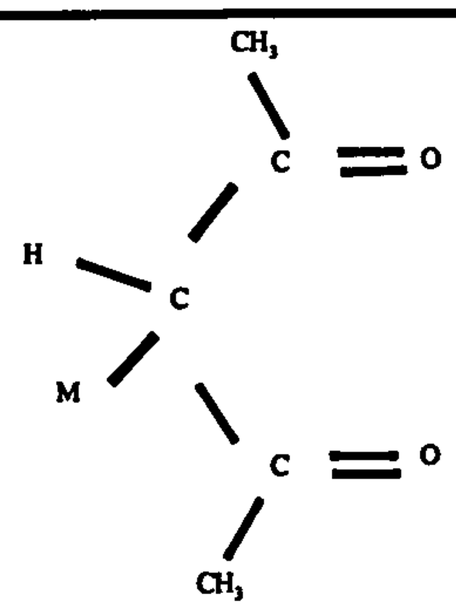	Pt (II) complexes, such as $K[Pt(acac)_2Cl]$ in which the metal is bound to the γ-carbon atom of the acetylacetonato ion Band around 1730-1600 cm^{-1}: ν (C = O)
E	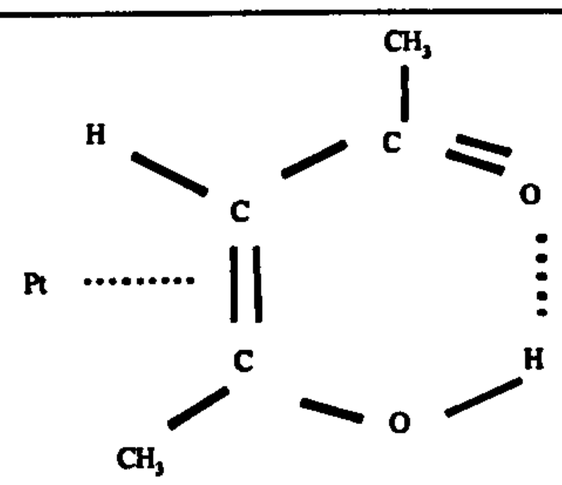	In a solution of $K[Pt(acac)_2Cl]$ which is acidified, the type D is converted into Type E Bands at 1652-1626 cm^{-1}: ν (C = O)

Table 4.9: Description of the six types of metallic complexes of acetylacetone [28].

The presence of the three bands at 1598 cm^{-1}, 1574 cm^{-1} and 1516 cm^{-1} in the spectra of annealed MHB in Figure 4.11 encourages comparison to the types A, C and E of the metallic complexes of acetylacetone. The common point of these three types is that acac is in the enol form.

The assignments of the bands of the annealed MHB adsorbed on Cu (110) are presented in Table 4.10.

Methyl-3-hydroxybutyrate in the liquid form		Methyl-3-hydroxybutyrate on Cu (110)		Annealed (R)-Methyl-3-hydroxybutyrate on Cu (110)	
3450	ν (OH)				
2960 vs	ν (CH_3)	2965	ν (CH_3)		
2920 m	ν (CH_2)	2947	ν (CH_2)		
2895 m	ν (CH)		ν (CH)		
2880 m					
2800 m					
1750	ν (C = O)	1676	ν (C = O)	1598	ν (C = O)
				1574	ν (C = O)
				1516	ν (C = C)
1440 - 1470	δ_{as} (CH_3)	1447	δ_{as} (CH_3)	1429	δ_{as} (CH_3)
1420	δ (CH_2)				
1380	δ_s (CH_3)	1415	δ_s (CH_3)	1392	δ_s (CH_3)
1360	δ (OH) or w (CH_2)	1360	δ (OH) or w (CH_2)		
1295	δ (CH)				
1260	δ (CH)				
1230	ν (CO - O_e CH_3)	1306	ν (CO - O_e CH_3)	1261	ν (CO - O_e CH_3)
1195	tw (CH_2)	1195	tw (CH_2)		
1180	ρ (CH_3)	1180	ρ (CH_3)		
1120	ν (C - OH)	1114	ν (C – OH)		
1060 - 1090	ν (C – CH_3)	1089	ν (C - CH_3)		
1010	ν (O_e – CH_3)	1060	ν (O_e – CH_3)	1004	ν (O_e – CH_3)
950	tw CH_3	942	tw CH_3	968	tw CH_3

Table 4.10: Description of the bands of the new product made by heating the (R)-MHB, ad their assignments compared to the assignment of (R)-MHB absorbed on a surface and to the assignment of MHB in the liquid form.

It is proposed, in the infrared spectrum of the annealed MHB adsorbed on Cu (110) that the two bands at 1599 cm^{-1} and 1562 cm^{-1} are assigned to the ν (C = O) stretching vibration for the ketone group and for the ester group, possibly coupled to the ν (C = C) stretching vibration. Indeed, these two groups are not equivalent because of the presence of the oxygen of the ester group, giving rise to two infrared bands. Besides, since these two bands are the strongest and sharpest ones, they represent the bonds which are the link of the molecule to the surface and which are normal to the surface.

The ν (C = C) stretching vibration presents a weaker band, since its bond is not normal to the surface, at 1516 cm^{-1}. This value can be compared to the frequency of the ν (C = C) stretching vibration of acac which is found at 1536 cm^{-1} [30].

The sharp peak at 1261 cm^{-1} can be attributed to the ν (CO - O_eCH_3) vibration. The frequency of this vibration has shifted from 1306 cm^{-1} as the (R)-MHB has been annealed and transformed into MAA. This is probably due to a re-organisation of the charges around the ring. The same phenomenon may have happened to the ν (O_e – CH_3) whose frequency may have shifted from 1060 cm^{-1} to 1004 cm^{-1}.

Bands due to the CH_3 group, at 1429 cm^{-1} and 1392 cm^{-1} are still very low in intensity in Figure 4.11, on the spectrum representing the MAA. This means that the C – CH_3 bond is neither parallel nor perpendicular to the surface.

The transformed (R)-MHB, MAA, is thus deduced to stand on the copper surface as presented in Figure 4.17 [23].

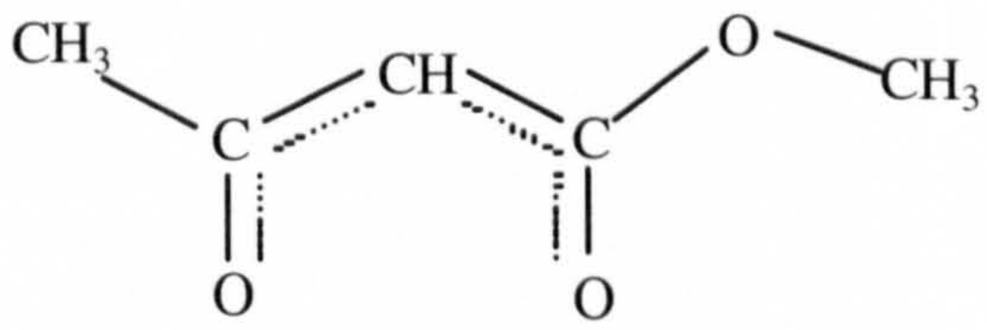

Figure 4.17: (R)-MHB transformed into MAA on Cu (110) [23].

4.2.3 TPD study of the (R)-MHB adsorbed on Cu (110) at 300 K

A TPD study of 15 L of (R)-MHB adsorbed on the Cu (110) at 300 K can confirm the results given in the previous section. On annealing (R)-MHB dehydrogenates and is transformed into MAA, following the reaction shown in Figure 4.18.

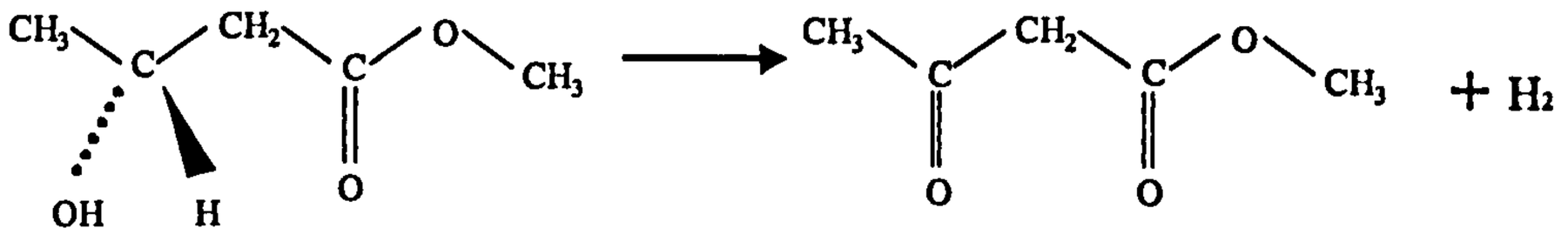

(R)-MHB MAA

Figure 4.18: Reaction of dehydrogenation of (R)-MHB into MAA on Cu (110).

The hydrogen coming off from the (R)-MHB should thus be noticed on the TPD spectra. Figure 4.19 presents the TPD spectrum of 15 L of (R)-MHB adsorbed on Cu (110) at room temperature.

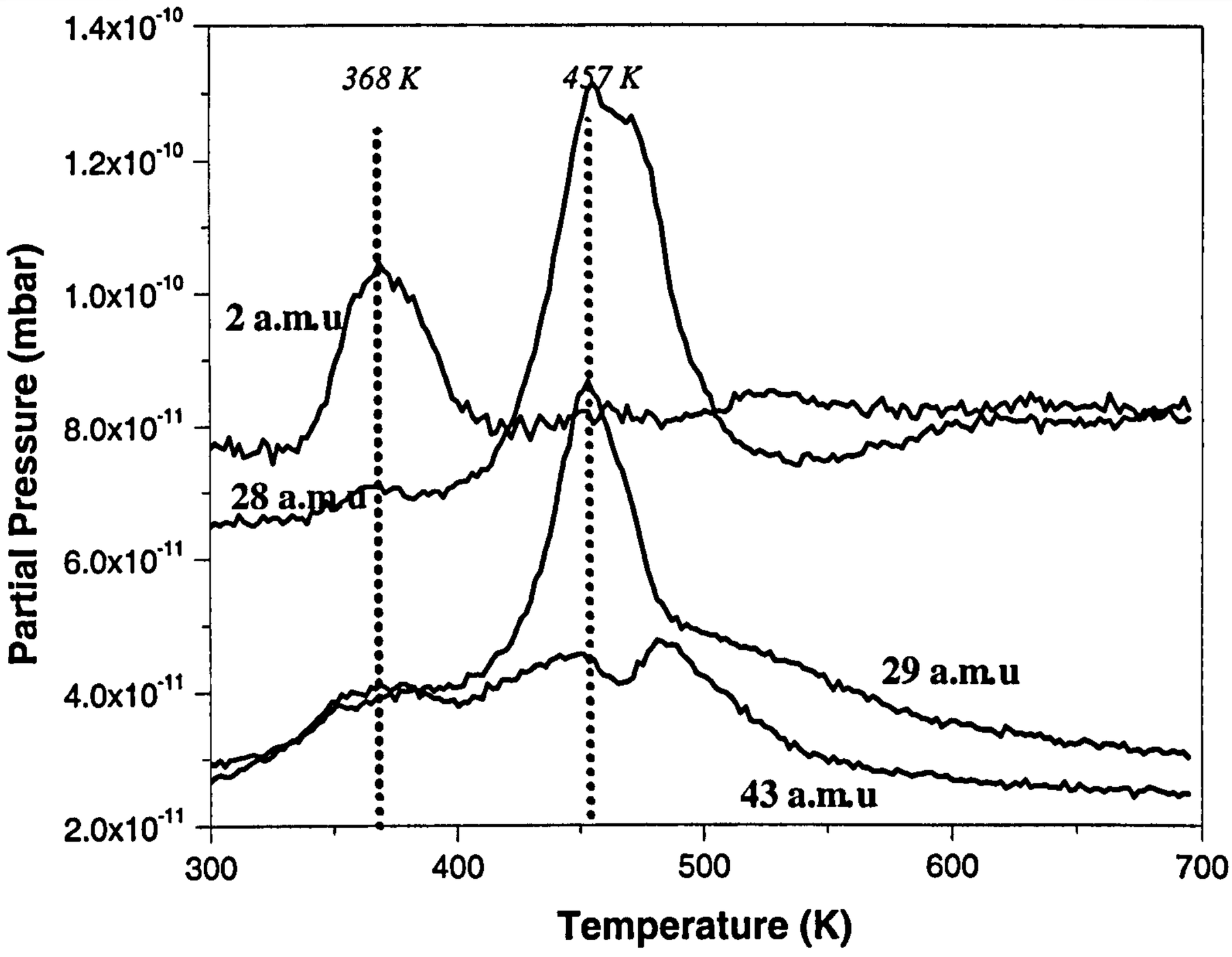

Figure 4.19: TPD spectrum of 15 L of (R)-MHB adsorbed on Cu (110) at 300K.

It can be noticed easily that the first species coming off the surface is the hydrogen, H_2, coming off at ~ 368 K for a dose of 15 L of (R)-MHB. This hydrogen can only come from the transformation of the (R)-MHB into MAA. Between the temperature of 370 K and ~ 420 K, the only molecular species present on the Cu (110) surface is the MAA. This first hydrogen peak is accompanied by two small peaks representing m / z = 29 a.m.u. and 43 a.m.u. This might be a small and insignificant amount of (R)-MHB desorbing. This amount may be qualified as "small and insignificant" due to the area of the main MHB peak at 1676 cm^{-1} being more or less equal to the area of the sum of the peaks at 1598 cm^{-1} and 1574 cm^{-1} on the infrared spectra. Thus, very little desorption of the MHB has occurred during the transformation to MAA.

4.2.4 Kinetic study of the transformation of (R)-MHB into MAA when adsorbed on Cu (110)

When the MHB adsorbs at room temperature, the term "room temperature" is not precise enough. Indeed, some changes, in the infrared spectra which are due to the disappearance of the MHB and appearance of MAA, are noticed. These changes are faster or slower depending on the temperature of the sample and on the time the (R)-MHB has been adsorbed on the sample.

Some kinetics experiments have been conducted. These were performed by keeping the sample at a desired temperature and dosing (R)-MHB, whilst recording successive RAIR spectra. The area of the band at 1674 cm^{-1}, due to the ν (C = O) stretching vibration was taken to be representative of the amount of (R)-MHB on the surface, and the time of recording each spectrum was registered using the "winfirst" software used to take and process the RAIR spectra.

Once the order of the reaction of transformation of (R)-MHB into MAA is well defined, it is possible to calculate the rate constant k to be measured at each temperature. From the knowledge of the rate, it is possible to plot the Arrhenius equation. The Arrhenius plot then yields the activation energy E_a for the reaction [31, 32].

The first step is to check the order of the reaction. This one cannot be zero since the area of the peak at 1674 cm^{-1} decreases exponentially with time, as shown in Figure 4.20. By looking if the half-life (i.e. the time for 50 per cent reaction) is independent of the initial number of molecules dosed, it is possible to differentiate a first order reaction from a second order reaction. Indeed, first order reactions have an important property which is that the half-life does not depend on the initial number of molecules; the following equations prove this. The first order rate law is defined as:

$$\frac{dx}{dt} = k(x_0 - x)$$

with x_0 the initial number of molecules, x the number remaining at time t, and k the rate constant.

Integrating this equation:

$$-\ln(x_0 - x) = k \times t + \text{constant}$$

Substituting for $t = 0$, $x = 0$ gives $(-\ln x_0) = \text{constant}$. Substituting for the constant:

$$k \times t = \ln \frac{x_0}{x_0 - x}$$

so, at half life, when $t = t_{1/2}$ and $x = x_0 / 2$:

$$\ln 2 = k \times t_{1/2}$$

This equation proves that for first order reaction, the half-life is not dependent of the initial number of reacting molecules.

Two extremes doses of (R)-MHB, 15 L and 3 L, were deposited on the Cu (110) surface at 323 K. Figure 4.20 shows the decrease of the area of the band at 1674 cm^{-1} with time. The area of this band is taken to indicate the amount of (R)-MHB still present on the surface. The interest of these measurements is the calculation and comparison of the half-life times, $T_{1/2}^{3L}$ and $T_{1/2}^{15L}$ as the two doses, 3 L and 15 L respectively, transform from (R)-MHB into MAA. $T_{1/2}^{3L}$ is the time by which half of the amount of 3L (R)-MHB deposited on the crystal (kept at the temperature of 323 K) at the beginning of the reaction will have disappeared; $T_{0.5}^{15L}$ is the same for an amount of 15 L of (R)-MHB.

It is clear, from Figure 4.20, that $T_{0.5}^{3L}$ and $T_{0.5}^{15L}$ are not the same. This means that the half-life is dependent of the initial dose of (R)-MHB deposited on the Cu (110) crystal. It can be concluded that disappearance of the (R)-MHB on the Cu (110) surface is a second-order reaction.

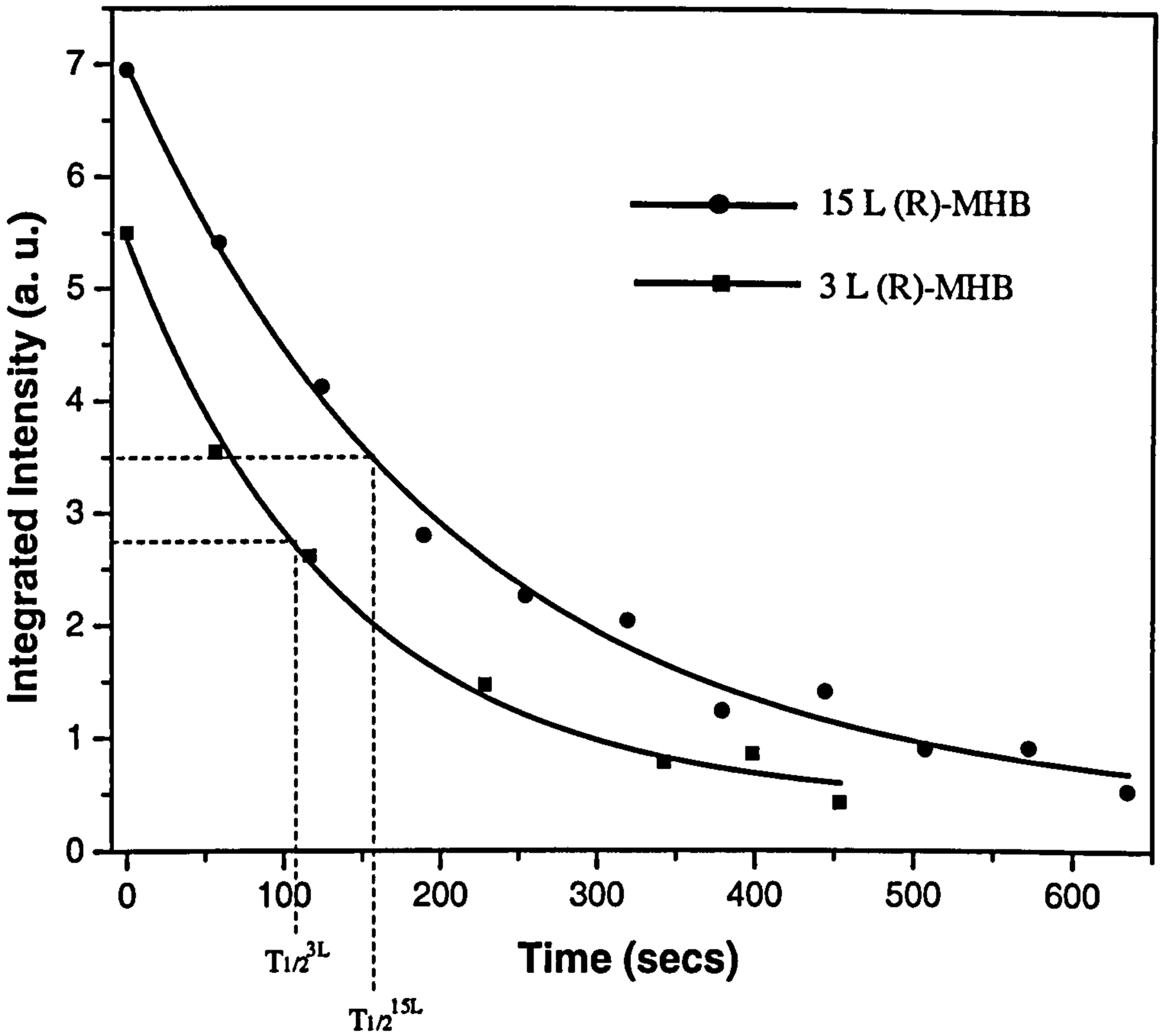

Figure 4.20: Measures of area of the band at 1674 cm^{-1} over time for a dose of 15L and a dose of 3 L of (R)-MHB adsorbed on Cu (110) at 323 K.

Since the order of the reaction is thus dependent of the amount of (R)-MHB dosed, a dose of 3 L was chosen for all the kinetics experiments in order to ease the cleaning of the UHV system between the experiments.

The second step is to measure the rate constant k of the reaction for four temperatures of crystal: 308 K, 313 K, 323 K and 333 K. To do this, the area of the band at 1674 cm^{-1} over time is measured for four temperatures; the spectra are shown in Figure 4.21 and the plotted areas over time in Figure 4.22.

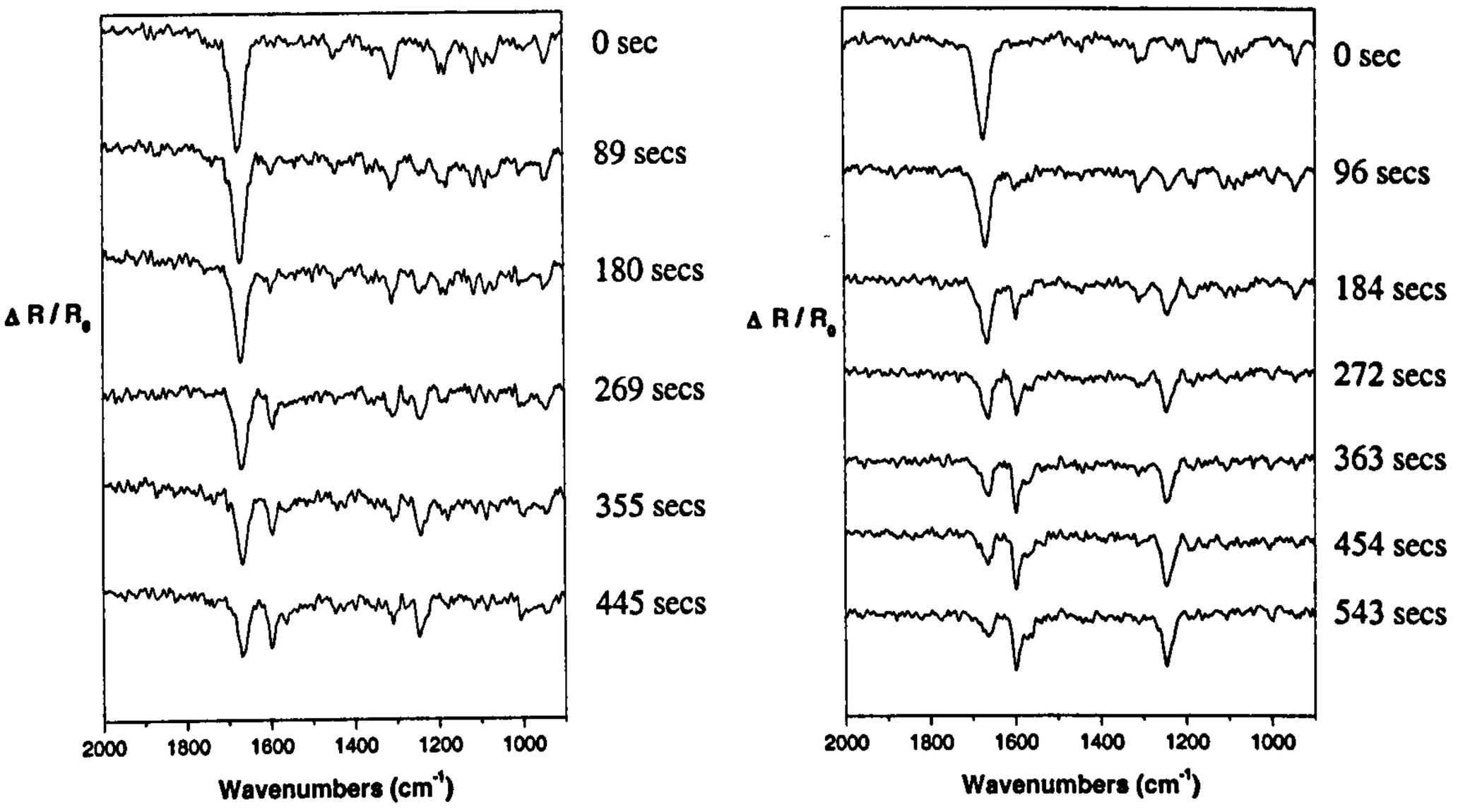

Figure 4.21: Successive RAIR spectra of a dose of 3 L of (R)-MHB transforming into MAA at temperature of: (a) 308 K, (b) 313 K, (c) 323 K and (d) 333 K.

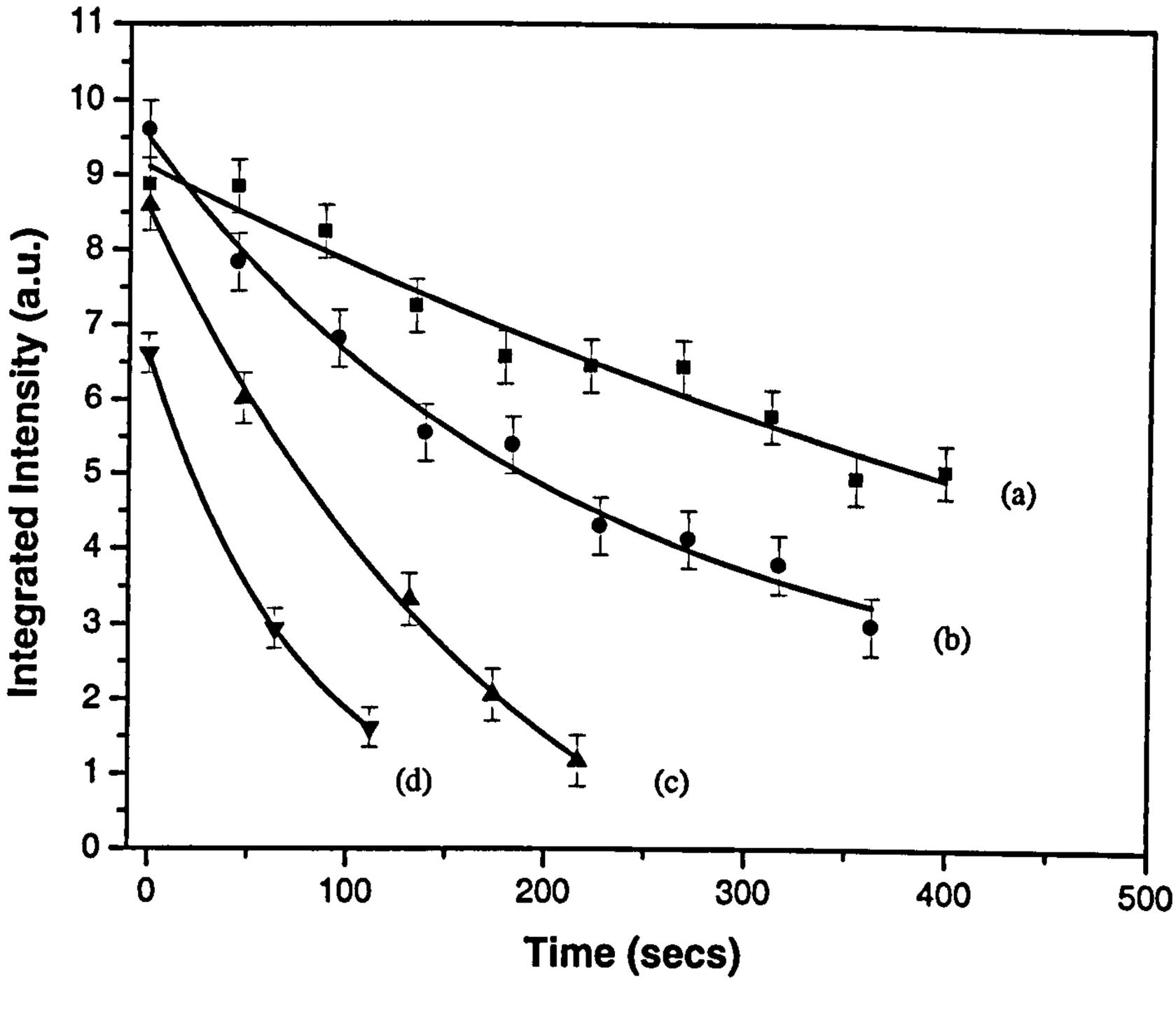

Figure 4.22: Decrease of the integrated intensity of the 1674 cm^{-1} band of (R)-MHB plotted as a function of time for the following temperatures: (a) 308 K, (b) 313 K, (c) 323 K and (d) 333 K.

From the plots in Figure 4.22, it can be noticed that at 333 K, in 100 secs, 75 % of the (R)-MHB has been converted; at 323 K, in the same time 50 % has been converted; at 313 K, 30 % has been converted and at 308 K, 12 % has been converted.

The following calculation was done to get the rate constant k for each temperature:

$$\frac{a_0 - a}{a_0 \times a} = k \times t \quad [32]$$

with the values of the initial area, a_0 and the values of the area a changing with the time t. Figure 4.23 presents the results for the four temperatures.

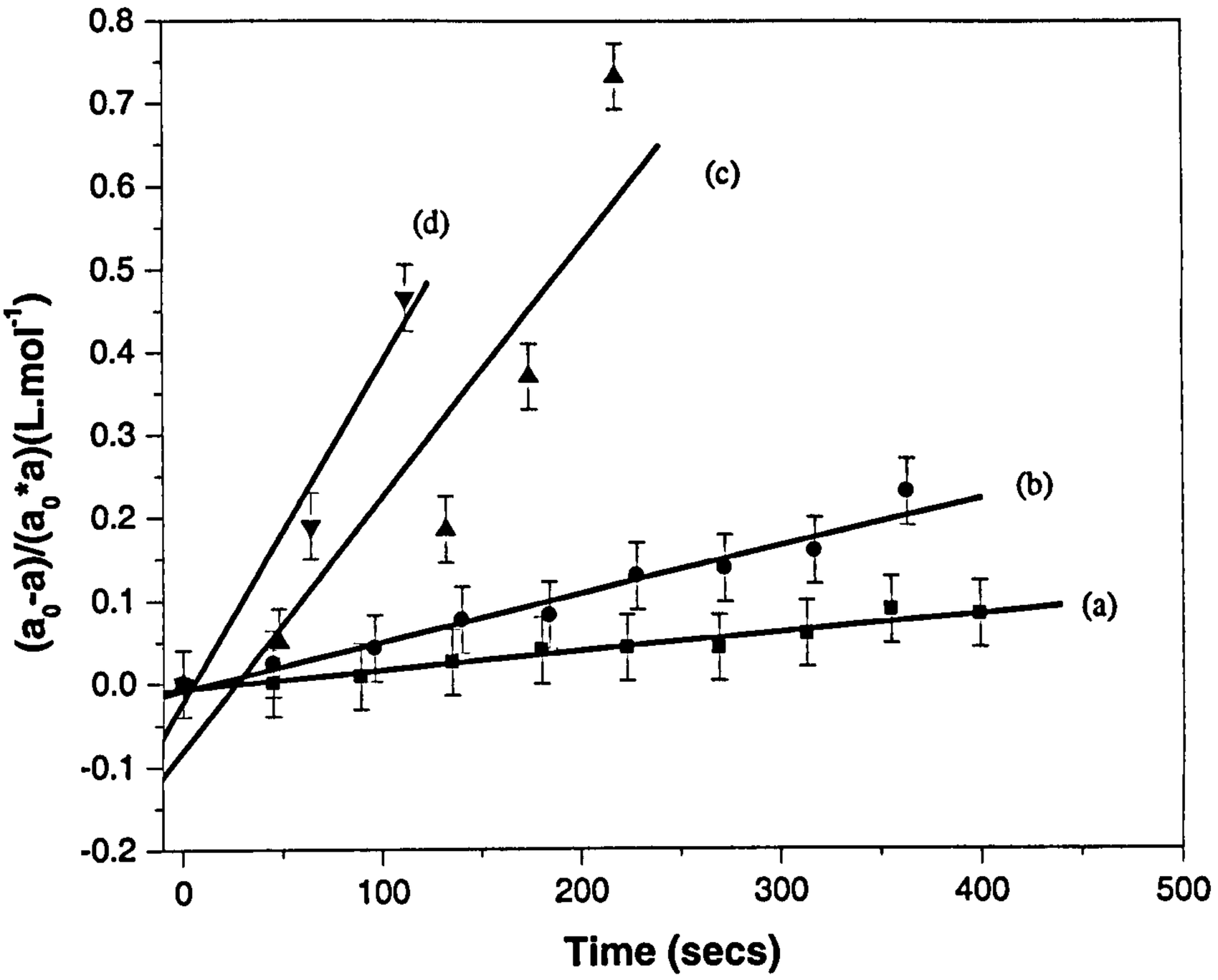

Figure 4.23: Equation $\frac{a_0 - a}{a_0 \times a} = k \times t$ plotted as a function of time for the following temperatures: (a) 308 K, (b) 313 K, (c) 323 K and (d) 333 K.

The gradient of each of the line in Figure 4.23 gives the rate constant k for each temperature. Each rate k is given in the Table 4.11 for each temperature.

Temperature T (K)	308	313	323	333
Rate constant k (s^{-1})	0.00023 (± 0.00001)	0.00058 (± 0.00004)	0.0030 (± 0.0007)	0.0040 (± 0.0007)

Table 4.11: Rate constant k for vanishing of (R)-MHB on Cu (110) at four temperatures.

The third and last step is the adaptation of the results to the Arrhenius equation, to get the value of the activation energy of transformation of (R)-MHB into MAA:

$$k = A \times \exp \frac{-E_a}{RT}$$

where A is a preexponential factor, E_a is the activation energy and R is a constant (R = 8.314 J. mol^{-1}. K^{-1} = 1.986 calories. mol^{-1}. K^{-1})

Transformation of this equation gives:

$$\ln k = \frac{-E_a}{RT} + \ln A$$

As a consequence, by plotting ln k = f (1 / T) and calculating the gradient g of this line, it is possible to get the activation energy E_a:

$$E_a = -R \times g$$

Table 4.12 gives the values of (1 / T) and ln k for each temperature.

Temperature T (K)	308	313	323	333
1 / T (K^{-1})	0.00325	0.00319	0.0031	0.003
Rate constant k (s^{-1})	0.00023 (± 0.00001)	0.00058 (± 0.00004)	0.0030 (± 0.0007)	0.0040 (± 0.0007)
ln k	-8.37 (± 0.04)	-7.45 (± 0.07)	-5.8 (± 0.2)	-5.5 (± 0.2)

Table 4.12: Values necessary to plot the Arrhenius equation: 1 / T and ln k for each temperature.

Figure 4.24 shows the linear of the Arrhenius equation (ln k = - E_a / RT + ln A) obtained from the kinetic data. From this, the activation energy E_a has a value of 100 ± 20 kJ. mol^{-1}.

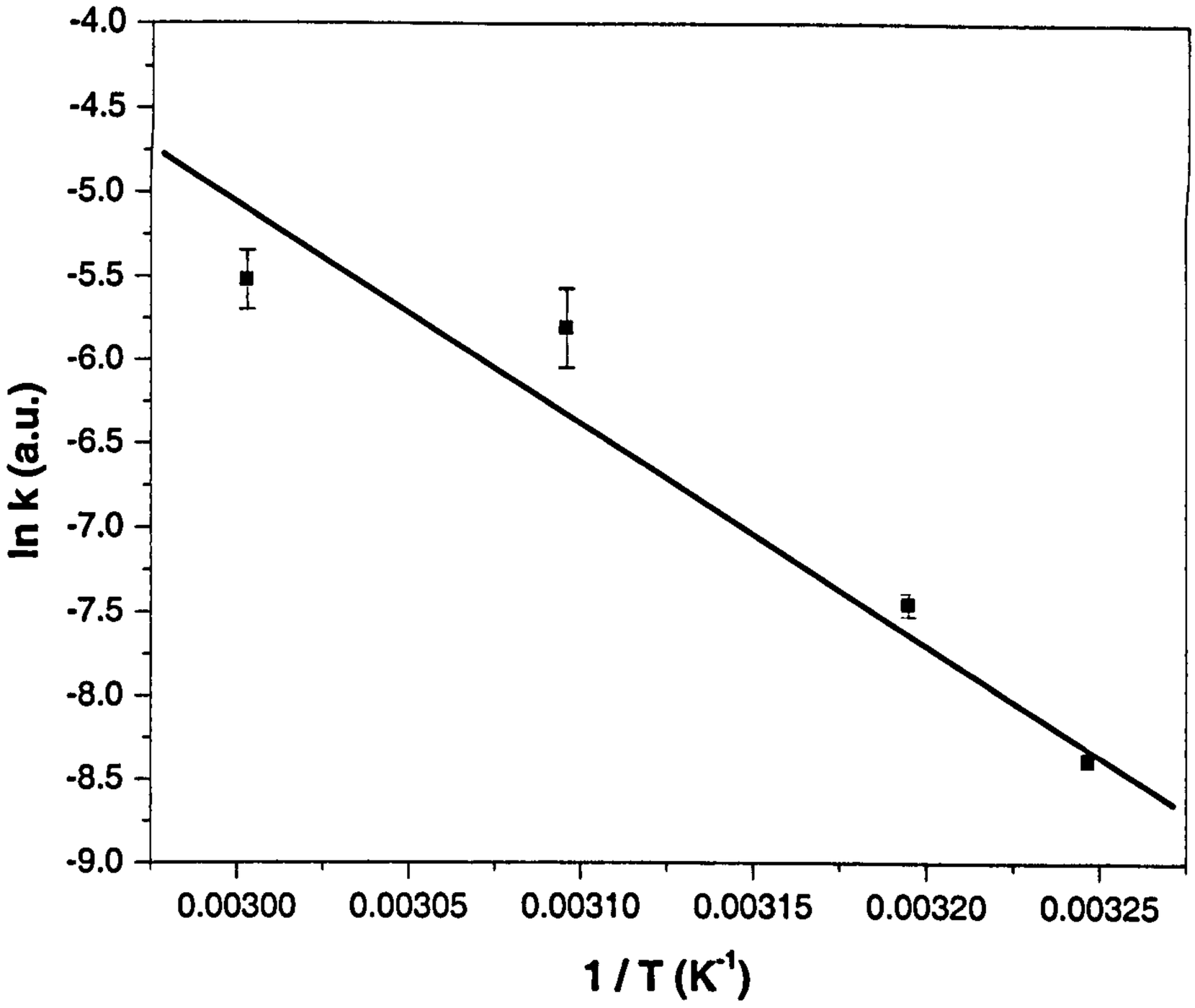

Figure 4.24: Linear of best fit to the Arrhenius equation ($\ln k = - E_a / RT + \ln A$) obtained from the kinetic data.

The value of this activation energy is superior to the value found for the second dehydrogenation of (R, R)-tartaric acid on Cu (110) which was 73 ± 2 kJ. mol^{-1} [33]. Tartaric acid adsorbs initially on the Cu (110) surface by one of its carboxylate groups in the monotartrate form. It loses the hydrogens of its second carboxylate group to be adsorbed in the bitartrate form. It has been noticed that this transformation is accompanied by a change in the two-dimensional organisation of the molecules which involves significant molecular mass transport and expansion in adsorption area.

It must be pointed out that two kind of errors are involved in the calculations of the activation energy: the error concerning each set of data corresponding to one temperature, and the error corresponding to the whole experiment.

The first error concerns the analysis of the data, or more precisely the calculation of the area of the peak at 1674 cm^{-1}. There are two roots of error: the noise of the spectrometer

present on each spectrum and the "human" error due to the difficulties in precisely calculating the area of the peaks. These errors can be seen when plotting the function:

$\frac{a_0 - a}{a_0 \times a} = k \times t$. Indeed, the equation expects that at time t= 0, a_0-a = 0; however, when linking all the data points by a line, this line does not go through the point {(x, y): (0, 0)}. The Origin software program gives the value of this error defined as (Δk). This error is represented as well on the linear plot of the Arrhenius equation, by its value (Δ(ln k)) which is determined by:

$$\Delta(\ln k) = \left| \frac{\ln(k + \Delta k) - \ln(k - \Delta k)}{2} \right|$$

This error is different for each set of data taken at different temperatures, and is consequently represented by an error bar of different length in Figure 4.24.

The second error, which is here ± 20 $kJ.mol^{-1}$, represents the error linked to variations between the results taken at the different temperatures at which the experiment has been carried out. For example, when the experiment has been conducted at 333 K, the time taken to get an infrared spectrum may have been sufficient for some of the molecules to be transformed. Indeed, the reaction at this temperature is very fast, compared to the reaction at 308 K. This error includes also the differences in the amounts of molecules adsorbed on the surface, event if the amount of molecules dosed has been kept the same for the four experiment. It includes the error in precisely regulating the temperature of the crystal and in minimising equally for each experiment the time between the dosing and the first RAIR spectrum. Therefore this further error may be seen as well as the "addition" of the errors of each of the four experiments.

4.3 (S)-MHB on Cu (110)

The simple hydrogenation of MAA into MHB using a non-modified metal catalyst gives a racemic mixture of the product. If the metal catalyst is modified with alanine, the product of the reaction can be switched to (R)-MHB or (S)-MHB depending on the chirality of the alanine.

The study of (S)-MHB on Cu (110) was carried out in the same way as was done with (R)-MHB i.e. the bonding of the molecule on the surface, its dehydrogenation into MAA and the kinetics of this reaction.

Figure 4.25 shows the RAIR spectrum when 3 L of (S)-MHB have been deposited on the surface, just before the transformation into MAA begins.

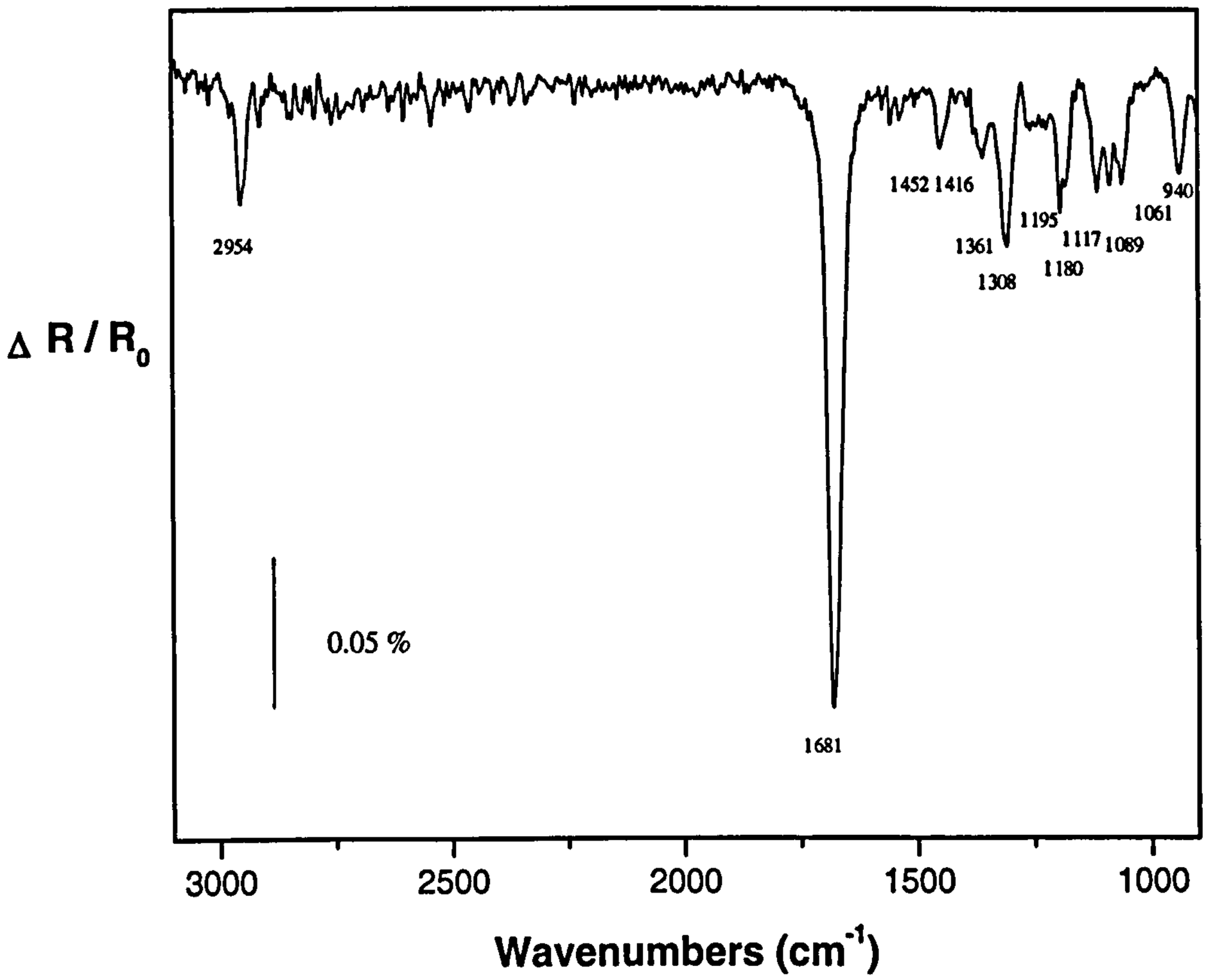

Figure 4.25: RAIR spectrum obtained during exposure of clean Cu (110) to 3 L of (S)-MHB at 289 K as soon as it adsorbs on the surface.

The IR frequencies of the (S)-MHB adsorbed on Cu (110) are compared with the ones for (R)-MHB in Table 4.13. The comparison between the values obtained for (R)-MHB and those obtained for (S)-MHB confirms that the assignments of the IR bands of the (S)-MHB are the same as those for (R)-MHB. From this, it is deduced that the bonding and orientation of the molecule of (S)-MHB, shown in Figure 4.26, are the same as for (R)-MHB.

(R)-Methyl-3-hydroxybutyrate on Cu (110) (this work)		(S)-Methyl-3-hydroxybutyrate on Cu (110) (this work)	
Wavenumbers (cm^{-1})	Assignments	Wavenumbers (cm^{-1})	Assignments
1676	ν (C=O)	1681	ν (C=O)
1447	δ_{as} (CH_3)	1452	δ_{as} (CH_3)
1415	δ_s (CH_3)	1416	δ_s (CH_3)
1360	δ (OH) or w (CH_2)	1361	δ (OH) or w (CH_2)
1306	ν (C –O_e)	1308	ν (C –O_e)
1195	tw (CH_2)	1195	tw (CH_2)
1180	ρ (CH_3)	1180	ρ (CH_3)
1114	ν (C – OH)	1117	ν (C – OH)
1089	ν (C - CH_3)	1089	ν (C - CH_3)
1060	ν (O_e – CH_3)	1061	ν (O_e – CH_3)
942	tw CH_3	940	tw CH_3

Table 4.13: Bands and assignments of (R)-MHB and (S)-MHB adsorbed on Cu (110).

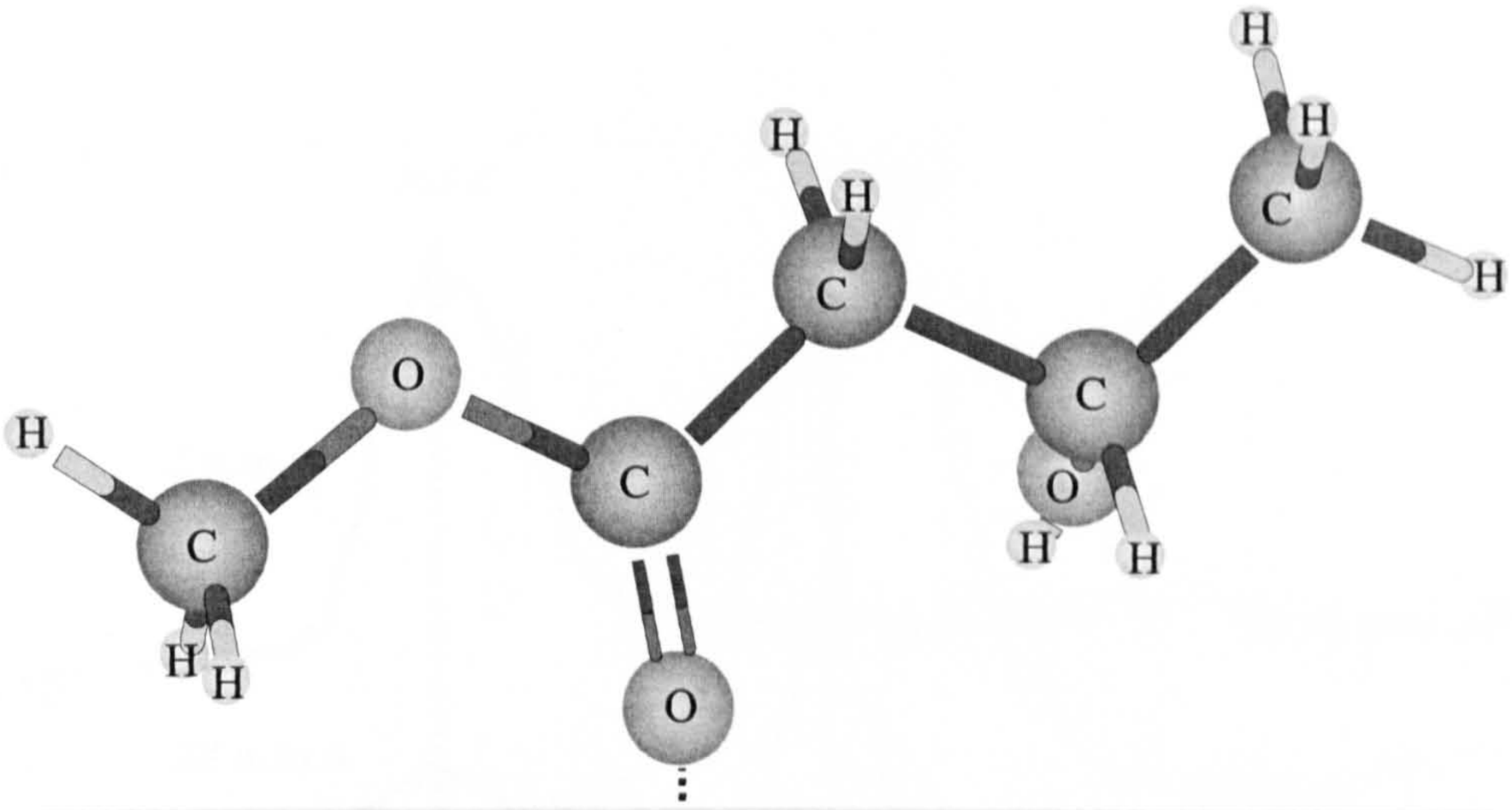

Figure 4.26: Schematic representation of one molecule of (S)-MHB adsorbed on the Cu (110) surface at 300 .K

The behaviour of the (S)-MHB on the surface is the same as the behaviour of the (R)-MHB at a given temperature, as shown in the TPD spectra in Figure 4.27. The desorption of H_2 takes place around 365 K, and between the temperatures of ~ 370 K and ~ 430K, the (S)-MHB does not exist on the surface as it has been transformed into MAA.

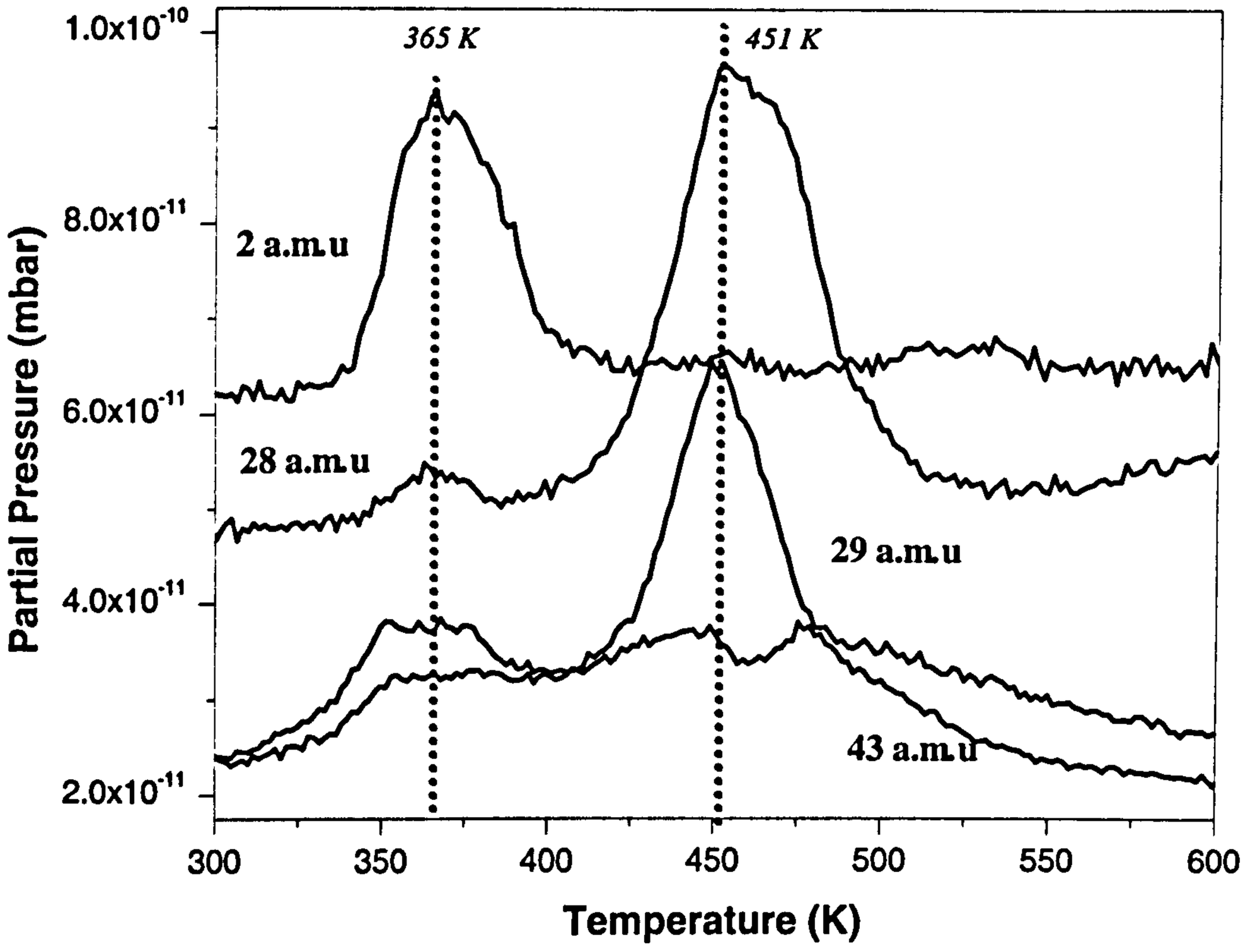

Figure 4.27: TPD spectrum of 10 L of (S)-MHB adsorbed on Cu (110) at 300K.

The kinetics of the transformation of (S)-MHB into MAA has also been studied using the identical method as for the (R)-MHB. The same conditions were applied to this experiment i.e. same dose of (S)-MHB, same temperatures and same calculation methods.

Figure 4.28 presents the RAIR spectra obtained for 3 L of (S)-MHB deposited on the Cu (110) surface at four temperatures: 308 K, 313 K, 323 K and 333 K. The area of the band at 1681 cm^{-1} representative of the amount of (S)-MHB has been measured and plotted as a function of time. Figure 4.29 presents these plots.

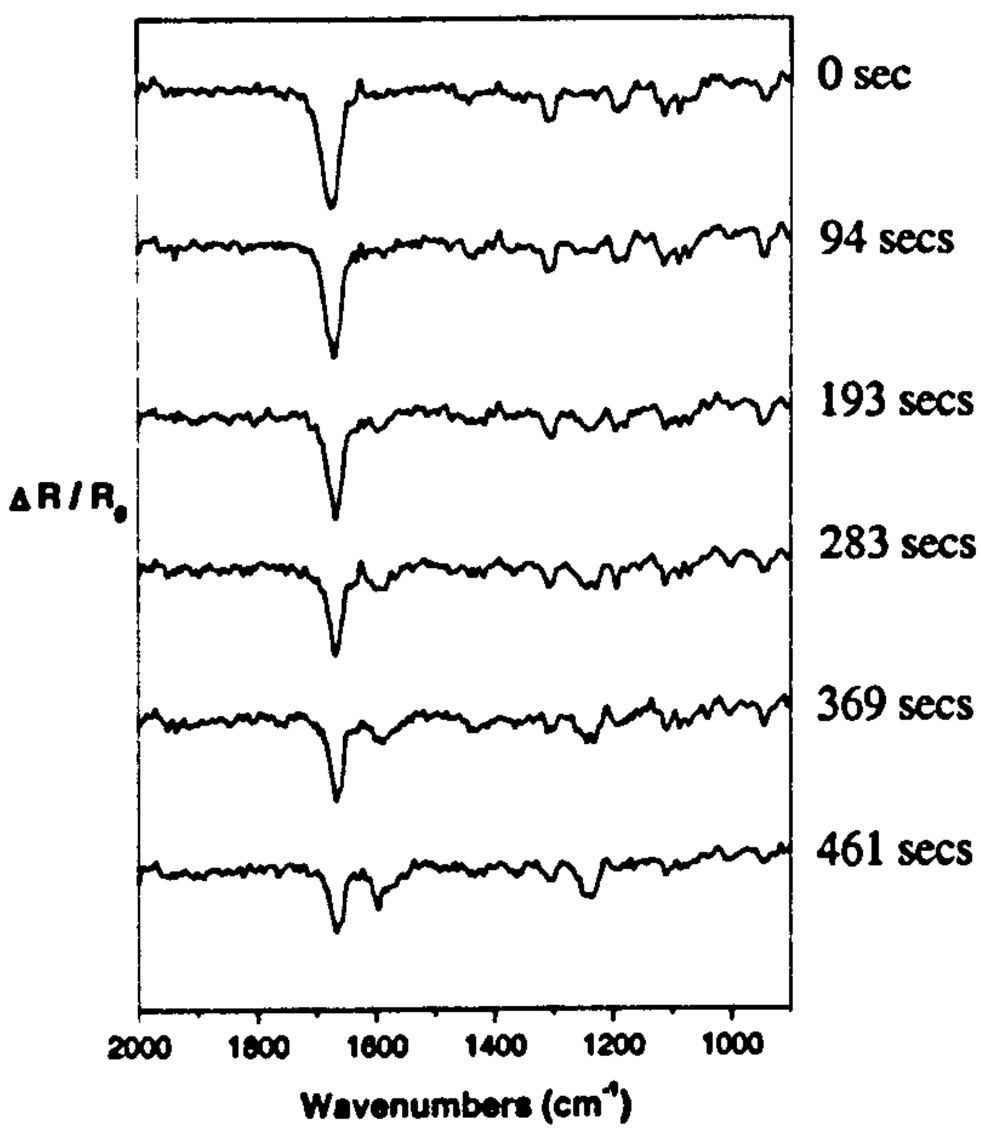

(a)

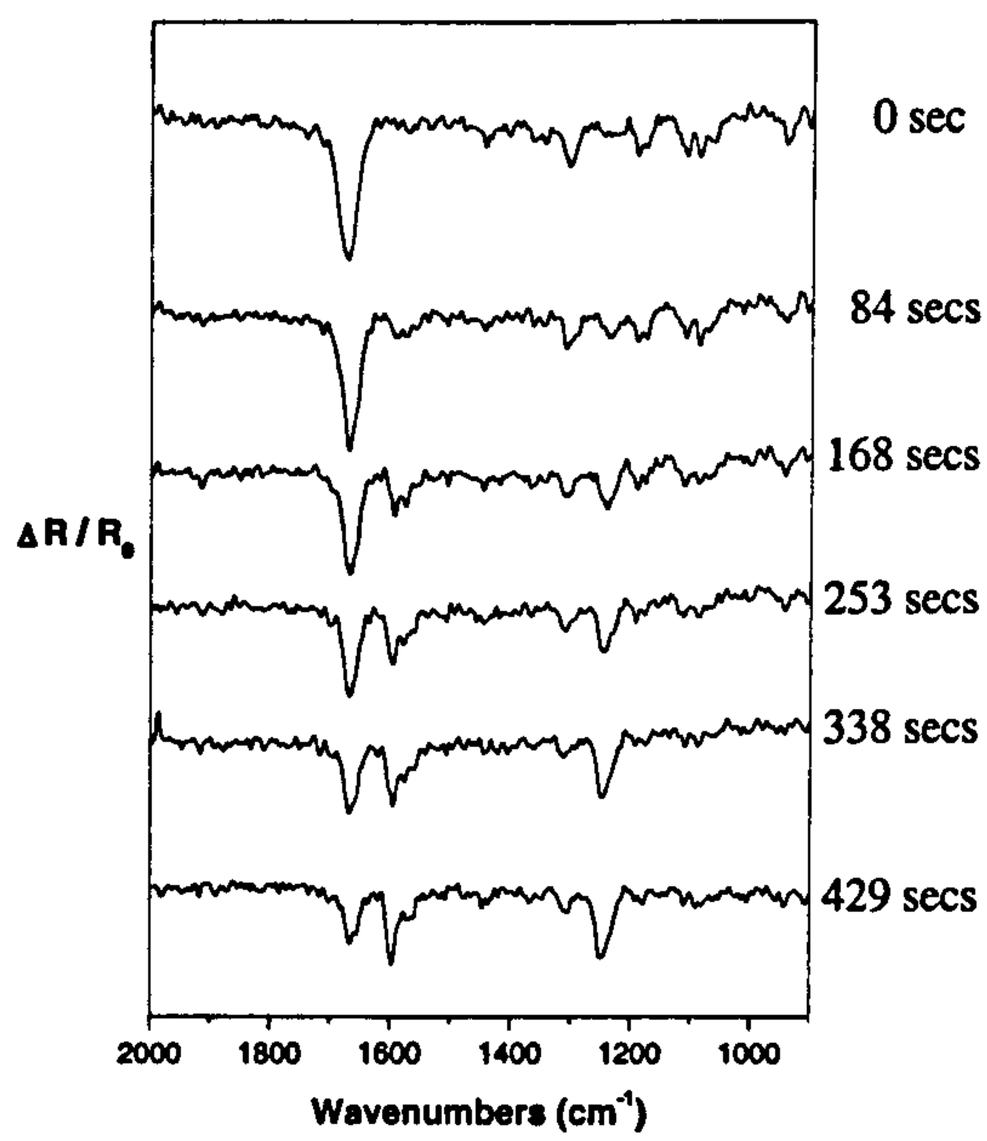

(b)

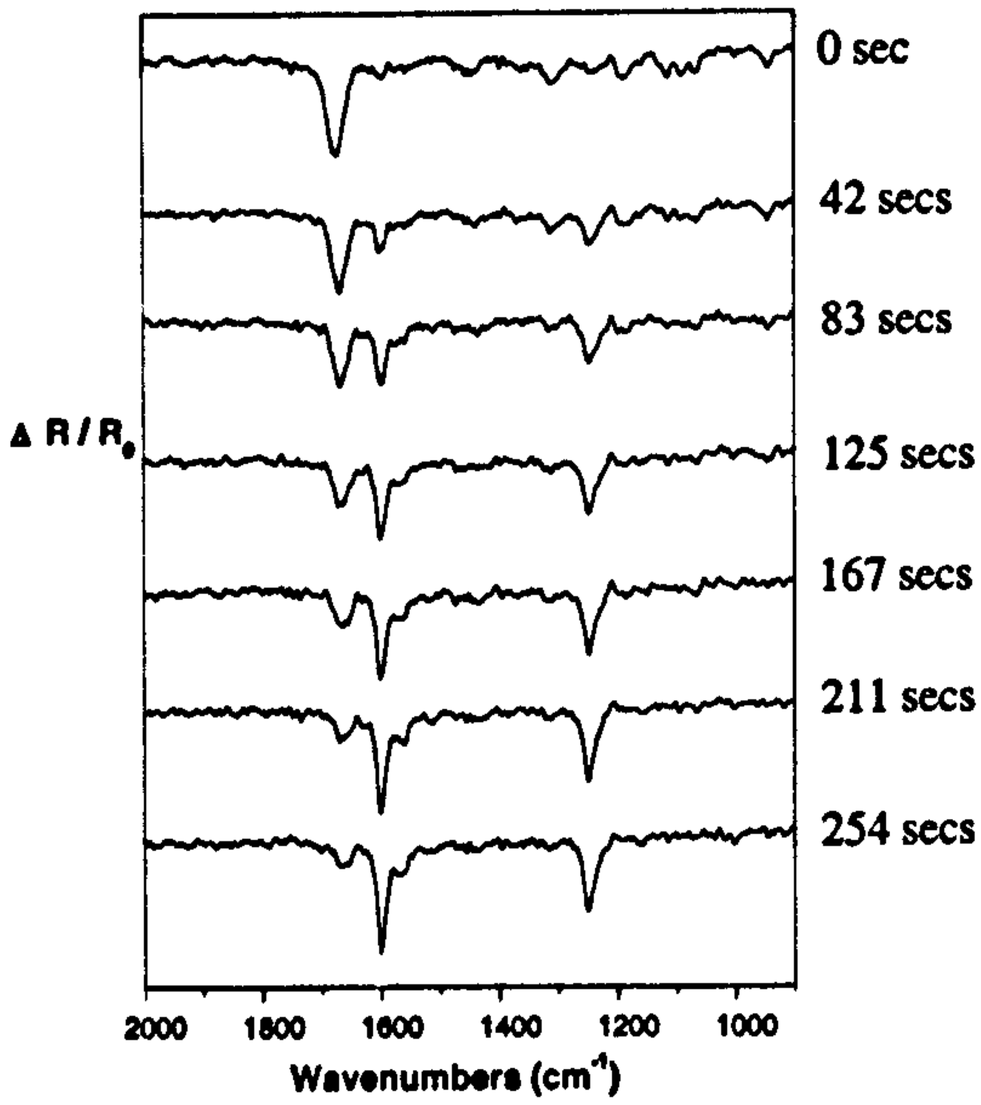

(c)

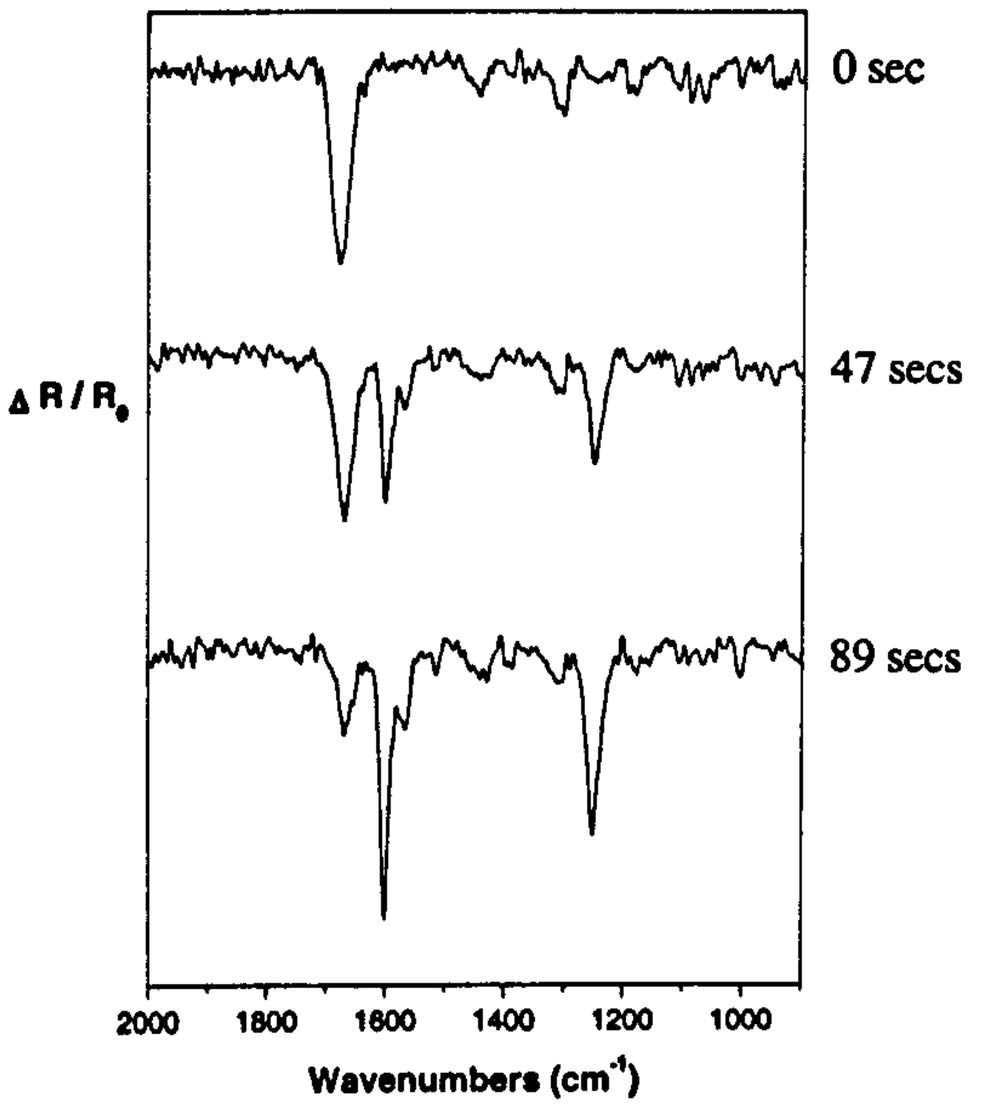

(d)

Figure 4.28: Successive RAIR spectra of 3 L of (S)-MHB transforming into MAA at temperature of: (a) 308 K, (b) 313 K, (c) 323 K and (d) 333 K.

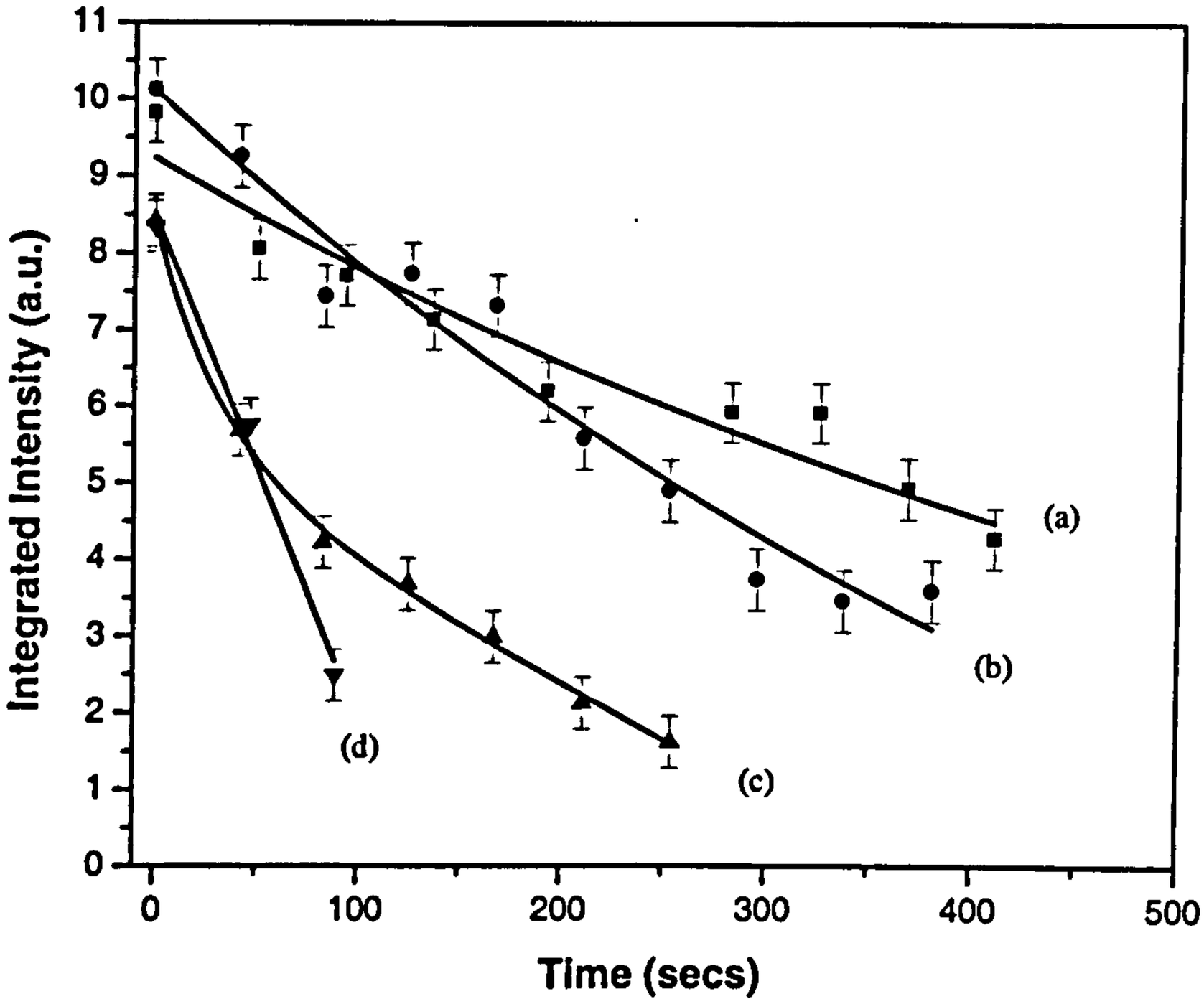

Figure 4.29: Decrease of the integrated intensity of the 1681 cm^{-1} band of (S)-MHB plotted as a function of time for the following temperatures: (a) 308 K, (b) 313 K, (c) 323 K and (d) 333 K.

From the plots in Figure 4.29, it can be noticed that at 333 K, in 100 secs, 75 % of the (S)-MHB has been converted; at 323 K, in the same time 50 % has been converted; at 313 K, 25 % has been converted and at 308 K, 20 % has been converted.

The rate constant k has also been calculated for the disappearance of the (S)-MHB on the Cu (110) for each temperature. The graphs representing the linear function:

$$\frac{a_0 - a}{a_0 \times a} = k \times t$$

has been plotted from each temperature and are presented in Figure 4.30.

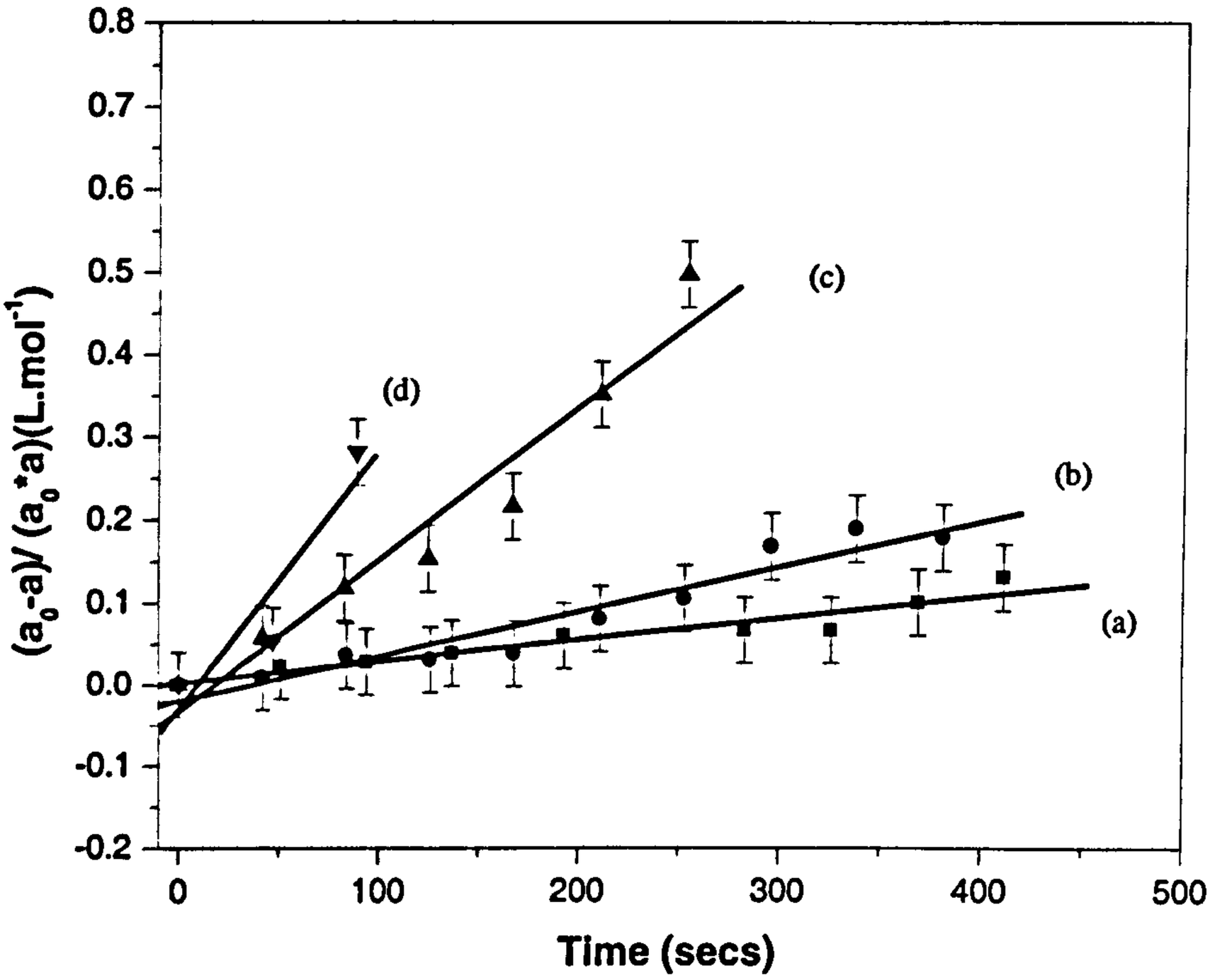

Figure 4.30: Equation $\frac{a_0 - a}{a_0 \times a} = k \times t$ plotted as a function of time for the following temperatures: (a) 308 K, (b) 313 K, (c) 323 K and (d) 333 K.

The gradient of each line in the plots presented in Figure 4.30 gives the value of k for the (S)-MHB dehydrogenation. These values are presented in Table 4.14 and compared to these obtained for (R)-MHB.

Temperature T (K)	308	313	323	333
Rate constant k (s^{-1}) for (S)-MHB	0.00020 (± 0.00002)	0.00050 (± 0.00005)	0.0018 (± 0.0002)	0.0031 (± 0.0012)
Rate constant k (s^{-1}) for (R)-MHB	0.00023 (± 0.00001)	0.00058 (± 0.00004)	0.0030 (± 0.0007)	0.0040 (± 0.0007)

Table 4.14: Rate constant k for evolution of (R)- and (S)-MHB on Cu (110) at four temperatures obtained from the plot of the linear function represented in Figure 4.30.

As the Cu (110) surface does not present any chiral discriminatory features, the values of the rate of reaction k are expected to be the same for the (R)- and the (S)-MHB. Table 4.14 shows that the rates are in good accordance for three temperatures, 308 K, 313 K and 333 K, since their values are similar when the error values are taken into account. However, for the temperature of 323 K, the error does not cover both rates obtained for the (R)- and the (S)-MHB. In addition the error bar for the values of k issues of the (S)-MHB experiment for the temperature of 333 K is very high compared to the ones for the three other temperatures. This may come from the fact that at this temperature, the reaction has already begun before it is possible to record the infrared-spectrum and has already finished when a minimum of infrared-spectra have been recorded.

From these values of k, the values designed to plot the Arrhenius equation were calculated; they are presented in Table 4.15.

Temperature T (K)	308	313	323	333
1 / T (K^{-1})	0.00325	0.00319	0.0031	0.003
ln k for (S)-MHB	-8.5 (± 0.1)	-7.6 (± 0.1)	-6.3 (± 0.1)	-5.7 (± 0.4)
ln k for (R)-MHB	-8.37 (± 0.04)	-7.45 (± 0.07)	-5.8 (± 0.2)	-5.5 (± 0.2)

Table 4.15: Values necessary to plot the Arrhenius equation: 1 / T and ln k for each temperature for (R)- and (S)-MHB.

Figure 4.31 shows the linear of the Arrhenius equation ($\ln k = - E_a / RT + \ln A$) obtained from the kinetic data for (S)-MHB. From this, the activation energy E_a has a value of 94 $\pm$ 17 kJ.mol^{-1}.

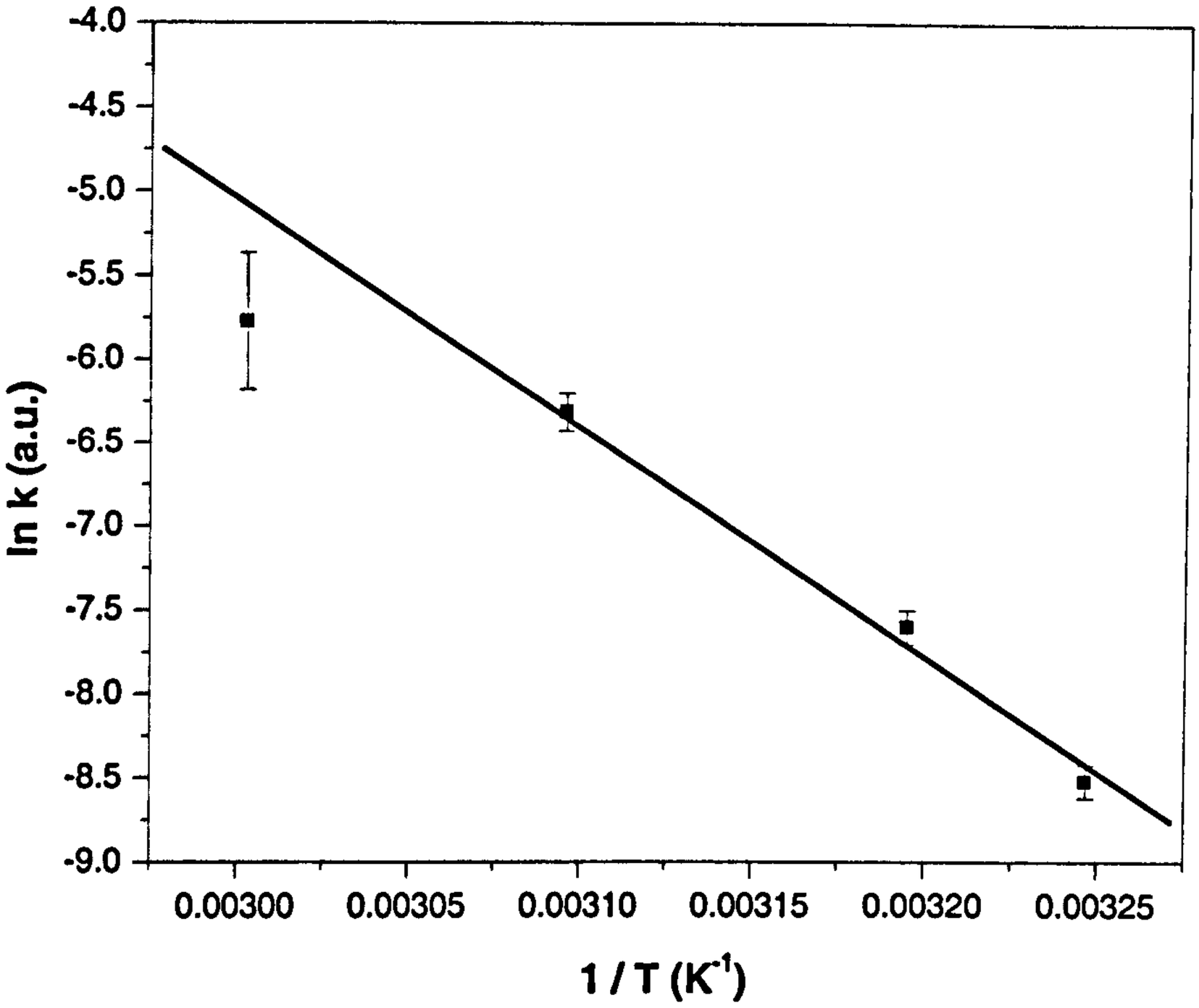

Figure 4.31: Linear of best fit to the Arrhenius equation ($\ln k = - E_a / RT + \ln A$) obtained from the kinetic data of the vanishing of (S)-MHB on Cu (110).

The activation energy for the (R)-MHB, which is 100 $\pm$ 20 kJ. mol^{-1} and the (S)-MHB, which is 94 $\pm$ 17 kJ.mol^{-1} are quite different but are still in the error bars which makes then to be the same. This was expected since each of these two molecules were evolving in a non-chiral environment.

4.4 Summary

The adsorption geometry and bonding of the enantiomers of MHB on the Cu (110) surface have been determined using RAIRS. The MHB molecule is bonded to the Cu (110) surface through the C = O bond of its ester group. This bond, whose characteristic normal mode of vibration is the ν (C = O) stretching vibration, is strong and in a position quite normal to the surface. The alcoholic part of the MHB molecule does not maintain any bonding with the surface.

The MHB molecule is subject to thermal changes. Both RAIRS and TPD experiments prove that the MHB molecule dehydrogenates into MAA even at room temperature with the rate increasing as the temperature increases. On RAIR spectra, some vibrational bands attributed to MAA replace MHB bands and other MHB bands disappear due to a new orientation of the MAA at the surface. The resulting MAA is bonded to the surface through the C ⥱ O bond of its ester part and also through the C ⥱ O bond of its ex-alcoholic part. On the TPD spectra, a hydrogen peak is present around 360 K, due to the desorption of hydrogen from the MHB. The hydrogen comes from the C-O-H and C-H groups of the alcoholic part of the MHB molecule. The MAA created then desorbs from the surface at a temperature of 450 K.

The kinetics of the transformation have been calculated. The activation energies for (R)-MHB and (S)-MHB to transform into MAA are 100 ± 20 kJ. mol^{-1} and 94 ± 17 $kJ.mol^{-1}$ respectively. The activation energies for both enantiomers are thus found to be the same within the error bars. This is not unexpected since both molecules were evolving in a non-chiral environment. It is clear, from the significant values of these activation energies, that the appearance of the MAA on the surface is associated with a very significant kinetic barrier.

An interesting question is: does this transformation involves mass transport and area expansion or diminution? The TPD reveals that during the initial desorption of hydrogen from the MHB, a small amount of MHB does desorb from the surface. Is this linked to an eventual area expansion when the MHB is transformed into MAA ? To resolve this point further studies of the two-dimensional organisation of the molecules on the surface are needed. The LEED pattern which presents a (1×1) unit cell with a high background for both the MHB and for the MAA adsorbed on the surface is not sufficient. It would have been certainly interesting to look at the organisation of the MHB and MHB transformed

into MAA molecules adsorbed on the Cu (110) using STM, and to compare the local coverage of MHB and MAA when adsorbed on Cu (110). However, it has not been possible to perform such experiments during the course of the current work.

References

[1] Y. Nakao, H. Sugeta, and Y. Kyogoku, Chem. Lett. 623(1984).

[2] D. M. P. Gigante, F. Long, L. A. Bodack, J. M. Evans, J. Kallmerten, L. A. Nafie, T. B. Freedman, J. Phys. Chem. A **103,** 1523 (1999).

[3] R. S. Rasmussen, D.D. Tuncliff, R.R. Brattain, J. Am. Chem. Soc. **71**, 1068 (1949).

[4] N. J. Leonard, H. S. Gutowsky, W. J. Middleton, E. M. Petersen, J. Am. Chem. Soc. **71,** 4070 (1952).

[5] H. Ogoshi, K. Nakamoto **45,** 3113 (1966).

[6] M. D. Newton, G. A. Jeffrey, J. Am. Chem. Soc. **99,** 2413 (1977).

[7] Infrared Spectrum of (S)-methyl-3-hydroxybutyrate, Aldrich company.

[8] M. Morssli, G. Cassanas, L. Bardet, B. Pauvert, A. Terol, Spectrochim. Acta, **47A,** 529 (1991).

[9] J. D. S. Goulden, Spectrochim. Acta **16,** (1960).

[10] C. Rozsa, M. Gonzalez, N. Galego, P. Ortiz, J. Martinez, R. Martinez, Ma. R. Gomez, Polym. Bull. **37,** 429 (1996).

[11] M. Avram, Gh. Mateescu, Infrared spectroscopy, p 259 (Wiley-Interscience, Romania, 1972).

[12] S. N. Vinogradov, R. H. Linnel, Hydrogen Bonding, p53, (Van Nostrand Reinhold Company, 1971).

[13] E. Zahidi, M. Castonguay, P. H. Mc Breen, J. Phys. Chem. **99,** 17906 (1995).

[14] E. Zahidi, M. Castonguay, P. H. McBreen, J. Am. Chem. Soc. **116,** 5847 (1994).

[15] B.A. Sexton, Surf. Sci. **88,** 319 (1979).

[16] B.A. Sexton, A.E. Hughes, N.R. Avery, Surf. Sci. **155,** 366 (1985).

[17] M.A. Barteau, M. Bowker, R.J. Madix, Surf. Sci. **94,** 303 (1980).

[18] S.D. Worley, J.T. Yates, J. Catal. **48,** 395 (1977).

[19] J. Wang, M Castonguay, J. R. Roy, E. Zahidi, P. H. McBreen, J. Phys. Chem. B **103,** 4382 (1999).

[20] G. J. Millar, C. H. Rochester, K. C. Waugh, J. Chem. Soc. Faraday Trans. **87,** 2785 (1991).

[21] M. Avram, Gh. Mateescu, Infrared spectroscopy, p 264 (Wiley-Interscience, Romania, 1972).

[22] M. Avram, Gh. Mateescu, Infrared spectroscopy, p 125 (Wiley-Interscience, Romania, 1972).

[23] M. Ortega-Lorenzo, PhD Thesis, Complexities and dynamics of the enantioselective site in heterogeneous catalysis : tartaric acid and methylacetoacetate on Cu(110) (Liverpool University, 1999).

[24] M. Avram, Gh. Mateescu, Infrared Spectroscopy, p. 380- 384 (Wiley-Interscience, Romania, 1972)..

[25] Infrared Spectrum of methyl-acetoacetate, Aldrich company.

[26] M. Avram and Gh. D. Mateescu, Infrared Spectroscopy, p. 384 (Wiley-Interscience, Romania, 1972).

[27] E. McCash, New Scientist, Inside Science, **93**, 1 (1996).

[28] K. Nakamoto, Infrared and Raman Spectra of Inorganic and Coordination Compounds, p.259 (Wiley-Interscience, New York Chichester Brisbane Toronto Singapore, 1986).

[29] R. Mecke, E. Funck, Z. Electrochem. **60**, 1124 (1956).

[30] M. Avram and Gh. D. Mateescu, Infrared Spectroscopy, p. 380 (Wiley-Interscience, Romania, 1972).

[31] G. A. Somorjai, Introduction to Surface Chemistry and Catalysis, p. 339 (Wiley-Interscience, New York, 1993).

[32] J. L. Latham, Elementary Reaction Kinetics (Butterworths, London, 1969).

[33] M. Ortega Lorenzo, V. Humblot, P. Murray, C. J. Baddeley, S. Haq, R. Raval, J. Catal. **205**, 123 (2002).

Chapter Five

Co-Adsorption of (R)- / (S)-MHB and (S)-Alanine on Cu (110)

5.1 Introduction

5.1.1 Activities and chiral discrimination at chiral surfaces

It has been possible to observe enantiomerically selective adsorption and chemistry of chiral organic molecules on naturally chiral surfaces.

The investigation of the chirality of certain metallic surfaces has begun with McFadden *et al* who have shown that it is possible to create metallic chiral surfaces [1]. Metallic surfaces are chiral if their kink sites on the high Miller index surfaces lack symmetry when the step lengths or step faces on either side of the kink are unequal. In such cases a new surface may be generated by reflection through a plane normal to the surfaces which possess kink sites with intrinsic (left or right) handedness. In terms of notation, in analogy to the Cahn-Ingold-Prelog rules, Mc Fadden *et al* gave the long step higher priority than the short step and the terrace lower priority than the short step. Viewed from above, the surface was designated $(hkl)^R$ if one spirals clockwise into the surface and $(hkl)^S$ if counterclockwise. However, Attard *et al* pointed out that this definition does not include all possible chiral surfaces and added an element to this definition by taking into account the individual symmetry of {111}, {100}, and {110} sites comprising the kink [2-4]. This new definition is based on an analogy with the Cahn-Ingold-Prelog sequences rules as well. When the kink site is view from above, if the sequence {111} → {100} →

{110} is found to run clockwise, the surface is denoted "R"; if the sequence {111} → {100} → {110} is found to run anticlockwise, the surface is denoted "S".

It was believed that because of the existence of chirality in kinked single crystal metal surfaces, it was possible to observe enantiomerically selective adsorption and / or chemistry of chiral organic molecules at kink sites. This would result if steric considerations allowed one enantiomer to interact more intimately with the kink site than the other. This phenomenon has been predicted theoretically by Sholl *et al* [5, 6], who used the Monte Carlo methods and calculated enantiomeric shifts in the binding energies of chiral hydrocarbons on chiral Pt surfaces. He also calculated and compared the binding energies of the (R)- and (S)- enantiomers of 1,2-dimethylcyclopropane adsorbed on Pt (643) and deduced that TPD was a good experimental technique to demonstrate the difference in the binding energies when two enantiomers are bound to a chiral surface. A small warning should be taken into account since Sholl *et al* demonstrated that not every chiral compound exhibits a significant enantiomeric shift when adsorbed on a chiral surface.

Electrochemical experiments conducted by Attard *et al* provided the first experimental demonstration of the enantiospecific properties of chiral single-crystal surfaces [2-4]. When achiral stepped Pt surfaces were used as electrodes, the differences in voltammetry between the oxidation of (D)- and (L)-glucose were negligible. When the same experiment was performed using Pt $(643)^R$ and Pt $(643)^S$ electrodes, the voltammetry profiles depended on the enantiomeric identity of the glucose. Similar experiments were performed using Pt $(531)^R$ and Pt $(531)^S$ electrodes. The differences between the voltammetry profiles for (D)- and (L)-glucose on Pt $(531)^R$ and Pt $(531)^S$ were larger than those for Pt $(643)^R$ and Pt $(643)^S$. This effect was attributed to the higher kink density on the Pt (531) surface. By performing experiments at 273 K and 293 K, Attard *et al* estimated the adsorption energies of (D)- and (L)-glucose on Pt $(643)^R$ and Pt $(643)^S$ differed by approximately 0.3 $kcal.mol^{-1}$.

To demonstrate the enantiospecific adsorption of molecules on chiral single-crystal surfaces, McFadden *et al* used temperature-programmed desorption (TPD) to measure the binding energy of several chiral alcohols on Ag (643) and Ag (-6 –4 –3) [1]. With these experiments, it should have been possible to resolve differences in binding energy as small as 0.1 kcal / mol. Unfortunately, no measurable differences between the binding energies of (R)- and (S)- 2-butanol on Ag (6 4 3) and Ag (-6 –4 –3) were detected. McFadden *et al* were also unable to measure any enantiospecific effects in the kinetics of

alkoxide decomposition on the same surface [1]. Thus, although the possibility of enantiospecific adsorption properties involving chiral single-crystal surfaces is clear, no demonstration of this phenomenon has been made by this experiment. However, Gellman *et al* have presented the first observation of a diastereomeric effect in the molecular desorption of a chiral molecule from naturally chiral single-crystal surfaces [7-9]. They have shown that the desorption of enantiomerically pure propylene oxide from the Cu (643) surface is influenced by the chirality of the surface. Besides, they have been able to observe a difference in the desorption energies of (R)-3-methyl-cyclohexanone of 0.22 ± 0.05 kcal / mole when this molecules is adsorbed on the Cu $(643)^R$ and Cu $(643)^S$. It has been shown as well by Gellman *et al* that the RAIRS spectra of adsorption of the enantiomers of butan-2-oxide on chiral Ag (643) present some differences [8].

In the work presented in this thesis, an alternative approach to create a chiral surface was used. Rather than cutting the underlying metal surface to make it chiral, the copper surface was modified using a molecule, (S)-alanine.

5.1.2 Co-adsorption experiments

As explained in Chapter One, the hydrogenation of MAA on a metal gives a racemic mixture of (R)- and (S)-MHB. If the metal is modified with (S)-alanine, the reaction is switched to give an enantiomeric excess of the (R)-MHB enantiomer; if the metal is modified with (R)-alanine, the reaction is switched to favour the production of the (S)-MHB enantiomer, as shown in Figure 5.1. It is not possible to directly determine the chirality of the reaction product using the surface science methods available for the hydrogenation reaction of MAA. However, the reverse dehydrogenation reaction of the chiral MHB giving the MAA can be observed. Thus, the aim of the work presented in this chapter is to investigate the way a chiral surface, such as the Cu (110) surface modified with (S)- or (R)-alanine, responds with respect to the chirality of the (R)- or the (S)-MHB. This response can be investigated by two equivalent ways: the co-adsorption of either the (R)-MHB or the (S)-MHB on a Cu (110) surface modified with (S)-alanine or alternatively the co-adsorption of either the (R)-MHB or the (S)-MHB on a Cu (110) surface modified with (R)-alanine. The first solution has been followed, even if it would have been reassuring to check that the results obtained with the surface modified with (S)-alanine are coherent with the results obtained with the surface modified with (R)-alanine:

(R)-MHB + (S)-alanine / (S)-MHB + (R)-alanine ⇒ same behaviour

(S)-MHB + (S)-alanine / (R)-alanine + (R)-MHB ⇒ same behaviour

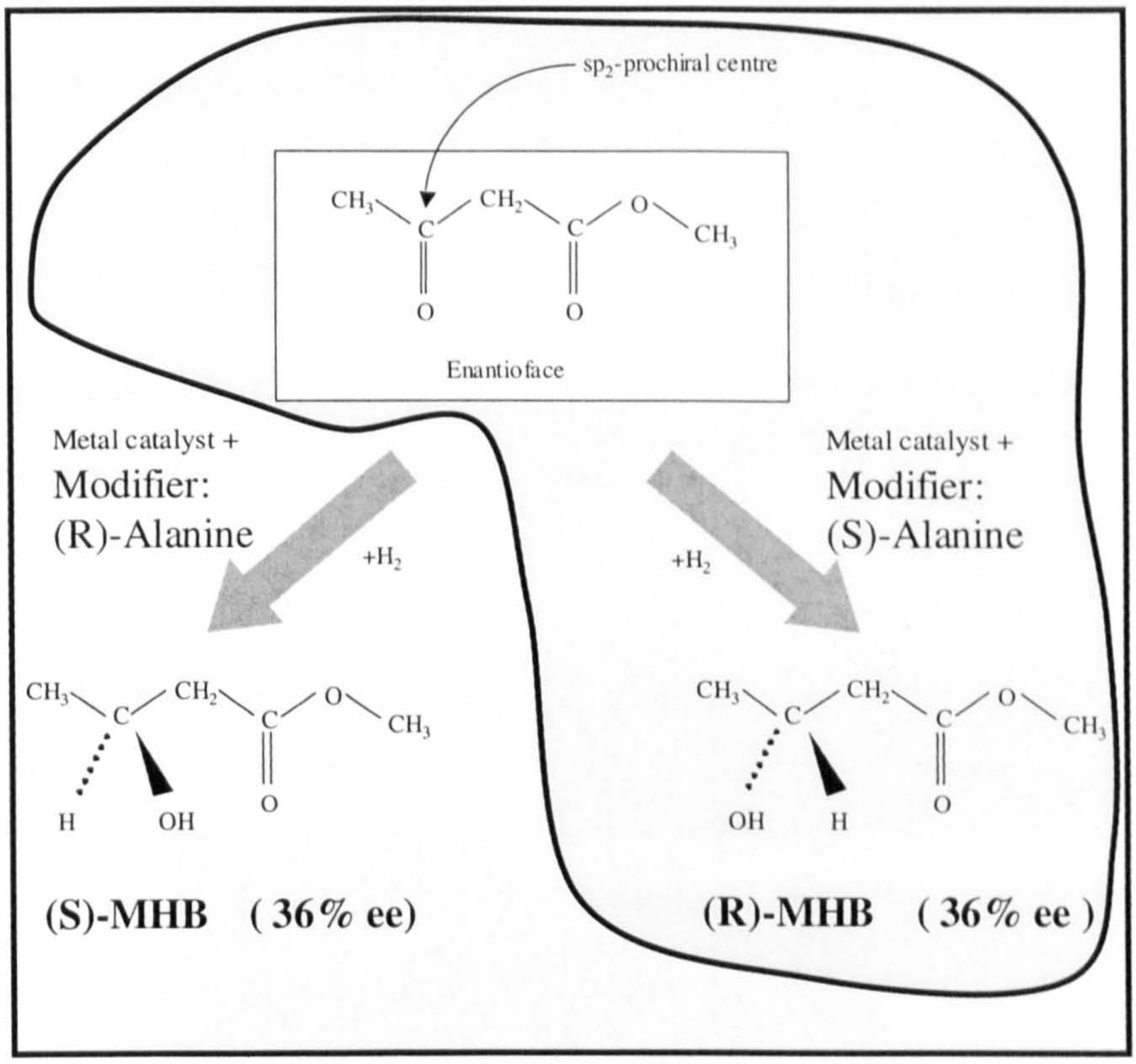

Figure 5.1: Hydrogenation of MAA in to (R)- or (S)-MHB depending on the enantiomers of alanine used.

Different preparations of the Cu (110) surface modified with (S)-alanine have been used corresponding to a range of coverage and temperature dependent phases. Details regarding the preparation of these various phases are well known from earlier work performed in our research group [10, 11]

5.2 Attempt to adsorb (R)-MHB on the extended chiral surface formed by (S)-alanine on Cu (110)

5.2.1 Presentation of the saturated extended chiral surface of (S)-alanine and aims of the experiment

To prepare the extended chiral surface, the (S)-alanine is first dosed on the Cu (110) crystal to saturation at room temperature to give the surface shown in Figure 5.2.

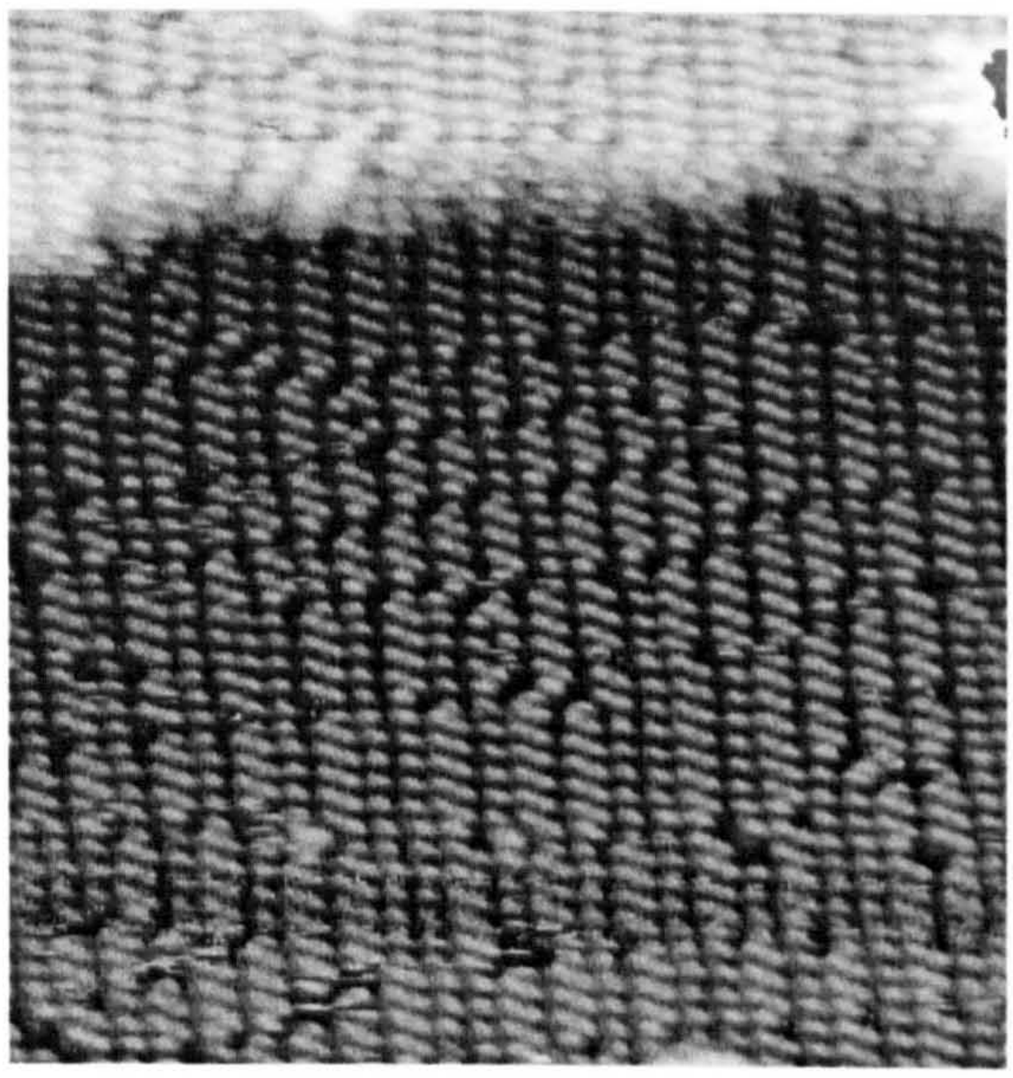

Figure 5.2: STM image showing the Cu (110) surface saturated of (S)-alanine *molecules* at room temperature; 140 Å × 140 Å [10].

On this surface, the (S)-alanine molecules are in the "high coverage" phase. This means there are two kinds of positions of the (S)-alanine molecule on the surface: the bidentate and the monodentate shown in Figure 5.3 (a) and (b) respectively.

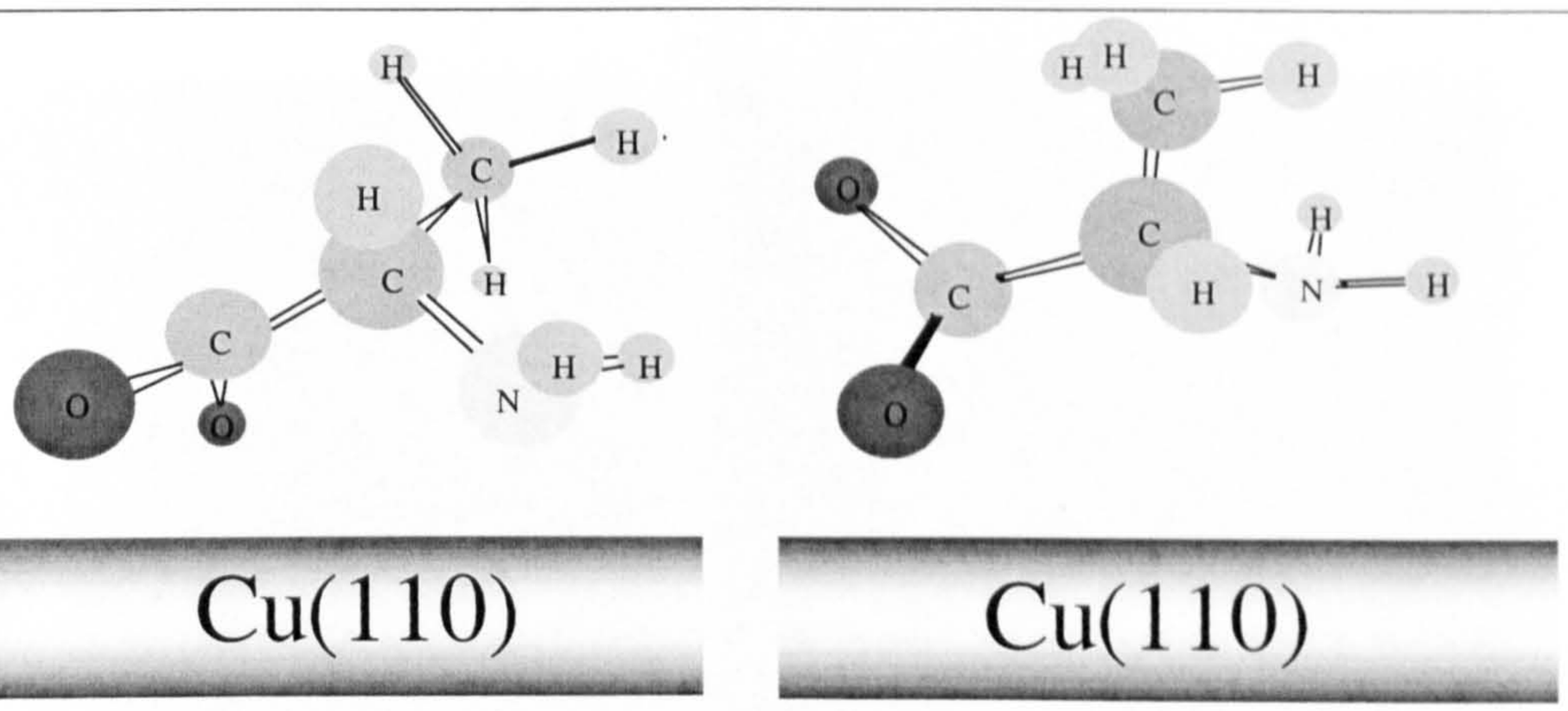

(a) (b)

Figure 5.3: Two species of (S)-alanine present on the Cu (110) surface at high coverage: (a) bidentate and (b) monodentate [11, 12].

As can be clearly seen on Figure 5.2, the (S)-alanine molecules fill up the area of this surface, and it would be hard to co-adsorb another molecule onto this densely packed surface. However, if this surface is then warmed gently to 430 K, a new organisation of the (S)-alanine molecules on the Cu (110) surface can be identified. This new surface, highly organised, is represented on the STM picture in Figure 5.4 (a). The LEED pattern of the structure, shown in Figure 5.4 (b) gives the unit cell of the overlayer structure in matrix notation (5 3, 2 - 2) [10].

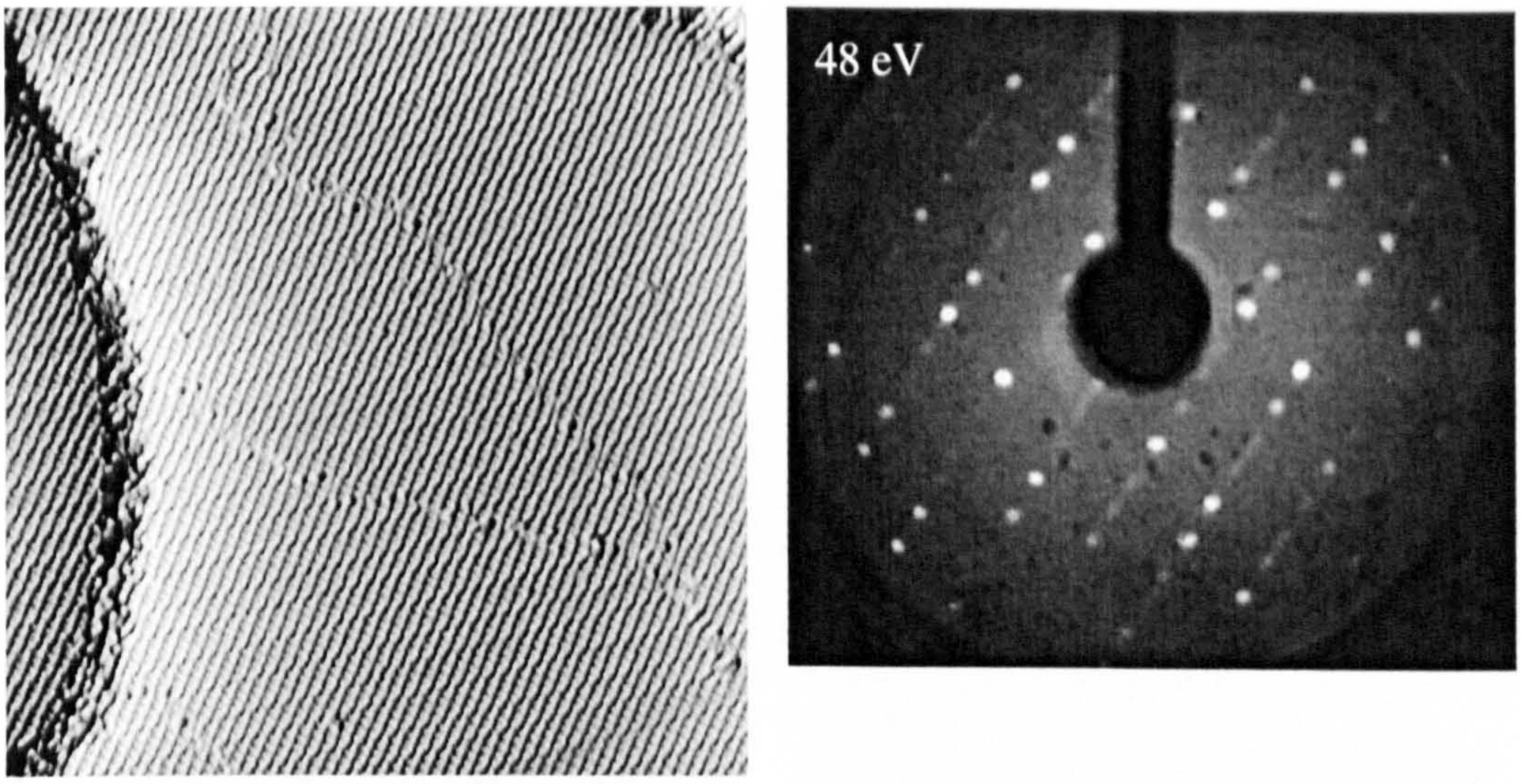

(a) (b)

Figure 5.4: (a) STM image showing the Cu (110) surface saturated of S-alanine molecules at room temperature and warmed to 430 K, 400 Å × 400 Å [10, 11]; (b) LEED pattern associated with this structure [10].

The RAIR spectrum of this newly created phase indicates that the two species of (S)-alanine, the monodentate and the bidentate, shown in Figure 5.3 are still present on the surface [10]. Figure 5.5 (a) shows a STM image of the structure which shows that the alanine molecules are organised in pack of six or eight molecules. Between each pack, some empty nanosized channels can be observed. The combination of STM, RAIRS and LEED allows the local and global structural model to be established as shown in Figure 5.5 (b).

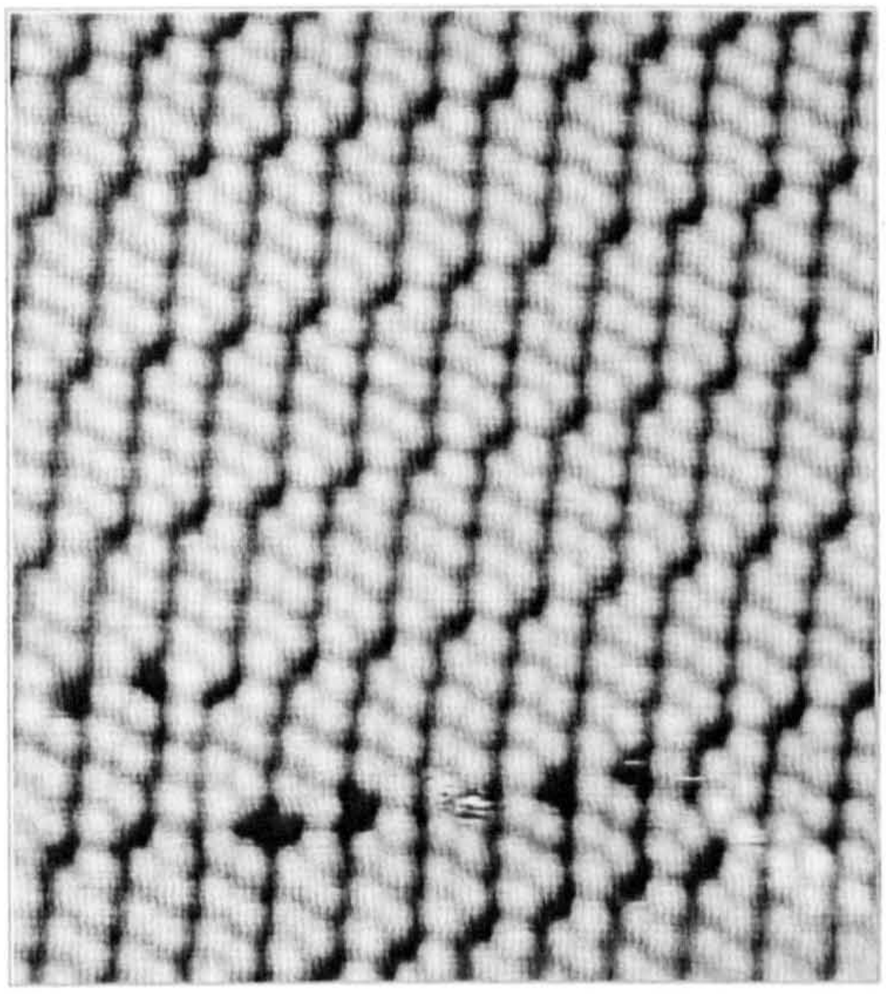

(a)

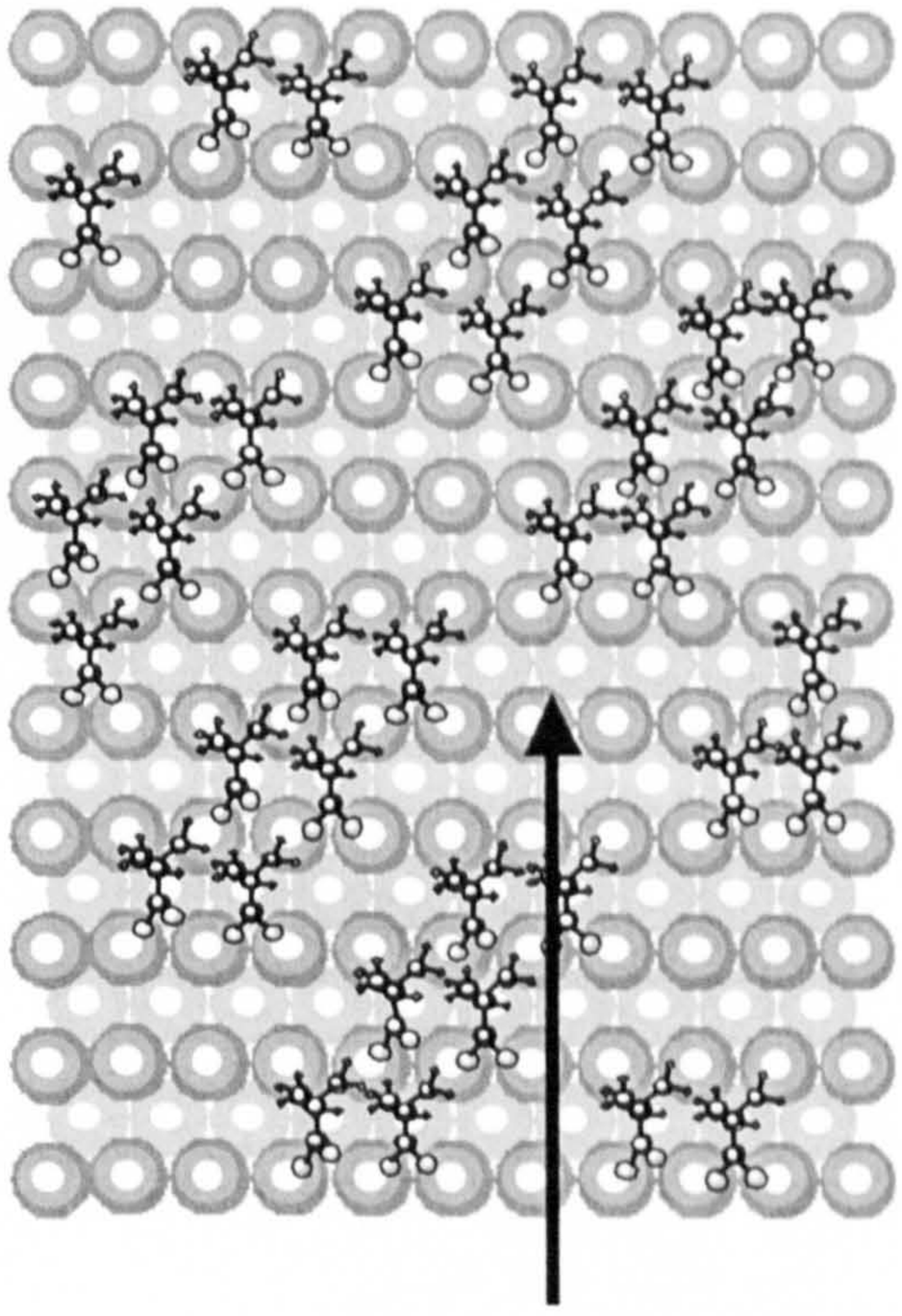

Empty Nanosized Channels =
Potential Molecular Landing Strips

(b)

Figure 5.5: Saturation layer of S-alanine on Cu (110) warmed to 430 K; (a) STM image of the structure, 100 Å × 100 Å; (b): Schematic representation of the structure [10].

The attractive facts to use this phase for the co-adsorption of the (R)-MHB are:

(i) This phase presents a two-dimensional order of the (S)-alanine molecules extended over long distances across the surface. The growth axis destroys the two mirror planes that exist at the fcc (110) surface, creating an extended chiral surface.

(ii) This phase presents some empty nanosized channels, which are mirrors of each other for the (S)-alanine and (R)-alanine, as has been shown in Chapter

One. It is supposed here that these channels are the enantiomeric catalytic place where the reaction of hydrogenation of the MAA into (R)-MHB or (S)-MHB, depending on the chirality of the alanine, takes place.

The aim of the experiments described in the next section was to investigate the recognition of the (R)- or the (S)-MHB from the channels created by (S)-alanine adsorbed on Cu (110). The extended chiral surface of (S)-alanine was created and an increased pressure of (R)-MHB put in the chamber. As (R)-MHB is the product of the reaction of the hydrogenation of MAA on a metal modified with (S)-alanine, it was hoped that (R)-MHB would adsorb into the channels formed by the (S)-alanine molecules.

5.2.2 Results

RAIRS was used to follow the adsorption of the (R)-MHB onto the previously created extended chiral surface of (S)-alanine on Cu (110). Figure 5.6 presents the spectra corresponding to the extended chiral surface (a), to which 1 L of (R)-MHB has been added (b), 3 L has been added (c) and 15 L have been added (d).

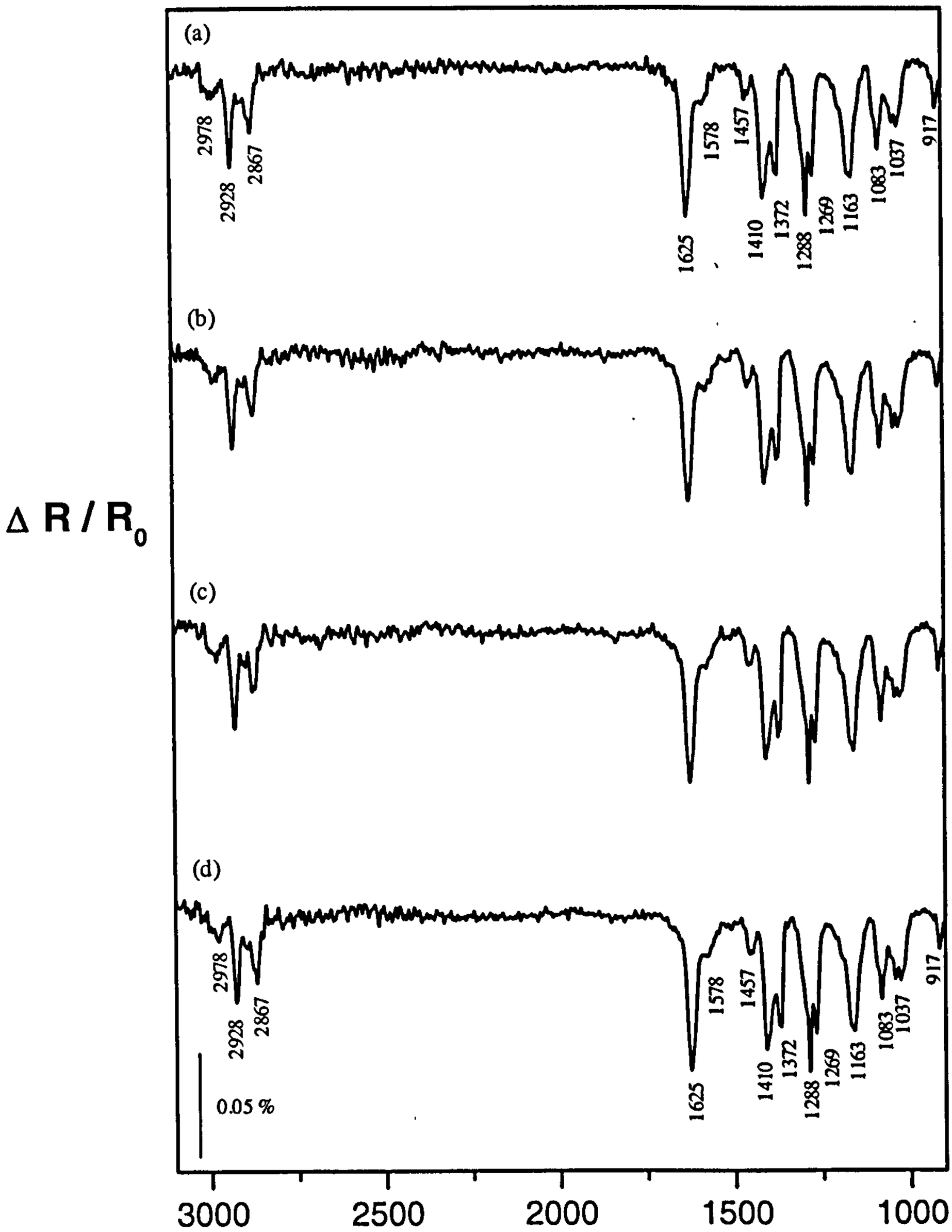

Figure 5.6: RAIR spectra corresponding to the experiment described in this section; (a) RAIR spectrum corresponding to the extended chiral surface, described in section 5.3.1; (b) with 1 L of (R)-MHB, (c) with 3 L of (R)-MHB, (d) with 15 L of (R)-MHB.

It can be easily noticed that no difference exists between the different RAIR spectra presented in Figure 5.6. The characteristic peaks of the MHB are absent from each RAIR spectrum. This obviously means that the (R)-MHB does not adsorb onto the (S)-alanine structure created, and does not adsorb into the channels, as represented in Figure 5.7 (a). The size of the channels must be too small for the (R)-MHB molecules to adsorb into them. The lack of adsorption of the (R)-MHB into the channels created by the (S)-alanine, demonstrates that the creation of the catalytic channels depends not only on the organisation of the (S)-alanine molecules on the Cu (110) surface but depends as well on the size of the reactant molecules.

It has also been previously recognised that these channels were too small for the MAA molecules to be inserted into them [10]. In this case, another method of preparation of the sample was necessary to be able to observe the MAA molecules adsorbing into the channels [10]. By co-adsorption with the MAA at room temperature, the (S)-alanine molecules re-organised themselves incorporating the MAA molecules into the channels when the mixture was heated to 430 K, as represented in Figure 5.7 (b). This was observed using STM. However, this procedure for putting the MAA molecules into the channels, which includes heating the crystal, cannot be adopted for the MHB molecules as any heat provided gives sufficient energy to dehydrogenate the MHB into MAA. The experiment then becomes meaningless.

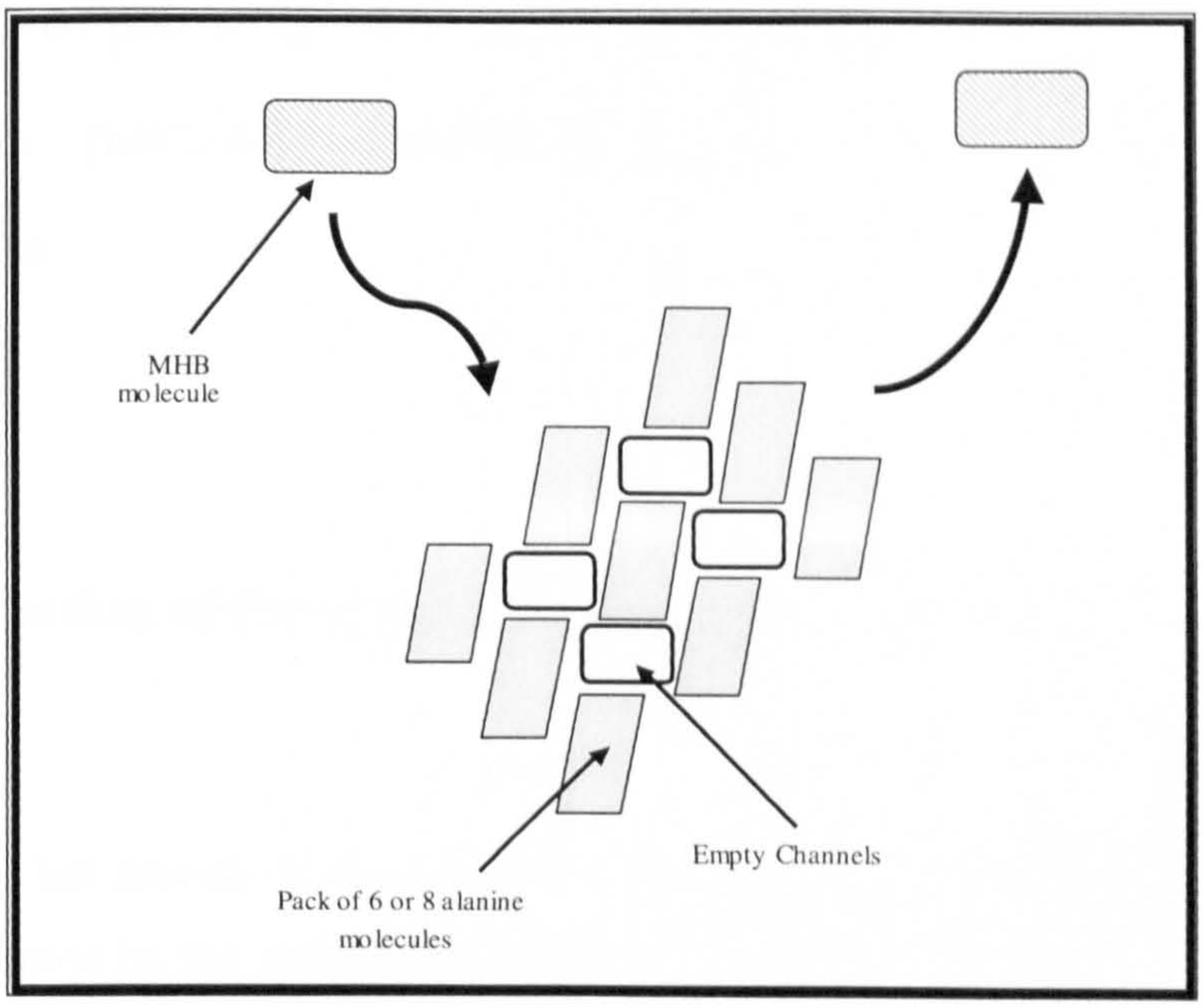

(a)

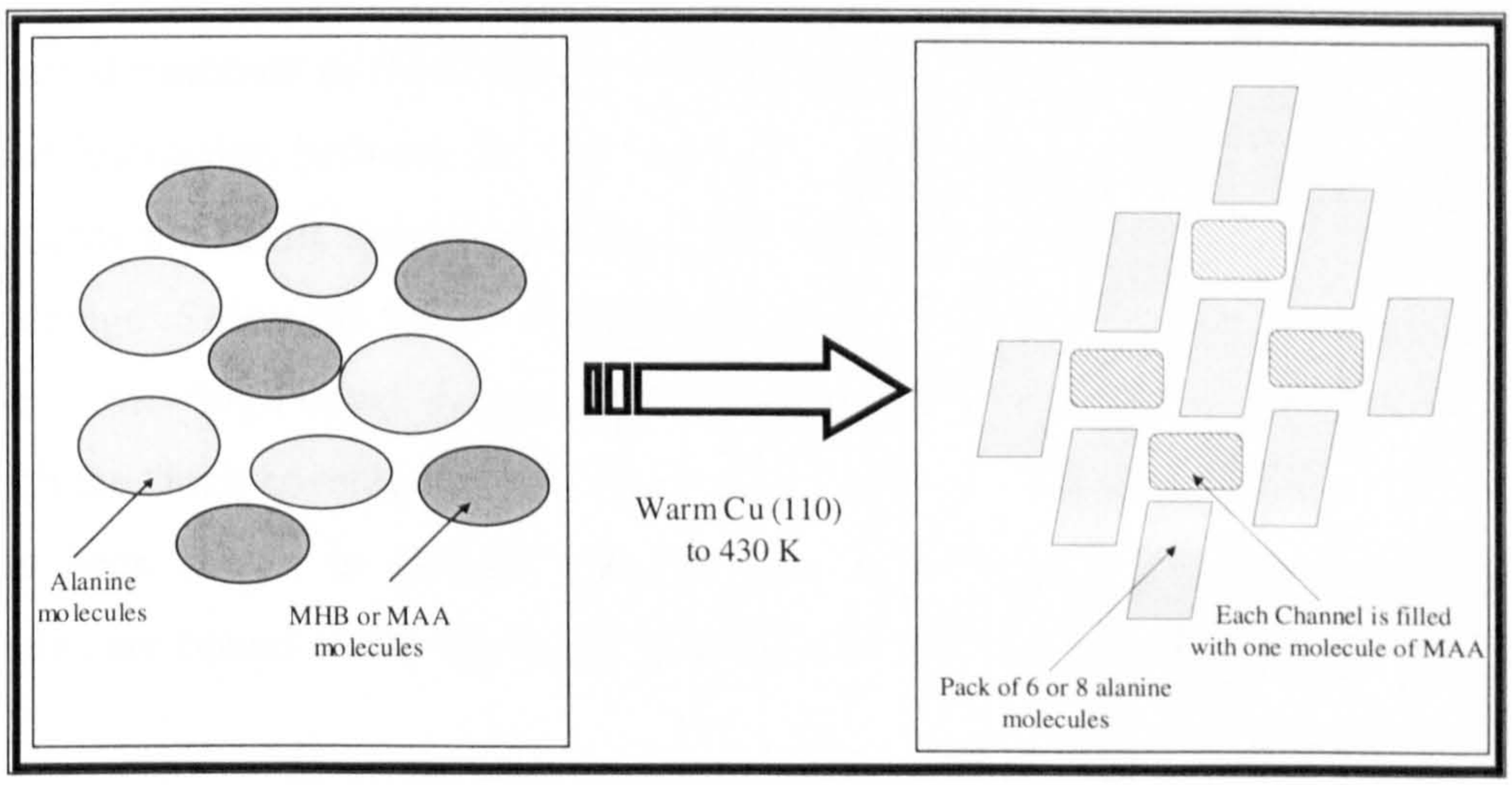

(b)

Figure 5.7: Two experiments conducted to adsorb the (R)-MHB into the channels: (a) when the extended chiral surface has been formed previously; (b) when the co-adsorption of the MAA and (S)-alanine are done before heating the crystal to 430 K.

5.3 Co-adsorption of (R)-MHB and (S)-MHB on a Cu (110) surface partially modified with a low coverage of (S)-alanine

5.3.1 Presentation of the surface used and aims of the experiment

As shown in the last section, it was impossible to co-adsorb the (R)-MHB molecules into the channels formed by the self-organised extended chiral surface created by a saturated coverage of (S)-alanine molecules adsorbed on the Cu (110) surface, the channels being too small. The aim then became to dose a smaller amount of (S)-alanine so that there was enough room on the Cu (110) surface for the co-adsorption of (R)-MHB or (S)-MHB. However, the amount of (S)-alanine dosed still needed to be relatively high to provoke an eventual interaction between the (R)-MHB or the (S)-MHB and the (S)-alanine. Figure 5.8 presents the RAIR spectra obtained when dosing (S)-alanine on Cu (110) increasing the coverage. Spectrum 5.8 (a) represents the "low coverage phase", spectrum 5.8 (c) represents the "high coverage phase"; spectrum 5.8 (b) represents the intermediate state in which the "high coverage phase" starts to be formed.

As has been shown in Chapter One, in the "low coverage phase", the (S)-alanine molecules are bound to the Cu (110) surface in their bidentate form as shown in Figure 5.9.

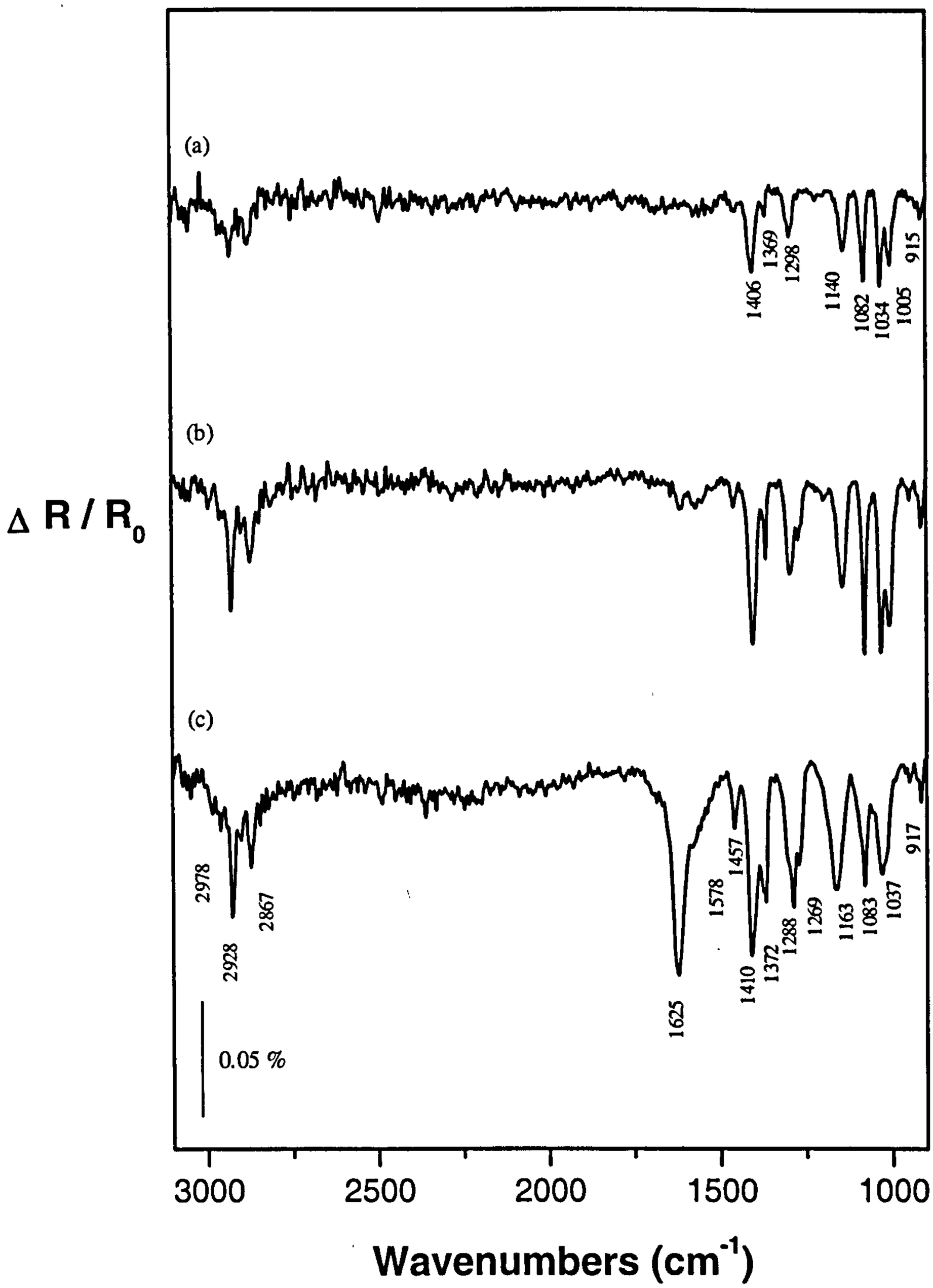

Figure 5.8: RAIR spectra of (S)-alanine adsorbing on the Cu (110) surface, increasing coverage.

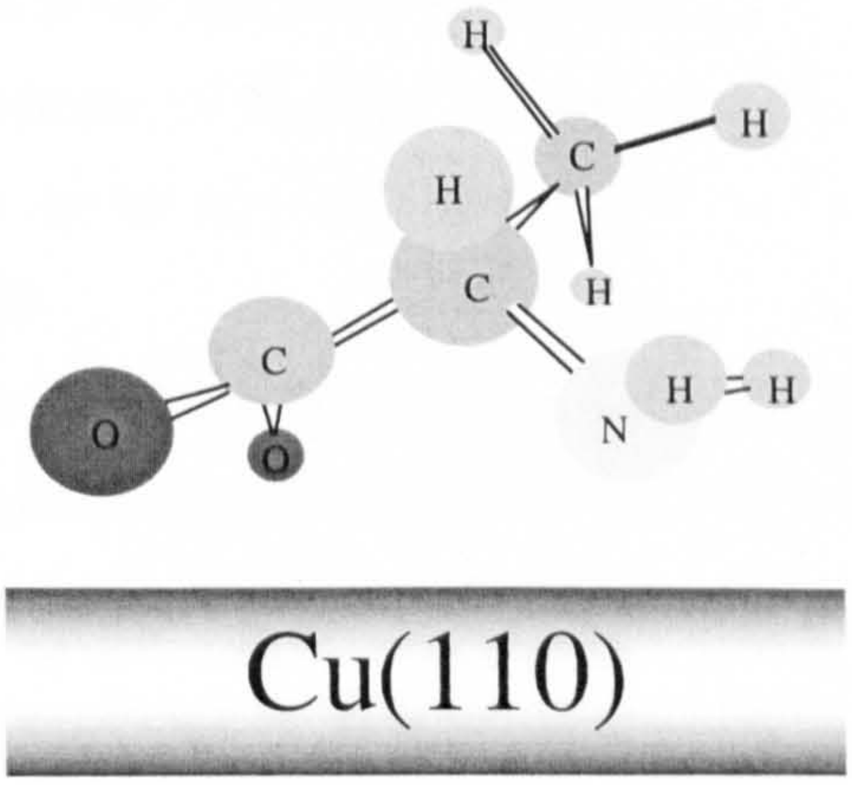

Cu(110)

Figure 5.9: Bidentate form of (S)-alanine present on the Cu (110) surface at low coverage [11, 12].

It is believed that this "low coverage phase" decorates the steps of the Cu (110) surface and is also present in small quantity on the terraces, as the STM image in Figure 5.10 shows.

Figure 5.10: STM image representing the "low coverage" of (S)-alanine adsorbed on the Cu (110) surface, 500 Å × 500 Å [10].

The aim of the experiments in the following sections was:

(i) to look for evidence of interaction between (R)- or (S)-MHB and the (S)-alanine present in its low coverage phase on the Cu (110) surface using RAIRS and TPD

(ii) if an interaction occurs, check if it is strong enough to modify the kinetics of the transformation of (R)-MHB into MAA in the presence of (S)-alanine

5.3.2 Co-adsorption and interaction investigated by RAIRS

5.3.2.1 RAIRS studies of the co-adsorption at 300K

As there is more space on the surface, it should be possible to co-adsorb some (R)-MHB or (S)-MHB with a low coverage of (S)-alanine on Cu (110). The idea was to see if there were some relevant indicators on the RAIR spectra of co-adsorption which would allow confirmation of an interaction between the MHB enantiomers and the (S)-alanine molecules. It would be even more interesting to see if there were differences between the co-adsorption spectra of (R)-MHB with (S)-alanine and those of (S)-MHB with (S)-alanine.

The experiment consisted of dosing an amount of (S)-alanine corresponding to the low coverage phase on the Cu (110) surface. This amount is represented in the RAIR spectrum of Figure 5.11 (a). When this amount was deposited on the surface, the dosing valve was closed. Then, (R)-MHB was introduced into the chamber; spectrum 5.11 (b) represents the spectrum of the co-adsorption. For comparison, a RAIR spectrum of (R)-MHB when it is by itself on the Cu (110) surface is presented in Figure 5.11 (c).

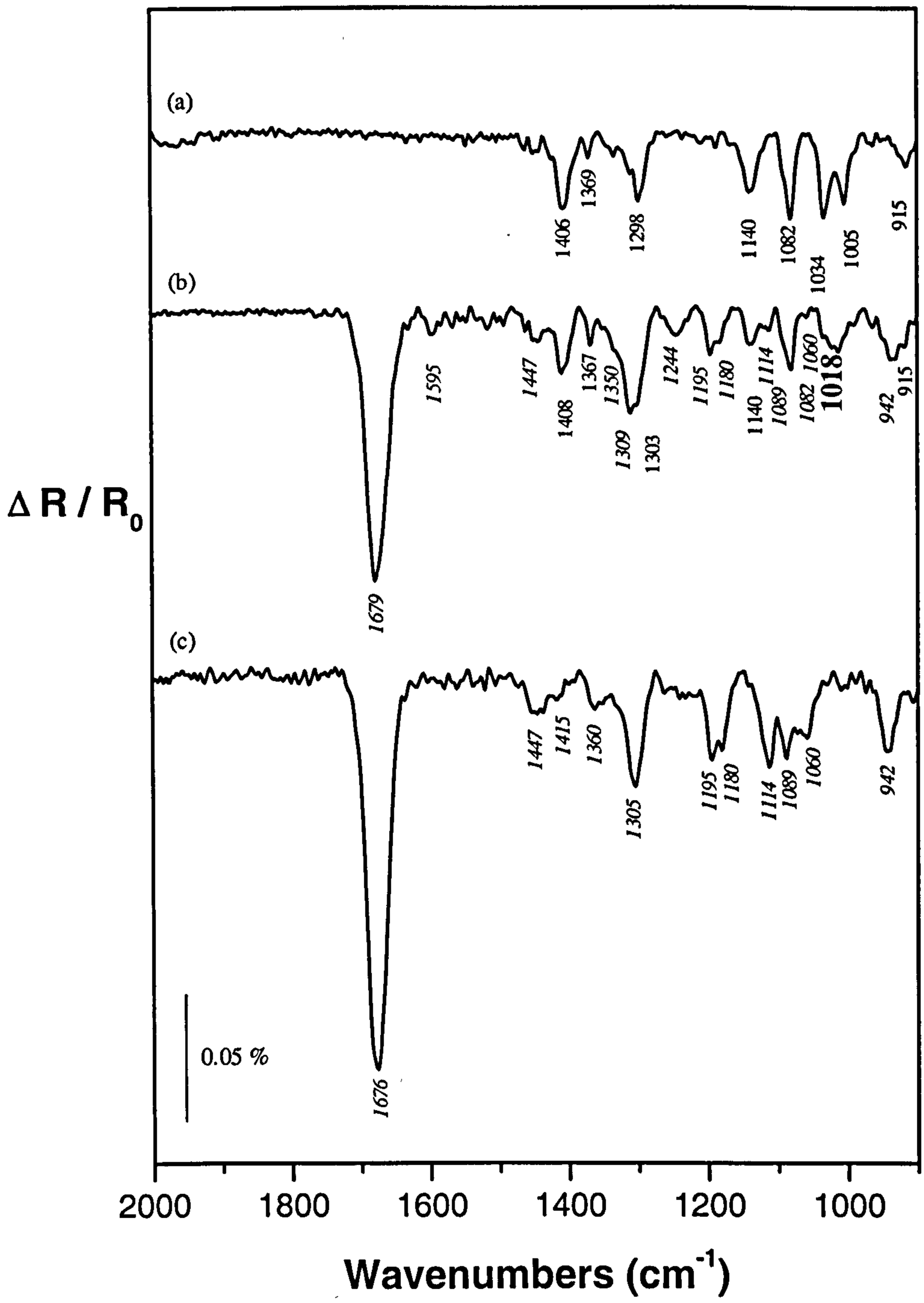

Figure 5.11: RAIR spectra corresponding to: (a) a low coverage of (S)-alanine on the Cu (110) surface; (b): the surface described in (a) with a dose of (R)-MHB; (c) a small coverage of (R)-MHB by itself on a Cu (110) surface, for comparison.

The main aim of the experiment was to be able to point out the signs of a possible interaction between the (S)-alanine and the (R)-MHB.

The comparison of the RAIRS peaks of the (R)-MHB in Figure 5.11 (c) and the RAIRS peaks of the (R)-MHB present in Figure 5.11 (b) show that the orientation of the (R)-MHB molecules does not undergo any change in the presence of the (S)-alanine on the surface. Indeed, from spectrum 5.11 (c) to spectrum 5.11 (b), the (R)-MHB peaks do not show any frequency shift. However, it is possible to notice some differences in the size of the (R)-MHB peaks but this has nothing to do with a possible interaction since the two spectra represent two different experiments in which the dosed quantity of (R)-MHB was not the same. The only difference between the two spectra are the appearance on the spectrum of co-adsorption, of two peaks which are at 1595 and 1244 cm^{-1}. As has been explained in Chapter Four, the MHB is being transformed into MAA when it is adsorbed on the Cu (110) and these two peaks show the beginning of the transformation of the (R)-MHB into MAA. On one hand, this phenomenon can not be related to the presence of the (S)-alanine in the surface since it has been observed when the (R)-MHB gets transformed into MAA when it is adsorbed by itself on the Cu (110) surface. However, on the other hand, it can be related to the presence of the (S)-alanine on the surface if the (S)-alanine perturbs the kinetics of the transformation of the (R)-MHB into MAA by its presence on the surface.

If now the (S)-alanine peaks are considered, it is expected that the only changes on the (S)-alanine peaks between spectra 5.11 (a) and 5.11 (b) are due to the addition of the (R)-MHB on the surface. Figure 5.11 (b) seems to show a superposition of the separate spectra of (S)-alanine by itself and (R)-MHB by itself, except a major transformation of the (S)-alanine peaks concerning the alanine bands at 1034 cm^{-1} and 1005 cm^{-1}. These bands have decreased in intensity and instead of presenting two bands, present one broad band which seems to have its frequency around 1018 cm^{-1} wavenumbers. Other slight changes are a shift or a deformation of one of the alanine bands at 1034 cm^{-1} and 1005 cm^{-1}. However, since no modification of the (R)-MHB bands can be defined, it is not possible to propose a model which would describe the interaction of the (R)-MHB molecule with the (S)-alanine molecule from the RAIR spectra.

From the RAIR spectra, the interaction between the molecules of (S)-alanine and (R)- or (S)-MHB does not seem to be intimate. It is proposed that (R)-MHB adsorb on the free space, the terraces, between the (S)-alanine molecules, maybe in islands.

In order to define more the "kind of interaction" between the (R)-MHB and the (S)-alanine or to see if this interaction is related to the chirality of one or the other molecule, the same experiment was conducted replacing the (R)-MHB with the (S)-MHB.

Figure 5.12 (b) presents the RAIR spectra obtained on the co-adsorption of the (S)-alanine with the (S)-MHB. For comparison, the spectra describing the adsorption of the (S)-alanine at low coverage by itself and the adsorption of the (S)-MHB by itself are also shown in the Figures 5.12 (a) and 5.12 (c) respectively. This spectrum 5.12 (b) confirms that a dose of (S)-MHB is able to co-adsorb with a low coverage phase of (S)-alanine on the Cu (110) surface.

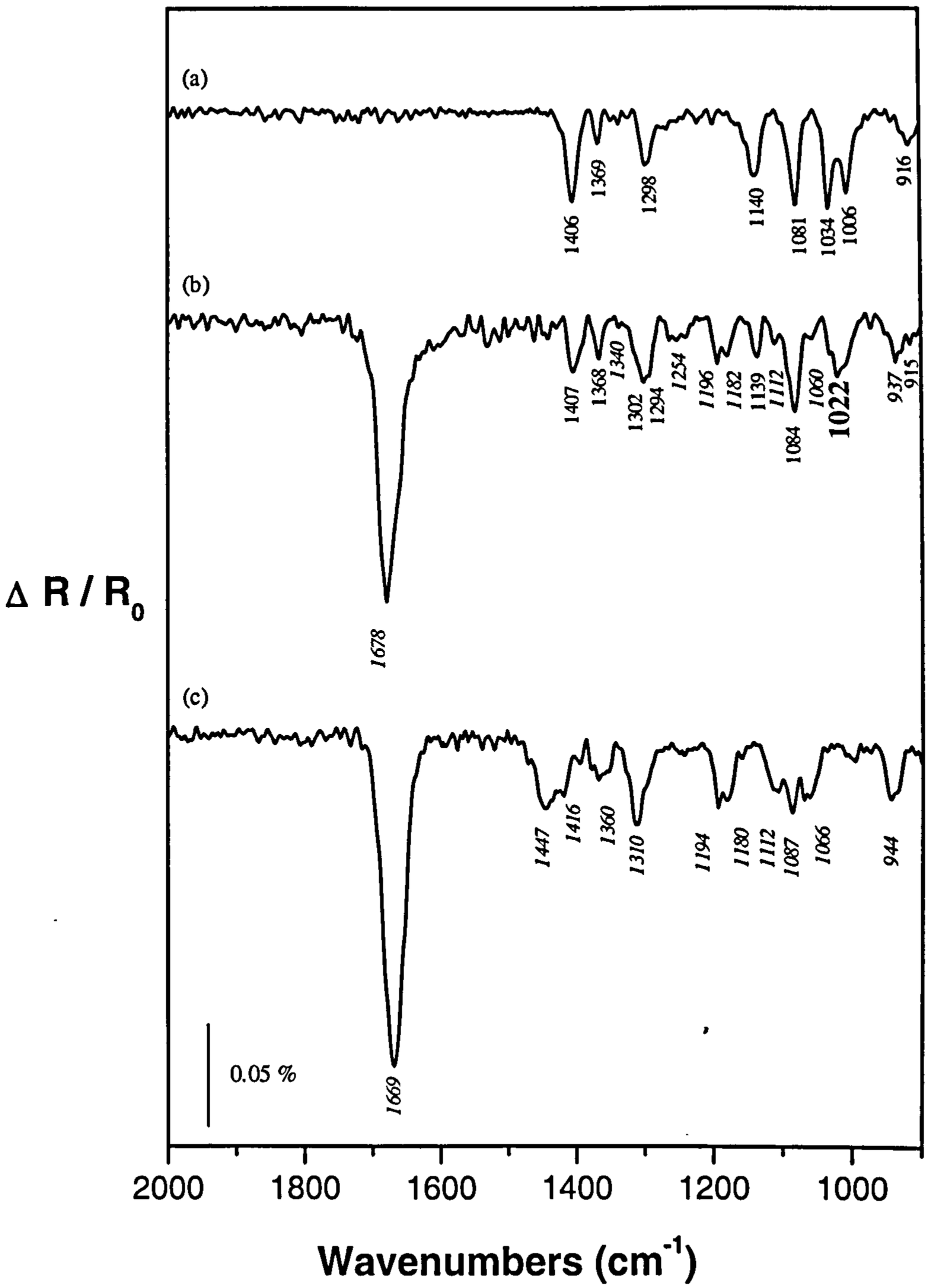

Figure 5.12: RAIR spectra corresponding to: (a) a low coverage of S-alanine on the Cu (110) surface; (b): the surface described in (a) with a dose of (S)-MHB; (c) a small coverage of (S)-MHB by itself on a Cu (110) surface, for comparison.

However, when comparing the infrared bands of (S)-MHB and those of (S)-MHB co-adsorbed with (S)-alanine, again no change can be observed, except the appearance of the band at 1254 cm^{-1} on co-adsorption, which is related to the transformation of the (S)-

MHB into MAA. When looking at the infrared bands of (S)-alanine, again the same changes in the spectrum of co-adsorption can be seen. The same two alanine bands at 1034 cm^{-1} and 1006 cm^{-1} are concerned. These two bands seem to melt into one single broad band whose frequency is at 1022 cm^{-1}.

The disappointing news here is that the same kind of modification of the infrared spectra can be observed for both the co-adsorption of (S)-alanine with (R)-MHB or with (S)-MHB. Thus the (S)-alanine molecules cannot discriminate the chirality of the enantiomers of the MHB.

5.3.2.2 RAIRS studies of the co-adsorption above 300 K

It has been shown in the last section that the co-adsorption of (S)-alanine with the (R)-MHB or the (S)-MHB does not allow the observation of any chiral discrimination between the two MHB enantiomers by RAIRS. However, on both spectra of co-adsorption, a new band has been seen around 1250 cm^{-1} which is an indication that the MHB begins to transform into MAA. The interest now is to investigate the behaviour of this "interaction" when the MHB is transformed into MAA.

The following RAIR spectra of co-adsorption of the (S)-alanine with the (R)-MHB shows the behaviour of the mixture when heated to different temperatures, Figure 5.13.
Spectrum (a) presents the infrared spectrum of the (S)-alanine by itself and spectrum (b) presents the infrared spectrum of the (S)-alanine co-adsorbed with the (R)-MHB at 300 K. Again here, a change in the two alanine bands at 1032 cm^{-1} and 1005 cm^{-1} can be noticed on co-adsorption. The mixture was then warmed and consequently the transformation of the (R)-MHB into MAA has been followed. By spectrum (e), when the mixture has been heated to 348 K, the infrared bands of the (R)-MHB have completely disappeared. As the temperature is increased, spectra (c), (d) and (e) show that the alanine bands around 1032 cm^{-1} and 1005 cm^{-1} change but are still deformed, even when the (R)-MHB has completely transformed into MAA.
The same behaviour has also been noticed when (R)-MHB is replaced by (S)-MHB, Figure 5.14. Again, the alanine bands at 1034 cm^{-1} and 1006 cm^{-1} are deformed when (S)-alanine is co-adsorbed with the (S)-MHB and remains so when heating the sample to transform the (S)-MHB into MAA.
The deformation of the two alanine bands are not only due to the presence of the (R)-MHB or the (S)-MHB on the surface, but are also due to the presence of the MAA on the surface. Thus it can be concluded again that the changes in the two bands have nothing to do with the chirality of the molecule co-adsorbed with (S)-alanine on the surface.

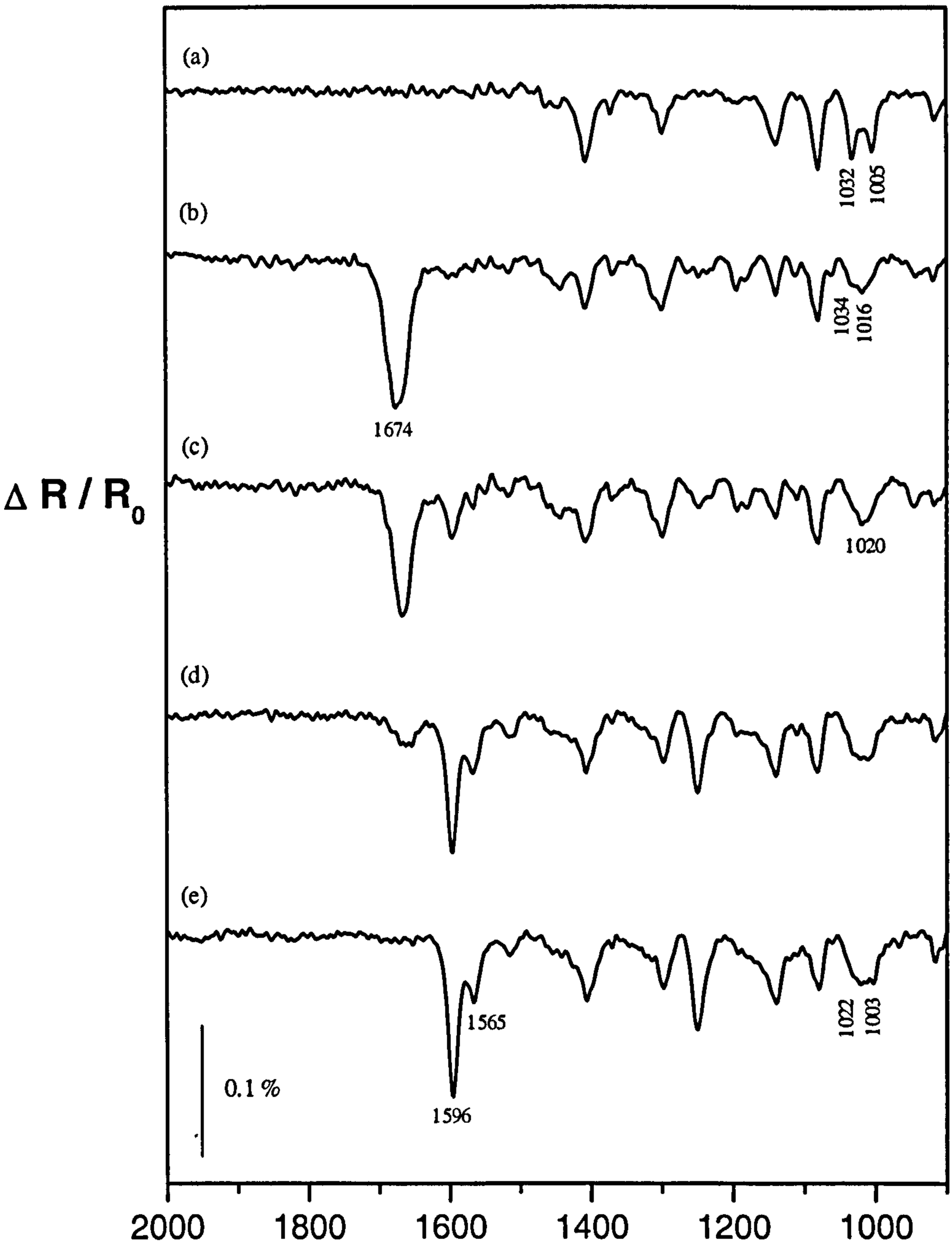

Figure 5.13: RAIR spectrum of: (a) low coverage of (S)-alanine; (b) low coverage of (S)-alanine co-adsorbed with 2 L of (R)-MHB at 300 K; (c) at 318 K; (d) 333 K; (e) 348 K.

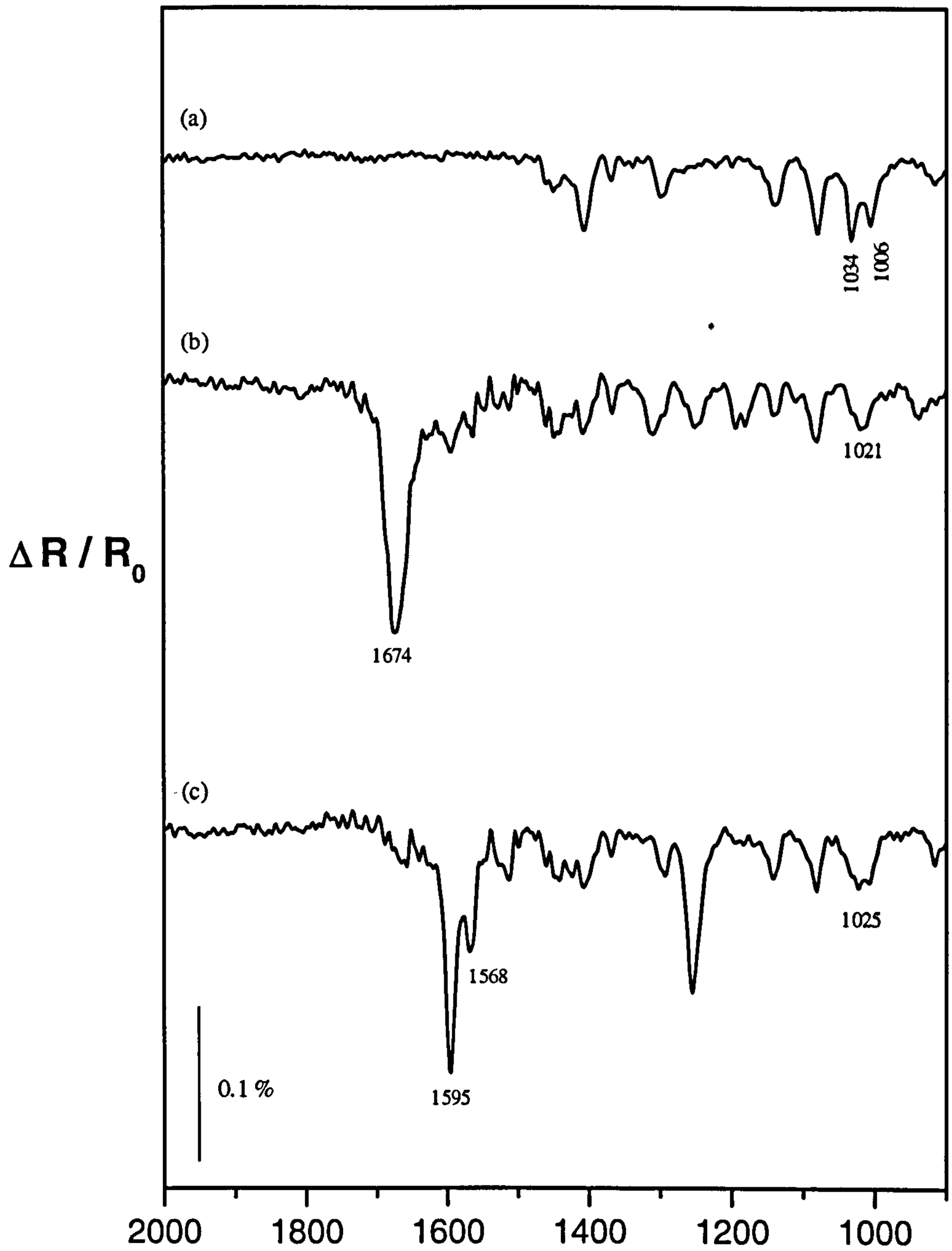

Figure 5.14: RAIR spectrum of: (a) low coverage of (S)-alanine; (b) low coverage of (S)-alanine co-adsorbed with 3 L of (S)-MHB at 300 K; (c) at 378 K.

5.3.3 Further co-adsorption studies for (R)- and (S)-MHB with (S)-alanine

RAIRS has shown that (R)- and (S)-MHB can co-adsorb with a low coverage of (S)-alanine on a Cu (110) surface and can possibly interact. However, the RAIR spectra for both co- adsorptions are the same and no chiral discrimination was evident.

Thus the next step consisted of checking if the interaction between the (R)- or (S)-MHB and (S)-alanine was strong enough to modify the temperature of desorption of the molecules and / or the temperature and the kinetics of the transformation of MHB into MAA. In order to do this, TPD and kinetics experiments were conducted. Figure 5.15 presents a summary of the aims of these further experiments as well as the results obtained by the initial RAIRS experiments (step I).

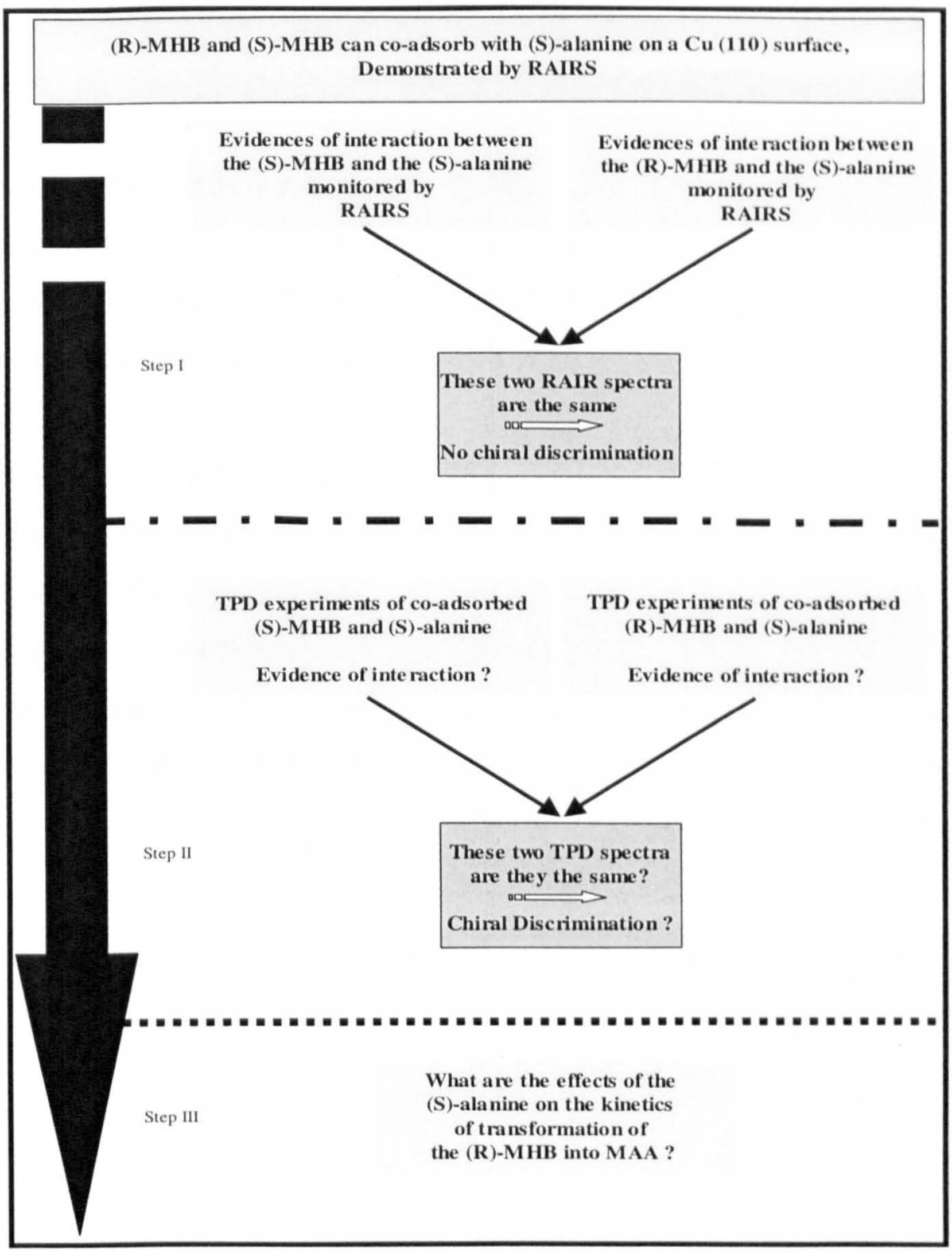

Figure 5.15: Summary showing the different experiments and the different techniques used.

5.3.3.1 TPD studies of the co-adsorption at 300K

The aim of these TPD experiments was to check if the enantiomers of MHB and the (S)-alanine desorb differently when they are co-adsorbed and if they dehydrogenate quicker in presence of (S)-alanine on the surface. It would be interesting to notice a difference in the temperature of dehydrogenation of the (R)-MHB and the (S)-MHB in presence of (S)-alanine.

Figure 5.16 shows the TPD spectra of the (R)-MHB and of the (S)-alanine alone, of the (R)-MHB and the (S)-alanine in co-adsorption and of the (S)-MHB and the (S)-alanine in co-adsorption on a Cu (110) surface.

These TPD plots can be considered in two parts. Between 300 and 425 K, the (R)- or (S)-MHB is transforming into MAA and hydrogen can be seen desorbing. Above 425 K, the resulting MAA is desorbing from the surface.

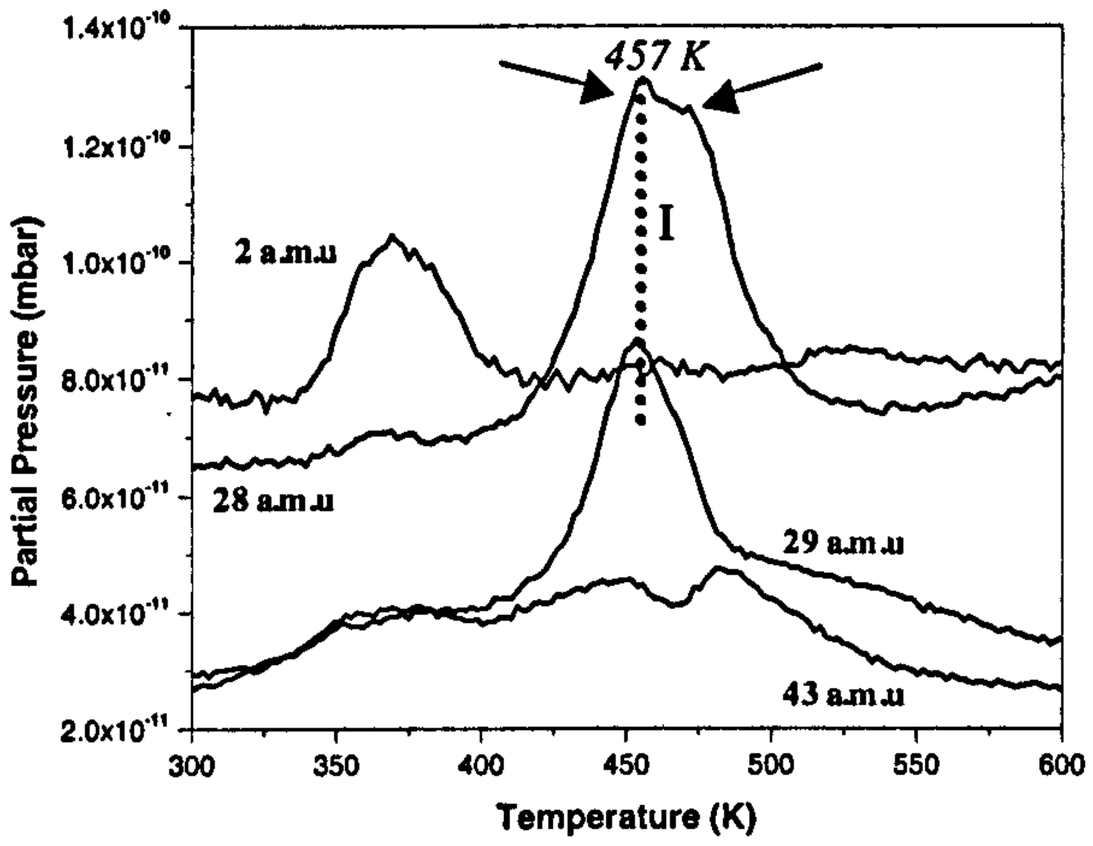

(a)

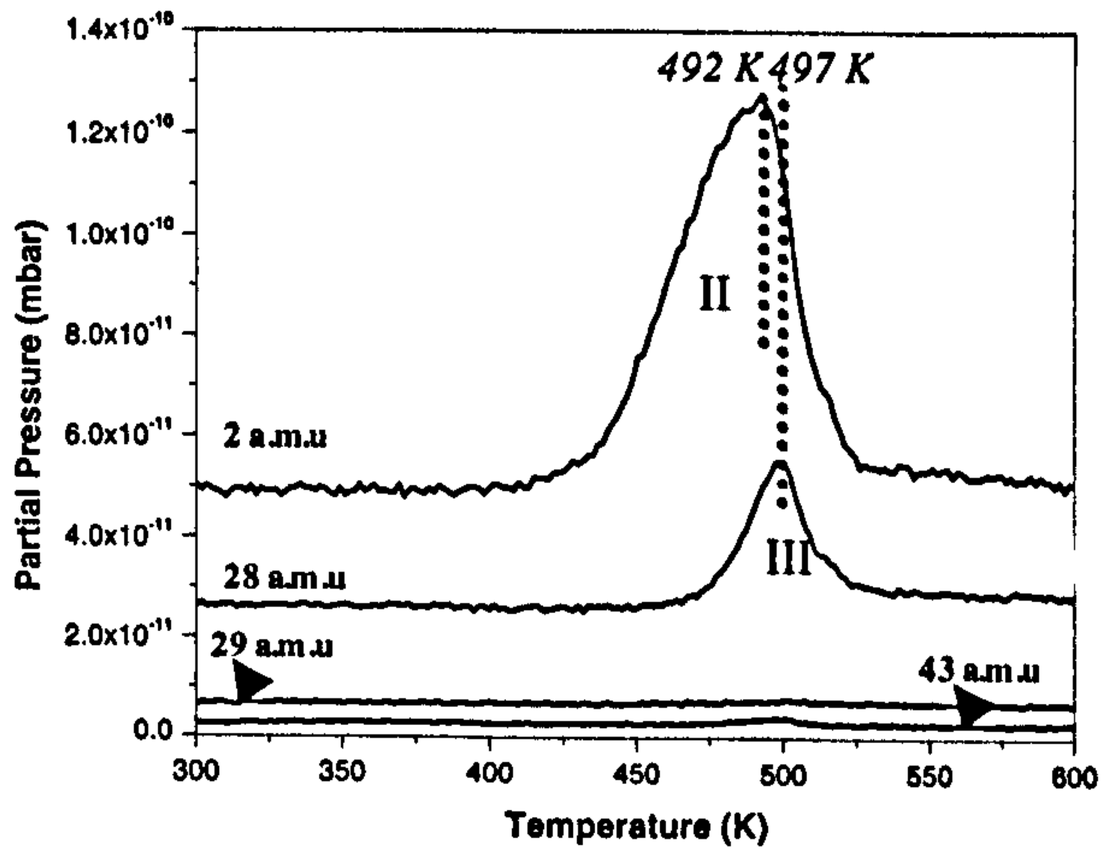

(b)

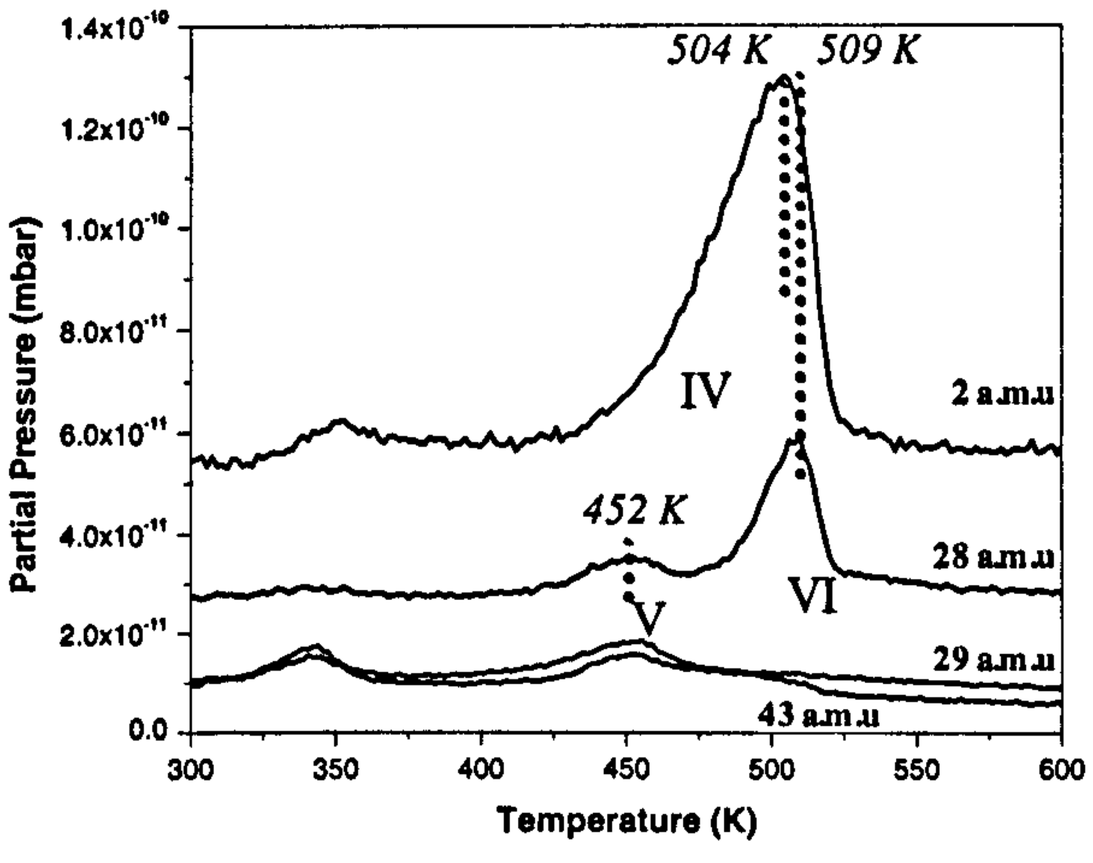

(c)

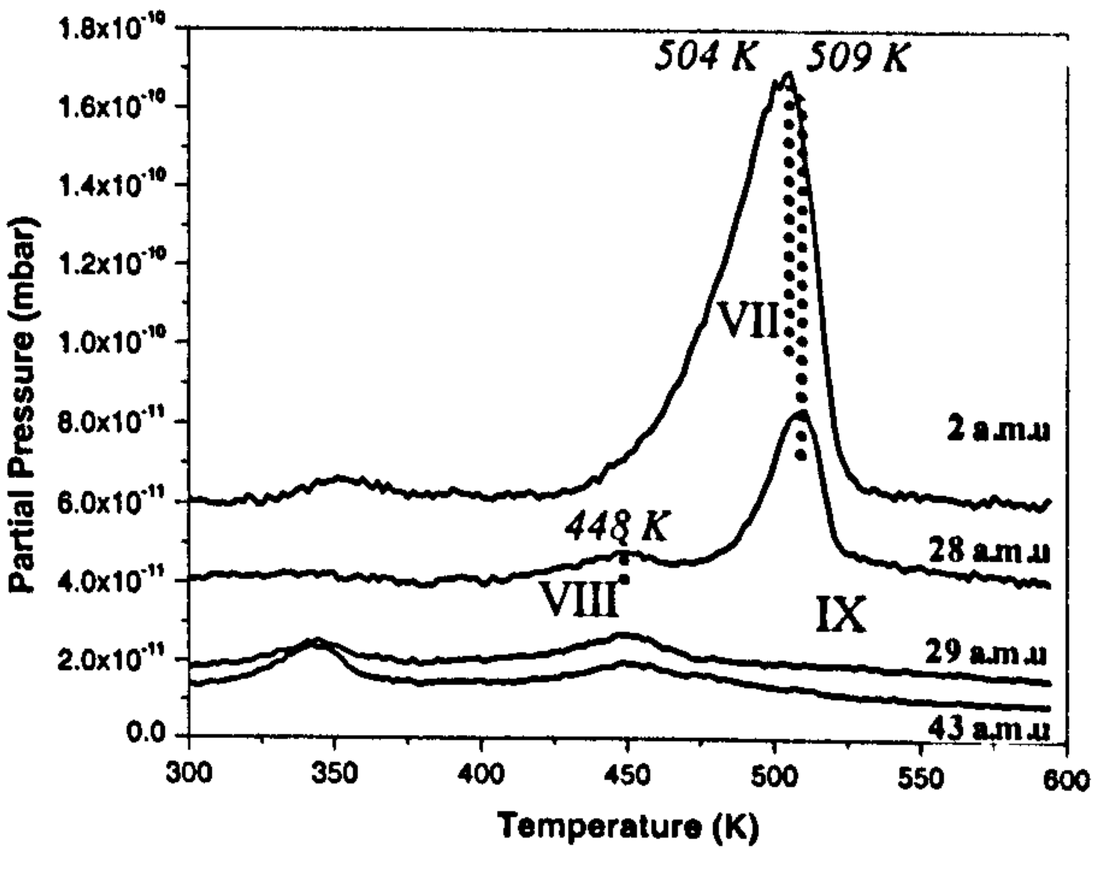

(d)

Figure 5.16: TPD of (a) 15 L of R-MHB; (b): low coverage of (S)-alanine; (c) 2 L of (R)-MHB co-adsorbed with a low coverage of (S)-alanine; (d) 2L of (S)-MHB co-adsorbed with a low coverage of (S)-alanine.

- ***Desorption of (R)-MHB or (S)-MHB and (S)-alanine in co-adsorption***

The region of interest from the TPD spectra, in this section, is the region between 425 K and 600 K which corresponds to the desorption of the (S)-alanine and the (R)-MHB or (S)-MHB which by this temperature has been transformed into MAA. As a consequence of this transformation, this temperature range is not expected to demonstrate any chiral discrimination between the co-adsorption of the (S)-alanine with the (R)-MHB or the (S)-MHB.

The TPD spectra of co-adsorption of the two enantiomers with (S)-alanine present exactly the same shape. Each of the TPD spectra of co-adsorption, spectra 5.16 (c) and (d), are the sum of the spectra of each of the species.
If the peaks of desorption representing m / z = 2 a.m.u. are considered, only one peak is present in both the spectra of (S)-alanine alone (peak II) and on co-adsorption with (R)- or (S)-MHB (peak IV and VII). If the peaks of desorption representing m / z = 28 a.m.u. are considered, only one peak is present in the spectra of both (S)-alanine (peak III) and (R)-MHB (dehydrogenated into MAA) (peak I) adsorbed alone. However, in the spectra of co-adsorption two peaks are present at m / z = 28 a.m.u., the lower temperature peak at a similar temperature to that for desorption of (R)-MHB alone (i.e. MAA) (peaks V and VIII) and the higher temperature peak similar to that for (S)-alanine alone (peaks VI and IX). So, these two peaks can be taken representative of MAA and (S)-alanine respectively. These peaks are summarised in Table 5.1.

	(R)-MHB	(S)-alanine	(R)-MHB + (S)-alanine	(S)-MHB + (S)-alanine
2 a.m.u.		492 (II)	504 (IV)	504 (VII)
28 a.m.u.	457 (I) [451 K for (S)-MHB]		452 (V)	448 (VIII)
		497 (III)	509 (VI)	509 (IX)

Table 5.1: Temperatures at which the desorption rate is maximum for m / z = 2 a.m.u. and m / z = 28 a.m.u. for (R)-MHB, (S)-alanine, (R)-MHB co-adsorbed with (S)-alanine and (S)-MHB co-adsorbed with (S)-alanine.

It can be observed that a m / z = 2 a.m.u., there is a difference in the temperature at which the desorption rate is a maximum of 12 K between (S)-alanine alone and co-adsorbed with (R)- or (S)-MHB. At m / z = 28 a.m.u., this difference on co-adsorption for the (S)-alanine peak is also 12 K. Compared to (R)-MHB (or MAA) alone, the difference for the MAA peak of the co-adsorbed species is 9 K maximum.

These differences in temperature may find their origin in at least three known or suspected facts. The first one is related to the laws of desorption kinetics; the second one can be related to the errors on the experiment; the last one could be related to the interaction between the alanine and the MAA on the Cu (110) surface.

When a species desorbs from a surface, it can obey some precise laws of kinetics [13-16]. Indeed, in some cases, the temperature at which the maximum rate occurs can decrease with the coverage increasing or in some others this temperature can increase with the coverage increasing. The relationship between the coverage of the species desorbing from the surface and their temperature of desorption should be checked in our case, since the comparison is done between 15 L of (R)-MHB adsorbed by itself and 2 L of (R)-MHB and (S)-MHB each adsorbed with a low coverage of (S)-alanine. However, in addition two points makes the system more complex.

On one hand, care should be taken when choosing the peak whose area is taken into account. Indeed, alanine and MAA are complex molecules; their desorption is monitored

by measuring the fragments of species such as CO (28 a.m.u.), H_2CN (28 a.m.u.), COH (29 a.m.u.), CO_2 (44 a.m.u.) and CH_3CO (43 a.m.u.). These different fragments can themselves break into further fragments which could then increase the desorption rate of another fragment. For example, if the desorption spectrum of (R)-MHB by itself is considered, the peak representing m / z = 28 a.m.u. is broad and presents two peaks shown by the arrows in Figure 5.16 (a). The first peak might be the desorption of the fragment CO (m / z = 28 a.m.u.), while the second peak might be the fragmentation of the XH group (m / z = 29 a.m.u.) into two other fragments CO (m / z = 28 a.m.u.) and H (m / z = 1 a.m.u.). This last fragment (H) would then recombine into H_2 (m / z = 2 a.m.u.) to increase the peak of 2 a.m.u.. The nature of the XH group is ambiguous; it might be due to the addition of a hydrogen to the CO group, after this has already desorbed from the surface.

In addition, it is believed that alanine dissociates into fragments on the Cu (110) substrate as it "explodes" off [11]. Indeed, the shape of the m / z = 2 a.m.u. presents a "tail" in front of the peak in spectrum 5.16 (b) i.e. the hydrogen H_2 species do not all start desorbing at the same temperature. This means that the TPD spectra of alanine do not give the temperature of desorption of the alanine from the surface, but give the temperature of desorption of the fragments of alanine. In contrast, the MAA (from the transformation of the MHB) show a different type of TPD curves. The curves m / z = 28 a.m.u and m / z = 29 a.m.u present the same shape, and the two species start to desorb at the same temperature, meaning that the MAA is desorbing as a whole body.

Being aware of these two points, the most plausible comparison for the TPD spectra concerns the peak at the lowest temperature on the MAA peaks representing m / z = 28 a.m.u. when the MAA is by itself on the surface and when it is co-adsorbed with (S)-alanine, i.e. the peak around 457 K. These TPD curves are presented in Figure 5.17.

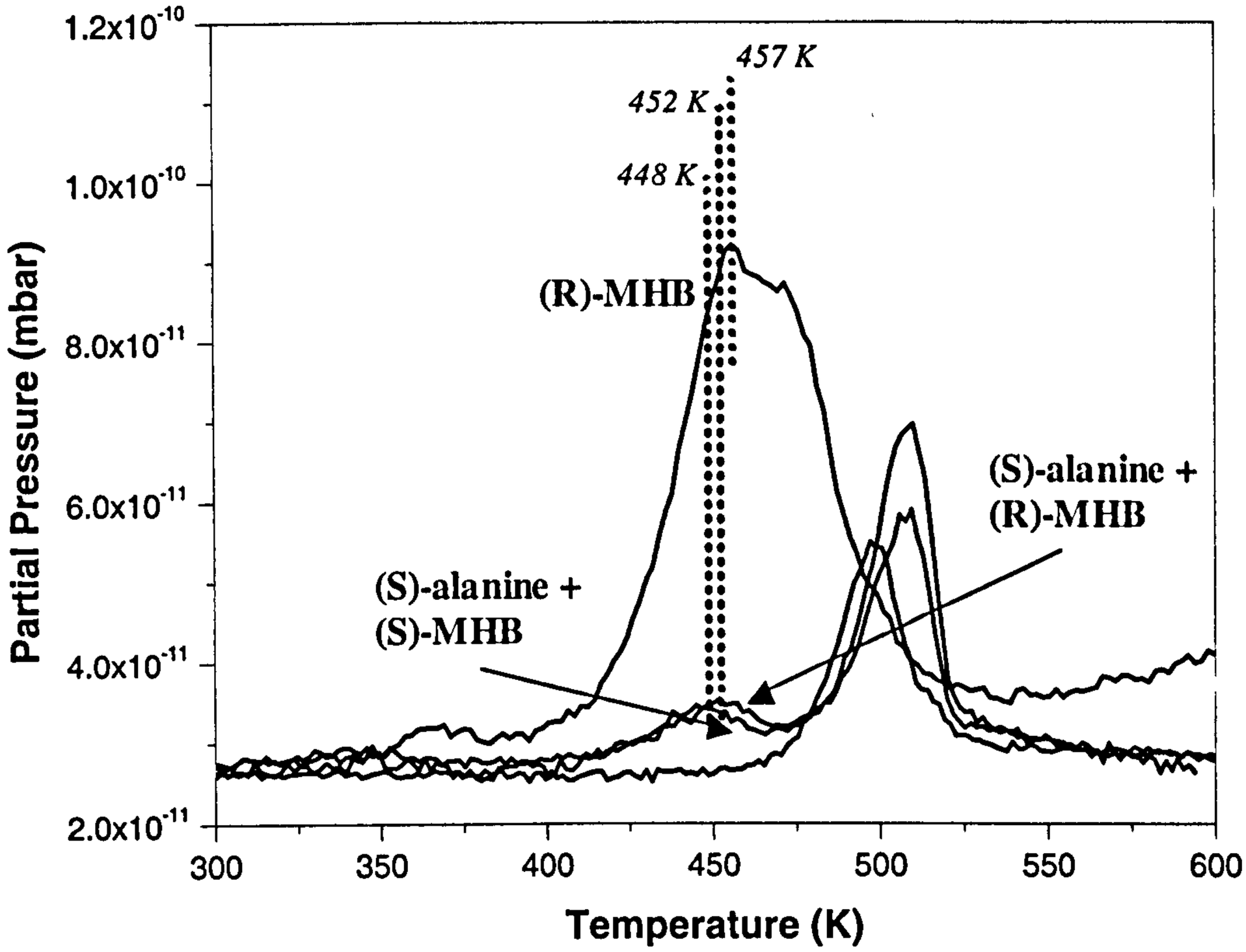

Figure 5.17: Comparison of the TPD curves obtained for 15 L of (R)-MHB; 2 L of (R)-MHB co-adsorbed with a low coverage of (L)-alanine and 2L of (S)-MHB co-adsorbed with a low coverage of (L)-alanine for m / z =2 a.m.u. between 400 K and 475 K.

From Figure 5.17, the temperatures at which the rate of desorption is maximum are 452 K and 448 K for 2 L of (R)-MHB and 2 L of (S)-MHB respectively when they are co-adsorbed with (S)-alanine and 457 K for 15 L of (R)-MHB transformed into MAA by itself. The coverage does not seem to affect the temperature of desorption. However, the differences in temperatures are within the level of expected experimental error in TPD measurements (see Chapter Three) so cannot be classed as significant.

- ***Desorption of hydrogen coming from the transformation of (R)-MHB or (S)-MHB into MAA when co-adsorbed with (S)-alanine***

The region of interest from the TPD spectra, in this section, is the region between 300 K and 425 K which refers to the dehydrogenation of the (R)-MHB or (S)-MHB into MAA. The aim of this section is to see if the presence of (S)-alanine on the surface has an effect on the temperature of desorption of hydrogen coming from the MHB.

The transformation of the enantiomers of MHB into MAA can be easily noticed on a TPD spectrum because of the presence of a peak around 350K on the m / z = 2 a.m.u. plot. Figure 5.18 shows the TPD spectrum of m / z = 2 a.m.u for 15 L of (R)-MHB on the Cu (110) surface, the TPD spectrum for 10 L of (S)-MHB, the TPD spectrum of 2 L of (R)-MHB co-adsorbed with a low coverage of (S)-alanine on the Cu (110) surface and the TPD spectrum of 2 L of (S)-MHB co-adsorbed with a low coverage of (S)-alanine on the same surface.

The TPD spectra presented in Figure 5.18 present a difference in the temperature of dehydrogenation of the enantiomers of MHB when they are by themselves on the surface and when they are co-adsorbed with (S)-alanine. This difference is 13 K minimum and can be as high as 17 K. The expected experimental error is not sufficient to explain this difference. An important point to keep in mind here is that the hydrogen H_2 is assumed to desorb from the MHB and not from the surface. However, this would not be the case if hydrogen coming from the molecule adsorbs on the Cu (110) surface. A dose of 100 L of hydrogen has been seen to adsorb on a Cu (110) surface at 130 K and desorb from this surface around 330 K [17]. The sticking coefficient of hydrogen on Cu (110) is smaller than 0.1. This value is very small compared, for example, to the sticking coefficient of hydrogen on Ni (110) which is 0.4 at 300 K [18]. Thus, it is unlikely that hydrogen produced by the dehydrogenation of MHB would stick on the Cu (110) surface and appear on the TPD spectrum in Figure 5.18. However, this has not been definitely confirmed to be the case.

It is not reasonable to answer the question of a potential interaction between the MHB enantiomers and the (S)-alanine which would facilitate or slow down the dehydrogenation of MHB at this point; some other experiments should be conducted, and some evidences to draw a such conclusion are missing. Figure 5.18 shows that, if (S)-alanine influences the temperature of dehydrogenation of both enantiomers of MHB, it does not discriminate between the enantiomers, unless this discrimination is supported by a difference of temperatures which is too small to be seen on this TPD experiment.

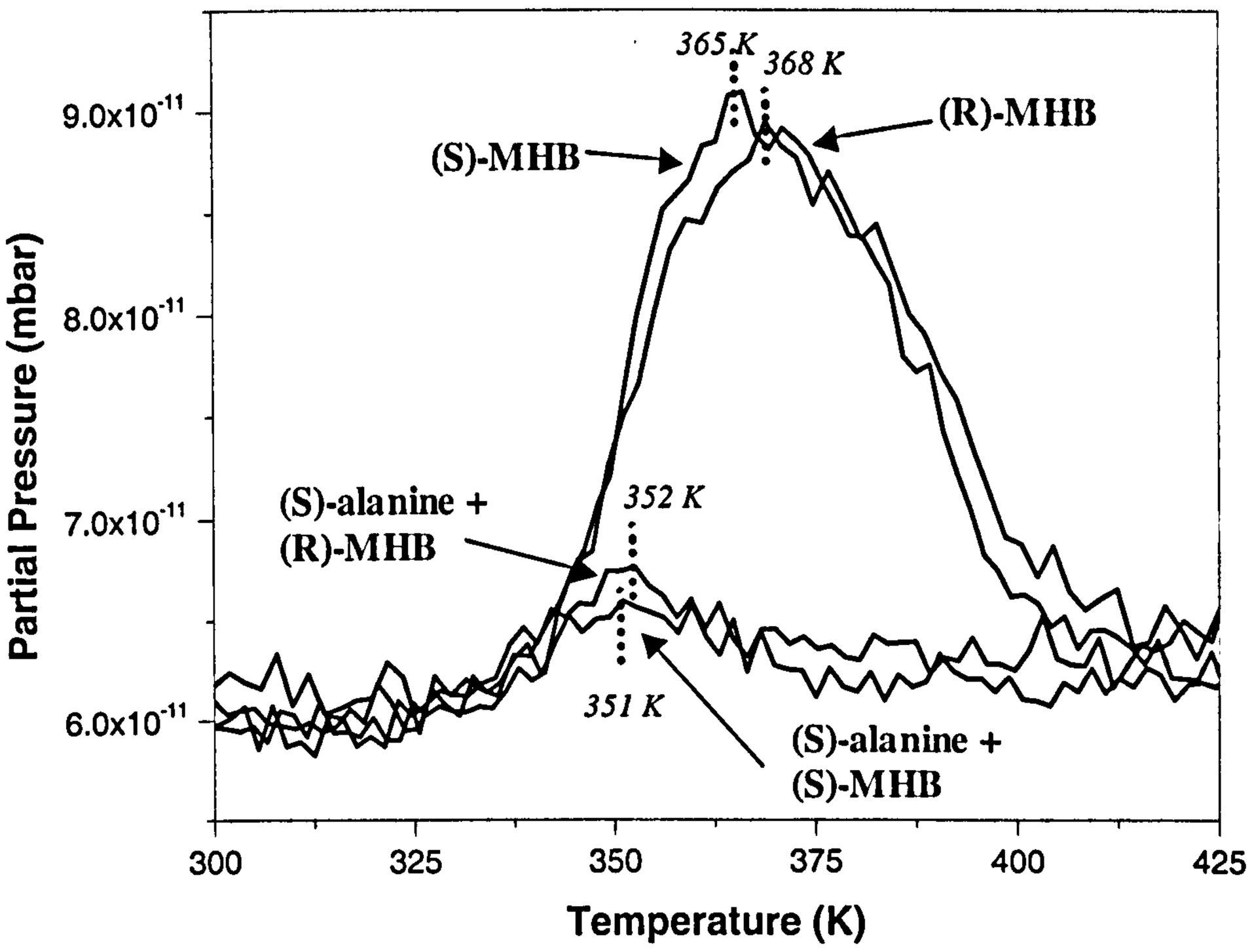

Figure 5.18: Comparison of the TPD curves obtained for 15 L of (R)-MHB; 2 L of (R)-MHB co-adsorbed with a low coverage of (S)-alanine and 2L of (S)-MHB co-adsorbed with a low coverage of (L)-alanine for m / z =2 a.m.u. between 300 K and 425 K, region corresponding to the desorption of the hydrogen resulting from the transformation of MHB into MAA.

5.3.3.2 Kinetics studies

The aim of the work described in this section was to investigate if the kind of "interaction" demonstrated was strong enough to modify the kinetics of the dehydrogenation of (R)-MHB when (S)-alanine was present on the Cu (110) surface.

- ***Calculations of the kinetics of (R)-MHB co-adsorbed with (S)-alanine***

This experiment was conducted in exactly the same way that the kinetics of (R)- and (S)-MHB transforming into MAA without (S)-alanine were conducted. The sample was kept at the desired temperature. A low coverage of (S)-alanine was deposited on the Cu (110) crystal. This was monitored and checked using RAIRS. As has been mentioned earlier in this chapter, the alanine coverage had to be small enough to allow the co-adsorption of the (R)-MHB onto the surface. Then a dose of 3 L of (R)-MHB was vaporised into the chamber. This was the same dose used for the (R)-MHB and (S)-MHB kinetics, but it was noticed that the effective amount of adsorbed (R)-MHB onto this alanine modified surface was smaller that the amount of adsorbed (R)-MHB on the clean Cu (110) surface. Again, the change in the area of the band at 1674 cm^{-1} representative of the dehydrogenation reaction was measured over time.

The RAIR spectra are presented in Figure 5.19 and the decrease of the area of the 1674 cm^{-1} over time is presented in Figure 5.20.

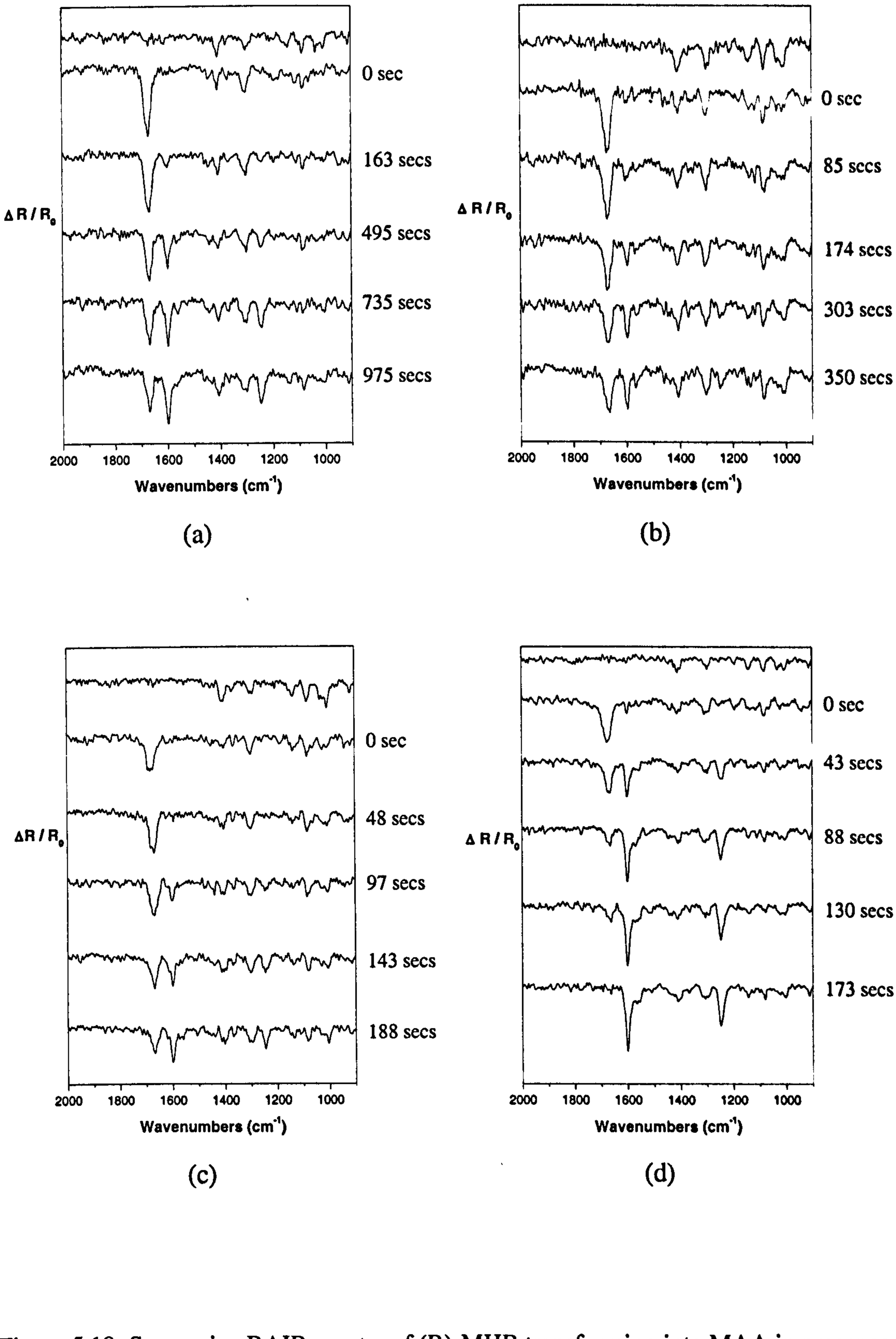

Figure 5.19: Successive RAIR spectra of (R)-MHB transforming into MAA in presence of (S)-alanine at temperature of: (a) 308 K, (b) 313 K, (c) 323 K and (d) 333 K.

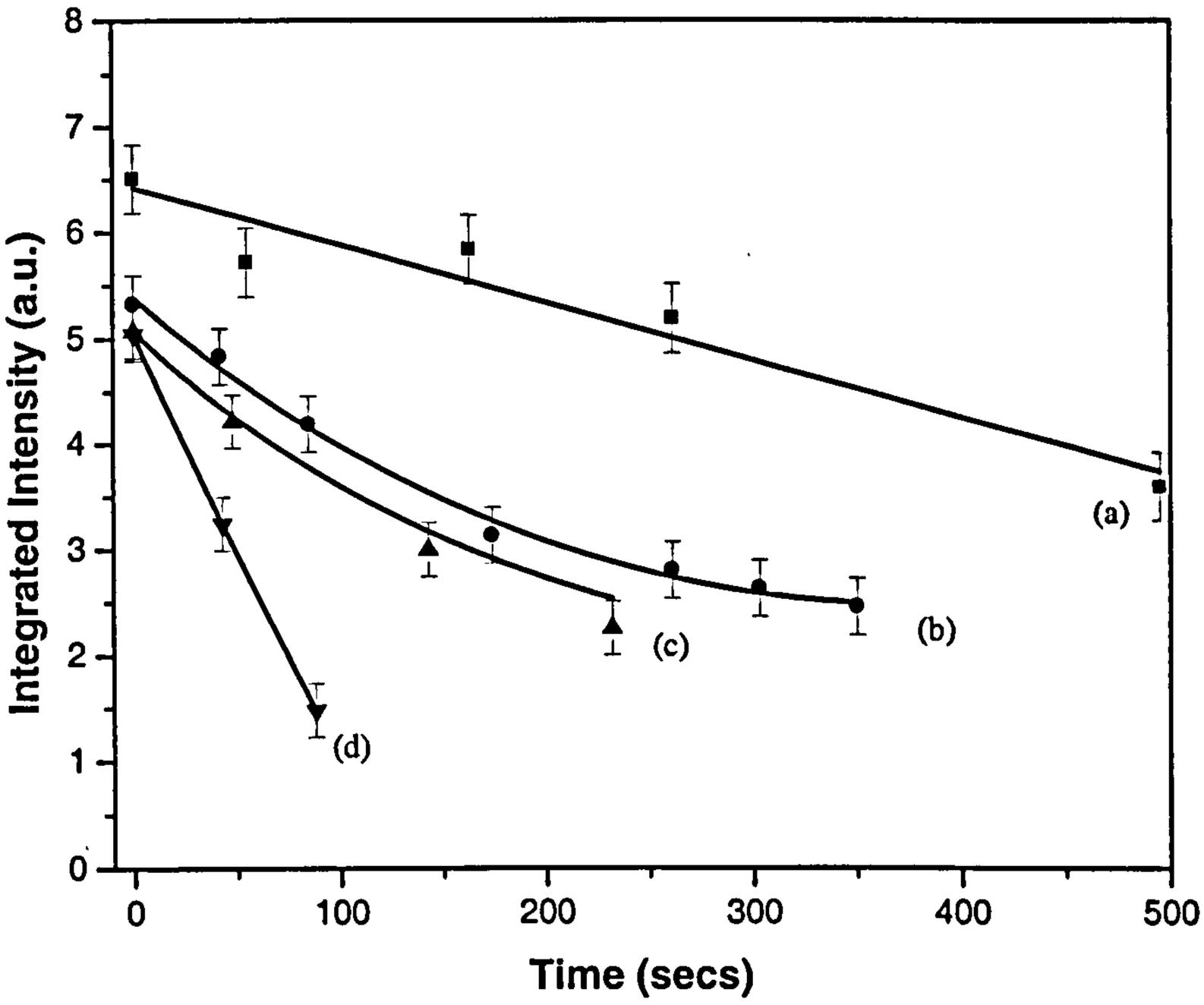

Figure 5.20: Decrease of the integrated intensity of the 1674 cm^{-1} band of (R)-MHB in co-adsorption with (S)-alanine plotted as a function of time for the following temperatures: (a) 308 K, (b) 313 K, (c) 323 K and (d) 333 K.

From the plots in Figure 5.20, it can be noticed that at 333 K, in 100 secs, 75 % of the (R)-MHB has been converted; at 323 K, in the same time 30 % has been converted; at 313 K, 25 % has been converted and at 308 K, 10 % has been converted.

The rate constant k has also been calculated for the disappearance of the (R)-MHB on the (S)-alanine modified Cu (110) surface for each temperature. The values of $\frac{a_0 - a}{a_0 \times a}$ have been plotted over t, in order to get the values of k.

The graphs representing the linear function $\frac{a_0 - a}{a_0 \times a} = f(t)$ for each temperature are presented in Figure 5.21.

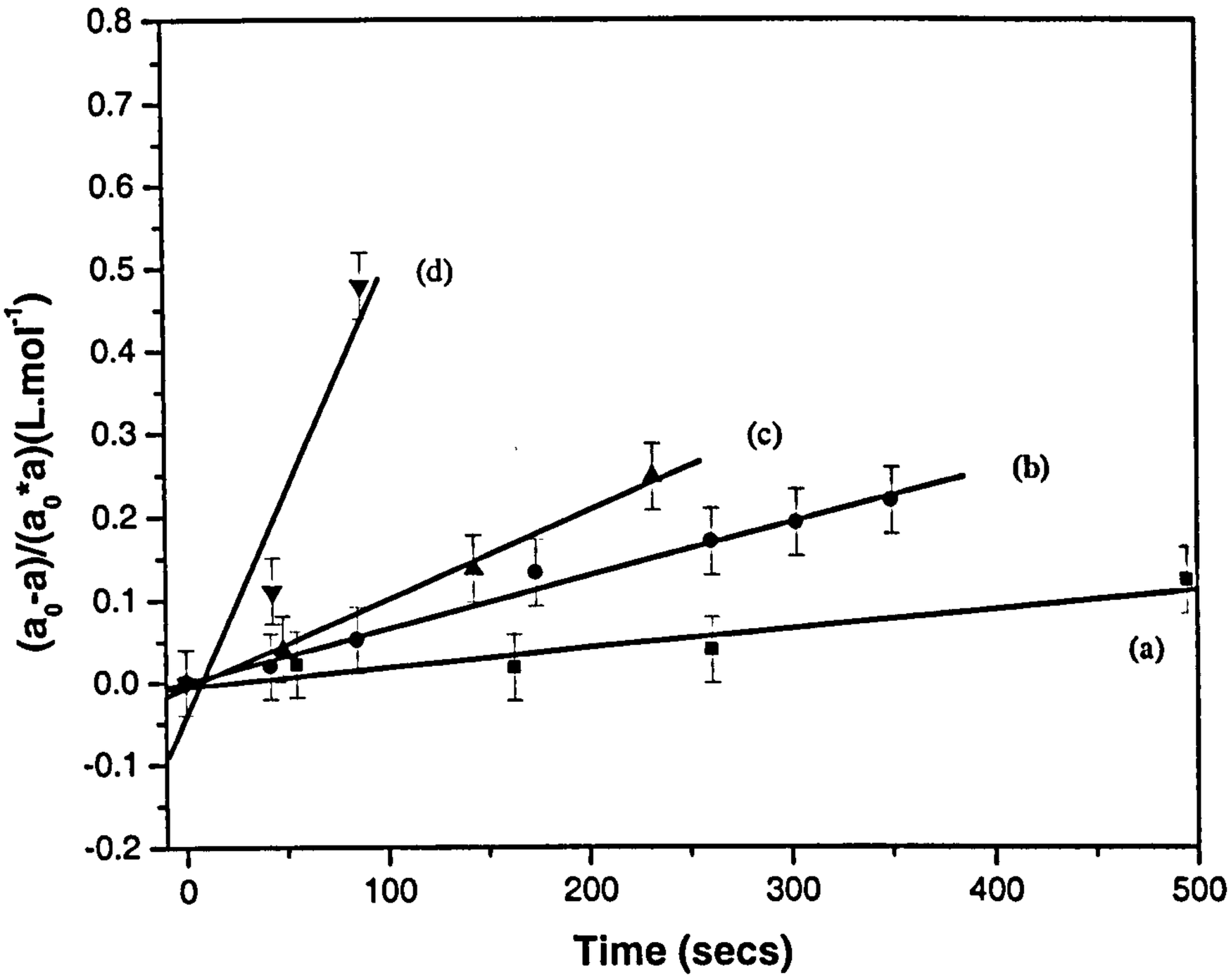

Figure 5.21: Values of $\frac{a_0 - a}{a_0 \times a}$ plotted as a function of time for the following temperatures: (a) 308 K, (b) 313 K, (c) 323 K and (d) 333 K.

The gradient of each line in the plots presented in Figure 5.21 gives the value of k. From these values of k, the values designed to plot the Arrhenius equation were calculated. All these values are presented in Table 5.2.

Temperature T (K)	308	313	323	333
1 / T (K^{-1})	0.00325	0.00319	0.0031	0.003
Rate constant k (s^{-1}) for (R)-MHB on Cu (110) modified with (S)-alanine	0.00023 (± 0.00004)	0.00064 (± 0.00003)	0.00107 (± 0.00005)	0.005 (± 0.001)
ln k	-8.37 (± 0.05)	-7.35 (± 0.04)	-6.84 (± 0.04)	-5.3 (± 0.2)

Table 5.2: Rate constant k for evolution of (R)-MHB co-adsorbed with (S)-alanine on Cu (110) at four temperatures obtained from the plot of the linear function $\frac{a_0 - a}{a_0 \times a} = f(t)$ and values necessary to plot the Arrhenius equation: 1 / T and ln k for each temperature.

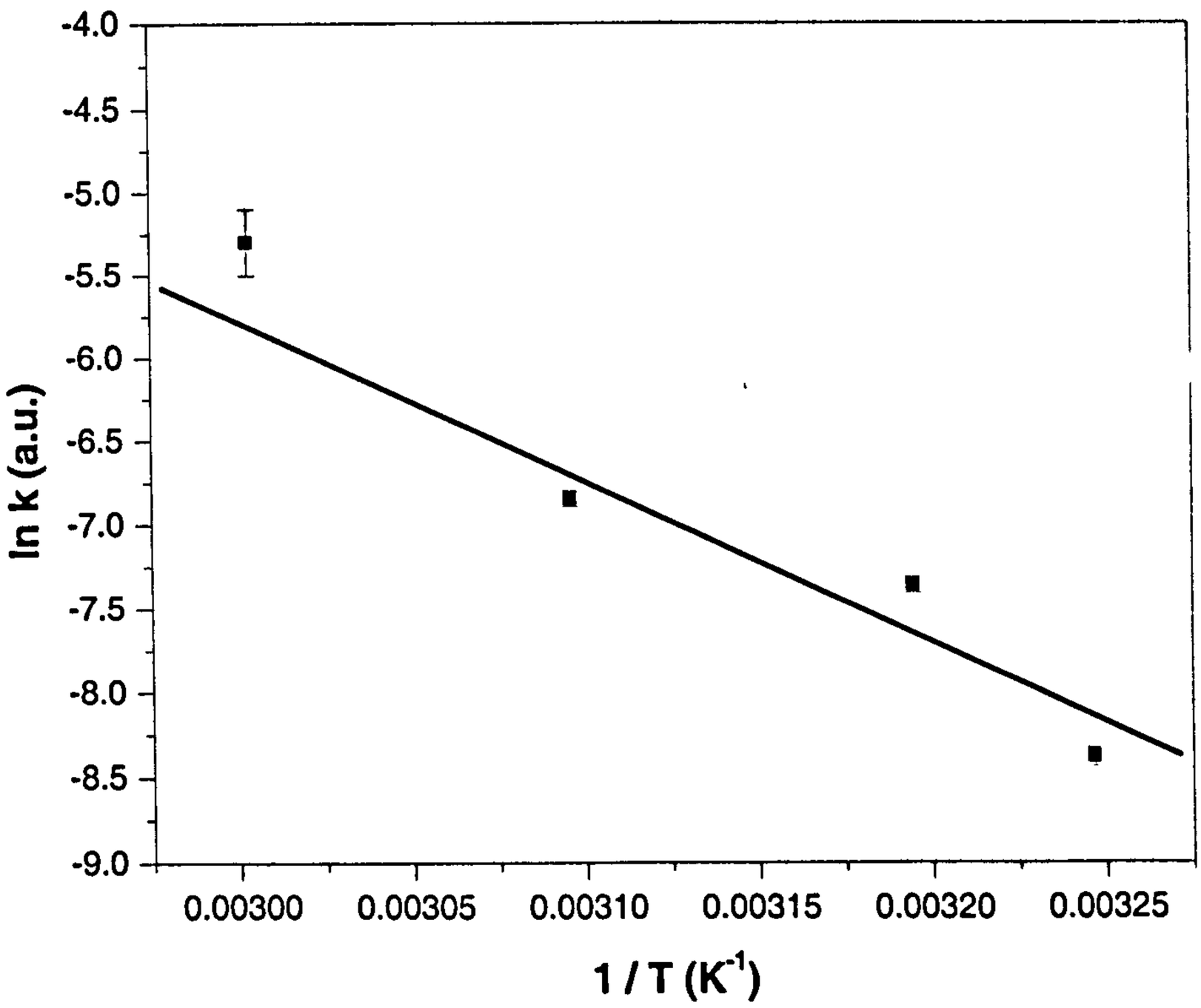

Figure 5.22: Linear of best fit to the Arrhenius equation ($\ln k = - E_a / RT + \ln A$) obtained from the kinetic data of the vanishing of (R)-MHB on Cu (110) modified with (S)-alanine.

Figure 5.22 shows the linear of the Arrhenius equation ($\ln k = - E_a / RT + \ln A$) obtained from the kinetic data. From this, the activation energy E_a has a value of 96 ± 15 kJ. mol^{-1}.

- ***Comparison between the kinetics of the enantiomers of MIIB absorbed on clean Cu (110) and the kinetics of (R)-MHB adsorbed on a Cu (110) surface modified with a low coverage of (S)-alanine***

In the reaction of hydrogenation of MAA into MHB, the (S)-alanine is the modifier of the catalyst, the catalyst being the metal [19, 20]. But, it has also been demonstrated that alanine can be responsible for the increase of the rate of hydrogenation of MAA into MHB at the time of experiments conducted in liquid [20]. Can alanine, which can have an effect on the hydrogenation of MAA, have an effect on the dehydrogenation of MHB when co-adsorbed with (R)-MHB or (S)-MHB on a Cu (110) surface in UHV?
The answer to this question implies the comparison of the kinetics of transformation of the enantiomers of MHB into MAA when (R)-MHB is co-adsorbed with or without (S)-alanine on the Cu (110) surface.
Table 5.3 presents the rate constant of the reaction for four temperatures.

Temperature T (K)	308	313	323	333
Rate constant k (s^{-1}) for (S)-MHB on clean Cu (110)	0.00020 (± 0.00002)	0.00050 (± 0.00005)	0.0018 (± 0.0002)	0.0031 (± 0.0012)
Rate constant k (s^{-1}) for (R)-MHB on clean Cu (110)	0.00023 (± 0.00001)	0.00058 (± 0.00004)	0.0030 (± 0.0007)	0.0040 (± 0.0007)
Rate constant k (s^{-1}) for (R)-MHB on Cu (110) modified with (S)-alanine	0.00023 (± 0.00004)	0.00064 (± 0.00003)	0.00107 (± 0.00005)	0.005 (± 0.001)

Table 5.3: Rate constant k for evolution of (R)- and (S)-MHB on clean Cu (110) and of (R)-MHB on (S)-alanine modified Cu (110) surface at four temperatures.

The rate constant of a reaction is defined as the decrease in concentration of one of the reactants or the increase of the product(s) per unit time [21, 22]. The higher is the rate, the faster or easier is the reaction.

In Table 5.3, the values of k for the temperature of 308 K, 313 K and 333 K can be said to be essentially the same for the dehydrogenation of both enantiomers of MHB over a clean Cu (110) surface. For the temperature of 308, 313 K, the values of k when the alanine is on the surface is comparable to the values of one or the other enantiomer. These values differ slightly for the temperature of 323 and 333 K, but the difference is not significant.

It was previously shown that the activation energies were 100 ± 20 kJ. mol^{-1} and 94 ± 17 $kJ.mol^{-1}$ for the dehydrogenation of (R)- and (S)-MHB respectively, on a clean Cu (110) surface. When the (S)-alanine is co-adsorbed with(R)-MHB, the activation energy of the reaction takes the value of 96 ± 15 kJ. mol^{-1}. However, this difference is still within the error bars of the experiment for the (R)- and (S)-MHB.

It can be concluded that the presence of the alanine on the surface does not change anything on the kinetics of dehydrogenation of MHB on the surface.

5.4 Summary

Attempts to co-adsorb (R)-MHB into the enantiomeric catalytic channels formed by the adsorption of the chiral phase (S)-alanine on Cu (110) have not been successful due to the size of the MHB molecule being larger than the size of the channels.

However, when the Cu (110) surface was modified with a smaller quantity of (S)-alanine, co-adsorption of (R)- or (S)-MHB has been possible and could be monitored by RAIRS. This technique has also shown limited evidence of an interaction between (S)-alanine and (R)- or (S)-MHB with some infrared bands due to the (S)-alanine being deformed. Since no modification of the (R)-MHB bands nor of most of the bands of (S)-alanine could be defined, it was not possible to propose any model to describe the interaction of the (R)- or the (S)-MHB molecule with the (S)-alanine molecule. The interaction between the molecules of (S)-alanine and (R)- or (S)-MHB molecules does not seem to be intimate. The deformation of the (S)-alanine bands that was observed did not depend on the chirality of the MHB since the same deformation was seen in the presence of either (R)-MHB, (S)-MHB or MAA.

TPD experiments were carried out in order to see if there was a difference in the desorption of the enantiomers of MHB in the presence of (S)-alanine. It was suspected that the (S)-alanine may be able to change the temperature of dehydrogenation of the MHB into MAA, and even to differentiate the (R)-MHB from the (S)-MHB on transformation into MAA. However, it was not possible to draw any such conclusions from these TPD experiments, partly due to the complexity of the process of desorption of the molecules from the surface, and also because of the difficulties in conducting such experiments which led to relatively large experimental errors.

The kinetics of transformation of (R)-MHB into MAA in the presence of (S)-alanine have been calculated and the activation energy of this reaction has the value of 96 ± 15 kJ. mol^{-1}. Without (S)-alanine the activation energy has been shown, in the previous chapter to be 100 ± 20 kJ. mol^{-1}. Thus the activation energy of the reaction of dehydrogenation of the MHB is not influenced in the presence of (S)-alanine.

It would be interesting to consider the organisation of the MHB molecules when they are co-adsorbed with (S)-alanine and to compare this with the situation when they are alone on the surface.

References

[1] C. F. McFadden, P.S. Cremer, A. J. Gellman, Langmuir **12,** 2483 (1996).

[2] A. Ahmadi, G. Attard, J. Feliu, A. Rodes, Langmuir **15,** 2420 (1999).

[3] G. A. Attard, A. Ahmadi, J. Feliu, A. Rodes, E. Herrero, S. Blais, G. Jerkiewicz, J. Phys. Chem. B **103,** 1381 (1999).

[4] G. A. Attard, J. Phys. Chem. B **105,** 3158 (2001).

[5] D. S. Sholl, Langmuir **14,** 862 (1998).

[6] D. S. Sholl, A. Asthagiri, T. D. Power, J. Phys. Chem. B **105,** 4771 (2001).

[7] J. D. Horvath, A. J. Gellman, J. Am. Chem. Soc. **123,** 7953 (2001).

[8] A. J. Gellman, J. D. Horvath, M. T. Buelow, J. Mol. Cat. A **167,** 3 (2001).

[9] J. D. Horvath, A. J. Gellman, J. Am. Chem. Soc. **124,** 2384 (2002).

[10] S. Louafi, PhD Thesis, Creating model enantio-differentiating surfaces: alanine enantiomers and methylacetoacetate adsorptions studies on Cu(110), (Liverpool University, 2001).

[11] J .Williams, PhD Thesis, Adsorption and characterisation of chiral amino acids on Cu (110) single crystal surfaces, (Liverpool University, 1988).

[12] J. Williams, S. Haq, R. Raval, Surface Science, 368 (1996) 303.

[13] P. A. Redhead, Vacuum **12,** 203 (1962).

[14] D. A. King, Surf. Sci. **47,** 384 (1975).

[15] J. M. Thomas, W. J. Thomas, Principles and practice of heterogeneous catalysis, p 226 (VCH Publishers, Germany, 1997).

[16] J. W. Niemantsverdriet, Spectroscopy in Catalysis, p. 24 (VCH Publishers, Germany, 1995).

[17] L .Thomsen, J. Onsgaard, P. J. Godowski, P. Moller, S. V. Hoffman, J. Vac. Sci. Techn. A **19,** 1988 (2001).

[18] K. Christmann, Surf. Sci. Rep. **1-3,** 1 (1988).

[19] M. A. Keane, G. Webb, J. Mol. Catal. **73,** 91 (1992).

[20] M. A. Keane, Langmuir **10,** 4560 (1994).

[21] J. L. Latham, Elementary Reaction Kinetics, p. 2 (Butterworths, London, 1969).

[22] J. M. Thomas, W. J. Thomas, Principles and practice of heterogeneous catalysis, p 460 (VCH Publishers, Germany, 1997).